



Universitat Autònoma de Barcelona

ADVERTIMENT. L'accés als continguts d'aquesta tesi queda condicionat a l'acceptació de les condicions d'ús establertes per la següent llicència Creative Commons:  http://cat.creativecommons.org/?page_id=184

ADVERTENCIA. El acceso a los contenidos de esta tesis queda condicionado a la aceptación de las condiciones de uso establecidas por la siguiente licencia Creative Commons:  <http://es.creativecommons.org/blog/licencias/>

WARNING. The access to the contents of this doctoral thesis it is limited to the acceptance of the use conditions set by the following Creative Commons license:  <https://creativecommons.org/licenses/?lang=en>



**Universitat Autònoma
de Barcelona**

Department of Chemistry

Faculty of Science

**Chromogenic and fluorogenic materials
based on micro and nanocapsules**

Àlex Julià López

PhD Thesis

PhD in Materials Science

2019

Supervisors:

Dr. Claudio Roscini

Dr. Daniel Ruiz Molina

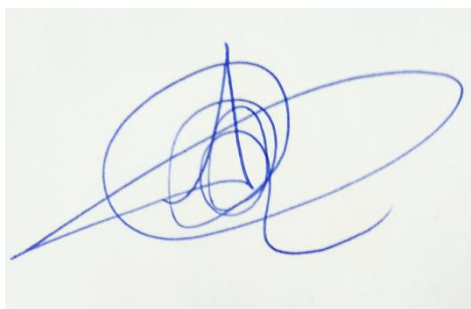
Tutor:

Dr. Jordi Hernando Campos

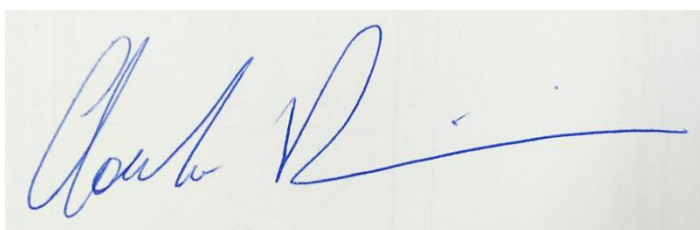
Memòria presentada per aspirar al Grau de Doctor per Àlex Julià López



Dr. Daniel Ruiz Molina



Dr. Claudio Roscini



Bellaterra 22/11/2019

ACKNOWLEDGEMENTS

Primero de todo me gustaría agradecer a mis supervisores: Dr. Daniel Ruiz Molina y en especial al Dr. Claudio Roscini por todo su apoyo, confianza, ideas y ayuda necesarias a lo largo de esta disertación.

También quiero agradecer al Servei de Ressonància Magnètica Nuclear (RMN) de la Universitat Autònoma de Barcelona; así como también a la división de Microscopia Electrònica y a los técnicos del Institut Català de Nanociència i Nanotecnologia, por el soporte técnico y ayuda prestada.

Gracias a los compañeros de trabajo presentes y pasados por hacer más fáciles los días de trabajo. Hasta en los peores días conseguíais sacarme una sonrisa y puedo decir que más que compañeros os habéis convertido en amigos. Gracias también a mis amigos del colegio por su apoyo incondicional en todo momento.

Finalmente, me gustaría agradecer a mi familia por su apoyo y cariño, sin ellos no habría llegado hasta aquí.

Gracias a todos.

ABSTRACT

During the last years smart materials community has paid special attention to systems exhibiting color and emission changes upon application of a certain stimulus (chromogenic). However, though there are a large variety of chromogenic/emissive examples in solutions producing complex effects, their integration into solid materials, relevant for real applications, always generates problems of reproducibility, tunability and modification or inhibition of the optical performances.

The aim of this thesis is to develop a straightforward and universal strategy that not only allows obtaining stimuli-responsive (light, temperature, pH) solid materials but gives also access to: i) direct transfer of bulk solution chromogenic/emissive properties (even combination of them) into the solid state, ii) easy tunability of the optical performances and iii) sophisticated chromogenic effects, beyond the typical photochromic and thermochromic response. Remarkably the tunability is easily achieved by using readily available components, without modifying the chemical structure of the active species. The general strategy relies on the assembling of chromogenic and emissive dyes with interacting media/molecules in micro/nanostructures obtaining performances that could not achieve otherwise. In all developed materials in this thesis the micro/nanostructures are based on: i) organic **dyes** (photochromic, thermochromic, fluorescent), ii) organic non-volatile **media** or **phase change materials** (which can be liquid or solid at RT) and, when needed other additives (*e.g.* color developer) that selectively interact (*via* complex formation, H-bonding or acid-base reaction) with the contained dye inducing specific optical properties in one of the two phases and, iii) structuration as polymeric **capsules** (core-shell or matrix type). Playing with the design of the architecture of these structures, highly tunable chromogenic micro/nanostructures that respond to different (multi)stimuli changing the color and/or the emission properties are obtained, in the solid state. As a proof of concept of this strategy three types of advanced chromogenic materials have been developed: i) polymeric films with tunable and switchable reverse photochromism, ii) multiresponsive (pH and temperature) materials, and iii) high-temperature threshold fluorescent sensors.

ABBREVIATIONS

ACQ: aggregation caused quenching

BA: bisphenol-A

Benz: *n*-octyl 4-hydroxybenzoate

COPV: cyano-oligo *p*-phenylene vinylene

Cyn: ketocyanine (I, II or III)

Cyn I: ketocyanine dye I

Cyn II: ketocyanine dye II

Cyn III: ketocyanine dye III

Cyn-H⁺: protonated form of ketocyanine dyes used.

Cyn/BA@TDOH: cyn I and BA dissolved in TDOH

Cyn/DPA@TDOH: cyn and DPA molecules dissolved in TDOH

Cyn/DPA@HDOH: cyn and DPA molecules dissolved in HDOH

Cyn/BA@HDOH: ketocyanine and BA molecules dissolved in HDOH

Cyn/DPA@HDOH@MF: melamine-formaldehyde capsules filled with HDOH solution of Cyn and DPA molecules

Cyn/DPA@HDOH@PS: polystyrene capsules filled with HDOH solution of Cyn and DPA molecules

Cyn I/DPA@HDOH_GS@GEL_GA: gelatine-gum Arabic capsules filled with mixture of 1-hexadecanol and glyceryl tristearate (50:50) with Cyn I and DPA molecules dissolved

Cyn/DPA@HDOH_GS: Cyn and DPA molecules dissolved in a mixture of 1-hexadecanol and glyceryl tristearate (50:50)

Cyn I/DPA@SA_GS@GEL_GA: gelatine-gum Arabic capsules filled with mixture of stearic acid and glyceryl tristearate (50:50) with Cyn I and DPA molecules dissolved

Cyn I/BA@HDOH_GS: Cyn and BA molecules dissolved in a mixture of 1-hexadecanol and glyceryl tristearate (50:50)

Cyn I/BA@HDOH_GS@GEL_GA: gelatine-gum Arabic capsules filled with mixture of 1-hexadecanol and glyceryl tristearate (50:50) with Cyn I and BA molecules dissolved

DPA: *n*-dodecylphosphonic acid

DA: dodecanoic acid

DCM: dichloromethane

F5-TPB: tetrakis(pentafluorophenyl) borate

GA: gum Arabic

GEL: gelatine

GS: glyceryl tristearate

HD: hexadecane

HA: heptanoic acid

HDOH: 1-hexadecanol

HDOH_GS: mixture of 1-hexadecanol and glyceryl tristearate (50:50)

HDOH-Benz: 1-hexadecanol and *n*-octyl 4-hydroxybenzoate mixture

HDOH-BA: 1-hexadecanol and bisphenol-A mixture

LLDPE: linear low density polyethylene

MC: merocyanine

MCH⁺: protonated merocyanine

M812: Myglyol®812

MF: melamine-formaldehyde

MCs: microcapsules

NA: nonanoic acid

NPs: nanoparticles

NIR: near infrared

PA: pentanoic acid

PDMS-OH: poly (dimethylsiloxane-*co*-diphenylsiloxane) dihydroxy-terminated

PCM: phase change material

PS: polystyrene

PC: poly(bisphenol-A carbonate)

PES: polyethersulfone

PLGA: poly(D,L-lactide-*co*-glycolide)

PMMA: poly(methyl methacrylate)

PP: pre-polymer

PZPER: N,N'-bis(2-(1-piperazino)ethyl)-3,4,9,10-perylenetetracarboxylic acid diimide dichloride

PC: polycarbonate

PEI: polyetherimide

QY: quantum yield

RhB: rhodamine b base

R18: rhodamine B octadecyl ester

Ref.: reference

RT: room temperature

RhB-zw: rhodamine b base in the zwitterionic form

R-Pery: N, N'-bis-(R)-(1'-phenylethyl)-perylene-3, 4, 9, 10-tetracarboxyldiimide

RhB@PS: rhodamine b base loaded polystyrene NPs

RhB/DA: rhodamine b base molecules dissolved in dodecanoic acid

RhB/DA@PS: rhodamine b base and dodecanoic loaded polystyrene NPs

RhB/DA@PMMA: rhodamine b base and dodecanoic loaded poly (methyl methacrylate) NPs

RhB/DA@PES: rhodamine b base and dodecanoic loaded polyethersulfone NPs

RhB/DA@PES: rhodamine b base and dodecanoic loaded poly (bisphenol A carbonate) NPs

RhB/DA@PEI: rhodamine b base and dodecanoic loaded polyetherimide NPs

RhB@PMMA: rhodamine b base loaded poly (methyl methacrylate) NPs

RhB@PES: rhodamine b base loaded polyethersulfone NPs

RhB@PC: rhodamine b base loaded poly (bisphenol A carbonate) NPs

RhB/DA@PEI: rhodamine b base loaded polyetherimide NPs

SLMs: solid lipid microparticles

SA: stearic acid

SA_GS: mixture of stearic acid and glyceryl tristearate (50:50)

SMA: stearic-maleic anhydride

SEM: scanning electron microscopy

SP-1: 1',3',3'-trimethyl-6-nitrospiro [1 (2H)-benzopyran-2,2'-indoline]

SP-2: 1'-(2-hydroxyethyl)-3',3'-dimethyl-6-nitrospiro [1 (2H)-benzopyran-2,2'-indoline]

SP-3: 1',3',3'-dihydro-8-methoxy-1',3',3'-trimethyl-6-nitrospiro [2H-1-benzopyran-2,2'-(2H)-indole]

SP-4: 1',3',3'-trimethylspiro [1 (2H)-benzopyran-2,2'-indoline]

SP-5: 6-bromo-1',3',3'-trimethylspiro [1 (2H)-benzopyran-2,2'-indoline]

SP-6: 8-methoxy-1', 3', 3'-trimethylspiro [1 (2H)-benzopyran-2,2'-indoline]

SP-X/NA: SP molecules dissolved in NA

SP-1/NA-DPA: SP-1 molecules dissolved in NA mixed with DPA

SP-1/PDMS-OH: SP-1 molecules dissolved in PDMS-OH

SP-X/NA@PMMA: PMMA capsules filled with NA solution of SP

SP-1/NA-DPA@PMMA: PMMA capsules filled with NA-DPA solution of SP-1

SP-1/PDMS-OH@PMMA: PMMA capsules filled with PDMS-OH solution of SP-1

SP-X/TA-BA: Spiropyran molecules dissolved in TA-BA mixture

SP-X/HDOH-BA: spiropyran molecules dissolved in HDOH-BA mixture

SP-X/HDOH-BA@PC: PC capsules filled with HDOH-BA mixture of SP molecules

SP-X/HDOH-BA@PES: PES capsules filled with HDOH-BA mixture of SP molecules

SP-X/TDOH-BA@PES: PES capsules filled with TDOH-BA mixture of SP molecules

SP-4/TDOH-BA@PC: PC capsules filled with TDOH-BA mixture of SP molecules

SP-X/DA: spiropyran molecules dissolved in DA

SP-X/DA@PMMA: PMMA capsules filled with DA solution of SP molecules

TA: Trilaurin

TA-BA: Trilaurin and bisphenol-A mixture

TDOH: 1-tetradecanol

TDOH-BA: 1-tetradecanol and
bisphenol-A mixture

T_g: glass transition temperature

T_m: melting point

Table of Contents

TABLE OF CONTENTS

Chapter 1 *General Introduction*

1.1 Smart materials	3
1.2 Photochromic materials	3
1.2.1 Spiropyrans and spirooxazines	6
1.2.3 Photochromism in the solid state	7
1.3 Thermochromic materials	11
1.3.1 Conjugated polymers	11
1.3.2 Thermochromic polymer composites	12
1.3.3 Liquid crystals	13
1.3.4 Organic thermochromic mixtures	14
1.4 Encapsulation	20
1.4.1 Encapsulation methods	21
1.4.2 Phase separation	24
1.4.3 <i>In-situ</i> polymerization	26
1.5 Phase change materials and solid lipid particles	28
1.6 Framework of the thesis	30
1.7 References	32

Chapter 2 *Objectives*

2.1 General objectives	39
------------------------------	----

Chapter 3 *Tunable and switchable reverse photochromism in solid materials*

3.1 Introduction	43
------------------------	----

Table of contents

3.1.1 Tunable reverse photochromism	43
3.1.1.1 From liquid solution to the solid state.....	43
3.1.2 Switchable photochromism (direct vs reverse)	48
3.1.3 Designing tunable and switchable reverse photochromic materials	49
3.2 Objectives.....	53
3.3 Results and discussion	54
3.3.1 Tuning reverse photochromism.....	54
3.3.1.1 Tuning reverse photochromism by changing the dye.....	54
3.3.1.2 Tuning reverse photochromism of nitro-SP by changing the medium	57
3.3.1.2.1 Reverse photochromism of capsules of nitro-SP/solvent.....	60
3.3.1.3 Tuning reverse photochromism of no nitro-SP by changing medium.....	65
3.3.1.3.1 Reverse photochromism of capsules of no nitro-SP/solvent	70
3.3.2 Switchable photochromism.....	79
3.3.3 Photochromic films	89
3.3.3.1 Tunable reverse photochromic films	90
3.3.3.2 Switchable reverse photochromic films	92
3.4 Summary	94
3.5 References	96

Chapter 4 *Multi-responsive thermochromic materials based on ketocyanine dyes*

4.1 Introduction.....	101
4.1.1 Spectral tunability of thermochromic materials in the visible and NIR spectral regions	101
4.1.2 Cyanine dyes	103
4.1.3 Ketocyanine dyes	104
4.1.4 Designing cyanine-based thermochromic materials.....	105
4.2 Objectives.....	108
4.3 Results and discussion	109
4.3.1 Tri-component bulk mixtures of ketocyanines	109

4.3.2 Structuration of the bulk mixture.....	120
4.3.2.1 <i>In-situ</i> polymerization: Melamine-formaldehyde	121
4.3.2.2 <i>In-situ</i> polymerization: Radical polymerization of styrene.....	123
4.3.3 Structuration of the bulk Cyn/DPA@HDOH as solid lipid microparticles.....	124
4.3.3.1 Cyn/DPA@HDOH SLMs	124
4.3.3.2 Mixture of PCMs: Cyn/DPA@HDOH_GS	129
4.3.4 Preparation of multi-responsive functional capsules	131
4.3.4.1 Cyn I/DPA@HDOH_GS@GEL_GA	131
4.3.4.2 Tunability of the chromogenic properties of the capsules	136
4.3.4.2.1 Cyn I/DPA@SA_GS@GEL_GA	138
4.3.4.2.2 Cyn I/BA@HDOH_GS@GEL_GA	141
4.4 Summary	147
4.5 References	149

Chapter 5 Nanostructured High-temperature thermofluorochromic sensors

5.1 Introduction.....	153
5.1.1 Polymers: tool for high temperature fluorescent sensing	153
5.1.2 Polymeric NPs as novel off/on fluorescent sensors	156
5.2 Objectives.....	159
5.3 Results and discussion	160
5.3.1 RhB-loaded polymeric nanoparticles.....	160
5.3.2 RhB/DA@PS nanoparticles	164
5.3.3 RhB/DA@Polymeric nanoparticles	173
5.3.4 Tunable threshold temperature sensors.....	180
5.3.5 Preparation of a thermofluorochromic device.....	182
5.4 Summary	185
5.5 References	186

Table of contents

Chapter 6 *General conclusions*

6.1 General conclusions.....	191
------------------------------	-----

Chapter 7 *Experimental Section*

7.1 Materials.....	197
7.1.1 Polymers and surfactants.....	197
7.1.2 Color developers and phase change materials	197
7.1.3 Dyes.....	197
7.1.4 Solvents.....	198
7.2 Characterization techniques.....	198
7.2.1 Optical microscopy (OM).....	198
7.2.2 Scanning electron microscopy (SEM)	198
7.2.3 Absorption spectra.....	198
7.2.3.1 Time-dependent absorption measurements.....	198
7.2.3.1 Temperature-dependent absorption spectra.....	199
7.2.4 Fluorescence spectra.....	199
7.2.4.1 Temperature-dependent fluorescence measurements.....	199
7.2.4.2 Heating process of the NPs for T-dependent fluorescence study.....	199
7.2.5 Proton nuclear magnetic resonance (¹ H-NMR).....	199
7.2.6 Differential Scanning Calorimetry (DSC)	200
7.3 General procedures.....	200
7.3.1 Lyophilisation.....	200
7.3.2 Irradiation methods.....	200
7.3.3 Synthesis of photochromic microcapsules.....	201
7.3.3.1 Synthesis of SP-X/NA@PMMA	201
7.3.3.2 Synthesis of SP-1/NA-DPA@PMMA.....	201
7.3.3.3 Synthesis of SP-1/PDMS-OH@PMMA.....	201
7.3.3.4 Synthesis of SP-4/TDOH-BA@PC and SP-5/TDOH-BA@PES	201
7.3.3.5 Synthesis of SP-X/DA@PMMA	201

7.3.4 Thermo and pH-responsive solid lipid particles and capsules	202
7.3.4.1 Synthesis of Cyn/DPA@HDOH particles	202
7.3.4.2 Synthesis of Cyn/DPA@HDOH_GS particles	202
7.3.4.3 Synthesis of Cyn/DPA@HDOH_GS@GEL_GA capsules.....	202
7.3.4.4 Synthesis of Cyn/DPA@SA_GS@GEL_GA capsules.....	203
7.3.4.5 Synthesis of Cyn/BA@HDOH_GS@GEL_GA capsules.....	203
7.3.5 Synthesis of RhB@polymer NPs.....	204
7.3.6 Preparation of polymeric films	204
7.3.6.1 PVA films preparation	204
7.3.6.2 PA films preparation	205

CHAPTER 1

General introduction

The following chapter includes a general overview of chromogenic (photochromic and thermochromic) materials in the solid state and their actual applications. Moreover, it also encompasses an introduction to encapsulation and the main methods employed for the synthesis of polymeric capsules, which represents the key structure of this thesis.

1.1 Smart materials

Chromogenic and fluorogenic materials are defined as materials that reversibly change their absorption and/or emission properties as response to external stimuli (e.g. temperature, light, pH, etc.).¹ These systems are considered smart and “chameleonic” because they adapt their color according to the environmental conditions. In these materials A turns to a species B (which has different optical properties) when exposed to a certain stimulus (**Figure 1.1**).

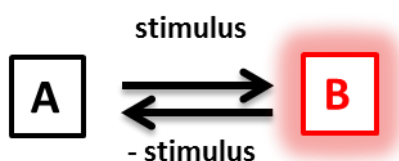


Figure 1.1: schematic representation of the interconversion between two different species A and B, of different color/emission properties, induced by an external stimulus.

The change of color (in terms of absorption or emission properties), is related to the alteration of the electronic properties (e.g. increase or decrease π -conjugation) of the compound or substance caused by the stimulus. The two species can be chemically different or could be the same species in a different physical state. The stimulus may cause different effects to the substances involved such as acid-base or redox reactions, dimerizations, isomerizations, bond cleavage/formation (chemical changes) or aggregation-disaggregation processes (physical changes), among others. Depending on the external stimulus used to induce the color change, the phenomenon is described as photochromism (light), thermochromism (temperature), halochromism (pH), solvatochromism (solvent), electrochromism (voltage), etc. Given the chromogenic effects of the smart materials in this thesis work, some of these chromic phenomena are described into more details in the present chapter.

1.2 Photochromic materials

Photochromism is the reversible transformation between two chemical species, A and B, with different absorption properties, induced by absorption of

electromagnetic radiation (**Figure 1.2**).²⁻⁴ When A absorbs a photon, it interconverts to B, the thermodynamically less stable species.

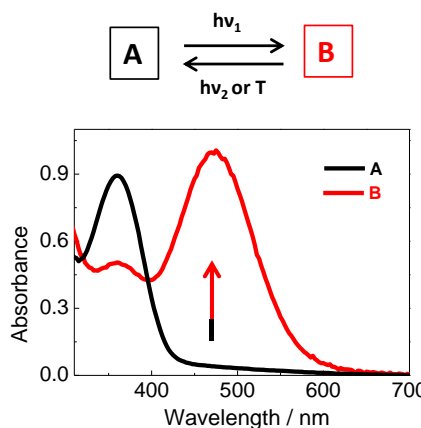


Figure 1.2: schematic representation of a photochromic interconversion between two different species A and B and the typical spectral variation associated due to the different absorption properties.

The back process (from B to A) can occur thermally (**T-type** photochromism) and the initial form A is formed spontaneously once radiation is removed due to the limited thermal stability of B. On the other hand, when the photochemically induced form B is thermally stable, A is only recovered upon irradiation with light of a different frequency (**P-type** photochromism).^{3,4}

Well-known examples of both types of photochromic dyes are shown in **Figure 1.3**. Typical T-type photochromic dyes are azobenzenes, spiropyrans and naphthopyrans that often interconvert from colorless to colored, upon UV irradiation (**Figure 1.3a**). The photogenerated species are thermally unstable, and revert to the initial form in the dark, at room temperature.

Fulgides and diarylethenes (**Figure 1.3b**), which generally change from colorless to colored upon UV exposure, are widely-known P-type photochromic dyes that only recover the initial colorless state after irradiating with visible light.⁵

In most of the cases the photochromic process consists of a unimolecular isomerization reaction such as *trans-cis* isomerization (of azobenzene) or ring-opening/ring-closure reactions (i.e. spiropyrans, naphthopyrans, diarylethenes or fulgides).

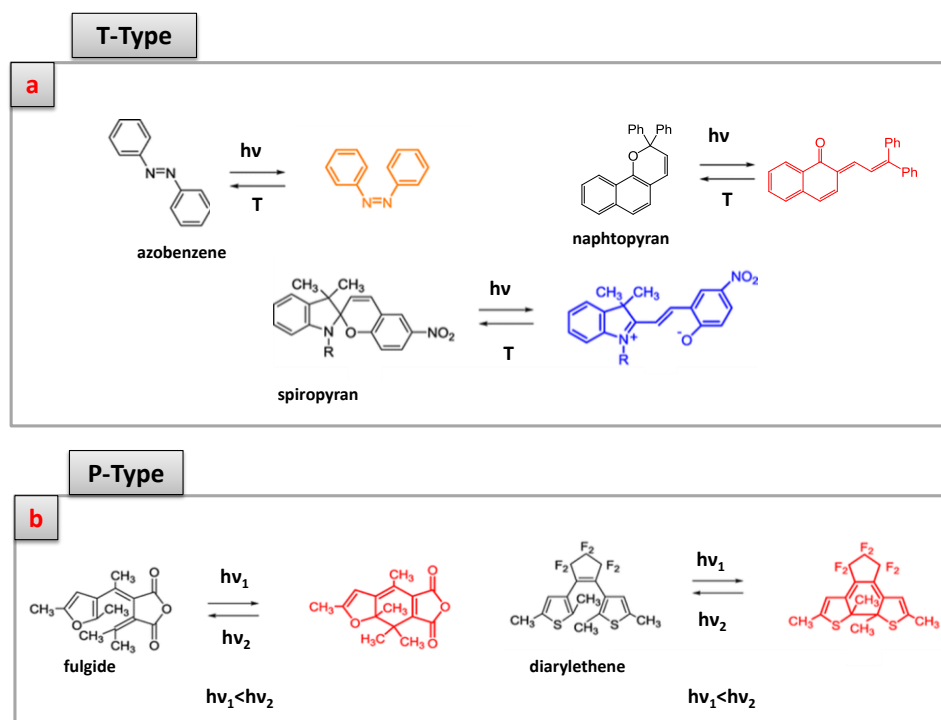


Figure 1.3: molecular structures of typical a) T-type and b) P-type photochromic molecules. Adapted from ref. 5.

When the initial species A absorbs at longer wavelengths than the photoinduced species B ($\lambda_{\max}(A) < \lambda_{\max}(B)$), the phenomenon is known as **positive** or **direct photochromism**. On the contrary, when the photoinduced species B absorbs at higher energy than the initial one A ($\lambda_{\max}(A) > \lambda_{\max}(B)$) the process is known as **negative** or **reverse photochromism**. In the latest case if the species A absorbs in the visible region and B absorbs in the UV region, the photoirradiation of the colored form originates a colorless state (photoinduced fading).

The direct photochromism exhibited by T-type photochromic dyes, is a property industrially exploited to obtain dynamic photoprotective coatings for ophthalmic lenses and smart windows.⁶ These coatings smartly self-adapt to the light intensity, becoming colored under sunlight exposure (filtering the UV and Vis light) and colorless in the dark. Nowadays, in the industry real applications for reverse photochromism exhibited by T-type photochromic dyes are still scarce. However, reported examples show their potential applications in anti-counterfeiting technologies, rewritable displays, and optical data storage systems.⁷⁻¹¹ On the other hand, the bi-stability of P-type photochromic dyes is

proposed for data storage and logic gates.^{12,13} However, the applications of P-type dyes are still on a research stage.

1.2.1 Spiropyrans and spirooxazines

Among all the T-Type photochromic dyes, spiropyrans and spirooxazines are among the most investigated organic photochromic molecules during the last decade. Commercially available spiropyran molecules have been used during the development of this thesis. The most common spiropyrans are based on indoline and benzopyran moieties connected through a spirocarbon. This basic structure can bear substituents in the indoline or benzopyran moieties (alkyl, alkoxy, nitro, halogen, etc.), and can be extended to more conjugated structures, upon substitution of the benzopyran and the indoline moieties, with naphthopyran or thioindoline, respectively.¹⁴

Spirooxazines have similar structure to spiropyrans (the alkenic CH of the pyran ring is replaced by a nitrogen atom, **Figure 1.4**) and undergo analogous photoinduced reaction.^{2,3,15}

In such compounds, UV light irradiation of the spiro closed form (SP, colorless in non-polar media) leads to the spirocarbon–oxygen bond cleavage (ring-opening reaction) of the pyran ring, followed by a *cis–trans* isomerization to finally reach the merocyanine (MC) form (colored). The latter isomer has two resonant forms, with zwitterionic and quinoidal character (**Figure 1.4**). The predominance of one resonant structure or the other depends on the polarity of the environment and the electronic properties of the substituents.¹⁶ The main existing form of the ring-opened spirooxazines is the quinoidal structure, stabilized by the nitrogen in the oxazine ring, which is involved in electron delocalization.¹⁷ In spiropyrans, the zwitterionic character is generally predominant. The electron delocalization of the MC form originates an intense absorption band in the visible region of the electromagnetic spectrum. On the contrary, in the closed form, the conjugation is broken in the spirocarbon atom and the molecule is colorless and absorbs in the UV region. In non-polar media the closed form is the most stable isomer and the metastable MC form is temporally induced upon UV irradiation. However, the MC isomer may form spontaneously in the dark if stabilized through chemical

modifications of the parent molecular structure or by the media (i.e. polar or acidic solvents).¹⁸ The MC form in these cases is also photochromic (visible light). Generally, the quinoidal MC of spiropyrans and the zwitterionic MC of spiropyrans show positive (red shift of the spectrum as the polarity increases) and negative (blue shift of the spectrum as the polarity increases) solvatochromism, respectively.¹⁹

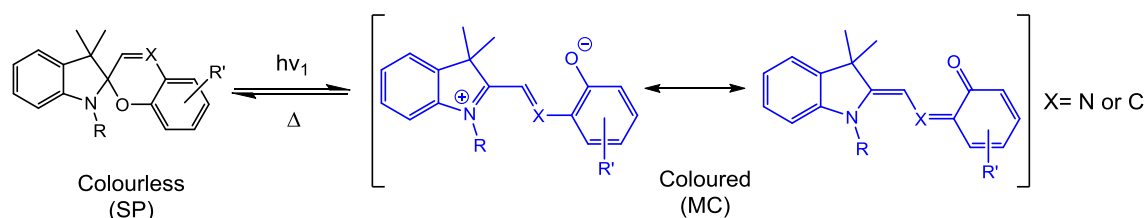


Figure 1.4: scheme of the photochromic interconversion of spiropyrans (X=C) and spiropyrans (X=N).

1.2.3 Photochromism in the solid state

- **Current applications of direct photochromism**

From a practical standpoint, the photochromic switching has to occur in a robust matrix such as polymeric materials. In order to prepare photochromic polymers, the dye molecules are embedded in the matrix by covalently binding to the polymer chain backbone or through direct dispersion in the matrix. The photoinduced interconversion between two species that differ for their spatial geometry and chemical nature can be exploited to produce smart materials that reversibly vary their wettability²⁰⁻²² and the mechanical properties (i.e. actuators, molecular motors).²³⁻³² However, these applications are still under development in the academic community.

Regarding the industry, the photoinduced reversible coloration of T-type photochromic materials is what nowadays is mostly exploited. It is found in novelty items such as in toys and T-shirts, but it is in the eyewear industry (**Figure 1.5a**) where photochromic compounds are more broadly used.⁶ Their use can be exploited as well to obtain smart windows that become colored upon sunlight exposure (**Figure 1.5b**) and colorless in the dark.



Figure 1.5: digital images of applications of T-type direct photochromism in a) eyewear glass and b) in smart windows.

Spirooxazines and naphthopyrans are the most used dyes in the industrial sector due to their enhanced fatigue resistance and scaled-up production.^{2,33} Normally, these dyes are directly embedded in the matrices to yield photochromic materials. However, when embedded in solid polymeric materials, the micro and nano-environmental properties of the matrix, such as local polarity and the rigidity can affect the photochromic performances. Generally, photochromic transitions are slower in a polymer matrix, as compared to solution. This effect is attributed to the limited free volume available for the dye molecules in a polymeric medium, which imposes steric restrictions to the isomerizations.³⁴ This is known as “matrix effect” and was described for the first time by Krogauz *et al.*³⁵ Furthermore, aggregation of photochromic dyes in solid materials can also influence kinetic and spectral properties. Several strategies have been designed to avoid these problems.³⁶⁻³⁸ In particular the methodology developed in Nanosfun group and reported by N. Vazquez *et al.*³⁹ allows transferring the photochromic behavior of liquid solutions (which minimizes the matrix effect) to solid materials. This strategy is based on the encapsulation of a liquid photochromic solution in core-shell capsules (**Figure 1.6a**) and the embedment of these capsules into a polymeric film. The capsule protects the photochromic solution and avoids the immobilization of the molecules within the rigid matrix. As a result, the photochromic behavior is enhanced (faster) compared to a film in which the photochromic molecules are directly embedded (**Figure 1.6b-c**).³⁹ Overall the encapsulation strategy allows transferring fast photochromic behavior, which is only observed in solution, to solid materials.

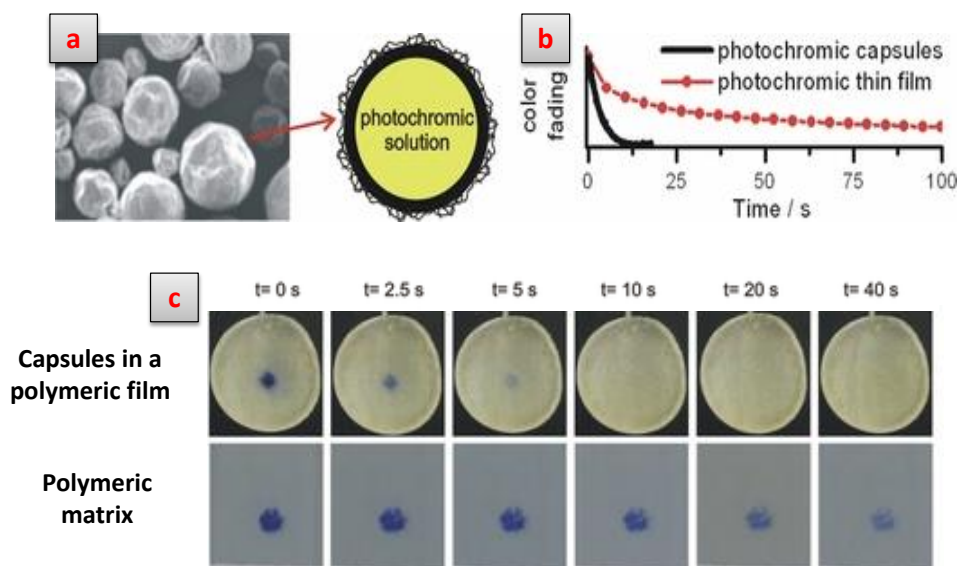


Figure 1.6: a) SEM image and scheme of the capsules enclosing a photochromic solution, b) comparison of the fading of the photochromic capsules and the film with spirooxazine molecules embedded; and c) digital images of acrylate-based polymeric photochromic films, with and without capsules, after being irradiated with UV light and the corresponding discoloration process. Data adapted from ref. 39.

- **Potential applications of reverse photochromism**

Reverse photochromism, as well as direct photochromism, can be exploited to change the physical properties of functionalized polymers. Again, among all the T-type photochromic compounds, spiropyrans and spirooxazines, are the most studied. The open MC isomer can be stabilized *via* intra or intermolecular interactions with functional groups of the polymer matrix. When this happens, these molecules could be used to achieve reverse photochromism, as upon visible irradiation the colorless spiro isomer is temporally induced. The isomerization of the MC to the spiro form is used to change the mechanical properties and/or 3D-structure of MC-functionalized polymers.⁴⁰⁻⁴⁴ This is obtained by using the less harmful and more easily accessible visible light which induces less fatigue to the dyes.

The use of visible light as a trigger in reverse photochromic polymers opens up the possibility to control also biological processes by changing the structure of macromolecules or opening and closing biological transport channels.⁴⁴⁻⁴⁶ It enables the reversible switching with visible light, without requiring the use of UV radiation, which is potentially harmful for biological systems and less penetrating.

Chapter 1

In the recent years much effort has been devoted to develop light-induced rewritable displays. However, most of the systems developed until now, use direct photochromism to generate writings or patterns that erase after a certain time.^{47,48} Nowadays, the interest is focused on obtaining these rewritable devices based on reverse photochromism, which allows the possibility to operate with the visible light. An example of this approach is shown in **Figure 1.7**, in which Zhang and co-workers⁴⁹ used a spiropyran-based photoacid (PAH, **Figure 1.7a**) together with a pH sensitive dye (methyl orange, **Figure 1.7a**) to develop rewritable paper. When the PAH (yellow color), stabilized in the MC form, is irradiated with visible light (blue light) the spiro closed form (colorless) is induced (**Figure 1.7a**, reverse photochromism) and, subsequently, a proton is released. The proton is taken by the methyl orange (MO), which changes its electronic structure and thus, develops the red color observed after irradiation. The mixture of MO and PAH was applied on top of filter paper (**Figure 1.7b**) and when irradiated with blue light (in the presence of a dark mask with text) a red text appeared in the paper. After certain time (hours) or upon heating, the text was erased allowing the possibility to write again.

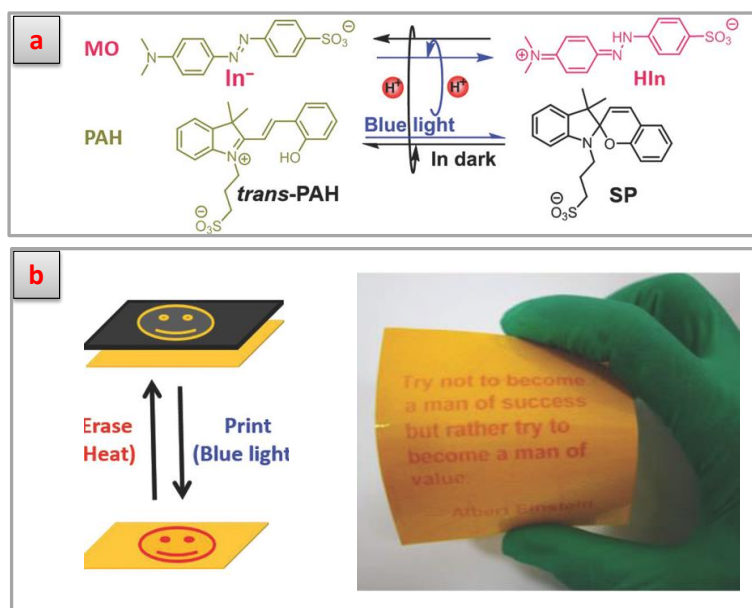


Figure 1.7: a) schematic representation of the photoinduced (blue light) proton transfer between the spiropyran derivative (photoacid, PAH) and methyl orange (pH-sensitive dye, MO) and b) images of a rewritable paper, coated with the photoacid and the methyl orange, after irradiating with blue light in the presence of a black mask with text. Data adapted from ref. 49.

Although real products using T-type direct photochromism are already available, the same could not be affirmed for reverse photochromism. Despite the advantages provided by reverse photochromism, the lack of applications is partially due to the difficulty of achieving this property in the solid state. The example showed above, is based on specific molecules designed and synthesized for this purpose. However, a general strategy to obtain solid materials with tunable photochromic performances (in terms of color and interconversion rates) is still not available. For this reason in this thesis, we aimed to adopt an equivalent strategy to the one reported by Nuria *et al.*³⁹ (**Figure 1.6**) to transfer, through the encapsulation, **reverse photochromic** response, which is more widely studied in solution, to solid polymeric materials (more difficult to achieve) and open up the possibility to exploit the potentiality of reverse photochromism in real applications. A more detailed overview on how to obtain reverse photochromism in solution and in the solid state is described in **Chapter 3**.

1.3 Thermochromic materials

Thermochromism is the property of substances able to change color due to a variation of temperature. Thermochromic polymers can be obtained exploiting the inherent properties of specific polymers (i.e. conjugated polymers),⁵⁰⁻⁵⁵ by designing thermochromic polymer composites or through embedding thermochromic pigments based on leuco dyes or cholesteric liquid crystals⁵⁵ into polymers.

1.3.1 Conjugated polymers

A **conjugated polymer** consists of a polymer backbone structure with a conjugated π -electron system. Polyacetylenes, polydiacetylenes, polythiophenes, and poly(*p*-phenylene vinylenes) belong to this class of polymers. An example of the general structure of polydiacetylenes (PDA) is shown in **Figure 1.8a**. A large number of conjugated polymers absorb light in the visible range leading to the appearance of color. Any change of the effective conjugation length of the π -electron system in the polymer backbone with temperature results in a shift of the absorption (and/or emission) spectrum and thus in thermo(fluro)chromism (**Figure 1.8b**).⁵⁰⁻⁵⁵ Even small variations of the conformational structure of the

polymer can cause significant color changes, especially if they affect the planarity of the polymer chain. These color changes can occur gradually within a phase or discontinuously during the phase transition of the polymer. Thermochromic effects of conjugated polymers are in principle reversible but can also be irreversible.

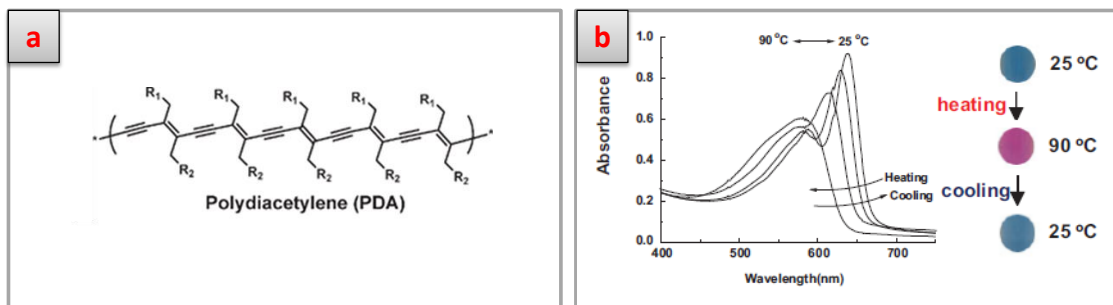


Figure 1.8: a) general structure of PDA and b) temperature-dependent absorption spectra and photographs of the PDA suspension. Data adapted from ref. 50.

1.3.2 Thermochromic polymer composites

Thermochromic polymer composites are made by a multilayer of two or more different polymers in which at least one of the layer materials alters thickness and/or refractive index with temperature. The common and easiest way to design these types of materials is by spin-coating or self-assembling alternating thermoresponsive and non-thermoresponsive polymer layers.⁵⁶⁻⁵⁸ Temperature changes vary the thickness of the thermoresponsive polymer layer (**Figure 1.9a**) inducing a change in the optical properties of the material. These color changes occur from the constructive light interference of the reflected light at the boundaries between polymer layers. Poly(*N*-isopropylacrylamide) (PNIPAM) is well-known polymer that has very high temperature-responsive volume change in aqueous media.⁵⁹ As long as the temperature is below the lower critical solution temperature (LCST) the polymer network is hydrated and swollen. When heated above LCST the hydrated state dehydrates providing a volume change. Hayward *et al.*⁵⁶ employed a polymer composite made of spin-coated alternating layers of PNIPAM-polyacrylic acid copolymer (PNIPAM-co-PAA, **Figure 1.9b**) and the non-responsive poly(*p*-methyl styrene) (PpMS, **Figure 1.9b**), finally crosslinked together by photopolymerization. The resulted composite changed color (from

orange to magenta passing through yellow and green) when heated from 23°C to 50°C (**Figure 1.9c**).

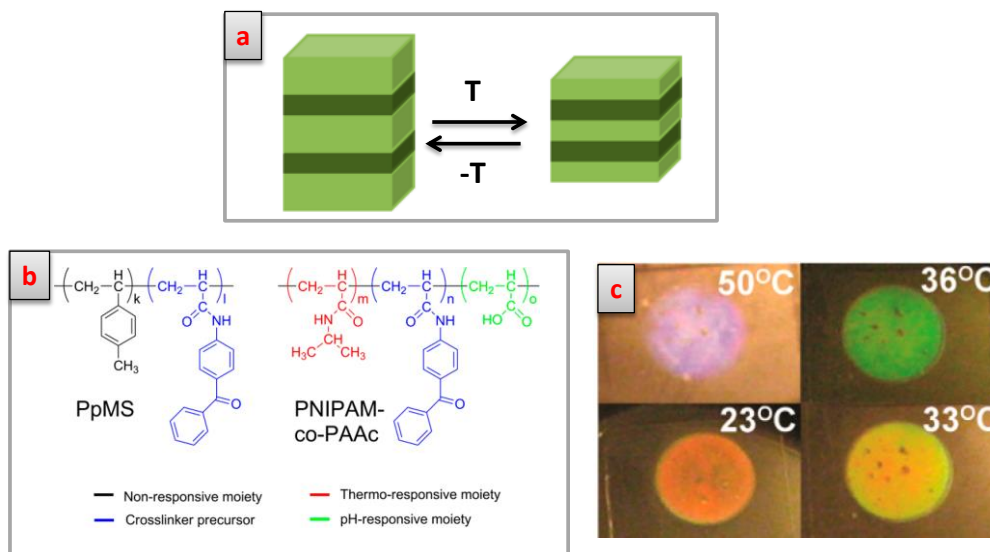


Figure 1.9: a) scheme of a thermochromic polymer composite built from alternating layers of thermoresponsive and non-thermoresponsive polymer materials; b) molecular structures of PpMS and PNIPAM-*co*-PAAc copolymer used for the fabrication of a thermochromic polymer composite; and c) digital images of the thermochromic composite swollen in water at different temperatures (23, 33, 36, 50 °C). Data adapted from ref. 56.

1.3.3 Liquid crystals

In another family of thermochromic materials, the temperature-dependent light reflection is achieved using cholesteric **liquid crystals (CLC)**.⁶⁰⁻⁶³ The liquid crystal molecules organize and orient in a preferred direction, which varies periodically along the axis perpendicular to the LC phase (**Figure 1.10a**). The pitch is defined as the distance, along the direction of periodicity, at which different layers have the same orientation. Typical values of the pitch can be of the order of the wavelength of visible light (400 to 700 nm). As a result, the visible light hitting the LC undergoes Bragg reflection from the subsequent layers, and the color of the liquid crystal corresponds to the wavelength of light for which maximum constructive interference occurs.^{64, 65} In cholesteric liquid crystals, changes in temperature result in thermal expansion, which leads to a variation of the pitch, and hence of the maxima of the constructive light interference, producing temperature-dependent colors (**Figure 1.10b**). Since the pitch varies gradually

(not discrete), the produced colors also changes smoothly and some CLC allow passing from black to red through orange, yellow, green, blue and violet, according to the reached temperature. An illustration of the thermochromic effect provided by cholesteric liquid crystals is shown in **Figure 1.10c**.⁶³

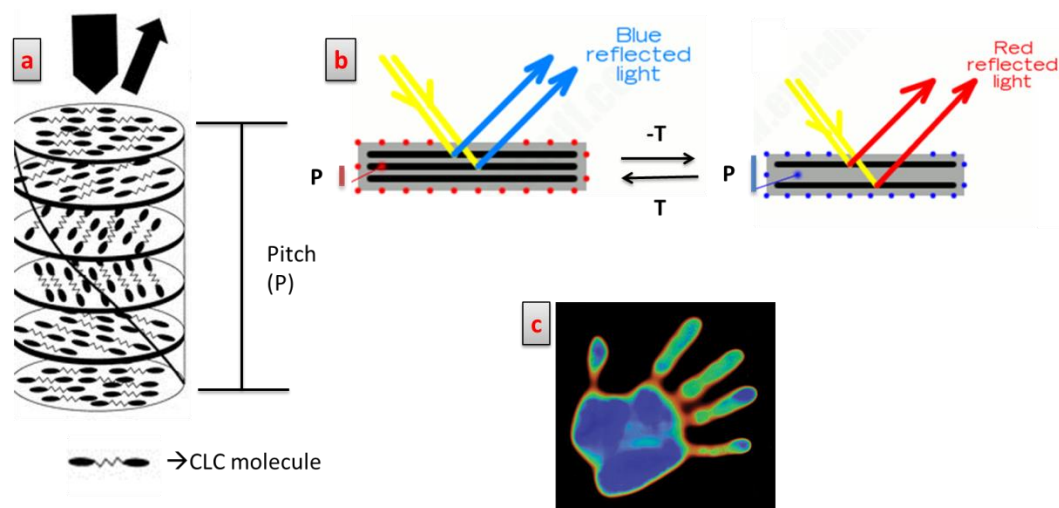


Figure 1.10: a) schematic representation of the pitch cholesteric liquid crystals and b) the variation of the pitch-dependent color upon temperature changes; c) digital image of a thermochromic CLC after being exposed to the human hand heat. Data adapted from ref. 63

The CLC thermochromic materials have been investigated for a large variety of applications such as in the thermal mapping of electronic components, aerodynamic tests and in medical applications.⁶⁶ However, these materials are currently used to produce thermochromic textiles fashion products (e.g. T-shirt).

In order to utilize these CLC in fabrics, they have to be encapsulated in core-shell capsules to preserve the orientation properties of the CLC molecules (required for color generation) once adhered to the textile materials.⁶⁷ Although suitable and highly sensitive color effects can be achieved by this strategy, liquid crystals-based thermochromic materials have limited use in textile owing their high cost and low color density, which implies that to maximize the visual effect, they must be printed in a black background (**Figure 1.10c**).

1.3.4 Organic thermochromic mixtures

The other major category of materials used to impart colors that change with temperature and largely employed in commercial products such as textiles and

other novelty products, involves color changing organic dyes. For this strategy, different architectures have been developed, that vary on the number and type of components employed.

- **Tri-component thermochromic mixture**

In order to design thermochromic materials based on organic dyes, a mixture of chemical components is required.^{63, 66} These components are:

i) the dye: these are usually leuco dyes, which are able to switch between two chemical forms, one of which is colorless. Dyes commonly used in thermochromic organic mixtures are spirolactones, such as fluorans (e.g. crystal violet lactone) (**Figure 1.11a**),^{66,68} spiropyrans (**Figure 1.11b**),^{2,69} or fulgides.² Strictly speaking, these dyes are not themselves thermochromic but rather change their color upon a variation of the pH (**halochromism**), as shown in the equilibrium reaction of crystal violet lactone or the spiropyran of **Figure 1.11**, between the closed form and the open protonated state (colored). In solution, the colored protonated form predominates at acidic pH (<4), while the colorless spiro form is obtained in more alkaline solutions.^{66, 69} The pH-dependent behavior of these dyes has been utilized to produce thermochromism. In this case the position of this equilibrium is shifted with temperature upon melting/solidification of a mixture that depending on its state (solid or liquid) favors one of the two forms of the equilibrium.

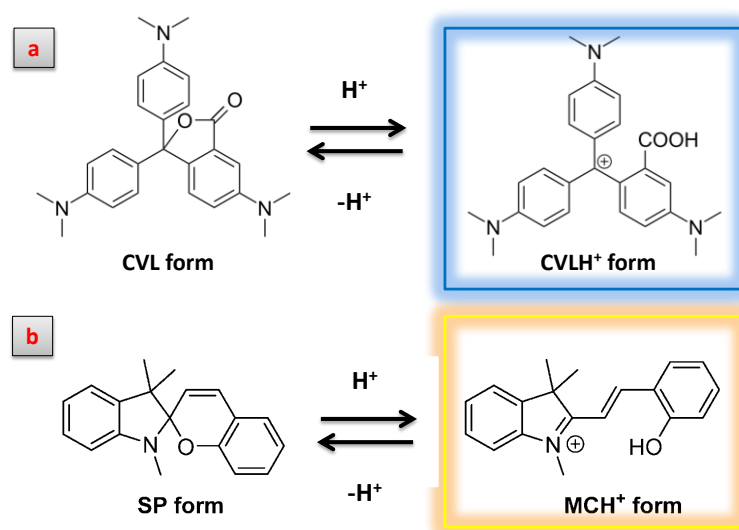


Figure 1.11: acid-base equilibrium of a) crystal violet lactone and b) a spiropyran dye.

ii) the color developer: this component affects the equilibrium position of the dye molecule by establishing hydrogen-bonding interactions or an acid-base reaction with the dye, only in one of the two phases of the solvent. Well-known examples of color developers are bisphenol A (**Figure 1.12a**), octyl *p*-hydroxybenzoate, methyl *p*-hydroxybenzoate (**Figure 1.12b**),⁷⁰ 1,2,3-triazoles, and 4-hydroxycoumarin derivatives (**Figure 1.12c**), which are all weak acids.⁷¹ Weak acids are generally used to impart the reversible temperature-induced color change to the mixture, while stronger acids lead to irreversible color variations (irreversible thermochromism). This component is also responsible for the color intensity of the final product.

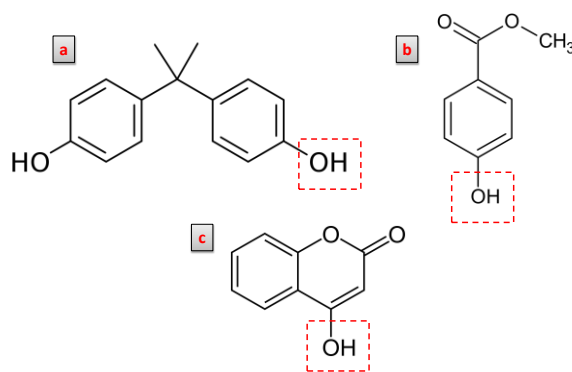


Figure 1.12: chemical structure of a) bisphenol A, b) methyl *p*-hydroxybenzoate and c) 4-hydroxycoumarin.

iii) the solvent: the third component of the mixture is generally a non-volatile polar solvent such as an alcohol, ester, ketone, or ether with long hydrocarbon chains. Examples of these include lauryl alcohol (1-dodecanol), cetyl alcohol (1-hexadecanol), myristyl alcohol (1-tetradecanol, **Figure 1.13a**) and butyl stearate (**Figure 1.13b**).⁷² All these materials are also termed phase change materials (PCM), which are substances generally known for storing and releasing large amount of heat when undergoing a phase transition.⁷³ As the heat is supplied, the materials change their phase from solid to liquid at a constant temperature until they completely convert into liquid. Similarly, the materials change from liquid to solid until solidify completely releasing the stored heat.

Alcohols and esters based PCMs are preferred to increase the solubility of the other two components in the molten state of the PCM. In thermochromic materials the crossing of the melting point (T_m) of the PCM triggers the interaction between

the color developer and the dye and thus, the temperature at which the color change takes place. By changing the PCM, the triggering temperature for the color switch can be varied.

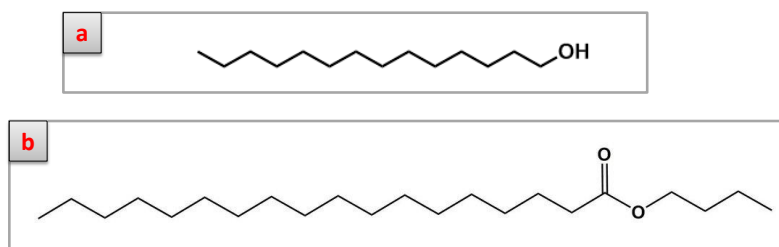


Figure 1.13: chemical structure of a) 1-tetradecanol and b) butyl stearate.

The mixture of dye, color developer and PCM presents color when kept below the T_m of the PCM and discolor upon heating above the PCM. It is somewhat surprising that three-component mixtures are colored at low temperature (below the melting point of the solvent component) and colorless at higher temperature (in the molten state). Given the fact the interaction between the color developer and the dye is a bimolecular process, it is expected to happen preferably in solution (PCM in the liquid phase). The mechanism of their operation is not yet known definitively. Possible explanations for the preferential stabilization of the highly polar, colored form in the solid matrix include:

- i) an increased **dielectric constant** in the host matrix upon solidification.
- ii) **phase separation** of one or the two components on solidification of the PCM.
- iii) a more favorable **steric** situation for the colored species in the solid host matrix.⁶⁶

In (iii) the effect could be due to the smaller steric requirement of the colored species compared with the lactone form, since the former is almost planar and the latter has a tetrahedral structure. According to (i) and (ii) the polar developer might segregate from the PCM upon its solidification, dragging the dye molecules with which interacts. The resulted increased polarity of the segregated microenvironment of the dye should favor the colored form (**Figure 1.14a**).⁶⁶ This is one of the proposed explanations for the thermochromic transition, though the lack of experimental evidences make this and other hypothesis mere speculative and more fundamental research is still needed.

Chapter 1

The basics of the thermochromic tri-component mixture have been used during the development of this thesis in **Chapter 4** with cyanine dyes (also pH-responsive dyes) to generate advanced thermochromic properties.

- **Bi-component thermochromic mixture**

In the bi-component thermochromic system there is no need of the color developer since the solvent already does this function when in its liquid state. This means that **bi-component thermochromic mixtures** work in the opposite way, since the interaction between the dye and the PCM and thus, the color development is only established at temperatures at which the solvent is in the molten state ($>T_m$).^{74,75} On the other hand, in the solid state of the PCM the dye does not interact with the PCM and remains in the colorless form (**Figure 1.14b**). Typical solvents to induce this behavior are acids with long hydrocarbon chain (such as octadecyl phosphonic acid,⁷⁵ dodecyl phosphonic acid, dodecanoic acid, etc.). The colored protonated form of the dye is favored above the T_m of the acid (which acts as both a proton donor and a solvent), and the colorless state is achieved at lower temperatures. This principle is exploited in this thesis to obtain reversible and switchable photochromism (from direct to reverse) and this topic is treated into more details in **Chapter 3**.

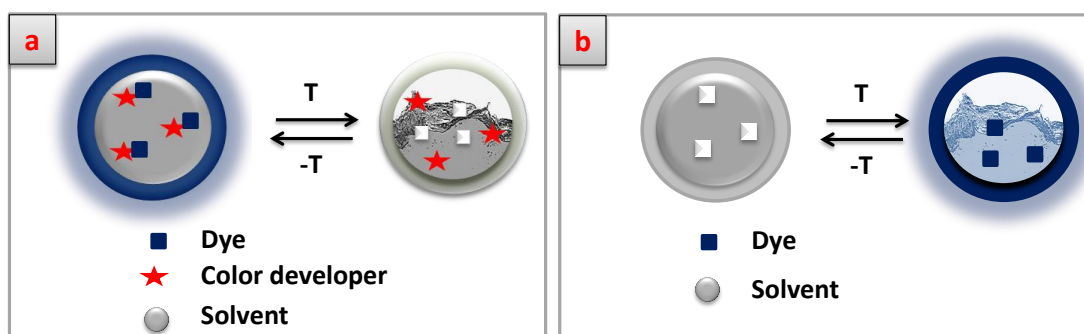


Figure 1.14: scheme of the mechanism proposed for the encapsulated a) tri-component thermochromic system and the b) bi-component thermochromic systems.

The color development exhibited by these organic thermochromic systems is dependent on and related to the T_m of the incorporated solvent. Consequently, to ensure that a homogeneous mixture is maintained throughout the melting/solidification process the thermochromic composition must be kept in a

closed system.^{66,70} This is achieved by encapsulation of the mixture, i.e. surrounding it with colorless, impermeable polymeric coating.⁶³

These thermochromic capsules are used as coating in toys and other novelty products (**Figure 1.15**), for printing inks, paints, and textile materials.⁷⁰



Figure 1.15: digital images of gadgets coated with thermochromic paints.

- **Thermochromism by self-assembling of dye-dye aggregates**

Another strategy to achieve temperature-induced color changes with organic dyes without the need of a color developer is by employing the so-called aggregachromic dyes. These dyes can form H- or J-aggregates through π - π stacking interactions among their planar aromatic backbones. The dye aggregation is accompanied by pronounced changes of the absorption properties which have their origin either in charge transfer interactions within the dye aggregates or in conformational changes of the dye structure. For H-aggregates (plane to plane parallel stacking) absorb at lower wavelengths than the non-aggregated molecules, whereas for J-aggregates (head to tail stacking) shift their absorption towards lower energies. Aggregachromic dyes present i) a highly conjugated and aromatic moieties, which promote π - π stacking interaction between dye molecules; ii) electron-withdrawing and/or electron-donating substituents conjugated to the aromatic core to modulate the optical properties of the dye and the aggregation tendency; and iii) absence of bulky substituents, which would cause a steric hindrance of dyes self-assembly.

Thermochromism is obtained when the dye and/or the dye aggregates absorb in different regions of the spectra and a temperature-dependent dye aggregation-disaggregation arises (**Figure 1.16**).⁷⁶ Polymers and PCMs are often used to trigger

Chapter 1

the aggregation or disaggregation of dyes due to the temperature-induced morphological or viscosity changes that they suffer.

Most of aggregachromic dyes are also fluorescent so temperature-dependent emission changes (**thermofluorochromism**) are generally accomplished as well. The temperature-dependent aggregachromism was exploited in this thesis to obtain high-temperature threshold fluorescence sensors. A more detailed explanation of these systems is given in **Chapter 5**.

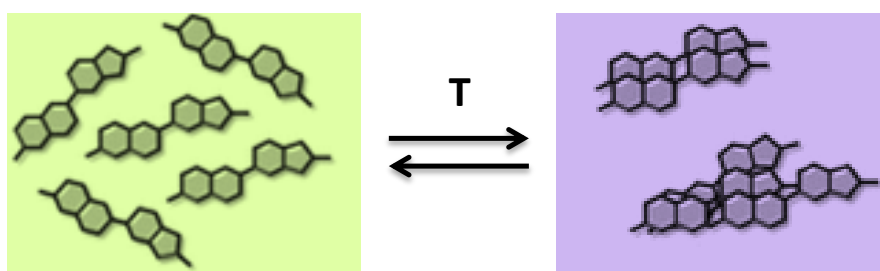


Figure 1.16: scheme of the mechanism of reversible aggregation-disaggregation of an aggregachromic dye triggered by temperature. Image adapted from ref. 76.

Some of the photochromic and thermochromic materials shown previously use the **encapsulation** to preserve the chromogenic properties in polymeric films or fabrics. Since the encapsulation has also been used in this thesis to obtain different chromogenic and fluorogenic materials, in the next session of this chapter the encapsulation methods, relevant for this work, are reported

1.4 Encapsulation

The encapsulation is a process where particles or droplets are coated with a polymer material that separates the internal from the external environment. The capsules possess different useful properties and are used in various applications.⁷⁷⁻⁷⁹ The capsules allow obtaining a wide range of products depending on the properties of the substance enclosed and the material used for the encapsulation. In our systems the encapsulation offers several advantages to chromogenic mixtures:

- (i) the protection of sensitive substances from the external environment improving the stability and the resistance of the final product.

- (ii) to prevent the leakage of a liquid material or PCM during its solid-liquid transition.
- (iii) to combine the properties of different types of materials.
- (iv) to manipulate liquid as solid powdered materials, allowing safe handling.
- (v) to retain the characteristics of the encapsulated substances when dispersed into another material (e.g. polymer matrix) and improve their compatibility preventing agglomeration and allowing a uniform dispersion.

1.4.1 Encapsulation methods

Capsules are composed of: i) a loaded substance that generally carries the functionality (payload); and ii) the shell that encloses the former. Although they can present different shapes, spherical capsules are among the most common and widely reported in the literature.⁸⁰⁻⁸² The spherical capsules mainly present two different structures, named core-shell (**Figure 1.17a**)^{80,82} and matrix-type (**Figure 1.17b**).⁸¹ Core-shell capsules are based on particles hollow in the interior (with one or more compartments) and composed of a solid shell surrounding the core material (**Figure 1.17a**). The mononuclear core-shell capsules can be thought equivalent to a liquor chocolate “bonbon” where the cortex (chocolate shell) surrounds the core material (the liquor inside). The multinuclear structure can be thought as a porous cake where the polymer matrix surrounds multiple core materials. The core of the capsules can be solid, liquid or gaseous containing dispersed and/or dissolved materials.

In the matrix-type structure the loaded material (e.g. dye, drug, etc.) is homogeneously dissolved in the entire volume of the particle matrix (**Figure 1.17b**).^{81,83} Polymers and silica-based materials are often selected to form the outer layer(shell) of the capsules due to their stability and robustness.^{84,85}

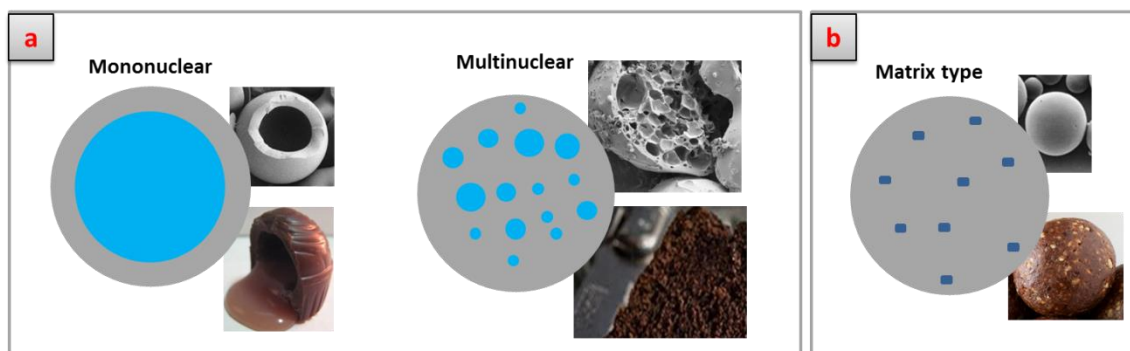


Figure 1.17: scheme of the possible structures, SEM images and photographs of similar macroscopic structures of a) core-shell polymeric capsules (mononuclear and multinuclear) and b) structure of a matrix-type polymeric capsule.

All capsules prepared along the present thesis are based on polymeric shell material and contain in the interior the chromogenic mixture of interest. Depending on the functionality it was meant to obtain core-shell or matrix type polymeric capsules. All methods employed for the preparation of the capsules used in this thesis are based on two basic steps: ⁸⁶

i) the formation of an oil-in-water (O/W) **emulsion** by mixing energetically an organic phase into an aqueous phase that contains a stabilizing agent (**Figure 1.18**).

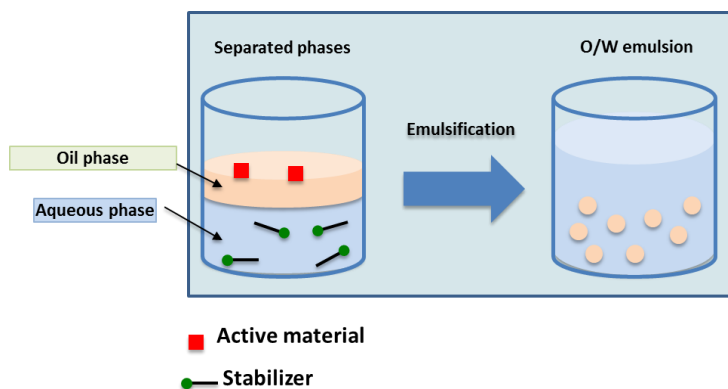


Figure 1.18: scheme of the emulsification process followed during an encapsulation method

A stabilizing agent can increase the viscosity of the media (stabilizer) or reduce the surface tension of the organic droplets (surfactant). The use of stabilizers and/or surfactants reduces the energy required to form the droplets and increase their lifetime since they inhibit the mechanisms for the phase separation (coalescence, flocculation, sedimentation, etc.) Typical examples of stabilizers are

water soluble-polymers (e.g. polyvinyl alcohol, PVA, or polyvinylpyrrolidone, PVP), whereas sodium dodecyl sulfate (SDS) and sorbitan monooleate (Span®80) are widely used ionic and non-ionic surfactants, respectively.

By mixing energetically the organic phase into the aqueous phase, a macroemulsion or a nanoemulsion is formed, depending on the experimental conditions, which are thermodynamically unstable. This means that with time, the tiny organic droplets tend to reform the more stable separated phase through coalescence and flocculation to the air-water interface. On the one hand, macroemulsions (droplet size: 600 nm-1000 μ m), which are also kinetically unstable, quickly undergo phase separation. These usually appear as a turbid or opaque suspension due to light scattering produced by the droplets of size of the range of the visible light wavelength (**Figure 1.19a**). On the other hand the nanoemulsion (30-500 nm) characterize for requiring more energy to be formed ($\Delta G_2 > \Delta G_1$), though are kinetically stable ($\Delta G_2^* > \Delta G_1^*$) once formed. In this case the dispersion can be stable for a larger period of time (hours-months). Due to the reduced size of the nanodroplets, the nanoemulsions appear transparent or slightly turbid (**Figure 1.19b**).⁸⁷ The emulsification step determines the size of the final capsules. In both cases energy is needed to form the emulsion. The macroemulsions can be obtained through magnetic stirring or by using a homogenizer, whereas in the nanoemulsions more energy is required, which is obtained through high-pressure homogenizers or ultrasounds. Both types of emulsion have been performed during the thesis work to obtain microcapsules or polymeric nanoparticles (matrix-type capsules), respectively.

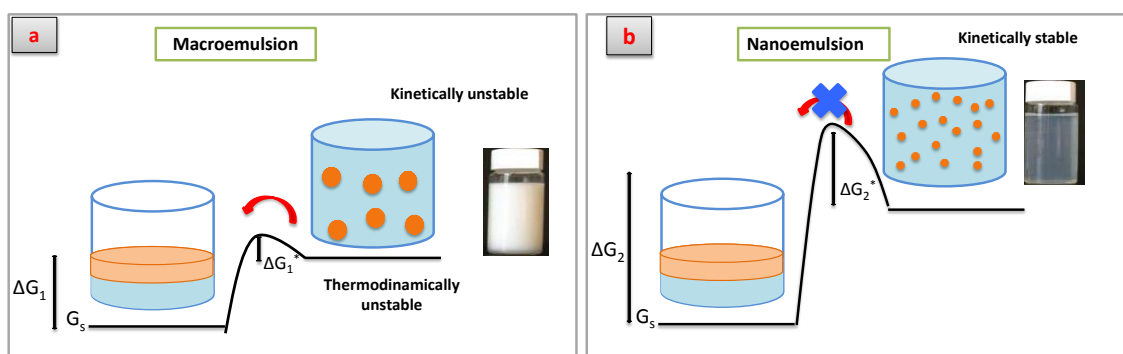


Figure 1.19: digital images and schematic representation of the energy diagram for a) a macroemulsion and b) a nanoemulsion.

ii) the formation of an impermeable **polymeric shell** around the oil droplets (**Figure 1.20**).

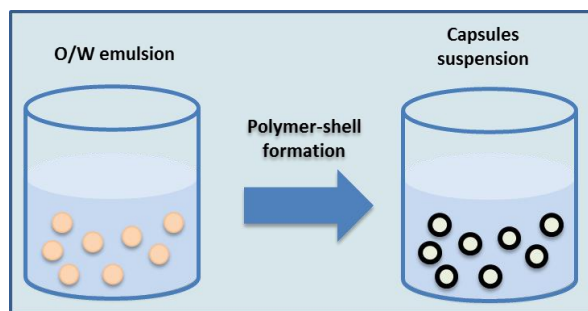


Figure 1.20: scheme of the polymer-shell formation around the emulsified droplets

Different strategies are used for the formation of the polymeric shell around the oil droplets. In this thesis the phase separation and the *in-situ* polymerization methods are described into more details as they have been used to achieve the functional capsules.

1.4.2 Phase separation

The phase separation method includes all strategies that involve the precipitation of a preformed polymer, previously dissolved in one of the two phases (organic phase or aqueous phase), as consequence of the forced reduction of the polymer solubility in the medium in which it had been dissolved.

- **Solvent evaporation**

This method starts from an organic (dispersed) phase and an aqueous (continuous) phase. To prepare the organic mixture, both the hydrophobic core material (e.g. an oil or PCM solution of the dye) and the preformed shell polymer are dissolved in an organic volatile, non-miscible with water solvent (e.g. chloroform or dichloromethane).⁸⁸ Generally the organic phase is emulsified in the aqueous phase, which is immiscible with both the core material and the shell polymer. Successively, the solvent is evaporated from the dispersed solution and, as a result, the polymer precipitates forming particles (matrix-type capsules) or deposits at the oil-in-water interface of the hydrophobic core droplets (templates) enclosing the material (core-shell capsules, **Figure 1.21**).⁸³To obtain core-shell capsules instead of matrix-type particles at the end of the process, the polymer and

the core material must not be miscible. On the other hand, good miscibility of the core material and the polymer favors the formation of matrix-type structures.

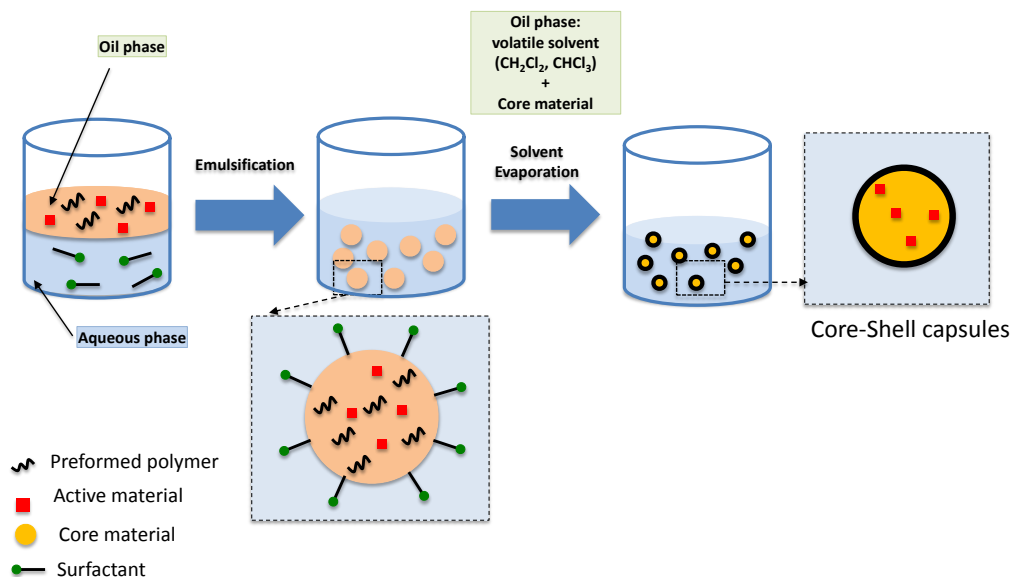


Figure 1.21: schematic representation of the solvent evaporation method.

- **Coacervation**

Coacervation is a term used in colloidal chemistry to denote the associative phase separation process of polymers induced by modification of the media environment (pH, ionic strength, temperature, solubility) under controlled conditions. In this case the polymeric material is dissolved in the water phase. In the coacervation, the polymer-rich phase is known as coacervate, while the phase containing very little amounts of colloidal polymer is known as the equilibrium phase. Based on the used polymers and the mechanism of phase separation, two types of coacervation can be distinguished: simple and complex coacervation. In the simple coacervation, a single polymer is involved and coacervates are formed due to a dehydration or “water deficit” mechanism caused by the addition of a salt or desolvation liquid. An example of simple coacervation is the phase separation of gelatin when sodium sulfate (Na_2SO_4) or ethanol is added into its solution. On the other hand, in complex coacervation the electrostatic interactions between two or more oppositely charged ionic polymers, usually proteins and polysaccharides, lead to the coacervate formation. Complex coacervation was also used for the preparation of capsules in this thesis.

If complex coacervation is used, the mixture to be encapsulated (e.g. an oil solution of a dye) is emulsified in the aqueous phase, which contains a water-soluble polyelectrolyte. Successively, a second aqueous solution of another water-soluble hydrophilic polymer is added to the dispersion at a certain (e.g. 40°C) temperature (**Figure 1.22**). Once added the second polymer, the pH of the water is varied to maximize the electrostatic interactions between the two polymers (whose charge is dependent on the solution pH). The polymers, thus, form the coacervates since the formed polymer complex becomes water-insoluble. The coacervates are made by insoluble polymeric materials that contain high amount of water and are formed when the isoelectric point of the two initially water-soluble polyelectrolytes, at a certain pH and temperature, is reached. The formed coacervates deposit on the surface of the droplets and after cooling they reticulate (gelation) forming a protective polymeric shell. Gelatin and gum Arabic are commonly used polymers in this method.⁸⁹ A schematic representation of the process followed is presented in **Figure 1.22**.

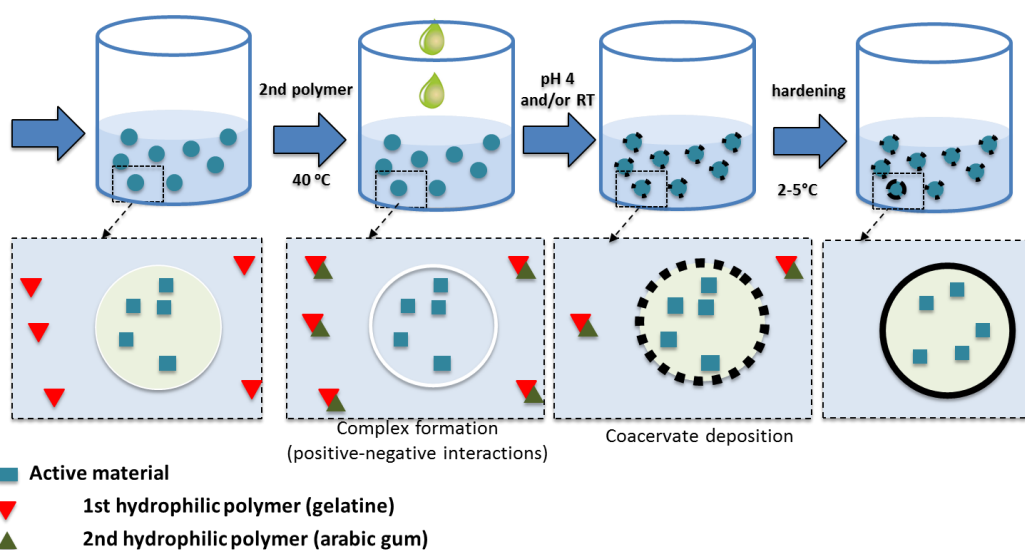


Figure 1.22: schematic representation of the complex coacervation method.

1.4.3 *In-situ* polymerization

Differently from the phase separation, this method consists in the *in-situ* polymerization of precursor polymer molecules, which initially are either in the water (e.g. melamine-formaldehyde)⁹⁰ or in the organic phase (e.g. styrene, Sty, methyl methacrylate, MMA). After the emulsification step upon polymerization, the formed oligomers or polymers reduce their solubility as their molecular weight

increases and precipitate forming matrix-type capsules or enclosing the encapsulated material (core-shell structure) depending on the miscibility between the core and the polymer.⁹¹

- **Melamine-formaldehyde**

The melamine-formaldehyde method consists of i) the formation of an O/W emulsion, usually performed with a surfactant with functional groups that attract the monomeric materials and make it polymerize in the interface between the organic droplets and the aqueous phase. The melamine-formaldehyde pre-polymer (hydrophilic monomer, PP), which can be either dissolved in the initial water phase or added after the preparation of the emulsion, polymerizes after a reduction of the pH of the media forming the melamine-formaldehyde polymer. The decrease of the pH can be accompanied with heat to induce a higher degree of polymerization. The MF pre-polymer polymerizes in the interface of the droplets forming a polymeric shell and enclosing the material of interest (**Figure 1.23**).

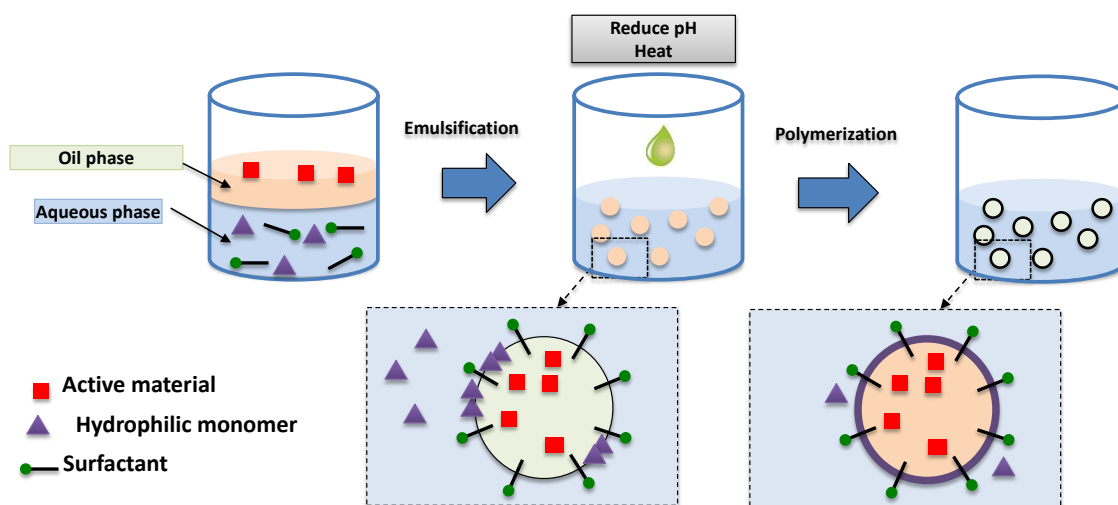


Figure 1.23: schematic representation of the *in-situ* polymerization of melamine-formaldehyde.

- **Radical polymerization**

The radical polymerization method consists of i) the preparation of an O/W emulsion in which the organic phase contains the core material, the monomer (e.g. Sty, MMA) and the radical initiator (e.g. azobisisobutyronitrile, AIBN), and ii) a subsequent polymerization of the monomer. The polymerization is carried out

under N_2 atmosphere to avoid oxygen scavenging of the radicals and at high temperature, at which the initiator decompose to radical species. The radical species initiate the polymerization of the monomer and the polymer/oligomer chains formed, which become insoluble, migrate to the interface forming the shell of the capsules or form matrix-type capsules depending on the miscibility between the core material and the formed polymer (**Figure 1.24**). A crosslinker agent can be added to the initial organic phase, which after polymerizing enhances the thermal and chemical stability of the polymeric shell of the capsules.

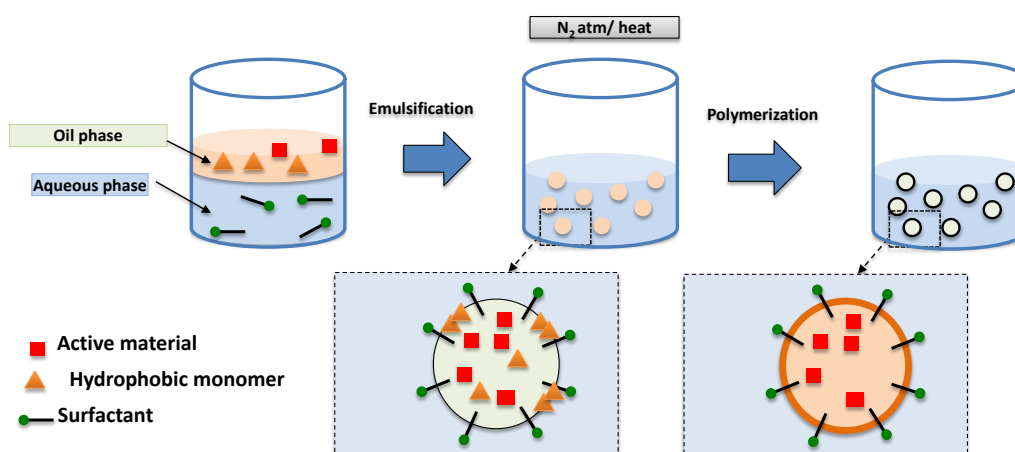


Figure 1.24: schematic representation of the *in-situ* polymerization via radical polymerization.

Many of the capsules-based chromogenic materials prepared along this thesis uses PCM to trigger their optical properties. Given the solid state of these PCMs at room temperature, these can be directly structured as solid lipid particles and used to encapsulate color changing dyes. In the next section the main types of PCM used in this work and the general procedure to form SLPs are summarized.

1.5 Phase change materials and solid lipid particles

PCMs are substances that are generally known for storing and releasing large amount of heat when undergoing a phase transition. Among the different type of PCMs (organic, inorganic, eutectic), the organic PCMs are the most studied due to their chemical and thermal stability and the potential use in energy building applications.⁹² Organic PCMs are divided in two subgroups: paraffin and non-paraffin.

Paraffin is composed of a straight long chain alkane mixture ($\text{CH}_3-(\text{CH}_2)_n-\text{CH}_3$), whereas non-paraffin PCMs are long-alkyl chain compounds with functional groups of different types in the structure (e.g. alcohols, esters or acids). In this thesis our interest was focused on the non-paraffin PCMs since their functional groups enhance the solubility of the chromogenic dyes. Importantly, the phase transition of these PCMs induces changes of the optical performances of these dyes due to specific interactions established with the functional groups of the PCM. Some examples of organic non-paraffin PCMs used along the thesis work are nonanoic acid, dodecanoic acid, 1-hexadecanol, 1-tetradecanol, glyceryl tristearate, trilaurin, etc.

The structuration of the PCMs can be obtained through the encapsulation methods explained before or in the form of solid lipid particles (SLPs), as most of these PCMs are solid at room temperature. For the preparation of SLPs in this thesis we selected a reaction and solvent-free method, known as emulsion-cooling method.⁹³ It consists of: i) an O/W emulsification of the PCM at temperature above the T_m of the PCM ($T_{m, \text{PCM}}$) and subsequently ii) cooling of the emulsion by adding cold water (2-5°C), during which the droplets of the emulsion precipitates in the form of particles (**Figure 1.25**). Depending on the energy employed during the emulsification process, solid lipid nanoparticles (SLNs) or solid lipid microparticles (SLMs) could be obtained

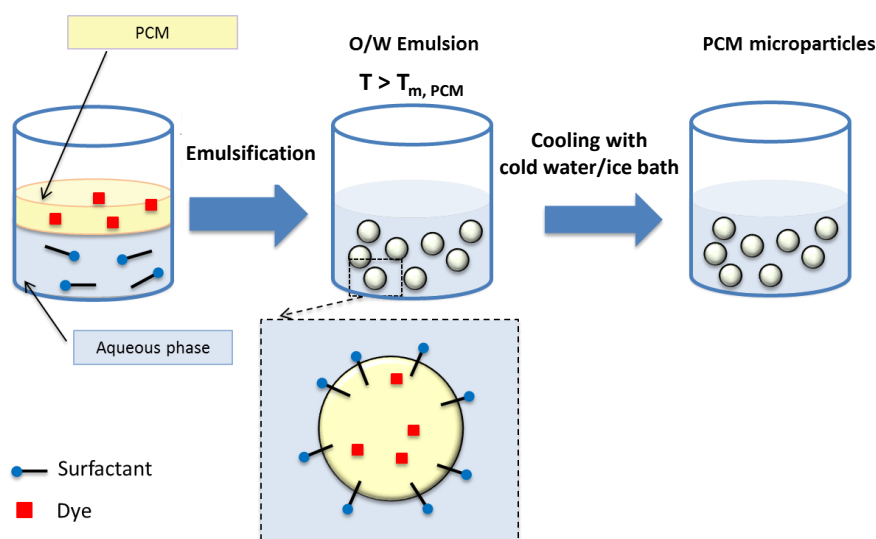


Figure 1.25: schematic representation of the emulsion-cooling method for the preparation of solid lipid particles.

1.6 Framework of the thesis

Overall, in the recent years, photochromic and thermochromic materials have been deeply studied in the academic community to develop smart materials with real applications. However, in most of the cases they have problems of reproducibility, tunability or inhibition of the optical properties. One of the possible solutions to overcome these limitations, as explained before, could be the encapsulation of bulk mixtures to transfer enhanced solution optical properties to solid materials. Indeed, there are some products in the market (mostly thermochromic) that work with this strategy (encapsulation). Nevertheless, these types of materials can be seen only in low-cost commercial products such as cups, T-shirts or common toys. For this reason, the field of smart solid materials is still in a very early stage of development and there is a plenty of room and potential to work in it.

In this thesis we aimed to enhance the properties of the typical photochromic and thermochromic materials by direct transfer of bulk solution chromogenic properties into the solid state. For this, a common trend in the entire thesis was followed:

- 1- The study and preparation of bulk mixtures with sophisticated chromogenic effects (**Figure 1.26**). The mixtures in all the cases are composed of organic dyes (photochromic, thermochromic, fluorescent), phase change materials and other additives. The latest, when needed, allows increasing the level of complexity of the system (e.g. multi-responsiveness).
- 2- The micro/nanostructuring of these mixtures into polymeric capsules (**Figure 1.26**).
- 3- The integration of the micro/nanostructures to functional devices (**Figure 1.26**).

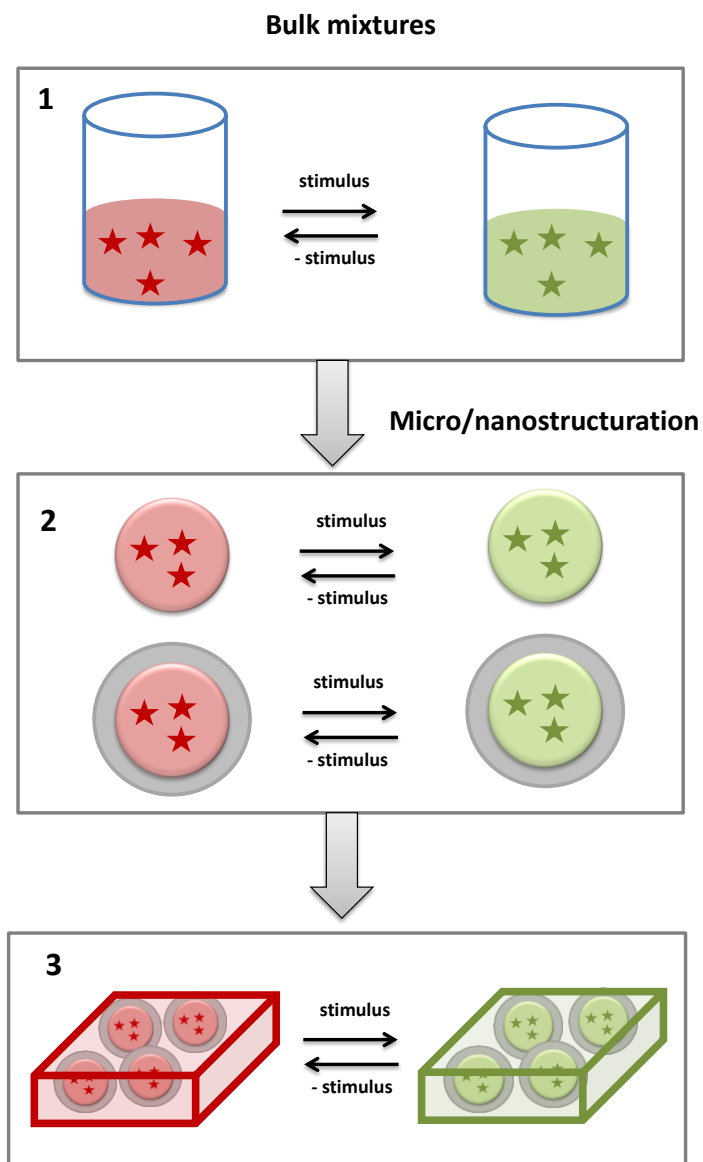


Figure 1.26: schematic representation of the: (1) preparation of chromogenic bulk solutions, which can respond to different stimuli giving different responses, (2) the micro/nanostructuring of the bulk mixtures and (3) the integration into devices (e.g. polymeric films).

1.7 References

1. C. M. Lampert, *Mater Today*. **2004**, 7, 28.
2. J. C. Crano, R. J. Guglielmetti, *Organic Photochromic and Thermochromic Compounds*; Plenum Press: New York and London, **1998**.
3. H. Bouas-Laurent, H. Dürr, *Pure Appl. Chem.* **2001**, 73, 639.
4. H. Dürr, H. Bouas-Laurent, *Photochromism: molecules and systems*, Elsevier, **2003**.
5. M. Irie, T. Fukaminato, K. Matsuda, S. Kobatake, *Chem. Rev.* **2014**, 114, 12174.
6. S. N. Corns, S. M. Partington, A. D. Towns, *Color. Technol.* **2009**, 125, 249.
7. R. Klajn, *Chem. Soc. Rev.* **2014**, 43, 148.
8. R. Pardo, M. Zayat, D. Levy, *Chem. Soc. Rev.* **2011**, 40, 672.
9. U. Pischel, *Angew. Chem., Int. Ed.* **2007**, 46, 4026.
10. P. L. Gentili, *Phys. Chem. Chem. Phys.* **2011**, 13, 20335.
11. P. L. Gentili, *Dyes Pigm.* **2014**, 110, 235.
12. S. Kawata, Y. Kawata *Chem. Rev.* **2000**, 100, 1777.
13. M. Sliwa, S. Létard, I. Malfant, M. Nierlich, P. G. Lacroix, T. Asahi, H. Masuhara, P. Yu, K. Nakatani, *Chem. Mater.* **2005**, 17, 4727.
14. E. Fischer, Y. Hirshberg, *J. Chem. Soc.* **1952**, 4522.
15. G. Berkovic, V. Krongauz, V. Weiss, *Chem. Rev.* **2000**, 100, 1741.
16. S. Swansburg, E. Buncel, R.P. Lemieux, *J. Am. Chem. Soc.* **2000**, 122, 6594.
17. Dinesh G. Patel, M. M. Paquette, R. A. Kopelman, W. Kaminsky, M. J. Ferguson, N. L. Frank, *J. Am. Chem. Soc.* **2010**, 132, 12568.
18. W. Tian, J. Tian, *Dyes Pigm.* **2014**, 105, 66.
19. J. B. Flannery, *J. Am. Chem. Soc.* **1968**, 90, 5660.
20. L. Shuiping, T. Lianjiang, H. Weili, L. Xiaoqiang, C. Yanmo, *Mater. Lett.* **2010**, 64, 2427.
21. R. Rosario, D. Gust, M. Hayes, F. Jahnke, J. Springer, A. A. Garcia, *Langmuir.* **2002**, 18, 8062.
22. I. Vlassioux, C.-D. Park, S. A. Vail, D. Gust, S. Smirnov, *Nano Lett.* **2006**, 65, 1013.

23. A. H. Gelebart, D. J. Mulder, G. Vantomme, A. P. H. J. Schenning, D. J. Broer, *Angew. Chem., Int. Ed.* **2017**, 56, 13436.
24. T. Ube, T. Ikeda, *Angew. Chem., Int. Ed.* **2014**, 53, 10290.
25. C. L. van Oosten, C. W. M. Bastiaansen, D. J. Broer, *Nat. Mater.* **2009**, 8, 677.
26. M. Kathan, P. Kovaríček, C. Jurissek, A. Senf, A. Dallmann, A. F. Thünemann, S. Hecht, *Angew. Chem., Int. Ed.* **2016**, 55, 13882.
27. A. Fuhrmann, R. Göstl, R. Wendt, J. Kötteritzsch, M. D. Hager, U. S. Schubert, K. Brademann-Jock, A. F. Thünemann, U. Nöchel, M. Behl, S. Hecht, *Nat. Commun.* **2016**, 7, 13623.
28. F. Terao, M. Morimoto, M. Irie, *Angew. Chem., Int. Ed.* **2012**, 51, 901.
29. D. Kitagawa, H. Nishi, S. Kobatake, *Angew. Chem., Int. Ed.* **2013**, 52, 9320.
30. H. Nie, J. L. Self, A. S. Kuenstler, R. C. Hayward, J. Read de Alaniz, *Adv. Opt. Mater.* **2019**, 7, 1900224.
31. M. Irie, T. Fukaminato, K. Matsuda, S. Kobatake, *Chem. Rev.* **2014**, 114, 12174.
32. J. Boelke, S. Hecht, *Adv. Opt. Mater.* **2019**, 1900404.
33. V. A. Barachevsky, *J. Photochem. Photobiol. A Chem.* **2018**, 354, 61.
34. G. Such, R. A. Evans, L. H. Yee, T. P. Davis, *J. Macromol. Sci., Polym. Rev.* **2003**, 43, 547.
35. V. Krongauz, Environmental Effects on Organic Photochromic Systems in *Photochromism: Molecules and Systems*, ed. H. Dürr and H. Bouas-Laurent, Elsevier Science Publishing House, Amsterdam, **1990**.
36. R. A. Evans, T. L. Hanley, M. A. Skidmore, T. P. Davis, G. K. Such, L. H. Yee, G. E. Ball, D. A. Lewis, *Nat. Mater.* **2005**, 4, 249.
37. W. Sriprom, M. Néel, C. D. Gabbutt, B. M. Heron, S. Perrier, *J. Mater. Chem.* **2007**, 17, 1885.
38. D. Samanta, D. Galaktionova, J. Gemen, L. J. W. Shimon, Y. Diskin-Posner, L. Avram, P. Král, R. Klajn, *Nat. Commun.* **2018**, 9, 2.
39. N. Vázquez-Mera, C. Roscini, J. Hernando, D. Ruiz-Molina, *Adv. Opt. Mater.* **2013**, 1, 631.
40. J. ter Schiphorst, S. Coleman, J. E. Stumpel, A. B. Azouz, D. Diamond, A. P. H. J. Schenning, *Chem. Mater.* **2015**, 27, 5925.
41. K. Klaue, Y. Garmshausen, S. Hecht, *Angew. Chem., Int. Ed.* **2018**, 57, 1414.
42. K. Sumaru, M. Kameda, T. Kanamori, T. Shinbo, *Macromolecules* **2004**, 37, 4949.

Chapter 1

43. A. Szilagy, K. Sumaru, S. Sugiura, T. Takagi, T. Shinbo, M. Zrinyi, T. Kanamori, *Chem. Mater.* **2007**, *19*, 2730.
44. F. Ciardelli, D. Fabbri, O. Pieroni, A. Fissi, *J. Am. Chem. Soc.* **1989**, *111*, 3470.
45. Y. Ito, N. Sugimura, O. H. Kwon, Y. Imanishi, *Nat. Biotechnol.* **1999**, *17*, 73.
46. T. Hirakura, Y. Nomura, Y. Aoyama, K. Akiyoshi, *Biomacromolecules* **2004**, *5*, 1804.
47. M. I. Khazi, W. Jeong, J.-M. Kim, *Adv. Mater.* **2018**, *30*, 1705310.
48. G. Petriashvili, M. P. De Santo, L. Devadze, T. Zurabishvili, N. Sepashvili, R. Gary, R. Barberi, *Macromol. Rapid Commun.* **2016**, *37*, 500.
49. T. Zhang, L. Sheng, J. Liu, L. Ju, J. Li, Z. Du, W. Zhang, M. Li, S. X.-A. Zhang, *Adv. Funct. Mater.* **2018**, *28*, 1705532.
50. M. Leclerc, *Adv. Mater.* **1999**, *11*, 1491.
51. D. J. Ahn, S. Lee, J. M. Kim, *Adv. Funct. Mater.* **2009**, *19*, 1483.
52. D. J. Ahn, E.-H. Chae, G. S. Lee, H.-Y. Shim, T.-E. Chang, K.-D. Ahn, J.-M. Kim *J. Am. Chem. Soc.* **2003**, *125*, 8976.
53. Z. Yuan, C.-W. Lee, S.-H. Lee, *Angew. Chem., Int. Ed.* **2004**, *43*, 4197.
54. Y. Gu, W. Cao, L. Zhu, D. Chen, M. Jiang, *Macromolecules* **2008**, *41*, 2299.
55. L. Yu, S. L. Hsu, *Macromolecules* **2011**, *45*, 420.
56. M. C. Chiappelli, R. C. Hayward, *Adv. Mater.* **2012**, *24*, 6100.
57. Z. Wang, J. Zhang, J. Xie, Z. Wang, Y. Yin, J. Li, Y. Li, S. Liang, L. Zhang, L. Cui, H. Zhang, B. Yang, *J. Mater. Chem.* **2012**, *22*, 7887.
58. Y. F. Yue, M. A. Haque, T. Kurokawa, T. Nakajima, J. P. Gong, *Adv. Mater.* **2013**, *25*, 3106.
59. Y. Hirokawa, T. Tanaka, *J. Chem. Phys.* **1984**, *81*, 6379.
60. I. Sage, *Liq. Cryst.* **2011**, *38*, 1551.
61. T. J. White, M. E. McConney, T. J. Bunning, *J. Mater. Chem.* **2010**, *20*, 9832.
62. H. S. Kitzerow, C. Bahr, *Chirality in Liquid Crystals*; Springer: New York, **2001**.
63. M. A. White, M. LeBlanc, *J. Chem. Educ.* **1999**, *76*, 1201.
64. K. Nassau, *The Physics and Chemistry of Colour*; Wiley: New York, **1983**.
65. P.-G. de Gennes, J. Prost, *The Physics of Liquid Crystals*, 2nd ed.; Clarendon: Oxford, **1993**.
66. D. Aitken, S. M. Burkinshaw, J. Griffiths, A. D. Towns, *Rev. Prog. Coloration* **1996**, *25*, 1.

67. R. M. Christie, D. Bryant, *Color. Technol.* **2005**, 121, 187.
68. S. M. Burkinshaw, J. Griffiths, A. D. Towns, *J. Mater. Chem.* **1998**, 8, 2677.
69. J. T. C. Wojtyk, A. Wasey, N.-N. Xiao, P. M. Kazmaier, S. Hoz, C. Yu, R. P. Lemieux, E. Buncel *J. Phys. Chem. A* **2007**, 111, 2511.
70. Y. Shibahashi, N. Nakasuji, T. Kataoka, H. Inagaki, T. Kito, FR2494707A1, **1981**.
71. M. K. Björnsdotter, J. de Boer, A. Ballesteros-Gomez, *Chemosphere* **2017**, 182, 691.
72. D. C. Maclaren, M. A. White, *J. Mater. Sci.* **2005**, 40, 669.
73. M. M. Farida, A. M. Khudhaira, S. A. K. Razack, S. Al-Hallaj, *Energ Convers Manage.* **2004**, 45, 1597.
74. M. B. Hoyt, D.R. Kent, C. F. Helms, O. M. Ilg, US5888651A, **1997**
75. K. Tsutsui, T. Yamaguchi, K. Sato, *Jpn. J. Appl. Phys.* **1994**, 33, 5925.
76. A. Seeboth, D. Löttsch, R. Ruhmann, O. Muehling, *Chem. Rev.* **2014**, 114, 3037.
77. R. Dubey, T. C. Shami, K. U. B. Rao, *Def. Sci. J.* **2009**, 59, 82.
78. N. V. N. Jyothi, P. M. Prasanna, S. N. Sakarkar, K. S. Prabha, P. S. Ramaiah, G. Y. Srawanet, *J. Microencapsul.* **2010**, 27, 187.
79. K. P. S. Kumar, S. Tejbe, A. S. S. Banu, P. N. Lakshmi, D. Bhowmik, *Indian J. Res. Pharm. Biotechnol.* 2013, 1, 324.
80. S. B. Yoon, K. Sohn, J. Y. Kim, C.-H. Shin, J.-S. Yu, T. Hyeo, *Adv. Mater.* **2002**, 14, 19.
81. D. V. Volodkin, A. I. Petrov, M. Prevot, G. B. Sukhorukov, *Langmuir* **2004**, 20, 3398.
82. J.-W. Kim, J.-Y. Ko, J.-B. Jun, I.-S. Chang, H.-H. Kang, K.-D. Suh, *Colloid Polym Sci* **2003**, 281, 157.
83. A. Reisch, A. S. Klymchenko, *Small*, **2016**, 12, 1968.
84. R. Ciriminna, M. Sciortino, G. Alonzo, A. De Schrijver, M. Pagliaro, *Chem. Rev.* **2011**, 111, 765.
85. D. Lensen, D. M. Vriezema, J. C. M. van Hest, *Macromol. Biosci.* **2008**, 8, 991.
86. J. Rao, D. J. McClements, *J. Agric. Food Chem.* **2011**, 59, 5026.
87. P. Shah, D. Bhalodia, P. Shelat, *Sys. Rev. Pharm.* **2010**, 1, 24.
88. Y. Zhao, J. Fickert, K. Landfester, D. Crespy, *Small* **2012**, 8, 2954.
89. C. G. de Kruif, F. Weinbreck, R. de Vries, *Curr. Opin. Colloid Interface Sci* **2004**, 9, 340.

90. D. Yin, L. Ma, W. Geng, B. Zhang, Q. Zhang, *Int. J. Energy Res.* **2015**, 39, 661.
91. K. Landfester, *Angew. Chem. Int. Ed.* **2009**, 48, 4488.
92. B. Zalba, J. M. Marin, L. F. Cabeza, H. Mehling, *Applied Thermal Engineering*, **2003**, 23, 251.
93. S. A. Wissing, O. Kayser, R. H. Müller, *Adv. Drug Deliv. Rev.* **2004**, 56, 1257.

CHAPTER 2

Objectives

2.1 General objectives

The global aim of the current thesis was to develop solid materials with advanced and highly tuneable chromogenic/emissive performances. The strategy is based on i) the assembling of chromogenic/emissive dyes in interacting media/molecules; ii) the micro/nanostructuring of these solutions in the form of polymeric capsules and, iii) the integration of these onto substrates or films preserving the bulk solution properties. To demonstrate the feasibility of this approach, we aimed to develop three types of smart materials with enhanced chromogenic/emission properties.

- i) **Tuneable and switchable reverse photochromism** in solid materials, where i) the tuning of the initial colour and kinetic response of the dye performing the reverse photochromism is easily achieved by modifying the core material of the capsules and ii) the reversible switch between direct and reverse photochromism is activated by simple melting/solidification of the capsules core material. This could open the possibility to use these materials in anti-counterfeiting technologies, rewritable devices, and optical data storage. The studies performed on this topic are described in **Chapter 3**.
- ii) **Multi-responsive** (pH and temperature) chromogenic materials based on cyanine dyes, which would be potentially used for sensing or as multi-stimuli responsive materials for optical data storage devices. The encapsulation strategy not only preserves the bulk thermochromic-like behaviour in the solid state, but also presents a simple way of tuning the thermochromic properties (colors and transition temperature) on demand. The results obtained in this part of the thesis are shown in **Chapter 4**.
- iii) High **temperature-responsive off/on irreversible fluorescent materials**, where the switching temperature could be easily tuned by modifying the polymer matrix of the capsules. These particles were used

Chapter 2

for multi-threshold high temperature (100-200°C) fluorescent sensors.
This part is described in **Chapter 5**.

CHAPTER 3

3. Tunable and switchable reverse photochromism in solid materials

In this chapter a novel, straightforward, and universal strategy to achieve solid materials with highly tunable and switchable reverse photochromism is reported.

- *The **tunability** was accomplished by means of commercially available spiropyran dyes, which can produce different types of stable merocyanine states (i.e., non-protonated and protonated forms) displaying distinct reverse photochromic properties (i.e., colors and coloration rates). To finely control the concentration ratio of these species and, as such, tailor the optical performance of the photochromes, we exploited their differential interaction with surrounding media of distinctive nature (i.e. non-volatile protic and aprotic polar solvents).*
- *A more complex system (**switching** between direct and reverse photochromism) was attained by using acidic phase change materials solid at room temperature. Upon changing the phase (solid or liquid) of the medium, one of the two photochromic states of the system is selectively stabilized on demand, allowing for reversible interconversion between direct and reverse photochromism when thermally scanning through the melting temperature of the phase change material.*

To transfer this behavior to the solid state, core-shell capsules of these mixtures were prepared and used as ink materials for the fabrication of flexible polymeric photochromic films.

The results shown in this chapter have been published in: i) A. Julià-López, D. Ruiz-Molina, J. Hernando, C. Roscini, *ACS Appl. Mater. Interfaces* **2019**, 11, 11884; ii) A. Julià-López, D. Ruiz-Molina, J. Hernando, J. Sedó, P. González-Monje, C. Roscini, *Angew. Chem. Int. Ed.* **2016**, 55, 15044.

3.1 Introduction

3.1.1 Tunable reverse photochromism

During the last decades, both the industrial and the academic sectors have shown growing interest toward organic photochromes for the preparation of color-tunable functional materials.¹⁻³ Aiming to address specific applications, an increasing number of strategies are being developed to finely tailor the photochromic performance of these systems (e.g., switching colors, rates, and wavelengths). This is the case of T-type photochromes, whose capacity to undergo UV-induced coloration and subsequent spontaneous color bleaching in the dark (i.e., direct photochromism) is currently employed for the fabrication of photoprotective coatings on the industrial scale (e.g., in ophthalmic lenses and smart windows).³ However, a wealth of research is devoted to additionally accomplish reverse photochromism with these compounds (i.e., photoinduced color fading followed by thermal coloration after irradiation),^{4,5} which would not only allow operation with less energetic and harmless visible light but also grant access to novel applications, such as anti-counterfeiting technologies, rewritable displays, and optical data storage systems.⁶⁻¹⁰ In spite of this, functional solid devices based on reverse T-type photochromes are very scarce and only started to be reported recently (e.g., in multicolored light-responsive rewritable devices).¹¹⁻¹⁷

3.1.1.1 From liquid solution to the solid state

In the very last few years new families of dyes have been prepared to directly exhibit reverse photochromism. J. Abe *et al.* developed new bisimidazole-based compounds (**Figure 3.1a**),¹⁸⁻¹⁹ which exhibited very fast negative photochromism. These are colored in solution in the dark due to the high conjugation of the molecules, which is lost after irradiation with visible light *via* the formation of short-lived biradical specie. In the dark, the colorless form turns rapidly to the initial colored state. Another example of molecules exhibiting reverse photochromism was reported by J. R. de Aleniz *et al.* who synthesized a new class of organic compounds termed donor-acceptor Stenhouse adducts.²⁰ Upon irradiation with visible light the molecules interconvert from the triene derivative

to the metastable cyclopentenone form, which reverts thermally to the initial state when irradiation is stopped (**Figure 3.1b**).

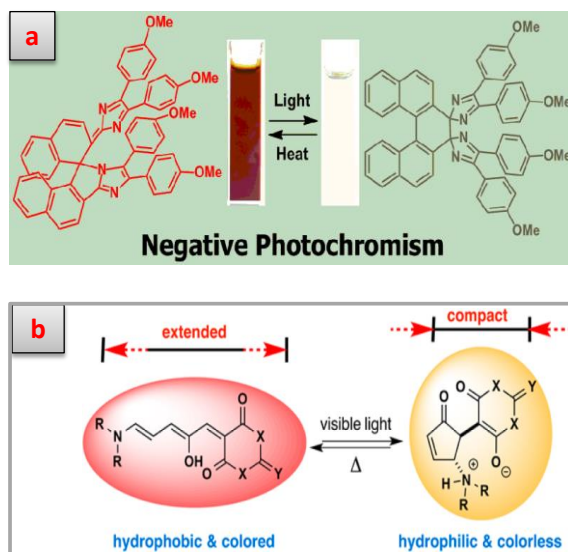


Figure 3.1: a) scheme of the bisimidazole derivative synthesized by J. Abe *et al.*, which shows the photoinduced chemical change and the consequent loss of color. Data adapted from ref. 18; b) scheme of the light induced reversible cyclisation of the donor-acceptor Stenhouse adducts before (more conjugated) and after (less conjugated) irradiating with visible light. Data adapted from ref. 20.

However, due to the specificity of these systems and the fact that they are not commercially available, much attention have been dedicated to achieve reverse photochromism by means of well-known, commercially available, and largely used T-type photochromes such as spirooxazines and spiropyrans.^{4,5} Normally, these compounds show direct photochromism because their thermodynamically stable form is the closed colorless spiro state, which isomerizes to the colored unstable merocyanine (MC) when irradiated.^{1,3} However, the MC form can be stabilized to such an extent that can be obtained as stable form in the dark. When this happens, these molecules could be used to achieve reverse photochromism, as upon visible irradiation the colorless spiro form is temporally induced. Several methodologies have been proposed to alter the relative stability of these isomers in solution:

i) the simplest approach is the dissolution of the dyes in highly **polar solvents** (such as methanol or ethanol, **Figure 3.2a**)^{21,22} or in **ionic liquids**^{23,24} where the equilibrium is more shifted towards the MC. Interestingly, due to the high sensitivity of the media of the MC isomer (solvatochromism) the color of the

solution in the dark can also be easily tuned, slightly varying the polarity of the solvent (**Figure 3.2a**).

ii) **chemical modification** of the dyes^{25–29} resulting in the opening of the SP form *via* a) the addition of more than one electro withdrawing group (e.g., NO₂) in the *ortho* and *meta* position of the phenolate moiety, b) a carboxylate (*ortho*) that participates in intramolecular hydrogen bond formation,²⁶ c) groups (i.e. crown ether) that favor the complexation between the phenolate and metals, d) or attaching functional groups that self-protonate the spiropyran stabilizing it in the protonated MCH⁺ form (**Figure 3.2b**).^{30–38}

iii) dispersion of the dyes in **acid media**, which stabilizes the protonated form MCH⁺ through acid–base reaction and also preserves reverse photochromism when irradiated with visible light.^{39–43} F. M. Raymo *et al.* reported how spiropyran can be stabilized to the MCH⁺ form, upon addition of CF₃COOH.⁴² The MCH⁺ presents visible light absorption at higher energy than the non-protonated MC (**Figure 3.2c**).

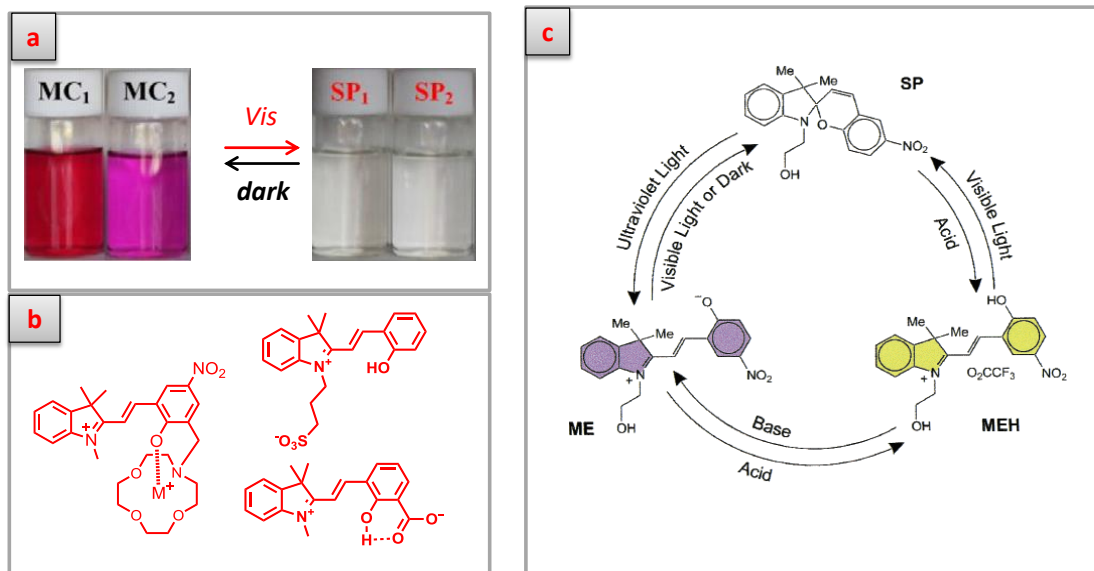


Figure 3.2: a) digital images of a nitrospiropyran derivative dissolved in methanol and ethanol solutions before and after irradiating with visible light. Data adapted from ref. 21; b) structure of spiropyran dyes in the stabilized MC forms bupon chemical substitution. Data adapted from ref. 25–30; c) scheme of the three states (SP, MC, MCH⁺) of a nitrospiropyran dye in presence of different stimuli (light, acid, base). Data adapted from ref. 42.

Overall, these strategies mentioned above allow obtaining and tuning reverse photochromism (color, recoloration rates) with spirocompounds in liquid media by using/adding protic solvents,^{21, 22} ionic liquids,^{23,24} metal ions²⁸⁻³⁶ or acids.^{42,43} However, these behavior in solution could not be transferred to the solid state, which is more relevant for practical applications. Therefore, a general strategy to obtain reverse photochromism in the solid state still needs to be developed.

A few examples of solid materials attaining reverse photochromism have been reported. Most of them are based on polar silica matrices, which stabilize the open MC via hydrogen bonding interactions between the high number of free-hydroxyl groups within the pores of the matrices and the dyes (**Figure 3.3a**).⁴⁴⁻⁴⁸ Makoto Ogawa *et al.* showed an example by adsorbing MC isomer onto dendritic fibrous nanosilica, which displayed reverse photochromism when irradiated with visible light (**Figure 3.3a**).⁴⁴ Other more specific examples exhibiting reverse photochromism are obtained by stabilizing the MC form in the mesoporous structure of an indium trimesate metal-organic framework (MOF)⁴⁹ (**Figure 3.3b**) or by the adsorption of SP molecules onto gold (Au) surface which converts the initial highly ordered SP islands into MC dimer chains (**Figure 3.3c**).⁵⁰ In the MOF cages and on the metal surface, the planar MC structures turn out to be the most stable. Y. Zhang *et al.* reported peptide MC conjugates that self-assemble into hydrogels.^{51,52} Hydrogels showed responses towards visible light and heat, and their sol-gel phase transition could be manipulated by the reverse photochromism of the corresponding spiropyran moiety (**Figure 3.3d**).

Tunable and switchable reverse photochromism in solid materials

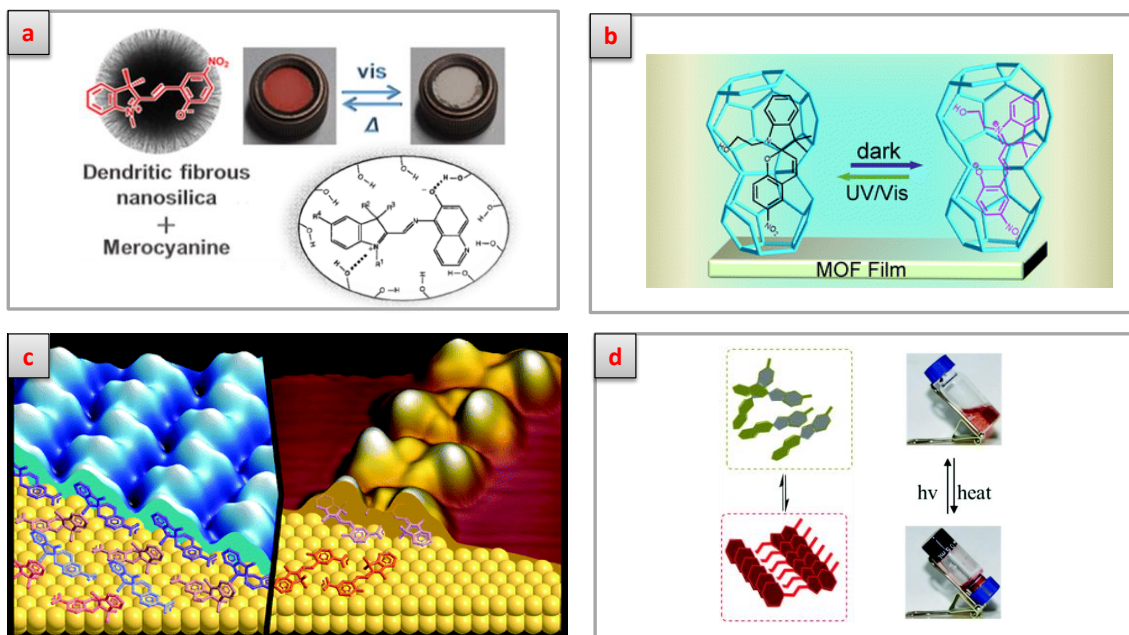


Figure 3.3: a) scheme and digital images of a nitrospiropyran derivative adsorbed onto dendritic fibrous nanosilica before and after irradiation. Data adapted from ref. 44; b) scheme of an indium trimesate MOF encapsulating a nitrospiropyran derivative in its mesoporous structure. Data adapted from ref. 49; c) scheme of SP molecules adsorbed onto Au surface before and after heating at 300 K and shows the conversion between ordered SP islands into MC dimer chains. Data adapted from ref. 50; d) digital images of the sol-gel transition of hydrogel of MC-peptide conjugates induced by reverse photochromism. Data adapted from ref. 51.

Though the examples described above provide reverse photochromism in the solid state, the adopted strategies do not allow flexible tunability of their photochromic responses (i.e., color in the dark and isomerization kinetics) because their properties are very dependent on the particular dyes and/or host matrices selected and, in some cases, even specific chemical modification of these species is needed. Therefore, the development of a simple approach to design and achieve **tunable reverse photochromism** in solid materials from readily available commercial dyes without requiring chemical derivatization would be highly desirable, thus paving the way for the broad use of this phenomenon in real applications.

3.1.2 Switchable photochromism (direct vs reverse)

Even more interestingly, if the reverse photochromic behavior of a material can be reversibly switched to direct photochromism on demand, the new material has input/output complexity level that its use could be extended to logic gates, information recording/processing, new anti-counterfeiting technologies and rewritable devices.⁶⁻¹⁷ Again, to date, most of the reported examples showing switchable photochromism were developed as proof-of-concept liquid solutions where chemicals had to be sequentially added to alter the relative stability of the SP and MC isomers: acids^{53,54} or metal ions³⁰⁻³⁸ to stabilize the colored form as MCH⁺ or metal–MC complexes and bases to compete with coordinating ligands, or complexing metals, to re-establish the non-colored SP isomer. In these examples, when the stabilized form is the SP, the solution displays direct photochromism, whereas when the stabilized isomer is the MC or MCH⁺, as seen above, reverse photochromism is obtained.

An alternative approach to selectively stabilize one of the isomeric forms of color-changing dyes (e.g., spirolactones^{55,56} and spirooxazines)⁵⁷ without the addition of external components is based on using acidic and/or hydrogen bonding phase change materials (PCMs), solid at RT. In the solid state, no interactions with the dye are produced because of the phase separation of the dye from the PCM (due to low solubility), whereas upon melting, these materials form the colored MC-like species in the dark through hydrogen-bonding interactions, dipole–dipole forces, or acid–base reactions. This strategy had been previously reported to obtain thermochromic materials based on spiropyran, spirolactones (as discussed in the introduction) and on spirooxazines.⁵⁷ In **Figure 3.4** it is showed an example of the color change produced in a 1-docosylphosphonic acid (DPO)/spirooxazine (SPO) film sandwiched between two glasses before and after heating above T_m^{DPO} (110 °C). In the molten state, DPO molecules protonate the dye inducing the formation of the red colored MCH⁺ form of the SP, which remained upon rapid cooling of the material. Thus, only after re-heating at 80 °C, below the T_m^{DPO} , the DPO molecules were able to reorganize to form a crystalline state, and induce dye molecules segregation and therefore the discoloration and recovery of the initial SP form. Although these PCM-based systems may undergo reversible temperature-controlled color changes (i.e., thermochromism, **Figure 3.4**) and, in some cases,

display direct photochromism,⁵⁷ they have not been used for switchable photochromism yet, possibly owing to the lack of photochromic activity of one, or both, dye isomers when dispersed in these materials. Another problem of these types of materials is that suffer from leaking when heating above the T_m . For this reason the development of a solid material with the capability of **switching** the type of **photochromism** is still a challenge.

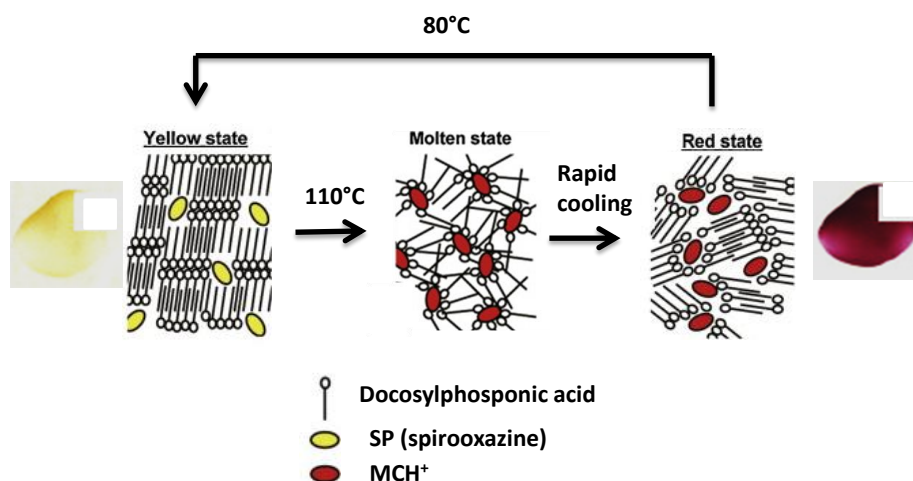


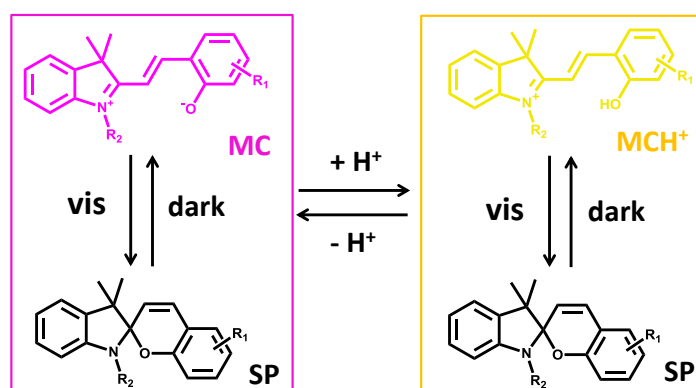
Figure 3.4: schematic representation of the mechanism for the coloration/discoloration of a spirooxazine derivative in 1-docosylphosphonic acid based films. Data adapted from ref. 57.

3.1.3 Designing tunable and switchable reverse photochromic materials

To achieve **tunable** and **switchable** reverse photochromism in the solid state, in this work, we propose a novel methodology that relies on:

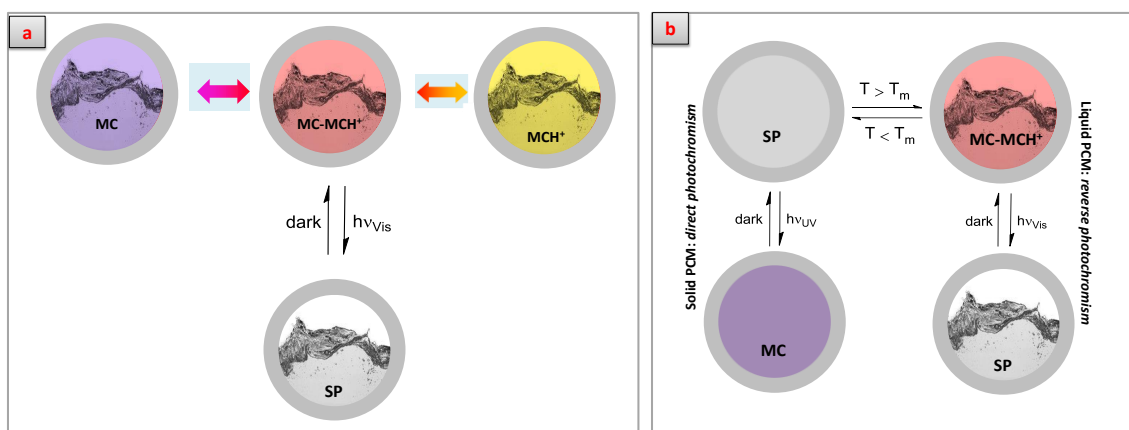
i) the embedment of readily accessible spiropyran dyes in rationally designed non-volatile media (with hydrogen bonding and/or acidic properties) to fine control the equilibrium between the differently colored merocyanine (protonated and non-protonated) forms and their relative concentration ratio (**tunability**, **Figure 3.1**). On the other hand we proposed the dispersion of the dyes in acidic solid PCMs, such that the relative stability of their SP and MC forms can be controlled by melting/solidifying the surrounding medium, enabling direct or reverse

photochromism (and thermochromism) depending on the applied temperature and without the need for chemical additives (**switching**).



Scheme 3.1: proposed scheme of the modulation of the colored merocyanine forms (non-protonated MC vs protonated MCH⁺ forms)

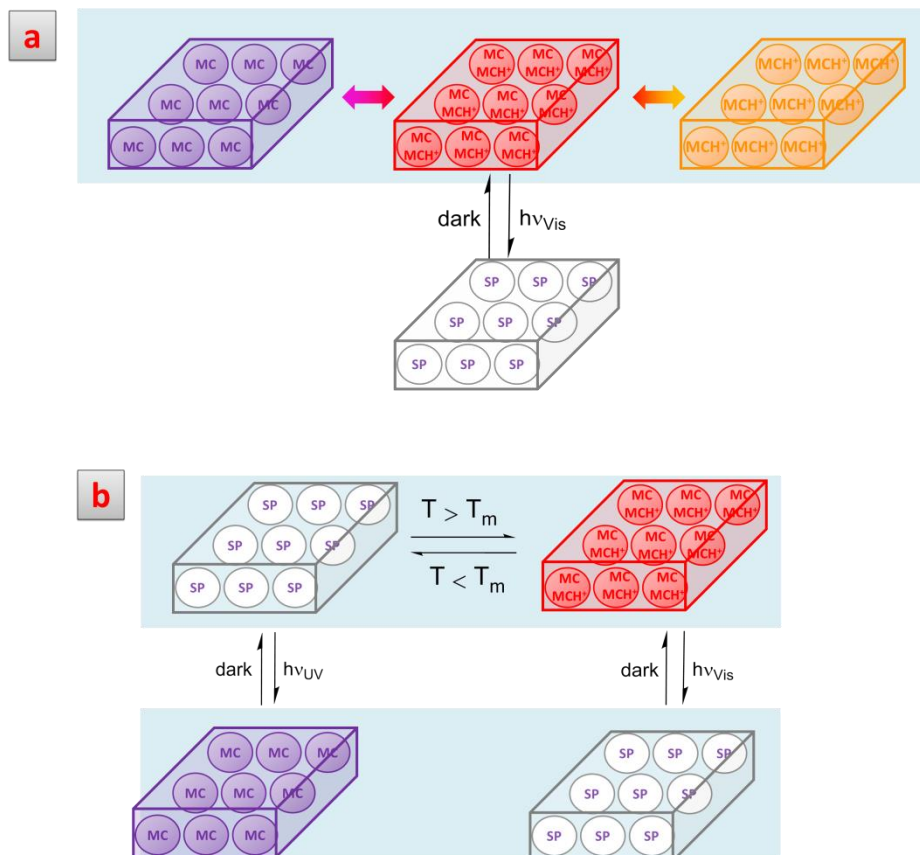
ii) the encapsulation of these dye-containing mixtures in core-shell polymer capsules to preserve in the solid state the **tunability** of reverse photochromism (**Scheme 3.2a**) and the **switching** between direct and reverse photochromism upon modification of the core material (**Scheme 3.2b**).



Scheme 3.2: a) encapsulation of the designed dye mixtures displaying different colors depending on the nature of the solvent encapsulated, and in all the cases maintaining the reverse photochromic properties; b) proposed scheme of capsules filled with acidic PCMs displaying direct and reverse photochromism triggered by temperature.

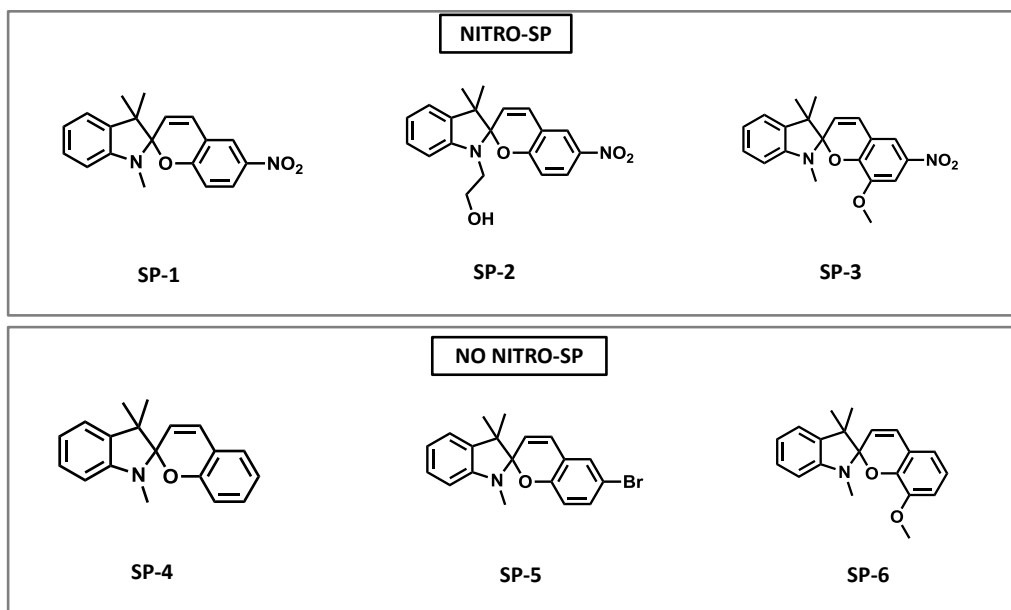
iii) the integration of these capsules in polymeric matrices to achieve solid materials with high and straightforward tunability of the reverse photochromic

performances (**Scheme 3.3a**) and interconversion between direct and reverse photochromism triggered by temperature (switching, **Scheme 3.3b**).



Scheme 3.3: schematic representation of the core-shell capsules integrated in solid films displaying a) tunable and b) switchable reverse photochromism.

For this study we selected six commercially available spiropyrans, holding different chemical and electronic properties: 1',3',3'-trimethyl-6-nitrospiro [1 (2H)-benzopyran-2,2'-indoline] (**SP-1**), 1'-(2-hydroxyethyl)-3',3'-dimethyl-6-nitrospiro [1 (2H)-benzopyran-2,2'-indoline] (**SP-2**), 1',3'-dihydro-8-methoxy-1',3',3'-trimethyl-6-nitrospiro [2H-1-benzopyran-2,2-(2H)-indole] (**SP-3**), 1',3',3'-trimethylspiro [1 (2H)-benzopyran-2,2'-indoline] (**SP-4**), 6-bromo-1',3',3'-trimethylspiro [1 (2H)-benzopyran-2,2'-indoline] (**SP-5**) and 8-methoxy-1',3',3'-trimethylspiro [1 (2H)-benzopyran-2,2'-indoline] (**SP-6**) that differ for the substituents in the chromene moiety, which causes significant differences on the basicity of the phenolate of the corresponding MC isomers. We divided the photochromes in two families: the nitro-substituted and no nitro-substituted (**Scheme 3.4**) in the 6 position of the chromene moiety.



Scheme 3.4: chemical structure of spiropyran dyes used along this work divided in two subgroups: nitro and no-nitro substituted spiropyrans in the 6 position of the chromene moiety.

3.2 Objectives

The purpose of the work described along this chapter is to achieve reverse photochromic behavior in the solid state, using a strategy that allows high tunability and switching of the photochromic performances. To achieve this main aim, specific objectives needed to be accomplished:

In particular, to obtain **tunable reverse photochromism**, it was aimed to:

- (i) identify and test non-volatile and hydrophobic media of different acidity that would be able to dissolve commercially available spiropyran dyes, stabilizing them in the protonated or non-protonated form and preserve the reverse photochromism.
- (ii) verify that the obtained solutions were also suitable for their encapsulation in core-shell capsules and that the obtained capsules retained the bulk photochromic behavior.

On the other hand, to obtain **switchable photochromism** (direct vs reverse), it was aimed to:

- (iii) identify and encapsulate different SP/acidic solid PCM mixtures into polymeric core-shell capsules and corroborate that distinct behavior were obtained at two different temperatures (below and above the T_m^{PCM}).

Finally, in all the cases,

- (iv) obtain that the optical performances of the initial mixtures is preserved in the final composite materials prepared by embedding the capsules into flexible polymeric films.

3.3 Results and discussion

3.3.1 Tuning reverse photochromism

3.3.1.1 Tuning reverse photochromism by changing the dye

The SP dyes (**Scheme 3.4**) were studied in media that were selected for: i) stabilizing the SP in the MC form and ii) being not miscible with water and non-volatile to allow the formation of stable capsules. In the literature it has been reported that polar solvents (e.g. methanol/ethanol)²¹ or acid media (e.g. trifluoroacetic acid)⁴² can stabilize respectively the MC or MCH⁺ form of spiropyrans. However, these solvents are volatile and miscible with water, what makes them very difficult to form stable capsules. As an alternative, the first investigated medium was nonanoic acid (NA), a weakly acidic oil (non-volatile medium), little miscible with water, which could stabilize the MC form through proton transfer (weak acid) and/or hydrogen-bonding interactions.

When the SP dyes (**SP-1-6**) were dissolved in NA (14-18 mM) different colors were developed in the dark that indicated the stabilization of the MC and/or MCH⁺ forms. As expected, the most basic spiropyrans, without any substituent in the 6-position of the chromene moiety (**SP-4** and **SP-6**), showed the formation of the yellow MCH⁺ ($\lambda_{\max}^{\text{SP-4}} = 430 \text{ nm}$, $\lambda_{\max}^{\text{SP-6}} = 400 \text{ nm}$, **Figure 3.5a-b**, **Table 3.1**). On the other hand, for the 6-nitrosubstituted SP, reddish (**SP-1, 2**, $\lambda_{\max}^{\text{SP-1}} = 528 \text{ nm}$, $\lambda_{\max}^{\text{SP-2}} = 530 \text{ nm}$) and violet (**SP-3**, $\lambda_{\max}^{\text{SP-3}} = 564 \text{ nm}$) colors were observed due to the higher contribution of the MC form (**Figure 3.5a-b**, **Table 3.1**). However the high absorption at around 430 nm for SP-1, 2 solutions indicates the MCH⁺ form is also present in NA.

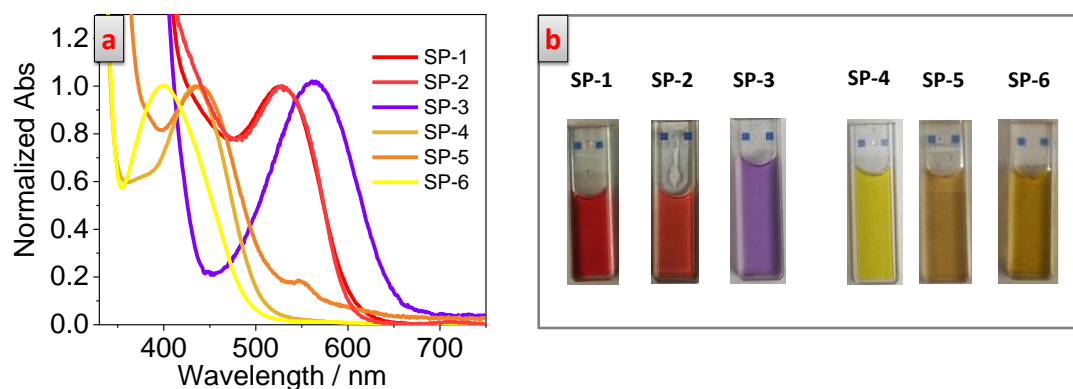


Figure 3.5: a) normalized absorption spectra and b) digital images of SP-1-6 in NA.

Worth to mention is how the presence of the methoxy group in **SP-3** induced a significant reduction of the absorption in the region around 430 nm, indicating a more selective formation of the non-protonated MC form, possibly due to the less basic character of the *ortho*-methoxy phenolate. Finally, **SP-5** (6-bromosubstituted spiropyran), which presents less basic character than **SP-4, 6**, but higher than **SP-1, 2, 3** in NA, leads to a yellow color solution from the predominant MCH⁺ (**SP-5**, $\lambda_{\max}^{\text{SP-5}} = 437$ nm, **Figure 3.5a-b, Table 3.1**) and residual contribution of the MC form (**SP-5**, $\lambda_{\max}^{\text{SP-5}} = 550$ nm).

Notably, irradiation with visible light (laser pointer at 532 nm and 470 mW/cm², white light-emitting torch with $\lambda_{\text{exc}} > 400$ nm and 20 mW/cm²) provoked color fading of all the NA solutions of **SP-1–SP-6**, a process that was reverted in the dark according to different first-order kinetics characteristic of photochrome back-isomerization in homogeneous liquid solutions ($k^{\text{SP-1/NA}} = 0.013$ min⁻¹, $k^{\text{SP-2/NA}} = 0.009$ min⁻¹, $k^{\text{SP-3/NA}} = 0.70$ min⁻¹, $k^{\text{SP-4/NA}} = 0.52$ min⁻¹, $k^{\text{SP-5/NA}} = 0.51$ min⁻¹, and $k^{\text{SP-6/NA}} = 6.1$ min⁻¹; **Table 3.1, Figure 3.6a-h**). This, together with the different colors obtained for each of these solutions, demonstrated that tunable T-type reverse photochromism can be attained by simply dissolving commercial SP dyes in NA, without requiring further chemical derivatization or the use of additives.

Solvent	NA					
	SP-1	SP-2	SP-3	SP-4	SP-5	SP-6
λ_{\max} (nm)	528	530	564	430	400	437
k (min ⁻¹)	0.013	0.009	0.70	0.52	0.51	6.1

Table 3.1: absorption maximum wavelengths (λ_{\max} in nm) and rate constants (k in min⁻¹) of the thermal recoloration process in the dark of **SP-1-6** in NA.

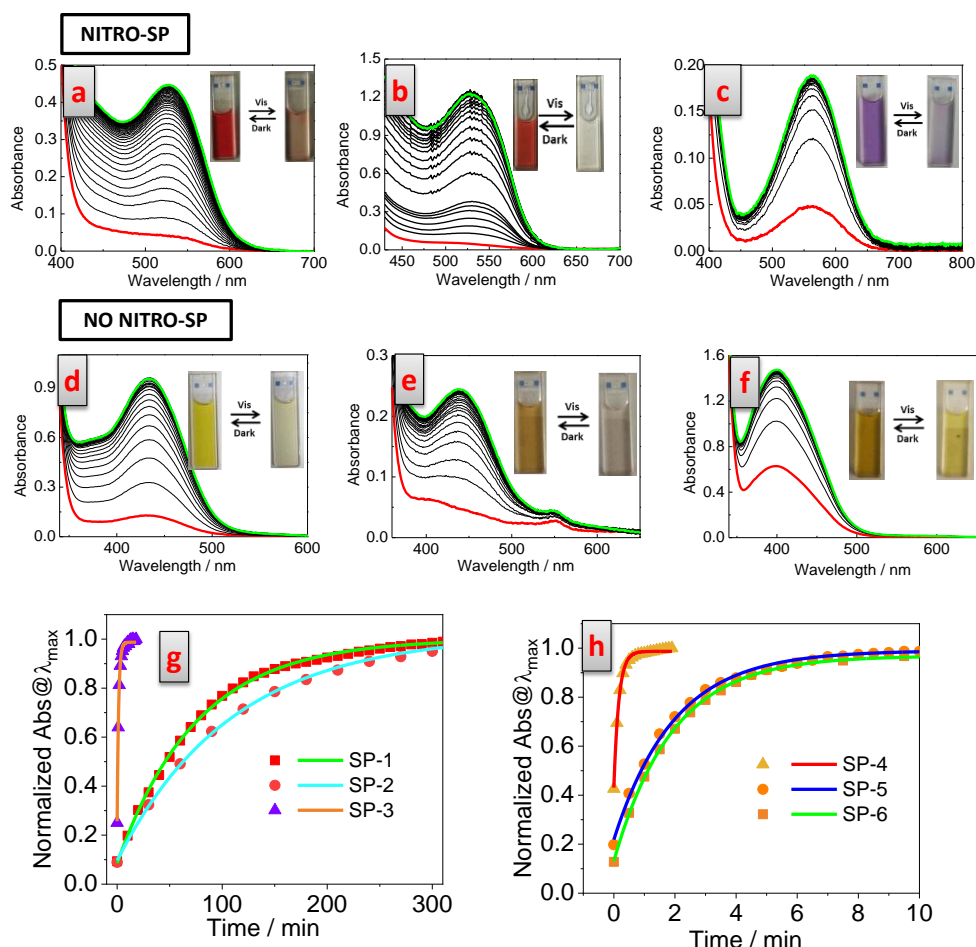


Figure 3.6: absorption spectra of a) **SP-1**, b) **SP-2** and c) **SP-3** d) **SP-4**, e) **SP-5** and f) **SP-6** in NA in the dark (green line), after irradiation with visible light (red line) and during the thermal reversion process (black lines) and recoloration kinetics (at $\lambda_{abs} = \lambda_{max}$) of g) the nitro-SPs and the h) no nitro-SPs.

Once demonstrated the tunability of colors and reversion rates of different SP in NA, we decided to exploit the high medium sensitivity of merocyanine forms of the SP to control and tune the photochromic performances of an individual SP by changing the properties of the medium. This study was started with **SP-1**, which in NA showed the presence of both MC and MCH⁺ forms in equilibrium between them (**Figure 3.5a**). We considered that by modifying the interacting mechanism between the medium and the dye (hydrogen bonding vs acid-base reactions) the formation of the yellow MCH⁺ or violet MC forms could be selectively controlled, providing tunability of the initial color.

3.3.1.2 Tuning reverse photochromism of nitro-SP by changing the medium

Color tuning of reverse photochromism was initially attempted exploiting the solvatochromism of the merocyanine isomer of **SP-1** in media of higher and lower polarity than NA. The medium polarity was reduced by adding increasing amounts (from 0 to 75% in volume) of non-polar hexadecane (HD), whereas it was increased by replacing NA with acids of shorter alkyl chains, i.e. heptanoic (HA) and pentanoic (PA) acids. Lowering the medium polarity induced a less effective stabilization of the merocyanine forms of the dyes and shifted the equilibrium toward the respective colorless spiro isomer (**Figure 3.7a**), as indicated by the lower absorbance in the visible region of the mixtures. The opposite behavior was obtained by increasing polarity, which resulted in higher absorbance in the visible region of the spectrum (**Figure 3.7b**). Regarding color tunability, the MC isomer of **SP-1** ($\lambda_{\text{abs, max}}^{\text{SP-1/NA}} = 528 \text{ nm}$) only showed very minor blue- or red-shifts of their absorption bands upon polarity variation (slightly negative solvatochromism, confirming the zwitterionic character of the MC form)^{21,22} and slightly changed the ratio between the protonated and non-protonated MC forms (**Figure 3.7c-d**). Overall, large color changes could not be obtained for **SP-1** only by changing the polarity of the medium.

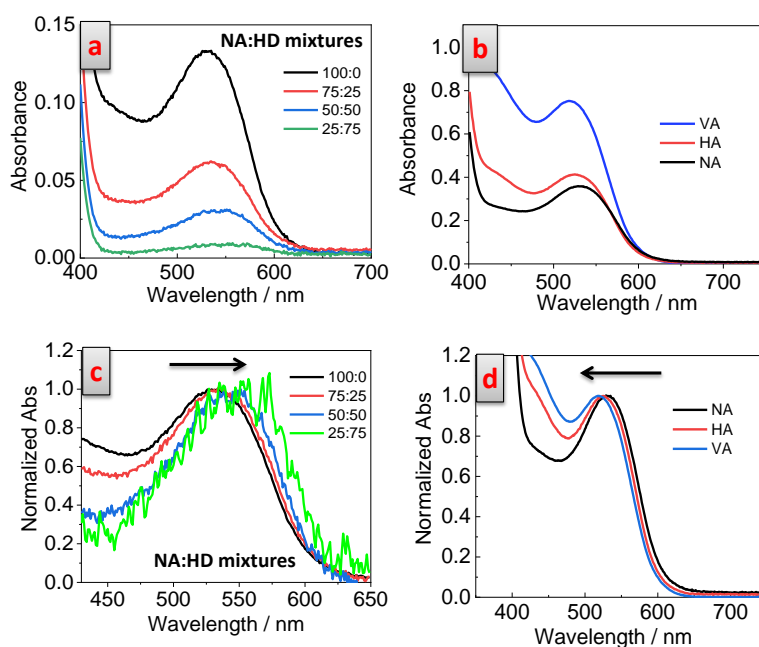


Figure 3.7: absorption spectra of **SP-1** in a) NA:HD mixtures prepared with different ratio ([**SP-1**]=6.2 mM), b) in VA, HA, NA ([**SP-1**]=5.5 mM) and c-d) normalized absorption spectra of the spectra in a) and b), respectively. The lower and higher polarity mixtures were prepared at different dyes concentrations to allow signal detection and avoid signal saturation.

On the basis of these results, we considered that much more tunable reverse photochromism could be reached for **SP-1** if the equilibrium between their non-protonated and protonated merocyanine forms could be altered by varying the acidity of the media, which would change the relative concentration of these species. Again, well-designed non-volatile hydrophobic solvents were used as they are more suitable for the fabrication of solid photochromic materials based on core-shell capsules.

To force the formation of the yellowish MCH^+ form of **SP-1** we selected *n*-dodecylphosphonic acid (**DPA**), which is a twelve carbon chain phosphonic acid, solid at RT ($T_m=70^\circ\text{C}$).⁵⁸ The reason for this choice was two-fold: i) it presents a pK_a value ($\text{pK}_a=1.25$) lower than NA and ii) the long hydrocarbon chain could confer good solubility in non-volatile organic solvents (i.e. NA) and low solubility in water, which is important for the correct formation of the capsules. Different amounts of DPA (4-40 mM) were thus added to a **SP-1/NA** solution (14 mM). Noteworthy, we realized that only very small amount of DPA (40 mM; DPA/NA molar ratio = 1/143) was needed to turn rapidly the solution from red to yellow ($\lambda_{\text{max}} = 421 \text{ nm}$, **Figure 3.8a-b**), with the corresponding disappearance of the band at 528 nm, suggesting the protonation of the MC form (**Figure 3.8a-b**). The acidity of **DPA** in NA is enough to shift the equilibrium towards the MCH^+ form.

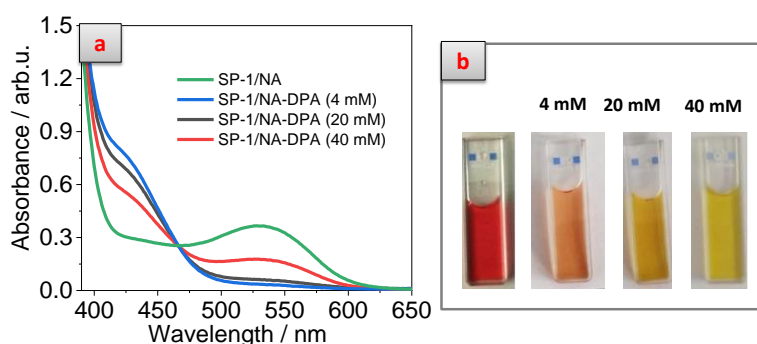


Figure 3.8: a) absorption spectra and b) digital images of **SP-1/NA** solution before and upon the addition of **DPA** (4, 20, 40 mM).

On the other hand, in order to stabilize the MC against MCH^+ we selected a non-acidic protic oil, poly(dimethylsiloxane-*co*-diphenylsiloxane) dihydroxy-terminated (**PDMS-OH**), which can stabilize the MC via hydrogen bonding. When **SP-1** was dissolved in **PDMS-OH**, the dye was selectively stabilized into its violet

MC form (there is no absorption contribution from the MCH^+ at around 430 nm) and presented a 30 nm red-shifted absorption spectrum respect to the **SP-1/NA** solution ($\lambda_{max}^{SP-1/PDMS-OH} = 551$ nm, **Figure 3.9a-b**). These results confirmed the color tunability that yields an individual dye (**SP-1**) when dissolved in different non-volatile organic solvents with different acidity (**Figure 3.9a-b**).

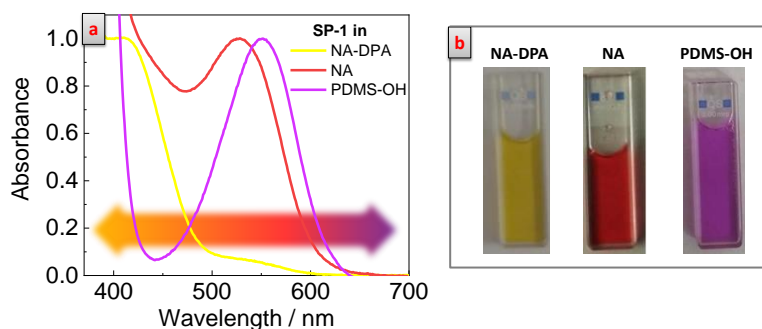


Figure 3.9: a) absorption spectra and b) digital images of solutions of SP-1 dissolved in NA, NA-DPA and PDMS-OH.

Interestingly, in both cases, reverse photochromism was preserved as the two **SP-1** solutions (**SP-1/NA-DPA** and **SP-1/PDMS-OH**) bleached when subjected to visible light irradiation and recolored in the dark (**Figure 3.9a-b**). Noticeably, different back-isomerization rate constants were measured for these samples and that in NA ($k^{SP-1/NA-DPA} = 0.0044 \text{ min}^{-1}$ and $k^{SP-1/PDMS-OH} = 0.037 \text{ min}^{-1}$), which indicates that not only the color but also the switching kinetics of photochromes can be modulated with this strategy (**Figure 3.10c**). Therefore, proper selection of the photochromic dye and of the surrounding medium should allow recoloration times to be tuned (from seconds to hours) according to the application requirements.

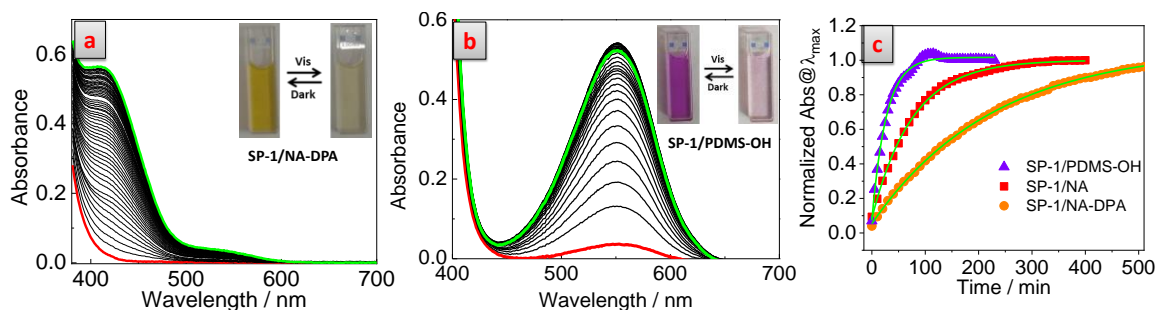


Figure 3.10: absorption spectra of SP-1 in a) NA-DPA and b) PDMS-OH before (green line), after irradiation with visible light (red line) and during recoloration in the dark (black lines); c) study of the recoloration kinetics at λ_{max} for SP-1 in NA, PDMS-OH and NA-DPA in the dark, after irradiating to the respective photostationary states.

Repetitive cycles of visible light-induced color fading and thermal recoloration in the dark were performed. The three bulk solutions (**SP-1/NA**, **SP-1/NA-DPA** and **SP-1/PDMS-OH**) showed good fatigue resistance (**Figure 3.11a-f**).

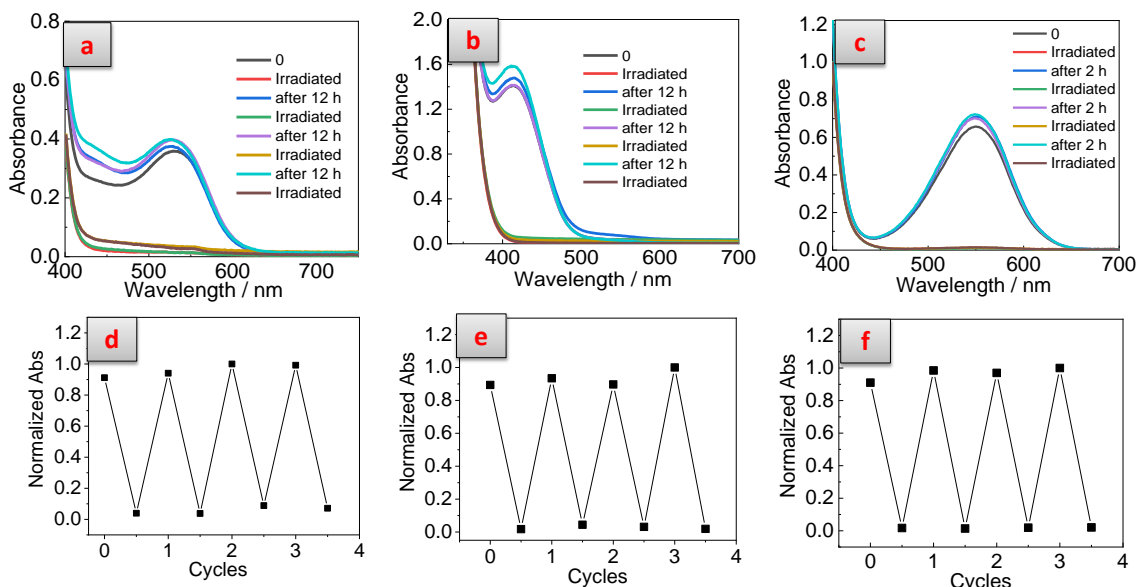


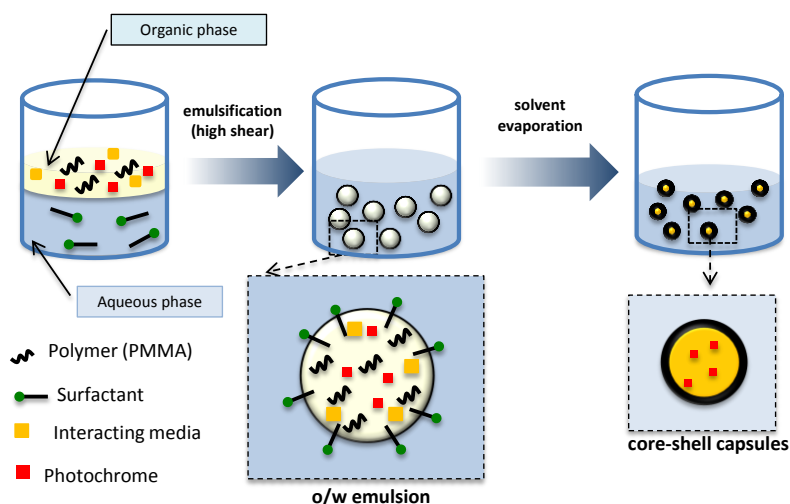
Figure 3.11: variation of the absorption spectra and of the absorbance (normalized to the highest value) at the spectral maxima for SP-1 mixtures in NA (a-d, 15.5 mM), NA-DPA (b-e, 3.1 mM) and PDMS-OH (c-f, 15.5 mM) when subjected to repetitive cycles of visible light-induced color fading and thermal recoloration in the dark.

All photochromic solutions were obtained with non-volatile solvents that should allow preparing stable core-shell capsules.

3.3.1.2.1 Reverse photochromism of capsules of nitro-SP/solvent

As mentioned before, the encapsulation strategy could be successfully used to transfer photochromic⁵⁹/thermochromic⁶⁰ properties to the solid state. The three mixtures of **SP-1** presenting three different photochromic performances were all made by non-volatile and quite lipophilic (non-miscible with water) media which, as demonstrated in the past in the group, are suitable to form stable core-shell capsules. For these mixtures the capsules were prepared through the reaction-free emulsion-solvent evaporation method adapted from the literature,⁶¹ which avoids any possible side reactions and consequent degradation of the photochromic dyes. Poly(methylmethacrylate) (PMMA) was used as shell polymer, as it was widely employed for successfully encapsulating different oil-based mixtures.⁶² The

polymer, the interacting media (NA-DPA, NA and PDMS-OH) and the dye are dissolved in an organic volatile solvent, immiscible with water. The organic solution is mixed with a surfactant-containing water solution to yield the oil-in-water(O/W) emulsion. Upon evaporation of the organic solvent the precipitation of the polymer in the interface between the water and the interacting media is induced yielding core-shell capsules (**Scheme 3.5**, see the experimental section 7.3.3.1 for the detailed synthesis).



Scheme 3.5: schematic representation of the solvent evaporation method used for the preparation of the capsules.

The freeze-dried capsules appeared yellow (**SP-1/NA-DPA@PMMA**), red (**SP-1/NA@PMMA**) and violet (**SP-1/PDMS-OH@PMMA**), and their absorption spectra ($\lambda_{\max} = 425, 528$ and 550 nm, **Figure 3.12a-b**) measured in reflectance mode, nicely reproduced those of the relative bulk solutions, indicating that the different non-volatile mixtures were successfully encapsulated and the respective stabilized MC forms were preserved also inside the capsules. SEM images showed the successful formation of the capsules ($1-5 \mu\text{m}$ for **SP-1/NA-DPA@PMMA**, $2-10 \mu\text{m}$ for **SP-1/NA@PMMA** and $20-30 \mu\text{m}$ for **SP-1/PDMS-OH@PMMA**, **Figure 3.12c-e**) and the core-shell structure of some broken capsules could be visualized (on top of **Figure 3.12d**).

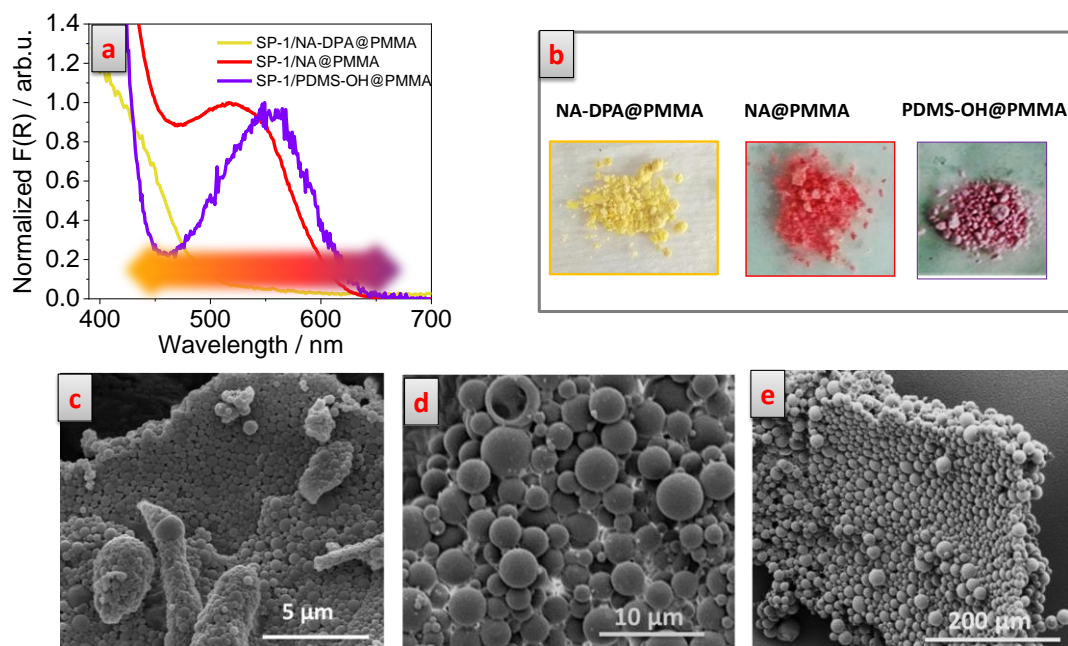


Figure 3.12: a) absorption spectra and b) digital and SEM images of c) **SP-1/NA-DPA@PMMA**, d) **SP-1/NA@PMMA** and e) **SP-1/PDMS-OH@PMMA** microcapsules.

$^1\text{H-NMR}$ spectra of **SP-1/NA-DPA@PMMA**, **SP-1/NA@PMMA** and **SP-1/PDMS-OH@PMMA** dissolved in CDCl_3 were recorded to determine the amount of the material (NA and PDMS-OH, respectively) encapsulated within the core of the capsules. Their spectra were compared with the spectra of pure NA, PDMS-OH and PMMA (Figure 3.13a-b). **SP-1/NA-DPA@PMMA** and **SP-1/NA@PMMA** presented the characteristic peaks of PMMA and of NA. The DPA could not be detected by this technique due to its low amount. Its encapsulation, however, was confirmed by the formation of the yellow MCH^+ form inside the capsules. In the case of **SP-1/PDMS-OH@PMMA**, the spectrum of the capsules presented the characteristic peaks of PMMA and PDMS-OH (Figure 3.13b). A controlled amount of DMF was added as standard reference to calculate the amount of encapsulated (payload) NA in **SP-1/NA-DPA@PMMA** (47 wt. %) and **SP-1/NA@PMMA** (52 wt. %) capsules and PDMS-OH in **SP-1/PDMS-OH@PMMA** (54 wt. %) capsules.

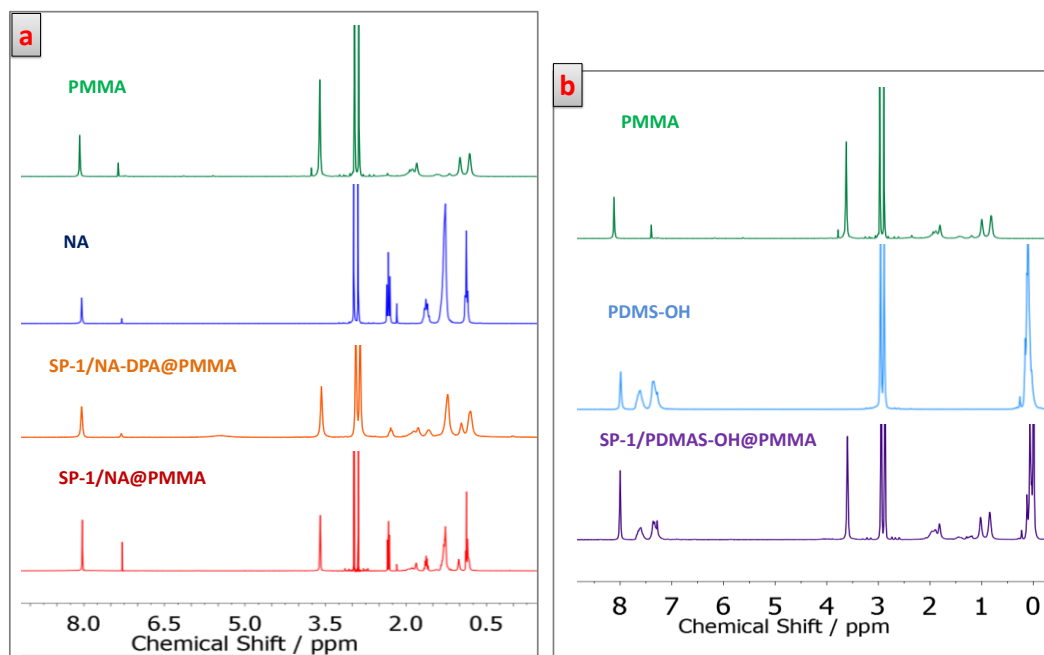


Figure 3.13: a) ¹H-NMR spectra in CDCl₃ of **SP-1/NA@PMMA** and **SP-1/NA-DPA@PMMA** microcapsules and b) ¹H-NMR spectra in CDCl₃ of **SP-1/PDMS-OH@PMMA**. For sake of comparison, ¹H-NMR spectra are also given for CDCl₃ solutions of NA and PMMA and PDMS-OH. **PMMA** presented the characteristic peaks at $\delta = 0.80\text{--}0.98$ (br., 3H, CH₃), 1.68–2.02 (br., 2H, CH₂) and 3.62 ppm (s, 3H, OCH₃), **NA** at $\delta = 0.79$ (t, 3H, CH₃), 1.25 (s, 10H, (CH₂)₅), 1.6 ppm (m, 2H, CH₂) and 2.40 (t, 2H, COCH₂) and **PDMS-OH** at $\delta = 0$ (m, 6H, (CH₃)₂-Si), 7.25 (m, 4H, ArH) and 7.6 (m, 6H, ArH).

Differential scanning calorimetry (DSC) measurements of the microcapsules were performed to demonstrate that the encapsulated oils were not mixed with the polymer forming a plasticized matrix (in which case no T_m or T_m at very different values respect to the pure compound is expected to be measured upon heating) that could alter the photochromic properties of the capsules. The DSC of **SP-1/NA@PMMA** and **SP-1/NA-DPA@PMMA** showed a melting point of NA at 12.4 and 4 °C, respectively, similar to pure bulk materials (9°C),⁵⁸ demonstrating that NA was not mixed with the shell polymer (**Figure 3.14a-b**). The lower T_m observed in the case of **SP-1/NA-DPA@PMMA** was attributed to the possible plasticizing effect of DPA mixed with NA. Unfortunately, in the case of **SP-1/PDMS-OH@PMMA** capsules, no T_m could be detected, most probably because the T_m of PDMS-OH ($T_m^{\text{PDMS}} = -50^\circ\text{C}$)⁵⁸ is below the limit of detection of the equipment (-20 ~ -30°C).

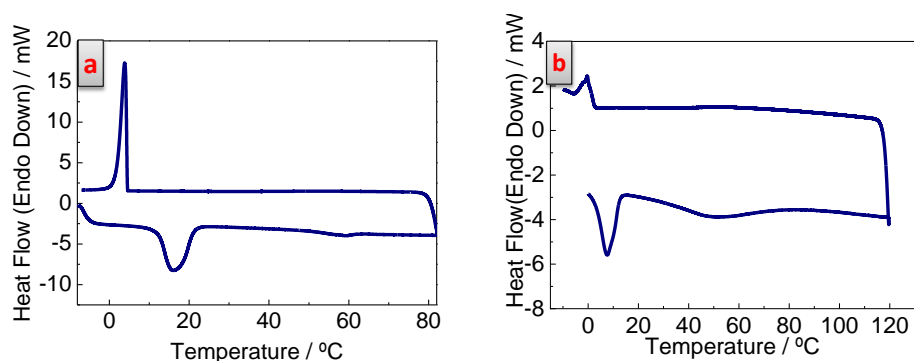


Figure 3.14: DSCs of: a) SP-1/NA@PMMA ($T_m = 12.5^\circ\text{C}$) and b) SP-1/NA-DPA@PMMA ($T_m = 4^\circ\text{C}$) microcapsules.

- **Photochromic performances**

Irradiation of the powders with visible light provided colorless capsules, which recolored in the dark (**Figure 3.15**) with similar rates ($k^{\text{SP-1/NA-DPA@PMMA}} = 0.0038 \text{ min}^{-1}$, $k^{\text{SP-1/NA@PMMA}} = 0.012 \text{ min}^{-1}$, $k^{\text{SP-1/PDMS-OH@PMMA}} = 0.042 \text{ min}^{-1}$) to the respective bulk mixtures (**Figure 3.15, Table 3.2**) indicating that also the photochromic kinetics (not only the initial color) were successfully transferred from organic non-volatile homogeneous mixtures to solid materials.

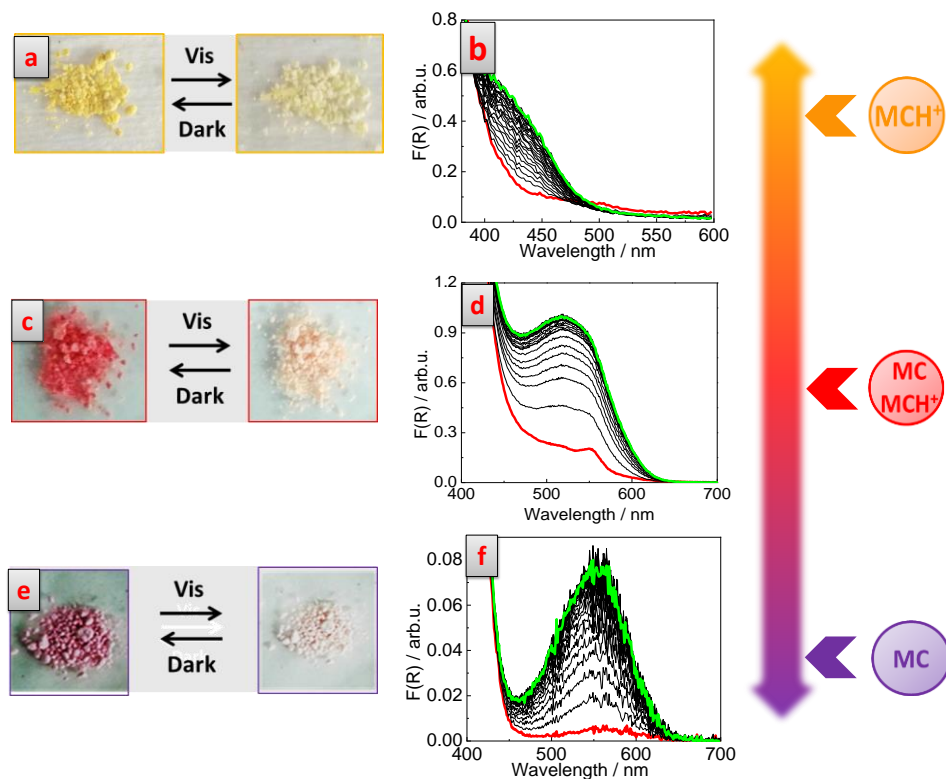


Figure 3.15: digital images and absorption spectra before (green), after (red) irradiation and during (black lines) recoloration in the dark of a) and b) SP-1/NA-DPA@PMMA, c) and d) SP-1/NA@PMMA and e) and f) SP-1/PDMS-OH@PMMA microcapsules.

Solvent		SP-1		
		NA-DPA	NA	PDMS-OH
λ_{\max} (nm)	Bulk solution	421 (shoulder)	528	551
	Microcapsules	425 (shoulder)	519	550
k (min ⁻¹)	Bulk solution	0.0044	0.013	0.037
	Microcapsules	0.0038	0.012	0.042

Table 3.2: absorption maximum wavelengths (λ_{\max} in nm) and rate constants (k in min⁻¹) of the thermal recoloration process in the dark of SP-1 in bulk solutions and microcapsules.

Once demonstrated the control and tunability of the MC/MCH⁺ equilibrium of nitro-SP in non-volatile, lipophilic media and the transfer to the solid state through the encapsulation, we decided to verify the universality of the strategy with no nitro-substituted spiropyrans. For this study we selected **SP-4** and **SP-5**.

3.3.1.3 Tuning reverse photochromism of no nitro-SP by changing the medium

SP-5, like **SP-1**, is stabilized into both, the MCH⁺ and the MC in NA (**Figure 3.5a**, $\lambda_{\max}^{\text{SP-5}} = 437$ nm and $\lambda_{\max, 2}^{\text{SP-5}} = 550$ nm). However, compared to **SP-1**, the equilibrium seems to be more shifted towards the MCH⁺ form, since the contribution of the band at 550 nm to the spectrum is much smaller. On the other hand, **SP-4** has a more basic character and thus the yellow MCH⁺ form is only obtained in NA (**Figure 3.5a**, $\lambda_{\max}^{\text{SP-4}} = 433$ nm). These two cases were quite challenging as the stabilization of the MC form against the MCH⁺ had to be carried out by using media less acidic than the weak acid NA.

To achieve this, we decided to use a mixture made of a phase change material (PCM) and a color developer (CD), a solid mixture (at RT) generally employed in thermochromic materials to stabilize the open form of spirolactones through hydrogen bonding interactions with the CD. The interaction is produced selectively in the solid state of the PCM as explained in the introduction.

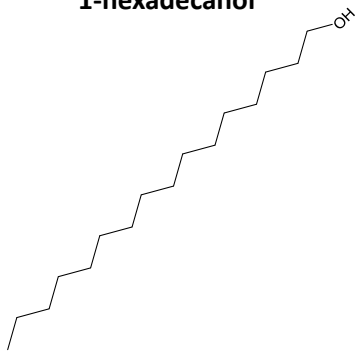
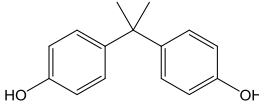
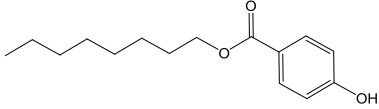
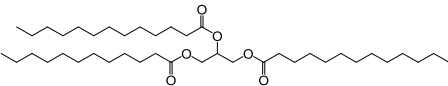
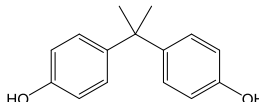
PCM, medium	Color developer
<p>1-hexadecanol</p> 	<p>Bisphenol A</p> 
	<p><i>n</i>-Octyl 4-hydroxybenzoate</p> 
<p>Trilaurin</p> 	<p>Bisphenol A</p> 

Table 3.3. PCMs and color developers used for the study of the bulk mixtures of **SP-4** and **SP-5**.

Three different bulk mixtures of PCM-CD were prepared for each **SP-4** and **SP-5** dye (**Table 3.3**):

- 1-hexadecanol (**HDOH**, $T_m=49^\circ\text{C}$) as PCM medium and bisphenol A (**BA**) as CD.
- 1-hexadecanol (**HDOH**) as PCM medium and *n*-octyl 4-hydroxybenzoate (**Benz**) as CD.
- Trilaurin (**TA**, $T_m=46.5^\circ\text{C}$) as PCM medium and bisphenol A (**BA**) as CD.

- When **SP-5** and **SP-4** were dissolved in the **TA-BA** mixture (**SP-5/TA-BA** and **SP-4/TA-BA**), an intense reddish color with a broad band in the visible region (**Figure 3.16a-d**) was observed when TA solidified. Noteworthy, in both cases the MC band at $\lambda_{\text{max}} = 550 \text{ nm}$, which was negligible (**SP-5/NA**) or undetected (**SP-4/NA**) in NA, increased significantly (respect to the one at $\lambda_{\text{max}} \sim 430 \text{ nm}$), indicating that part of the **SP-5** and **SP-4** molecules were successfully stabilized in the non-protonated MC form.

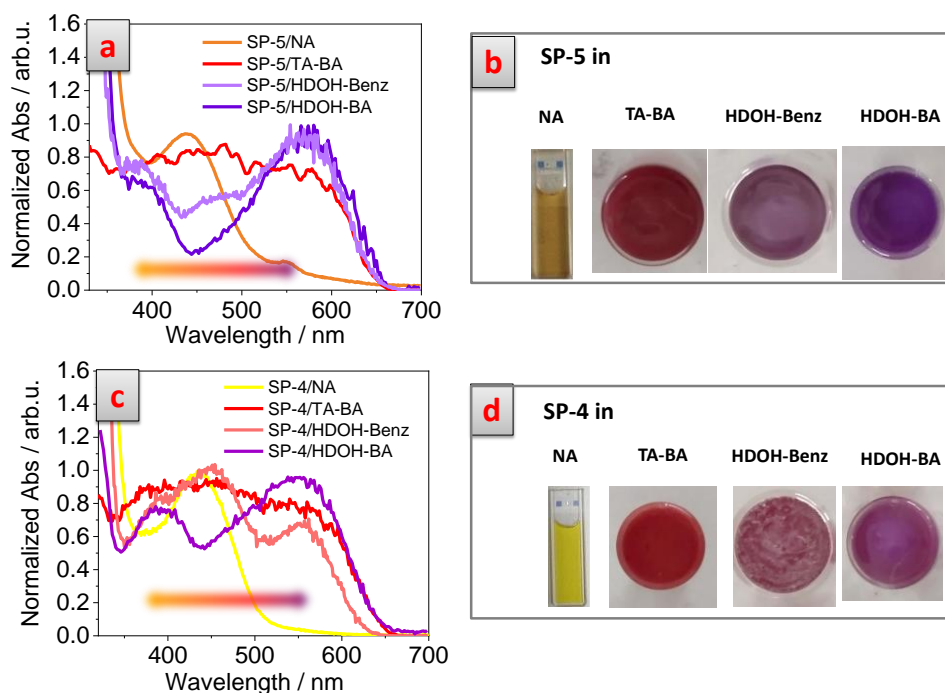


Figure 3.16: a) absorption spectra and b) digital images of SP-5 dissolved in NA, TA-BA, HDOH-Benz and HDOH-BA in the dark; c) Absorption spectra and d) digital images of SP-4 dissolved in NA, TA-BA, HDOH-Benz and HDOH-BA in the dark.

- The solid **HDOH-Benz** mixtures of **SP-5** and **SP-4** showed a violet and brown color, respectively (**Figure 3.16b, d**), and absorption spectra that have contribution of both MC ($\lambda_{max} = 560$ nm) and MCH⁺ ($\lambda_{max} = 455$ nm) forms. However, while in the **SP-5/HDOH-Benz** mixture the band at 560 nm is the most intense (**Figure 3.16a-b**), in the **SP-4/HDOH-Benz**, the most intense band is the one at 455 nm (related to MCH⁺, **Figure 3.16c-d**). Once more, this was explained by the higher basicity of **SP-4** than **SP-5** and thus, the higher tendency to be protonated in presence of **Benz** molecules.

- In **HDOH-BA** mixtures, both **SP-5** and **SP-4** dyes, showed violet color ($\lambda_{max}^{SP-5/HDOH-BA} = 570$ nm and $\lambda_{max}^{SP-4/HDOH-BA} = 565$ nm, **Figure 3.16a-d**), indicating the successful shift of the equilibrium towards the MC form.

These results confirmed again that high color tenability and control by using different non-volatile hydrophobic PCM-CD mixtures could be achieved even with no nitro dyes (**Table 3.4**).

- **Photochromic performances**

Importantly, in all cases reverse photochromism was observed since the mixtures faded to colorless when subjected to visible light (laser pointer at 532 nm) and recolored in the dark (**Figures 3.17a-f**).

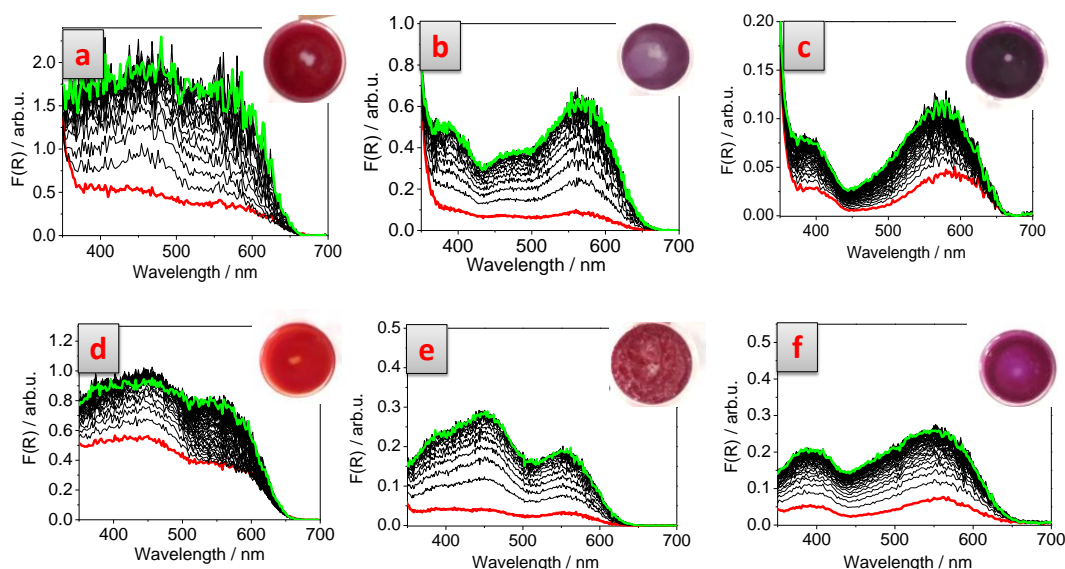


Figure 3.17: absorption spectra before (green), after (red) irradiation and during the recoloration process (black lines) of SP-5 in different media: a) TA-BA, b) HDOH-Benz and c) HDOH-BA and the same for SP-4 in the same media: d) TA-BA, e) HDOH-Benz and f) HDOH-BA.

The recoloration kinetics in the dark were monitored for the three solid mixtures (**TA-BA**, **HDOH-Benz** and **HDOH-BA**) at different wavelengths (the maxima of the absorption bands, λ_{\max}):

i) in the **TA-BA** mixtures, the bands at 450 and 550 nm of **SP-5** and **SP-4** were reformed, in the dark, with different rates ($k_{450}^{\text{SP-5/TA-BA}} = 0.14 \text{ min}^{-1}$, $k_{550}^{\text{SP-5/TA-BA}} = 0.37 \text{ min}^{-1}$ and $k_{450}^{\text{SP-4/TA-BA}} = 0.18 \text{ min}^{-1}$, $k_{550}^{\text{SP-4/TA-BA}} = 1.4 \text{ min}^{-1}$, **Figure 3.18a, d**, **Table 3.4**) confirming that they are associated to different species (**MC** and **MCH⁺**).

ii) On the other hand, in **HDOH-Benz** mixture of **SP-5**, the bands at 450 and 550 nm reformed with same rates ($k_{450}^{\text{SP-5/HDOH-Benz}} = 0.52 \text{ min}^{-1}$, $k_{550}^{\text{SP-5/HDOH-Benz}} = 0.53 \text{ min}^{-1}$), whereas for **SP-4** the bands were reformed with slightly different kinetics ($k_{450}^{\text{SP-4/HDOH-Benz}} = 0.70 \text{ min}^{-1}$, $k_{550}^{\text{SP-4/HDOH-Benz}} = 0.55 \text{ min}^{-1}$, **Figure 3.18b, e**, **Table 3.4**). Considering the two bands are related to the MC and MCH⁺ forms of **SP-5** and **SP-4**, they recovery was expected to occur with significantly different

rates, as seen in **TA-BA** mixtures. However, the recoloration of each species might be affected in different way by distinct media. This could explain why the MC and MCH⁺ had different recoloration rates in **TA-BA** and present similar or even the same behavior in **HDOH-Benz**.

iii) In **HDOH-BA** mixtures, both dyes, **SP-5** and **SP-4**, presented no significant contribution of MCH⁺ and the recoloration was studied in both cases at the maximum of the stabilized non-protonated MC ($k_{560}^{\text{SP-5/TA-BA}} = 0.42 \text{ min}^{-1}$ and $k_{556}^{\text{SP-4/TA-BA}} = 1 \text{ min}^{-1}$, **Figure 3.18c, f, Table 3.4**).

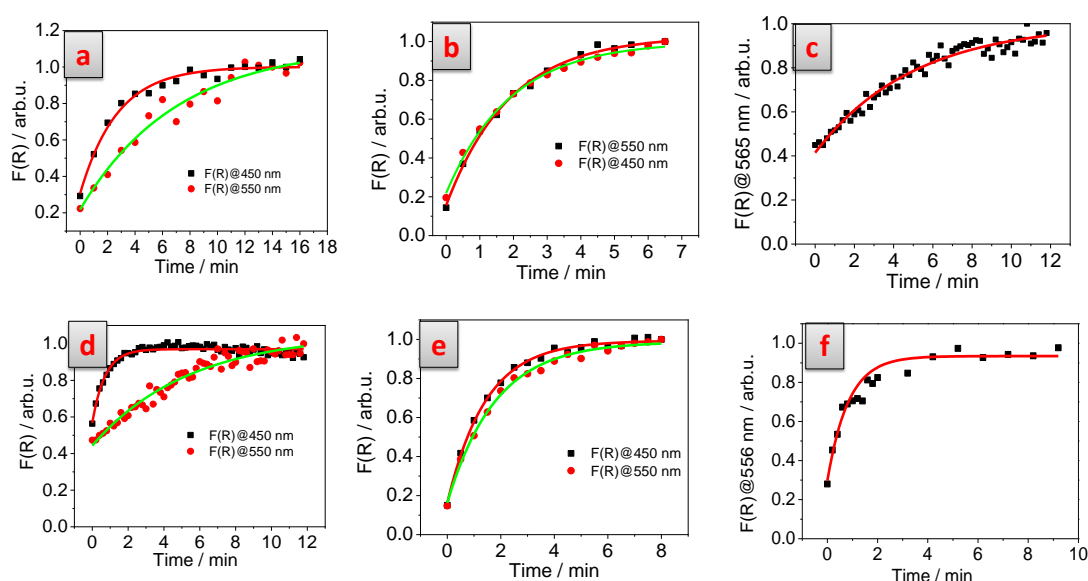


Figure 3.18: a-c) recoloration kinetics of SP-5 in different media: a) TA-BA, b) HDOH-Benz and c) HDOH-BA monitored at different wavelengths (λ_{max}) and of SP-4 in the same media d) TA-BA, e) HDOH-Benz and f) HDOH-BA monitored at different wavelengths (λ_{max}).

Mixture	SP-5			SP-4		
	TA-BA	HDOH-Benz	HDOH-BA	TA-BA	HDOH-Benz	HDOH-BA
λ_{max} (nm)	400-600 (broad band)	565 (shoulder at 462)	570	400-600 (broad band)	450 / 550	556
k_1 (min^{-1}) at $\lambda_{\text{max},1}$ (550-565 nm)	0.14	0.52	0.42	0.18	0.70	1
k_2 (min^{-1}) at $\lambda_{\text{max},2}$ (450 nm)	0.37	0.53	-	1.4	0.55	-

Table 3.4: maximum absorption wavelengths (λ_{max}) and rate constants (k in min^{-1}) of the thermal recoloration process in the dark of SP-5 and SP-4 in bulk mixtures at two different λ_{max} .

Once demonstrated the tunability of the photochromic performances of no nitro-substituted spiropyrans in non-volatile, lipophilic media, we decided to encapsulate 4 of the 8 investigated mixtures (**SP-4/HDOH-BA**, **SP-5/HDOH-BA**, **SP-4/NA** and **SP-5/NA**) as a proof-of-concept to demonstrate that also in these cases the photochromic behavior could be preserved in the solid state. The encapsulation was carried out through the solvent evaporation method (see experimental section 7.3.3.1).

3.3.1.3.1 Reverse photochromism of capsules of no nitro-SP/solvent

SP-4/NA@PMMA and **SP-5/NA@PMMA** capsules (2-10 μm) could be successfully obtained without modification of the method used to encapsulate the nitro-SP/NA mixtures (see experimental section 7.3.3.1). The freeze-dried capsules appeared as similar yellow color as the respective bulk mixtures, indicating the NA solutions were successfully encapsulated (**Figure 3.19a-b**). In both cases the dissolved capsules in CDCl_3 presented the characteristic $^1\text{H-NMR}$ peaks of **PMMA** and of **NA**.

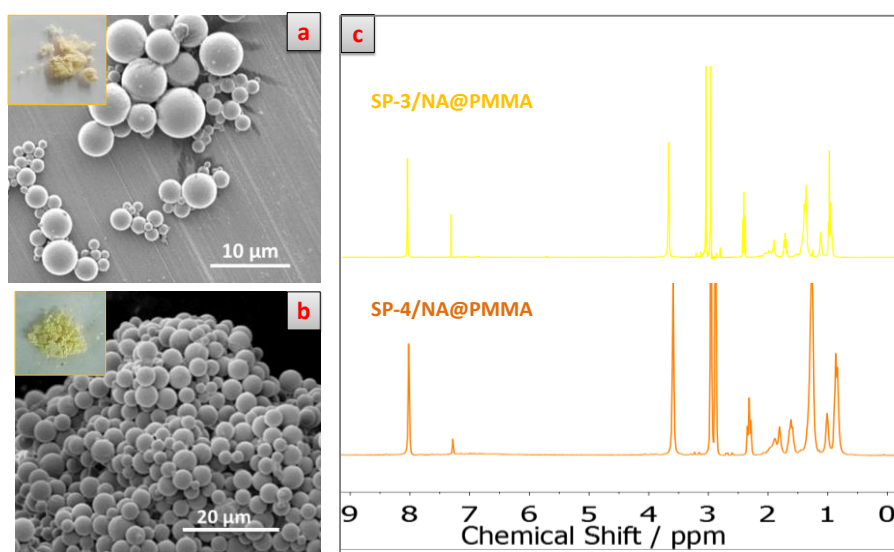


Figure 3.19: SEM and digital images (inset) of a) **SP-5/NA@PMMA** and b) **SP-4/NA@PMMA** microcapsules; c) $^1\text{H-NMR}$ spectra in CDCl_3 of **SP-5/NA@PMMA** and **SP-4/NA@PMMA** microcapsules. Characteristic peaks of **PMMA** at $\delta = 0.80\text{-}0.98$ (br., 3H, CH_3), $1.68\text{-}2.02$ (br., 2H, CH_2) and 3.62 ppm (s, 3H, OCH_3) and of **NA** at $\delta = 0.79$ (t, 3H, CH_3), 1.25 (s, 10H, $(\text{CH}_2)_5$), 1.6 ppm (m, 2H, CH_2) and 2.40 (t, 2H, COCH_2).

In both cases the DSC of the capsules showed a T_m similar to pure bulk NA ($T_m^{\text{SP-4/NA}} = 10.5$ $^\circ\text{C}$, $T_m^{\text{SP-5/NA}} = 9$ $^\circ\text{C}$, **Figure 3.20a-b**),⁵⁸ which supports that NA and

PMMA were not mixed and that the majority of NA was essentially confined in the core of the capsules.

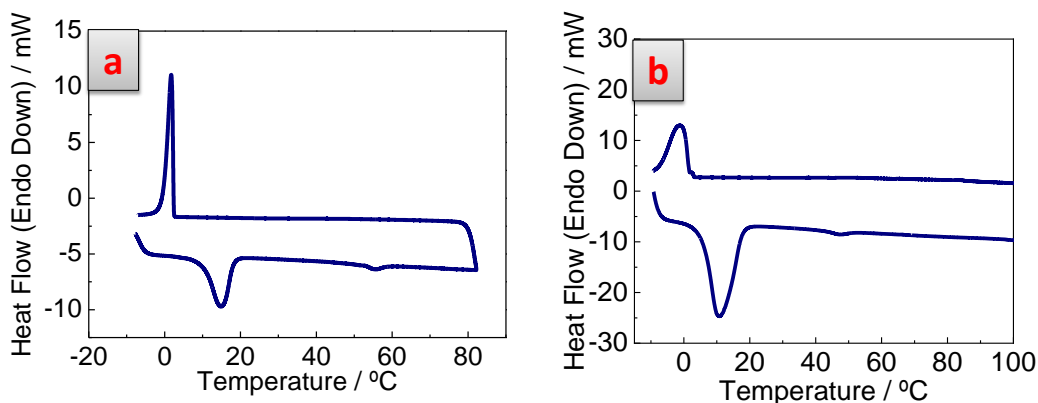


Figure 3.20: DSCs of: a) SP-4/NA@PMMA ($T_m = 12.5^\circ\text{C}$) and b) SP-5/NA@PMMA ($T_m = 9^\circ\text{C}$) microcapsules.

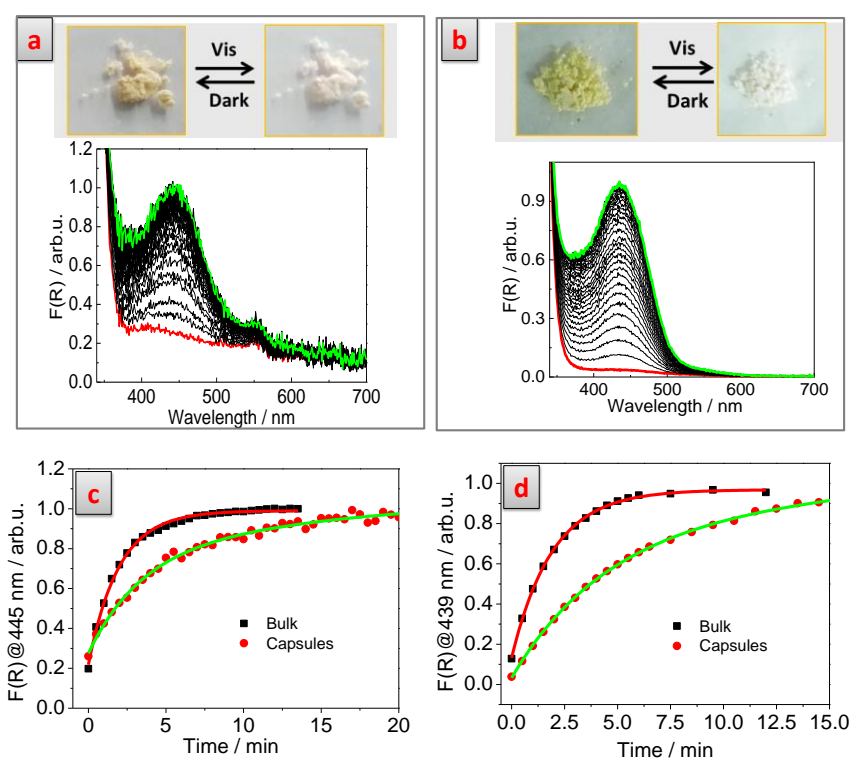


Figure 3.21: absorption spectra and digital images before (green line), after (red line) irradiation and during recoloration in the dark (black lines) of a) SP-5/NA@PMMA and b) SP-4/NA@PMMA; comparison of the recoloration kinetics of the c) SP-5/NA@PMMA and d) SP-4/NA@PMMA capsules with the corresponding bulk solutions.

The yellow color of SP-5/NA@PMMA and SP-4/NA@PMMA capsules ($\lambda_{\text{max}} = 434$ and 440 nm, **Figure 21a-b**) faded when irradiating with visible light and recolored in the dark ($k^{\text{SP-4/NA@PMMA}} = 0.17$, $k^{\text{SP-5/NA@PMMA}} = 0.16 \text{ min}^{-1}$, **Figure 21c-d**) with

lower growing kinetic rate compared with the respective bulk solutions (**Figure 21c-d**). This disagreement was ascribed to the fact that part of the dye/NA solution might be mixed with the shell polymer, creating more rigid subdomains that slow down the thermal isomerization process.

The fatigue resistance study of the capsules confirmed the photochrome stability after a few cycles of visible light-induced decoloration and recoloration in the dark (**Figure 3.22a-b**).

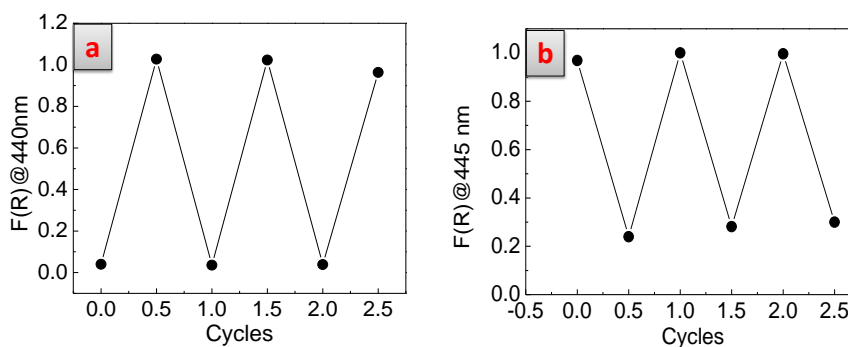


Figure 3.22: cycles of photoinduced color fading and recoloring in the dark of a) SP-4/NA@PMMA and b) SP-5/NA@PMMA microcapsules.

The encapsulation of **HDOH-BA** mixture of **SP-4** and **SP-5** required a process of optimization since the use of PMMA as polymer shell yielded solid particles with craters on the surface instead of a core-shell structure (**Figure 23a, b**). For this reason it was decided to change the polymeric shell. PMMA was substituted with polycarbonate (**PC**) and polyethersulfone (**PES**), which are commercially available polymers that can be suitable for the encapsulation via the solvent-evaporation method (soluble in chloroform or dichloromethane).

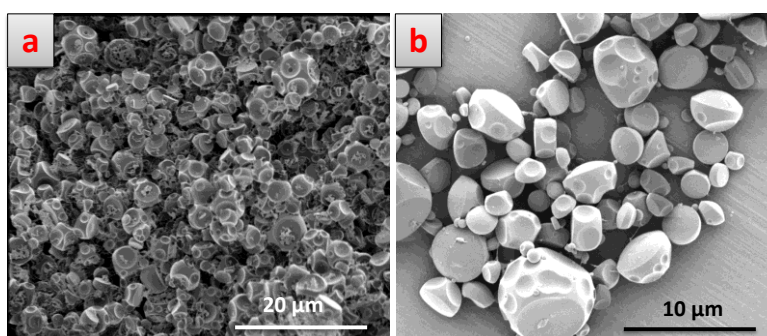


Figure 23: SEM images of HDOH@PMMA microcapsules.

Various syntheses were performed changing different parameters such as the polymer shell, the polymer/HDOH weight ratio and the rate of the emulsification process. The conditions are detailed in **Table 3.5**.

Synthesis Code	Polymer	HDOH/ polymer ratio	rpm
SP-5/HDOH-BA@PC	PC	2/1	1000
SP-5/HDOH-BA@PES	PES	2/1	1000
SP-5/HDOH-BA@PES_01	PES	2/1	5000
SP-5/HDOH-BA@PES_02	PES	1/1	5000

Table 3.5. Conditions and parameters changed during the optimization of the synthesis of SP-5/HDOH-BA@polymer capsules.

Unfortunately, none of the tested conditions yielded the desired core-shell capsules, while non-structured material or particles of only polymer or PCMs were obtained (**Figure 3.24a-b**). No improvements were achieved by increasing the rate of the emulsification step, which only yielded smaller particles.

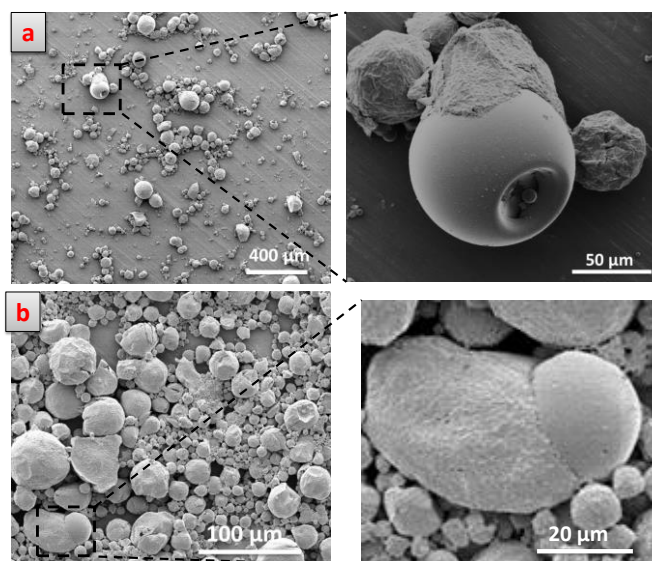


Figure 3.24: SEM images of attempts of synthesis of a) SP-5/HDOH-BA@PC, b) SP-5/HDOH-BA@PES and the corresponding 8x and 5x amplification, respectively, of a polymer particle (smooth surface) and non-structured HDOH (rough surface).

The lack of the core-shell structure was also corroborated by the formation of liquid material upon heating the freeze-dried powder that derived from the melting of the HDOH particles.

To overcome the encapsulation issues, it was decided to change the encapsulated media to 1-tetradecanol (TDOH), a PCM with a lower T_m ($T_m = 38^\circ\text{C}$) which should facilitate its encapsulation during the solvent evaporation (carried out at $T > 40^\circ\text{C}$,

see experimental section 7.3.3.4), avoiding the fast precipitation and phase separation that might be occurring with HDOH mixtures ($T_m = 49^\circ\text{C}$) during the solvent evaporation. Solid bulk **TDOH-BA** mixtures of **SP-4** and **SP-5** preserved the optical properties of the corresponding HDOH-BA mixtures: i) pink/violet color and ii) absorption bands at $\lambda_{\text{max}} = 390$ nm and 565 nm (**Figure 3.25a-b**). When irradiating with visible light (laser pointer at 532 nm) discoloration of both solids was observed, while recoloration occurred in the dark ($k^{\text{SP-4/TDOH-BA}} = 1.7 \text{ min}^{-1}$ and $k^{\text{SP-5/TDOH-BA}} = 0.70 \text{ min}^{-1}$, **Figure 3.25c-d**). The recoloration rates of these mixtures were faster than the corresponding HDOH-BA solutions ($k^{\text{SP-4/TA-BA}} = 1 \text{ min}^{-1}$ and $k^{\text{SP-5/TA-BA}} = 0.42 \text{ min}^{-1}$), probably due to the lower rigidity of the TDOH matrix respect to HDOH. Therefore, by changing the rigidity of the matrix, but maintaining the same type of interactions with the dyes (i.e. passing from **SP-X/HDOH-BA** to **SP-X-TDOH-BA**) it is possible to preserve the developed color in the dark and fine tune the kinetics response.

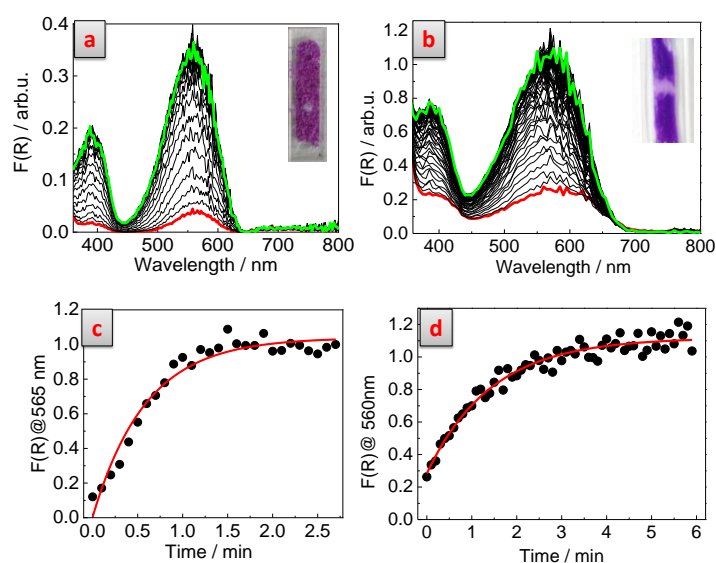


Figure 3.25: absorption spectra recorded before (green), after (red) irradiation and during (black lines) the recoloration process of a) **SP-4/TDOH-BA** and b) **SP-5/TDOH-BA**. Recoloration kinetics of c) **SP-4/TDOH-BA** and d) **SP-5/TDOH-BA** mixtures in the dark.

The two mixtures were encapsulated through the solvent evaporation method and using PES as shell material and PES/TDOH weight ratio of 1/2. SEM corroborated the formation of particles with smooth surface (**Figure 3.26a-b**), while the preservation of the spherical shape after heating the capsules at 50°C (above the T_m^{TDOH}) confirmed the PCM confinement within the PES shell (**Figure 3.26c**).

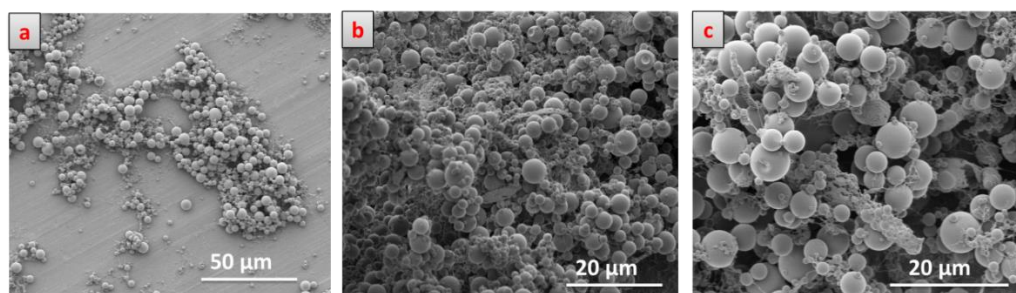


Figure 3.26: SEM images of a) **SP-5/TDOH-BA@PES** microcapsules and of **SP-4/TDOH-BA@PES** b) before and c) after heating at 50°C for 10 min.

The freeze-dried **SP-5/TDOH-BA@PES** capsules maintained the color ($\lambda_{\max}^{\text{SP-5/TD-BA@PES}} = 388$ and 546 nm) of the bulk solution as well as the reverse photochromic activity upon irradiation with visible light (**Figure 3.27a-c**).

On the other hand the color of the **SP-4/TDOH-BA@PES** capsules powder (pinkish, **Figure 3.27d**) and its absorption spectrum ($\lambda_{\max}^{\text{SP-4/TD-BA@PES}} = 546$ and 450 nm) were significantly different from that of the bulk solid mixture. The bands at $\lambda_{\max} = 450$ and 546 nm reformed in the dark after the light-induced discoloration, at different rate, confirming that they derive from two different species, i.e. the MCH^+ and MC, respectively (**Figure 3.27f**).

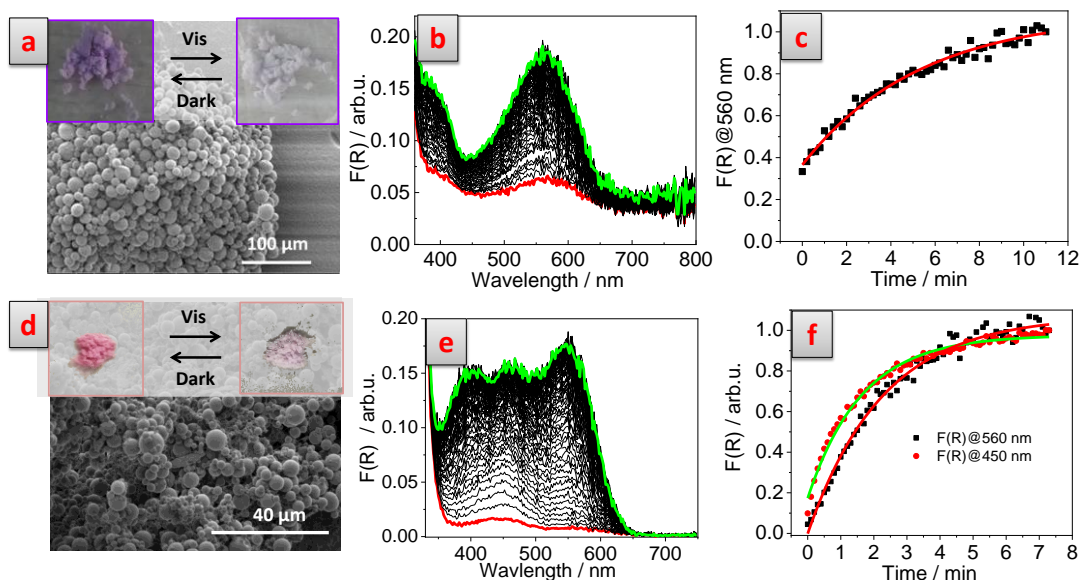


Figure 3.27: SEM and digital (inset) images of a) **SP-5/TDOH-BA@PES** and d) **SP-4/TDOH-BA@PES** microcapsules. Absorption spectra before (green), after (red) irradiation and during (black lines) the recoloration process of b) **SP-5/TDOH-BA@PES** and e) **SP-4/TDOH-BA@PES** microcapsules. Recoloration kinetics of the c) **SP-5/TDOH-BA@PES** and f) **SP-4/TDOH-BA@PES** capsules in the dark.

The formation of the MCH⁺ form once the **SP-4/TDOH-BA** was encapsulated was ascribed to the presence of species in the PES, acidic enough to protonate the MC form of SP-4. The acidic species could derive from the unreacted terminal monomers of the polymeric chains of PES or the residual monomeric bis(4-hydroxyphenyl) sulfone. This was not observed with **SP-5** possibly because its MC is less basic than the MC of **SP-4**.

Thus, it was decided to use PC (poly(bisphenol A carbonate)) as shell material, since its polymeric terminal units are expected to behave like a BA-like moiety, inducing therefore analogous color-developing properties. Finally using PC as shell material, the obtained freeze-dried **SP-4/TDOH-BA@PC** capsules maintained the color ($\lambda_{\max}^{\text{SP-4/TD-BA@PC}} = 390$ and 554 nm) of the bulk solution with almost no contribution of the band at 450 nm. The reverse photochromic activity was maintained upon radiation with visible light (**Figure 3.28a-c**).

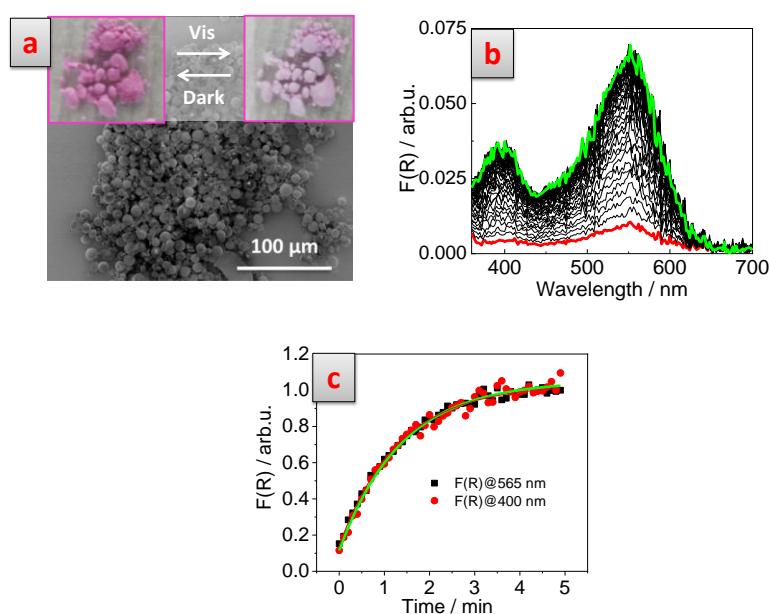


Figure 3.28: a) SEM and digital (inset) images, b) absorption spectra recorded before (green), after (red) irradiation and during (black lines) the recoloration process and c) recoloration kinetics at two different wavelengths (λ_{\max}) of **SP-4/TDOH-BA@PC**.

The differences ($k^{\text{SP-4/TD-BA@PC}} = 0.72 \text{ min}^{-1}$, $k^{\text{SP-5/TD-BA@PES}} = 0.19 \text{ min}^{-1}$, **Figure 3.27c**, **3.28c**) with the bulk re-coloration rate (**Table 3.6**) was again ascribed to the subdomains formed within the microcapsules due to partial miscibility between the shell and the core material.

In both cases, the encapsulation of the **SP-5, 4/TDOH-BA** mixtures was proved by $^1\text{H-NMR}$ and DSC (**Figures 3.29**). $^1\text{H-NMR}$ spectra of the dissolved **SP-5/TDOH-BA@PES** and **SP-4/TDOH-BA@PC** capsules presented the characteristic peaks of **TDOH** and of **PES** and **PC**, respectively. The payload in the capsules was 57 and 47 wt. %, respectively. The DSC of **SP-5/TDOH-BA@PES** and **SP-4/TDOH-BA@PC** showed melting points of 35.9 and 33.5 °C, respectively, in agreement with the T_m (38 °C) of the encapsulated media.

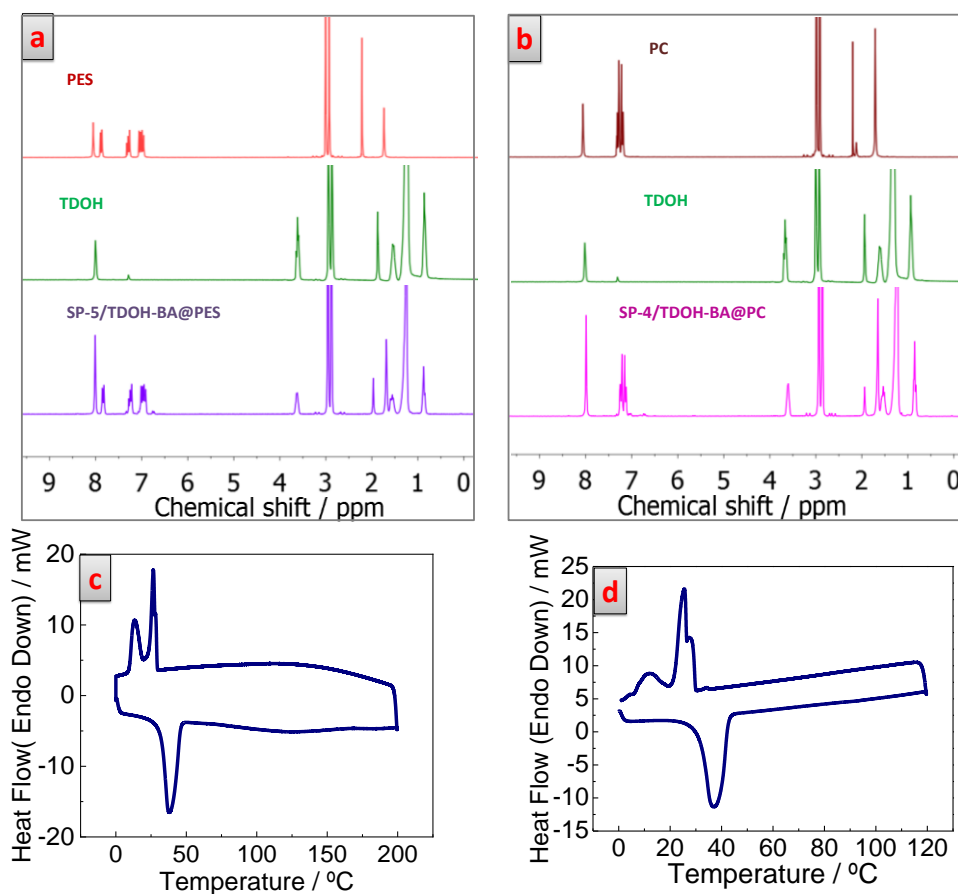


Figure 3.29: a) $^1\text{H-NMR}$ spectra in CDCl_3 and c) DSC of **SP-5/TDOH-BA@PES** microcapsules; b) $^1\text{H-NMR}$ spectra in CDCl_3 and d) DSC of **SP-4/TDOH-BA@PC** microcapsules. The **PES** characteristic peaks appear at $\delta = 1.6$ (s, 6H, $(\text{CH}_3)_2$), 6.9 (m, 8H, ArH), 7.1(m, 4H, ArH) and 7.9 ppm (m, 4H, ArH), the **PC** peaks at $\delta = 1.6$ (s, 6H, CH_3) and 7.1 ppm (m, 8H, ArH) and the **TDOH** ones at $\delta = 0.88$ (m, 3H, CH_3), 1.26 (s, 22H, $(\text{CH}_2)_{11}$), 1.53 (m, 2H, CH_2) and 3.63 ppm (m, 2H, OCH_2).

Solvent		SP-4		SP-5	
		NA	TDOH-BA	NA	TDOH-BA
λ_{\max} (nm)	Bulk solution	435	391 & 558	437	392 & 560
	Microcapsules	435	392 & 552	440	388 & 546
k (min ⁻¹)	Bulk solution	0.52	1.7	0.51	0.70
	Microcapsules	0.17	0.72	0.16	0.19

Table 3.6: absorption maximum wavelengths (λ_{\max} in nm) and rate constants (k in min⁻¹) of the thermal recoloration in the dark of SP-4 and SP-5 in bulk solutions and microcapsules.

Overall, we demonstrated the tenability of the photochromic performances of both, nitro and no nitro-SP (color, recoloration rates) in non-volatile and hydrophobic suitably designed media. The properties were fine controlled by modifying the type of dye, the chemical nature of the medium and its melting point. Moreover, it was showed that for all investigated cases it was possible to transfer these photochromic performances into core-shell capsules (in some cases the optimization of the capsules synthesis was required).

3.3.2 Switchable photochromism

After demonstrating the tunability of the reverse photochromism of spiropyrans in capsules filled with non-volatile solvents of different nature (NA, NA-DPA, PDMS-OH and TDOH-BA), we pursued switchable photochromism by replacing these solvents with an acidic PCM that is solid at room temperature.

Inspired by bi-component thermochromic systems (see introduction section 1.3.4), owing in which the dyes establishes different interactions with the solid and liquid states of the PCM (which also acts as color developer in the molten state), we expected that the photochromic SP and MC isomers of spiropyrans were selectively stabilized in each phase of the acidic PCM, thus allowing interconversion between direct and reverse photochromism upon thermally scanning through the T_m of the material.

For this purpose it was selected dodecanoic acid (**DA**) as medium, a twelve-carbon weak acid (pKa=5.3), solid at RT ($T_m = 43.8$ °C).⁵⁸ Below the T_m of the DA (solid state) no dye-matrix interaction is established and the spiropyran is expected to be

stabilized in the SP form. Therefore, the irradiation of the mixture at room temperature, with UV light should induce direct photochromism. On the other hand, in the liquid state (above the T_m), DA presents similar pKa of NA, which, as demonstrated above, has the capability to stabilize the MC or MCH⁺ forms of different SP dyes. Thus, upon heating the melted DA solution of spiropyran should develop the corresponding color of the MC or MCH⁺ form (thermochromism), which upon irradiation with visible light are expected to fade to the colorless SP isomer (reverse photochromism).

When the two no-nitro spiropyrans (**SP-4** and **SP-6**) were mixed with molten DA they were stabilized in the yellow MCH⁺ form as it occurred in liquid NA solution (**Figure 3.5**). Both mixtures become colorless upon solidification of DA.

The encapsulation of **SP-4/DA** and **SP-6/DA** mixtures was carried out through the emulsion–solvent evaporation method and PMMA was selected as the polymer shell for the preparation of microcapsules containing **SP/DA** mixtures. SEM confirmed the proper formation of the capsules with no signs of non-structured DA (**Figure 3.30a-b**). At room temperature, both **SP-4/DA@PMMA** and **SP-6/DA@PMMA** capsules were colorless with only residual absorption at 430 and 410 nm, respectively (**Figures 3.30c-d**). This indicated the stabilization of the photochromic molecules in their non-colored SP form under these conditions, probably owing to the weak interactions between solid DA and SP molecules. Interestingly, when the powders were heated above the DA melting point (60 °C), they became yellow, and an absorption band appeared in the visible region at $\lambda_{\max}^{\text{SP-4}}=430$ and $\lambda_{\max}^{\text{SP-6}} = 410$ nm. This thermochromic transition is related to the acid-induced stabilization of the MCH⁺ isomer in the liquid DA (**Figures 3.30c-d**).

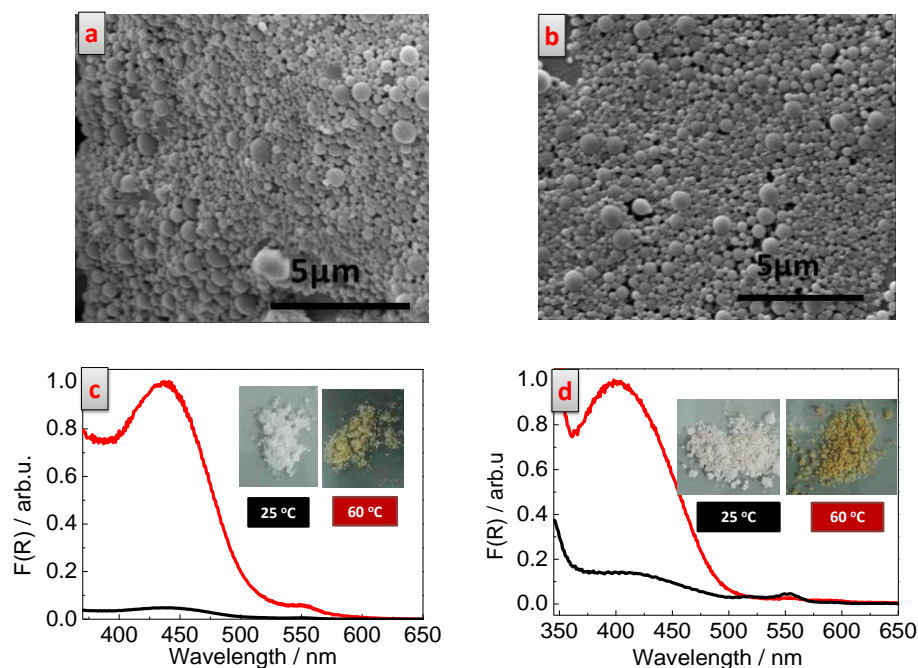


Figure 3.30: SEM images of a) **SP-4/DA@PMMA** and b) **SP-6/DA@PMMA** capsules and absorption spectra before and after heating of c) **SP-4/DA@PMMA** and d) **SP-6/DA@PMMA** microcapsules.

Although the capsules showed the expected thermochromic colorless-to-yellow color interconversion in the dark upon **DA** melting neither direct nor negative photochromism was observed. Indeed, when irradiating the white capsules with UV light at RT no color change was detected, nor loss of color was induced when irradiating them with visible light at 60°C. It is reported that the thermal recovery of the direct photochromism in solution is very fast ($\sim\mu\text{s}$)⁶³ and therefore not enough accumulation of the photoinduced colored species could be produced (with our UV sources) to be appreciated by naked-eye. On the other hand the thermal color recovery of the reverse photochromism (which was in the order of a few minutes in **NA** at RT), could be so dramatically accelerated at 60 °C that the photoinduced color loss could be hardly detectable. Given the impossibility to measure the photochromic behavior of these samples it was decided to change the encapsulated dyes.

The nitro-SP, **SP-2** and **SP-1** were selected for the preparation of the capsules due to the known slow direct photochromism and the slower reverse photochromic response observed in **NA** (~ 300 min).

At room temperature, both **SP-2/DA@PMMA** and **SP-1/DA@PMMA** capsules (5–10 μm , **Figure 3.31a-b**) were colorless (or very faintly pink) with only residual absorption around 530–540 nm (**Figure 3.31c-d**). This indicated again the stabilization of the photochrome molecules in their non-colored SP form. The core-shell structure could be detected in some broken capsules when inspected by SEM (inset **Figure 3.31a**). When the capsule powders were heated above the T_m^{DA} (60 °C), they became red, and an absorption band appeared in the visible region at $\lambda_{\text{max}} = 530$ nm confirming the thermochromic behavior of the **nitro-SP-2, 1/DA** capsules. The reddish color was deriving in both cases from the stabilization of the MC form against the MCH^+ , possibly through hydrogen bonding interaction between DA and the dyes, analogously to what observed for NA mixture of nitro-SP (section 3.3.1).

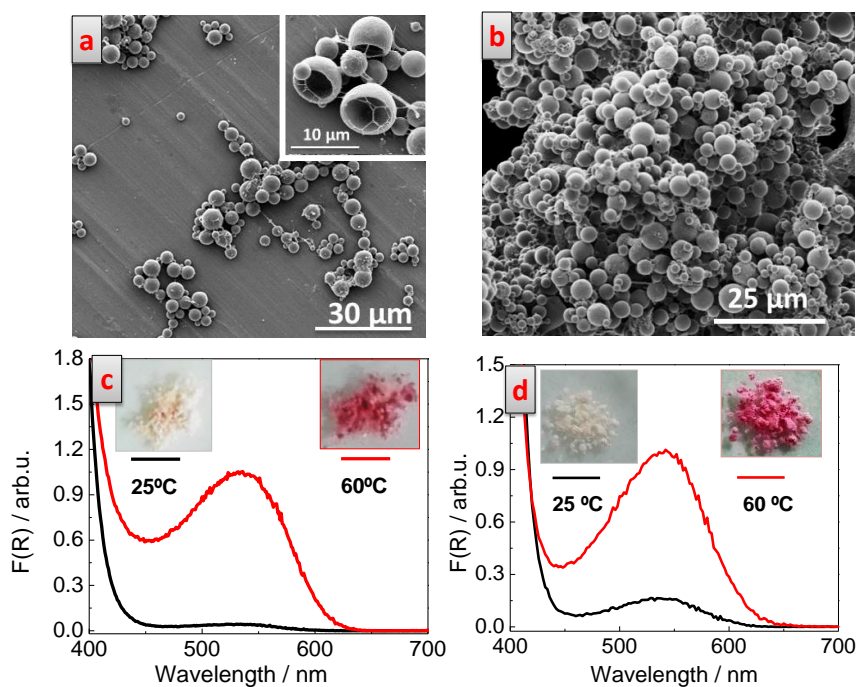


Figure 3.31: SEM images of a) **SP-2/DA@PMMA** and b) **SP-1/DA@PMMA** microcapsules and absorption spectra before and after heating at 60 °C of c) **SP-2/DA@PMMA** and d) **SP-1/DA@PMMA** microcapsules.

Macroscopically, from the capsule powders no leaking of DA was observed, after heating. Variable-temperature SEM showed that no melting or liquid ejection from the capsules was observed until temperatures around the PMMA glass transition temperature (105 °C) were reached,⁵⁸ confirming their thermal stability around the T_m^{DA} and the absence of non-encapsulated PCM (**Figure 3.32a-d**).

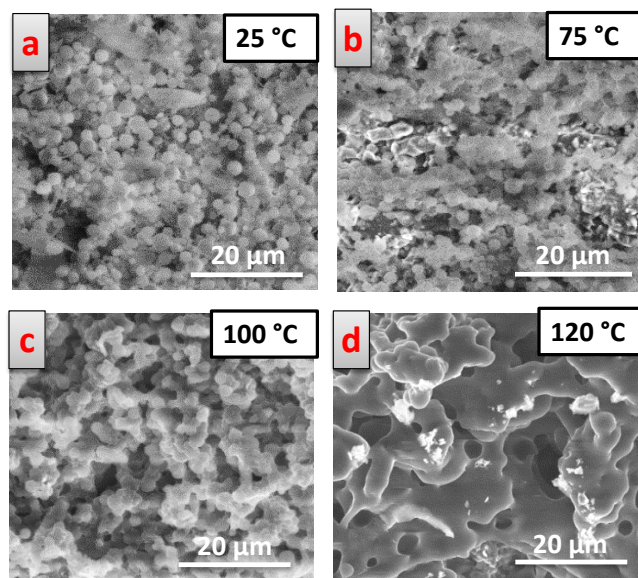


Figure 3.32: a) SEM images of **SP-2/DA@PMMA** capsules at different selected temperatures (25, 75, 100 and 120°C)

In both cases, the characteristic $^1\text{H-NMR}$ peaks of **DA** and **PMMA** were observed in the capsules (**Figure 3.33a**). The payload was calculated to be 64 and 63 wt. %, respectively for **SP-2/DA@PMMA** and **1/DA@PMMA** capsules. The higher payload values obtained for DA with respect to previous NA systems might be due to its lower polarity (higher hydrophobic/hydrophilic ratio) and reduced tendency to diffuse towards the water phase during the encapsulation. The DSC of the capsules powder revealed T_m values at 45.7 and 43.7 °C, respectively (**Figure 3.33b**), which match quite well with the melting point of the bulk DA ($T_m = 43.8^\circ\text{C}$).

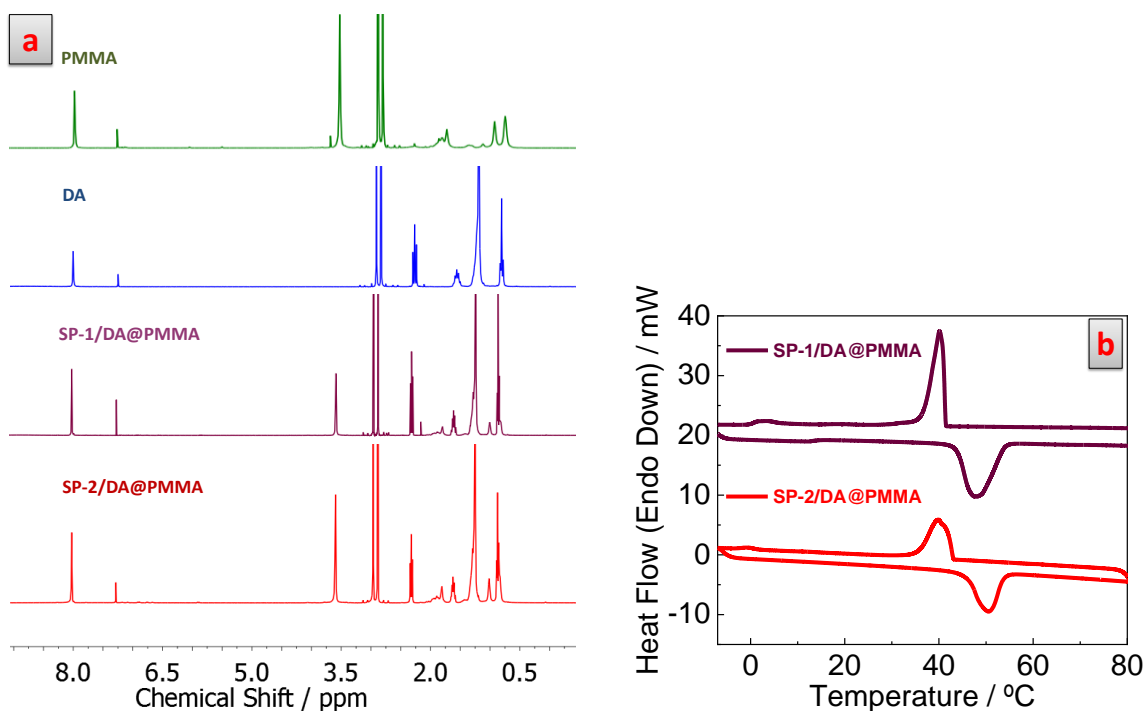


Figure 3.33: a) $^1\text{H-NMR}$ spectra recorded in CDCl_3 and b) DSC of **SP-2/DA@PMMA** and **SP-1/DA@PMMA** capsules. The $^1\text{H-NMR}$ spectra of pure PMMA and DA was recorded for comparison. Characteristic peaks of **DA** appeared at $\delta = 2.40$ (t, 2H, COCH_2), 1.6 (m, 2H, CH_2), 1.25 (s, 16H, $(\text{CH}_2)_8$), 0.79 (t, 3H, CH_3) and of **PMMA** at $\delta = 3.62$ (s, 3H, OCH_3), 2.02-1.68 (m, 2H, CH_2), 0.98-0.80 (m, 3H, CH_3).

- **Photochromic study of SP-2, 1/DA@PMMA capsules at $T < T_m^{\text{DA}}$**

Upon exposure to UV or blue-light irradiation at room temperature, the **SP-2/DA@PMMA** and **SP-1/DA@PMMA** capsule powder underwent rapid red coloration due to the light-induced MC formation (**Figure 3.34a, d**), as demonstrated by absorption measurements (**Figures 3.34b, e**). The color fading subsequently observed for these capsules, in the dark, confirmed the direct photochromic behavior, at 25 °C (**Figures 3.34b-c and 3.34e-f**). They recovered the non-colored state with different kinetics ($k_1^{\text{SP-2/DA@PMMA}} = 0.021 \text{ min}^{-1}$ and $k_2^{\text{SP-2/DA@PMMA}} = 4.9 \times 10^{-4} \text{ min}^{-1}$ and $k^{\text{SP-1/DA@PMMA}} = 3.2 \times 10^{-3} \text{ min}^{-1}$). The bi-exponential decay function of **SP-2/DA@PMMA** capsules was ascribed to the presence of the SP-2 dyes within the DA solid matrix and/or PMMA shell. However these rates were lower than those reported in less polar liquid solvents ($k^{\text{SP-2}} = 0.312 \text{ min}^{-1}$ ⁶⁴ and $k^{\text{SP-1}} > 4.7 \times 10^{-3} \text{ s}^{-1}$), which was ascribed to both the higher polarity and rigidity of the solid matrix.⁵⁹

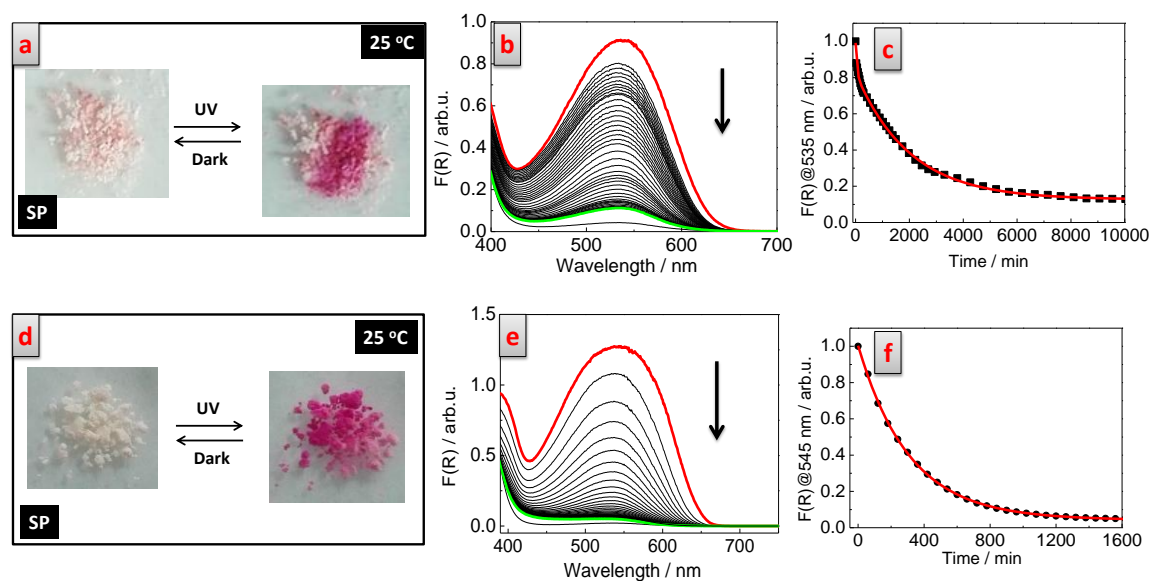


Figure 3.34: digital images of the freeze-dried a) **SP-2/DA@PMMA** and d) **SP-1/DA@PMMA** capsules before and after irradiating with UV light; absorption spectra of b) **SP-2/DA@PMMA** and e) **SP-1/DA@PMMA** capsules recorded in the dark at room temperature (green line) after irradiation (red line) and after the decoloration process (black lines); kinetic profile of the color fading of c) **SP-2/DA@PMMA** and f) **SP-1/DA@PMMA** capsules at the photochrome absorption maximum at 25 °C.

Noteworthy, no relevant degradation was observed after three irradiation cycles (**Figure 3.35c-d**), confirming the good stability of the dyes even in a rigid matrix.

Given the very slow recovery of the initial non-colored SP form, it was possible to study the fading kinetics of the solid-filled capsules at different temperatures (25, 30 and 35°C), below the T_m^{DA} to avoid the melting and the induced $SP \rightarrow MC$ transformation. The fading rates increased with temperature, as expected for a thermal isomerization reaction (**Figure 3.35**, **Table 3.7**). The k (min^{-1}) values obtained decreased two orders of magnitude when passing from measuring at 25°C to 35°C. Interestingly, the decoloration kinetics of **SP-2/DA@PMMA** capsules changed from a bi-exponential to a monoexponential decay function. This is possibly due to the higher mobility of the photochromic molecules at 35°C and the less contribution of possible aggregates in the solid PCM that could contribute to this bi-exponential decay.

T(°C)	k (min ⁻¹)	
	SP-2/DA@PMMA	SP-1/DA@PMMA
25	k ₁ = 2.1 · 10 ⁻² k ₂ = 4.9 · 10 ⁻⁴	3.2 · 10 ⁻³
30	k ₁ = 2.3 · 10 ⁻³ k ₂ = 6.8 · 10 ⁻⁴	9.5 · 10 ⁻³
35	2.9 · 10 ⁻³	3 · 10 ⁻²

Table 3.7: fading rate constant of the **SP-2/DA@PMMA** and **SP-1/DA@PMMA** capsules at different temperatures.

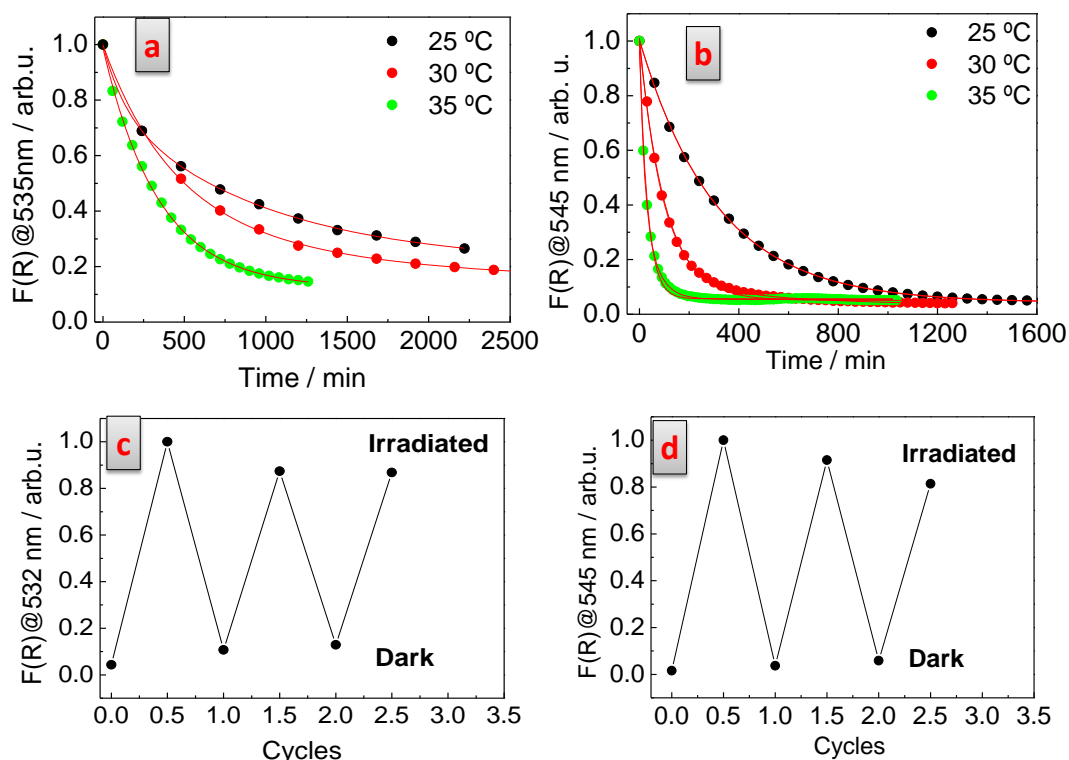


Figure 3.35: temperature dependent fading kinetics of a) **SP-2/DA@PMMA** and b) **SP-1/DA@PMMA**; fatigue resistance study of c) **SP-2/DA@PMMA** and d) **SP-1/DA@PMMA** capsules.

The presence of aggregates in spiropyran solution is a quite well-known phenomenon that originates principally from the low solubility of the zwitterionic MC isomer. This should be even more accentuated in low-polar media such as the DA. The presence of MC aggregates in the capsules could be detrimental for the photochromic performances (slower fadings) and dye stability.^{6,65-67} To investigate the presence of aggregates in these materials, different bulk DA solutions with different **SP-2, 1** concentrations were prepared and their spectral properties were measured. Spectral changes were observed at high dye loadings (3.3 wt. %) suggesting partial MC aggregation. These spectral changes consisted of:

i) significant residual absorption in the visible region, in the dark, possibly related to partial stabilization of aggregated MC (**Figure 3.36a-b**). The residual color in the dark disappear for less concentrated **SP-2, 1/DA** solutions (**Figure 3.36c-d**).

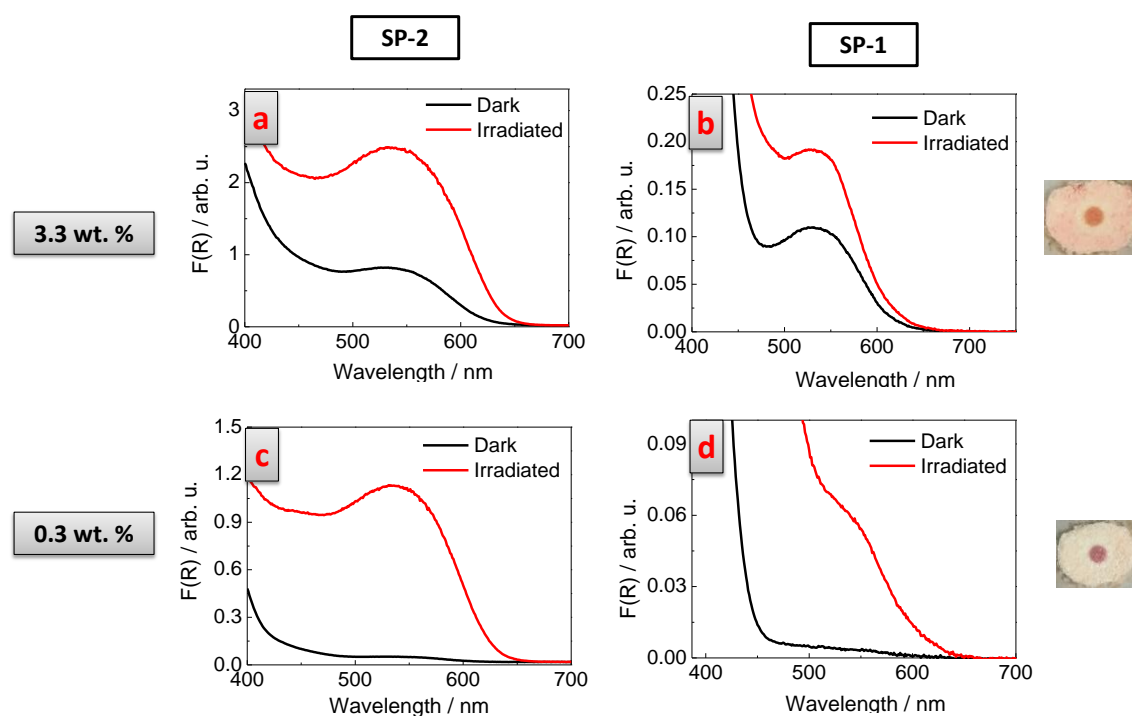


Figure 3.36: absorption spectra before (black line) and after irradiation (red line) of a) **SP-2/DA** and b) **SP-1/DA** solutions (3.3 wt. %) and c) **SP-2/DA** and d) **SP-1/DA** solutions (0.3 wt. %).

ii) bathochromic shifts and broadening of the MC absorption band, indicating the formation of J-stacks (**Figures 3.37a-b**).⁶ Similar features, red shift and broadening of the MC band, was observed when the concentration of the MC is higher (at the photostationary state, **Figure 3.37c-d**), thus indicating non-negligible photochrome aggregation. Nevertheless, this did not detrimentally affect the photochromic behavior of the materials.

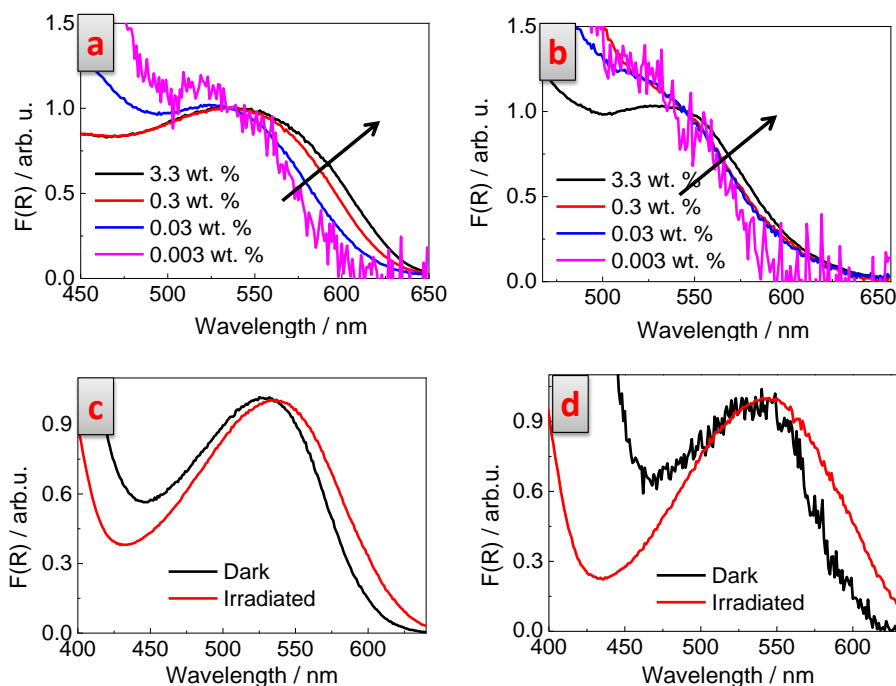


Figure 3.37: comparison of the normalized spectra of the absorption spectra of a) **SP-2/DA** and **SP-1/DA** solutions at different concentrations and normalized spectra of the irradiated and non-irradiated c) **SP-2/DA@PMMA** and d) **SP-1/DA@PMMA** microcapsules.

- **Photochromic study of the SP-2, 1/DA@PMMA capsules at $T > T_m^{DA}$**

Irradiation with visible light of the red-colored capsules kept at 60°C, induced the SP formation and the consequent loss of the red color and of the visible absorption band initially observed at this temperature (**Figure 3.38a, c**). This process was spontaneously reverted in the dark confirming the reverse photochromism of the **SP-2/DA@PMMA** and **SP-1/DA@PMMA** capsules, when these are kept at $T > T_m^{DA}$. By changing the PCM, the temperature at which the capsules switch from direct to reverse photochromism could be tuned. The recoloration rate occurred at higher rates ($k^{SP-2/DA@PMMA}=0.342 \text{ min}^{-1}$ and $k^{SP-1/DA@PMMA}=0.84 \text{ min}^{-1}$) than for the analogous capsules filled with liquid NA at 25 °C (**Figure 3.15, Table 3.2**), probably owing to the temperature effect on the thermal recovery of the most stable MC species (**Figure 3.38b, c, e, f**).

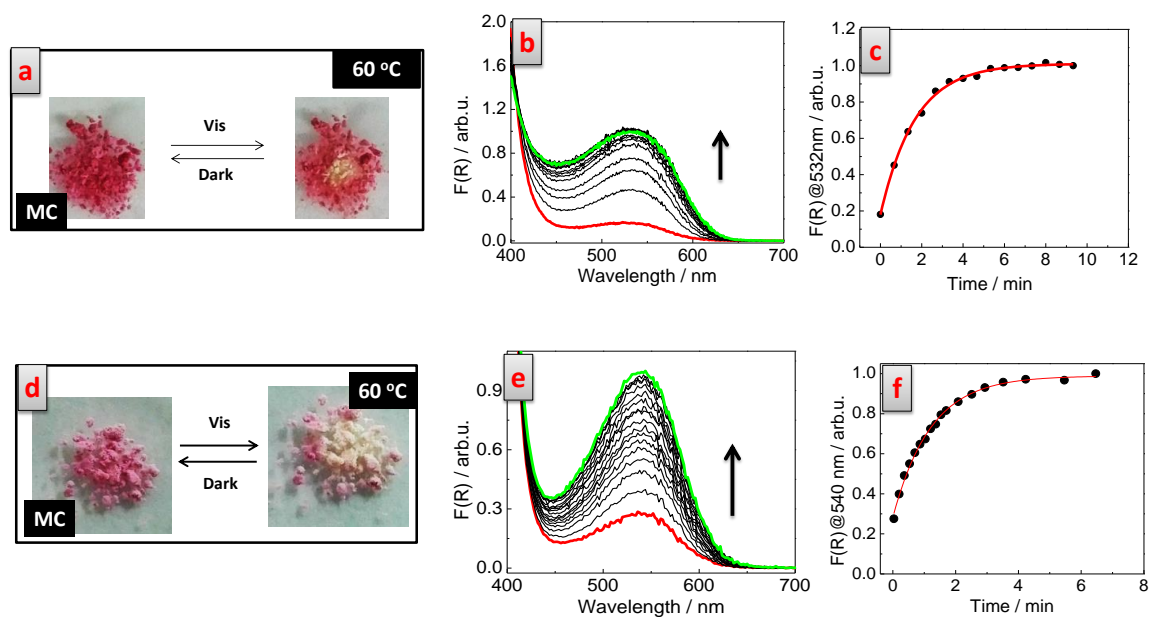


Figure 3.38: digital images of the freeze dried a) **SP-2/DA@PMMA** and b) **SP-1/DA@PMMA** capsules before and after irradiating with Vis light at 60°C, absorption spectra of b) **SP-2/DA@PMMA** and e) **SP-1/DA@PMMA** capsules recorded in the dark at 60°C and at different time delays before (green) and after (red) irradiation; kinetic profile of the color recovery of c) **SP-2/DA@PMMA** and f) **SP-1/DA@PMMA** capsules at the photochrome absorption maximum at 60 °C.

Once more, their performance was not affected by thermal degradation of the material as showed by the different photoinduced fading/recoloration cycles performed at 60°C (**Figure 3.39a-b**). By comparing this photochromism to that observed at 25 °C, it can be concluded that **SP-2, 1/DA@PMMA** capsules can interconvert between direct and reverse photochromism upon temperature variation. Moreover, the crossing of the T_m^{DA} produced thermochromism since the SP or MC form of the spiropyran was selectively stabilized in the solid and liquid DA, respectively. For both capsules, the thermochromic transition, and thus, the establishment of one of the two photochromic behavior was found to be reversible, though further irradiation with visible light was required to fully reestablish the colorless state of the capsules at 25 °C once the temperature had been reduced below the DA melting point.

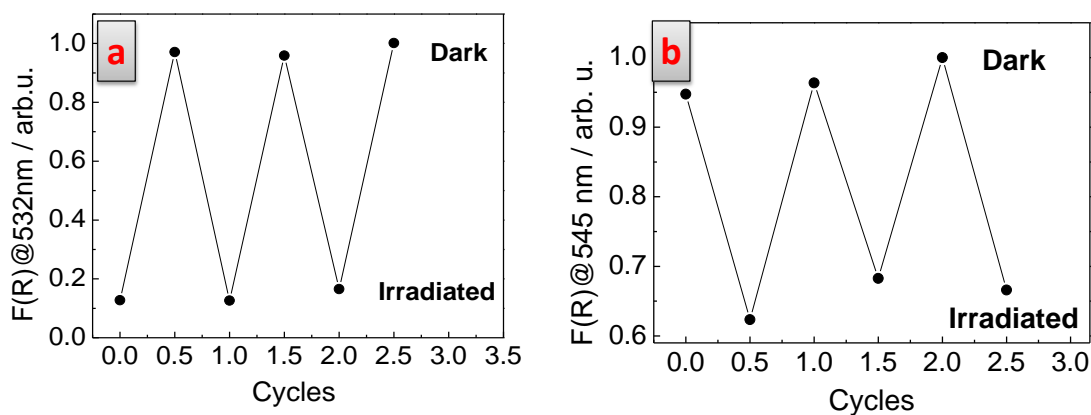
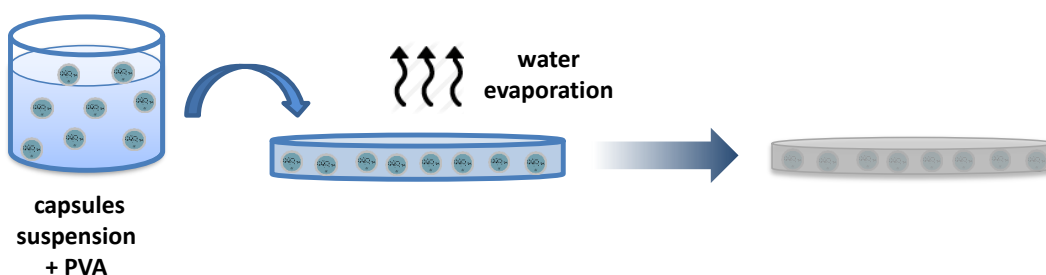


Figure 3.39: absorbance at 532 nm of the faded (irradiated) and colored (dark) a) **SP-2/DA@PMMA** and b) **SP-1/DA@PMMA** capsules during 3 cycles of visible light induced fading and recoloration in the dark at 60 °C.

3.3.3 Photochromic films

Flexible poly(vinylalcohol) (PVA) and polyacrylamide (PA) films, with the capsules embedded in, were prepared by casting a water suspension of the capsules in the presence of the water-soluble polymer (PVA or PA) on a petri plate. Upon evaporation of the water for 24-48 h, the water-soluble polymer precipitates entrapping the capsules in the solid matrix (**Scheme 3.6**). The dried film could be easily peeled out from the substrate.



Scheme 3.6: scheme of the preparation of polymeric films with the particles.

For these films the capsules obtained from **SP-1**, **SP-2** and **SP-5** in different media (NA, NA-DPA and PDMS-OH for **SP-1**, DA for **SP-2** and NA, TDOH-BA for **SP-5**) were used to show the color tunability and the switchable photochromism could be transferred to solid films, using these dyes (see the experimental section

7.3.3.5). The films were cut and the lateral part was inspected by SEM. Interestingly, in all cases the capsules maintained their shape and structure (Figure 3.40) after being embedded.

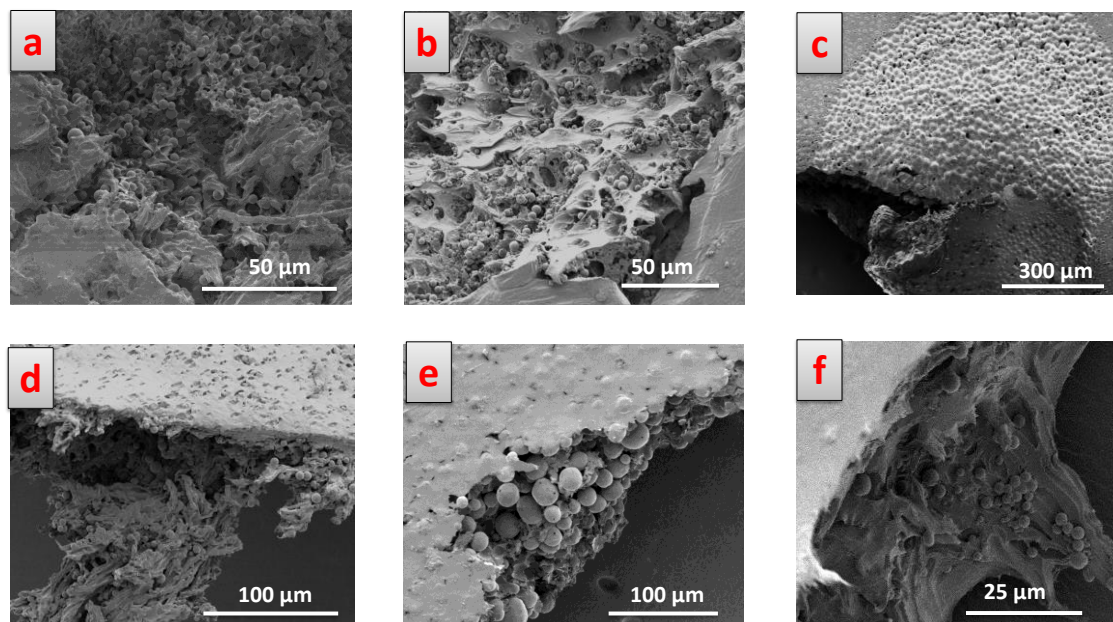


Figure 3.40: SEM images of sections obtained from: a) SP-1/NA@PMMA@PVA, b) SP1/NA-DPA@PMMA@PA, c) SP-1/PDMS-OH@PMMA@PVA, d) SP-5/NA@PMMA@PVA, e) SP-5/TDOH-BA@PES@PVA and f) SP-2/DA@PMMA@PVA films.

3.3.3.1 Tunable reverse photochromic films

As expected, the resulting films were all colored in the dark, according to the stabilized MC form of the combined dye/core medium system and all preserved the reverse photochromism showed by the capsules (Table 3.8, Figure 3.41).

From each photochromic dye (i.e. SP-1 and SP-5) it was possible to prepare two or more differently colored films, which could be used as light-induced rewritable device. As a proof of this concept, we explored the use of films containing SP-1- and SP-5-loaded capsules as rewritable films.

Solvent		SP-1			SP-5	
		NA	PDMS-OH	NA-DPA	NA	TDOH-BA
λ_{\max} (nm)	Microcapsules	519	550	425 (shoulder)	440	388 & 546
	Films	525	550	422 (shoulder)	446	388 & 553
k (min ⁻¹)	Microcapsules	0.012	0.042	0.0038	0.16	0.19
	Films	0.024	0.040	0.0040	0.15	0.13

Table 3.8: maximum absorption wavelengths (λ_{\max} in nm) and rate constants (k in min⁻¹) of the thermal recoloration process in the dark of SP-1 and SP-5 in microcapsules and polymeric films.

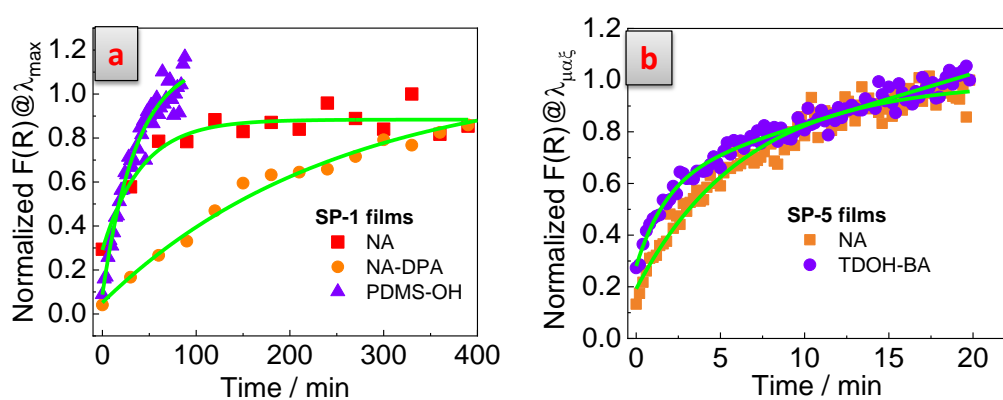


Figure 3.41: a) study of the recoloration kinetics in the dark at λ_{\max} for the films with **SP-1/NA@PMMA**, **SP-1/PDMS-OH@PMMA** and **SP-1/NA-DPA@PMMA** capsules; b) study of the recoloration kinetics in the dark at λ_{\max} for films with **SP-5/NA@PMMA** and **SP-5/TDOH-BA@PES** capsules.

Noticeably, by using only one single photochromic dye (e.g., **SP-1**), multicolored films could be written and erased several times with different black masks or handwriting with a 532-laser pointer and writings and draws with very good contrast and spatial resolution could be obtained (**Figure 3.42**).

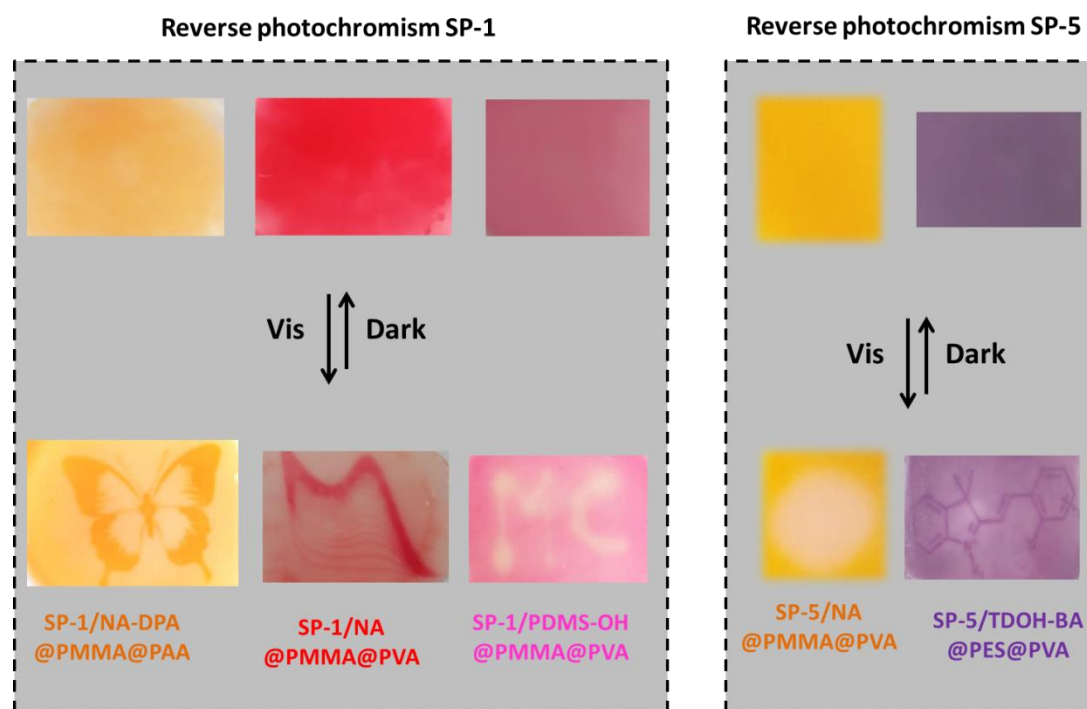


Figure 3.42: PVA and PA films obtained from the capsules of **SP-1** and **SP-5** with different core materials that provide reverse photochromism of different colors.

3.3.3.1 Switchable reverse photochromic films

When the **SP-2/DA@PMMA@PVA** film was illuminated with UV light in the presence of ICN2 shaped mask, it colored selectively in the non-covered regions (**direct photochromism**), as the loaded capsules had a solid interior that stabilize the colorless SP isomer (**Figure 3.43a**). Equivalent photoinduced color and color fading kinetics were measured for the film and the free capsules under these conditions (**Figure 3.43b, d**). Upon heating at 60 °C, coloration of the film in the dark was induced (thermochromism). At this temperature visible light light-induced fading was observed, as a result of the **reverse photochromism**. Also in this case an ICN2 pattern could be drawn by using a mask (**Figure 3.43c**). The thermochromic transition and the switch of the photochromic behavior were found to be completely reversible as the film recovered the initial non-colored state (and direct photochromism) after reducing the temperature and irradiating with visible light.

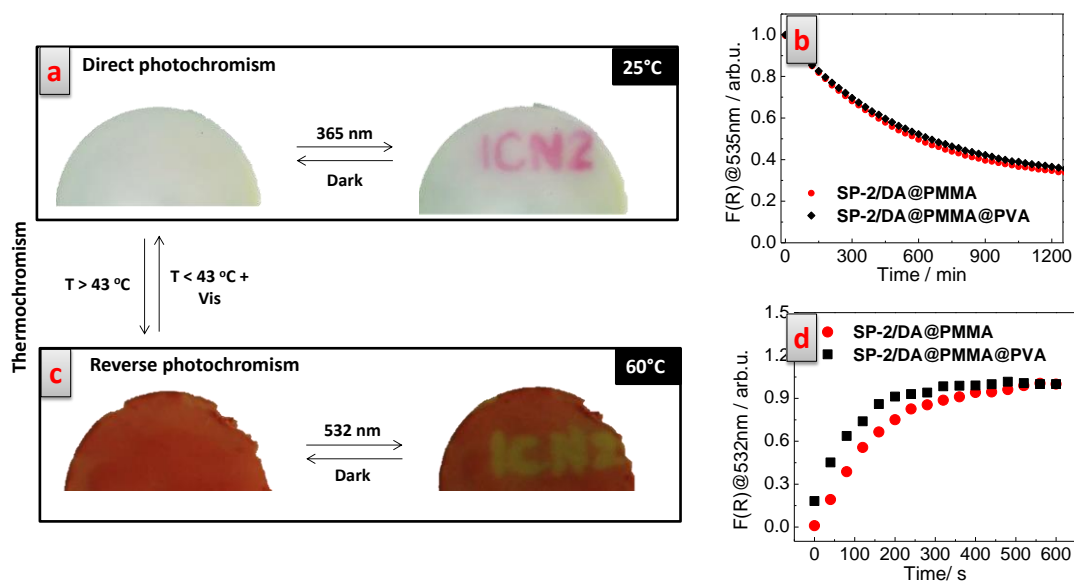


Figure 3.43: a) digital photos of the non-irradiated (left) and irradiated (right) **SP-2/DA@PMMA@PVA** film kept at 25°C, with UV radiation (UV lamp @ 365 nm, 2.7 mW/cm², 90 s) and in presence of an ICN2-shaped mask (**direct photochromism**); c) digital photos of a non-irradiated (left) and irradiated (right) **SP-2/DA@PMMA@PVA** film kept at 60°C with visible light and in the presence of ICN2-shaped mask (white light torch, **reverse photochromism**), kinetic profiles of the b) color fading and d) recoloration of the **SP-2/DA@PMMA@PVA** film at the photochrome absorption maximum ($\lambda_{\text{max}} = 535\text{ nm}$) and comparison with the fading and recoloration kinetics of **SP-2/DA@PMMA** capsules.

3.4 Summary

In summary, we reported a novel, reaction-free, universal, and straightforward strategy to achieve tunable and switchable reverse photochromism in solid materials. In particular for the **tunability** of reverse photochromism:

i) we demonstrated that distinct colors and recoloration rates could be obtained for commercially available spiropyrans by simply varying the nature of the dye or the surrounding medium without the need of chemical derivatization.

ii) non-volatile lipophilic media were used in all the cases to control the equilibrium between the MC and MCH⁺ forms and therefore the photochromic performances.

iii) we showed these mixtures could be trapped in core-shell capsules that in most of the cases preserved the photochromic performances (kinetics and absorption properties) of the initial mixtures.

iv) polymer films with up to three different photochromic responses (i.e., colors and isomerization kinetics) could be obtained from the same commercial dye by simply embedding the microcapsules in the polymeric matrix. The strategy provides an unprecedented tunability of the photochromic properties in the solid state.

v) Considering that more colors could be obtained by combining capsules of different types, which might also display thermochromic, halochromic, and/or fluorescence behavior, functional materials could be prepared from spiropyran dyes exhibiting multicolored and multi-stimuli responses.

- for controlling the photochromic behavior (**switching** direct/reverse):

i) we demonstrated that by preparing dye-loaded polymer capsules filled with a non-volatile acidic solid phase-change material, a thermochromic transition and a reversible interconversion between direct and reverse photochromism could be obtained, by thermally controlling the state of the encapsulated material (liquid vs solid).

ii) we achieved for the first time polymeric films, containing the capsules, with thermochromism and switchable photochromism, without requiring the addition of external additives or chemical modification of the photochromic dyes and the surrounding matrix.

Our approach could be highly relevant for the fabrication of different functional devices, from optical memories to writing/erasing displays, photoprotective coatings and anti-counterfeiting technologies.

The application of this approach to other photochrome families (e.g. spirooxazines), is currently under investigation.

3.5 References

1. R. C. Bertleson, S. Maeda, B. Van Gemert, Vol. 1; J. C. Crano, R. J. Guglielmetti, Eds.; Plenum: New York, **1999**.
2. M. Irie, *Chem. Rev.* **2000**, 100, 1683.
3. S. N. Corns, S. M. Partington, A. D. Towns, *Color. Technol.* **2009**, 125, 249.
4. V. A. Barachevsky, *J. Photochem. Photobio., A* **2018**, 354, 61.
5. S. Aiken, R. J. L. Edgar, C. Gabbutt, B. M. Heron, *Dyes Pigm.* **2018**, 149, 92.
6. R. Klajn, *Chem. Soc. Rev.* **2014**, 43, 148.
7. R. Pardo, M. Zayat, D. Levy, *Chem. Soc. Rev.* **2011**, 40, 672.
8. U. Pischel, *Angew. Chem., Int. Ed.* **2007**, 46, 4026.
9. P. L. Gentili, *Phys. Chem. Chem. Phys.* **2011**, 13, 20335.
10. P. L. Gentili, *Dyes Pigm.* **2014**, 110, 235.
11. M. I. Khazi, W. Jeong, J.-M. Kim, *Adv. Mater.* **2018**, 30, 1705310.
12. W. Wang, L. Liu, Y. Yin, *Small Methods* **2018**, 2, 1700273.
13. Z. Gao, L. Liu, Z. Tian, Z. Feng, B. Jiang, W. Wang, *ACS Appl. Mater. Interfaces* **2018**, 10, 33423.
14. T. Zhang, L. Sheng, J. Liu, L. Ju, J. Li, Z. Du, W. Zhang, M. Li, S. X. A. Zhang, *Adv. Funct. Mater.* **2018**, 28, 1705532.
15. G. Petriashvili, M. P. De Santo, L. Devadze, T. Zurabishvili, N. Sepashvili, R. Gary, R. Barberi, *Macromol. Rapid Commun.* **2016**, 37, 500.
16. A. Abdollahi, K. Sahandi-Zangabad, H. Roghani-Mamaqani, *ACS Appl. Mater. Interfaces* **2018**, 10, 39279.
17. A. Abdollahi, K. Sahandi-Zangabad, H. Roghani-Mamaqani, *Langmuir* **2018**, 34, 13910.
18. T. Yamaguchi, Y. Kobayashi, J. Abe, *J. Am. Chem. Soc.* **2016**, 138, 906.
19. S. Hatano, T. Horino, A. Tokita, T. Oshima, J. Abe, *J. Am. Chem. Soc.* **2013**, 135, 3164.
20. S. Helmy, F. A. Leibfarth, S. Oh, J. E. Poelma, C. J. Hawker, J. R. de Alaniz, *J. Am. Chem. Soc.* **2014**, 136, 8169.
21. W. Tian, J. Tian, *Dyes Pigm.* **2014**, 105, 66.
22. S. Keum, S. Roh, S. Kim, S. Lee, C. Cho, S. Kim, K.-N. Koh, *Bull. Korean Chem. Soc.* **2006**, 27, 187.
23. Y. Wu, T. Sasaki, K. Kazushi, T. Seo, K. Sakurai, *J. Phys. Chem. B* **2008**, 112, 7530.

24. S. Zhang, Q. Zhang, B. Ye, X. Li, X. Zhang, Y. Deng, *J. Phys. Chem. B* **2009**, 113, 6012.
25. J. D. Winkler, K. Deshayes, *J. Am. Chem. Soc.* **1987**, 109, 2190.
26. E. Inoue, H. Kokado, I. Shimizu, H. Kobayashi, Y. Takakashi, *Bull. Chem. Soc. Jpn.* **1972**, 45, 1951.
27. J. Vallet, J.-C. Micheau, C. Coudret, *Dyes Pigm.* **2016**, 125, 179.
28. H. Chen, Y. Liao, *J. Photochem. Photobiol., A* **2015**, 300, 22.
29. I. Shimizu, H. Kokado, E. Inoue, *Bull. Chem. Soc. Jpn.* **1969**, 42, 1730.
30. J. D. Winkler, K. Deshayes, B. Shao, *J. Am. Chem. Soc.* **1989**, 110, 770.
31. C. Zhang, Z. Zhang, M. Fan, W. Yan, *Dyes Pigm.* **2008**, 76, 832.
32. J. D. Winkler, C. M. Bowen, V. Michelet, *J. Am. Chem. Soc.* **1998**, 120, 3237.
33. R. A. Kopelman, S. M. Snyder, N. L. Frank, *J. Am. Chem. Soc.* **2003**, 125, 13684.
34. J. T. C. Wojtyk, P. M. Kazmaier, E. Buncel, *Chem. Mater.* **2001**, 13, 2547.
35. X. Guo, D. Zhang, G. Zhang, D. Zhu, *J. Phys. Chem. B* **2004**, 108, 11942.
36. M. Tanaka, M. Nakamura, M. A. A. Salhin, T. Ikeda, K. Kamada, H. Ando, Y. Shibutani, K. Kimura, *J. Org. Chem.* **2001**, 66, 1534.
37. M. Tanaka, T. Ikeda, Q. Xu, H. Ando, Y. Shibutani, M. Nakamura, H. Sakamoto, S. Yajima, K. Kimura, *J. Org. Chem.* **2002**, 67, 2223.
38. M. Inouye, Y. Noguchi, K. Isagawa, *Angew. Chem., Int. Ed.* **1994**, 33, 1163; *Angew. Chem.* **1994**, 106, 1226.
39. C. J. Roxburgh, P. G. Sammes, *Dyes Pigm.* **1995**, 27, 63.
40. S. Schneider, H. Grau, J. Ringer, *Mol. Cryst. Liq. Cryst. Sci. Technol., Sect. A* **1994**, 246, 267.
41. S. Giordani, F. M. Raymo, *Org. Lett.* **2003**, 5, 3559.
42. F. M. Raymo, S. Giordani, *J. Am. Chem. Soc.* **2001**, 123, 4651.
43. S. Giordani, M. A. Cejas F. M. Raymo, *Tetrahedron* **2004**, 60, 10973.
44. T. Yamaguchi, A. Maity, V. Polshettiwar, M. Ogawa, *Inorg. Chem.* **2018**, 57, 3671.
45. K. Kinashi, S. Nakamura, M. Imamura, K. Ishida, Y. Ueda, *J. Phys. Org. Chem.* **2012**, 25, 462.
46. K. Kinashi, S. Nakamura, Y. Ono, K. Ishida, Y. Ueda, *J. Photochem. Photobiol., A*, **2010**, 213, 136.
47. D. Levy, *Chem. Mater.* **1997**, 9, 2666.
48. T. R. Evans, A. F. Toth, P. A. Leermakers *J. Am. Chem. Soc.* **1967**, 89, 5060.

49. F. Zhang, X. Zou, W. Feng, X. Zhao, X. Jing, F. Sun, H. Rena, G. Zhu, *J. Mater. Chem.* **2012**, 22, 25019.
50. M. Piantek, G. Schulze, M. Koch, K. J. Franke, F. Leyssner, A. Krüger, C. Navío, J. Miguel, M. Bernien, M. Wolf, W. Kuch, P. Tegeder, J. I. Pascual, *J. Am. Chem. Soc.* **2009**, 131, 12729.
51. Z. Qiu, H. Yu, J. Li, Y. Wang, Y. Zhang, *Chem. Commun.* **2009**, 3342.
52. W. Wang, J. Hu, M. Zheng, L. Zheng, H. Wang, Y. Zhang, *Org. Biomol. Chem.* **2015**, 13, 11492.
53. E. B. Gaeva, V. Pimienta, S. Delbaere, A. V. Metelitsa, N. A. Voloshin, V. I. Minkin, G. Vermeersch, J. C. Micheau, *J. Photochem. Photobiol. A* **2007**, 191, 114.
54. A. Sugahara, N. Tanaka, A. Okazawa, N. Matsushita, N. Kojima, *Chem. Lett.* **2014**, 43, 281.
55. T. Horiguchi, Y. Koshiba, Y. Ueda, C. Origuchi, K. Tsutsui, *Thin Solid Films* **2008**, 516, 2591.
56. M. A. White, M. Leblanc, *J. Chem. Educ.* **1999**, 76, 1201.
57. K. Kinashi, T. Horiguchi, K. Tsutsui, K. Ishida, Y. Ueda, *J. Photochem. Photobiol. A* **2010**, 213, 189.
58. CRC Handbook of Chemistry and Physics, Internet Version, <http://www.hbcnpnetbase.com> (accessed November 21, 2018); Lide, D. R. Ed.; CRC Press: Boca Raton, FL, **2005**.
59. N. Vázquez-Mera, C. Roscini, J. Hernando, D. Ruiz-Molina, *Adv. Optical Mater.* **2013**, 1, 631.
60. N. A. Vázquez -Mera, C. Roscini, J. Hernando, D. Ruiz-Molina, *Adv. Funct. Mater.* **2015**, 25, 4129.
61. M. Li, O. Rouaud, D. Poncelet, *Int. J. Pharm.* **2008**, 363, 26.
62. A. Loxley, B. Vincent, *J. Colloid Interface Sci.* **1998**, 208, 49.
63. N. P. Ernsting, *Chem. Phys. Lett.* **1989**, 159, 526.
64. F. M. Raymo, S. Giordani, C. Gables, A. J. P. White, D. J. Williams, *J. Org. Chem.* **2003**, 68, 4158.
65. V. A. Krongauz, E. S. Goldburt, *Nature* **1978**, 271, 43.
66. Y. Onai, K. Kasatani, M. Kobayashi, H. Shinohara, H. Sato, *Chem. Lett.* **1990**, 1809.
67. H. Sato, H. Shinohara, M. Kobayashi, T. Kiyokawa, *Chem. Lett.* **1991**, 1205.

CHAPTER 4

Multi-stimuli responsive materials based on ketocyanine dyes

In this chapter it is reported the development of a novel and universal methodology for the preparation of pH and temperature-responsive solid materials based on ketocyanine dyes. This was achieved by means of the microstructuration of phase change materials together with a dye-developer duo and the subsequent encapsulation into core-shell capsules. The strategy allows easy tunability of the temperature transition by changing the nature of the phase change material and of the absorption spectra by changing the interaction between the dye and the color developer. Finally we ended up with a solid material with three colored-states (one of the states absorbing almost in the NIR region) that allows going from one state to the other changing the pH and/or the temperature of the environment.

4.1 Introduction

4.1.1 Spectral tunability of thermochromic materials in the visible and NIR spectral regions

The different strategies to obtain thermochromic materials in the solid state have been presented in the introduction (section 1.3). Most of the reported systems present color changes in the visible region between two forms. Tunability of the spectral properties of both forms can be accomplished, though it is not straightforward. This tunability becomes even more difficult if one of the two forms has to absorb and/or emit in the near infrared region (NIR). For example leuco-dye based thermochromic materials are based on spirolactones or spiropyrans that most of the times have one colorless form (absorbing in the UV) and a colored form (absorbing in the visible region). The parent structure of the compounds of this family can be modified through substitution, but achieving tunability scanning throughout the visible up to the NIR region is still a hard task. A similar conclusion could be given for the other strategies.

Recently, achieving dyes absorbing or emitting in the NIR region is becoming particularly interesting for the different applications in which they could be used (telecommunications,¹ bio-imaging,² information security display,³ solar energy conversion and thermal energy saving). Lots of research is being devoted to obtain such molecules.⁴⁻⁹ Even more interestingly and challenging is accomplishing systems able to selectively absorb or emit in this region (NIR) through external stimulus, such as temperature. For example molecular NIR-thermochromic materials could be used in smart windows to filter, selectively during hot sunny days, the NIR portion of the solar radiation (around 50% of the solar energy), reducing the necessity of using energy-consuming air conditioning devices. Thermo(fluoro)chromic dyes working in the NIR could be also used for imaging in biological systems² in which having NIR absorbing/emitting dyes⁴⁻⁷ would allow deeper penetration in detection and avoids the use of visible light that may cause tissue degradation. However, such tunable thermochromic dyes up to the NIR region, are still scarcely available.

A low-energy thermochromic material can be obtained by inducing a reversible aggregation/dissociation of dyes¹⁰ triggered by a temperature variation of the solution. A nice example of this approach is based on a butyronitrile solution of a Pt complex (alkynylplatinum (II) terpyridyl), which presents absorption close to the NIR ($\lambda_{\text{max}} = 690 \text{ nm}$, **Figure 4.1a-b**) at 190K due to dye aggregation and in the Vis region ($\lambda_{\text{max}} = 410 \text{ nm}$, yellow color) when the temperature increases up to 230 K (the monomeric form is recovered).¹¹

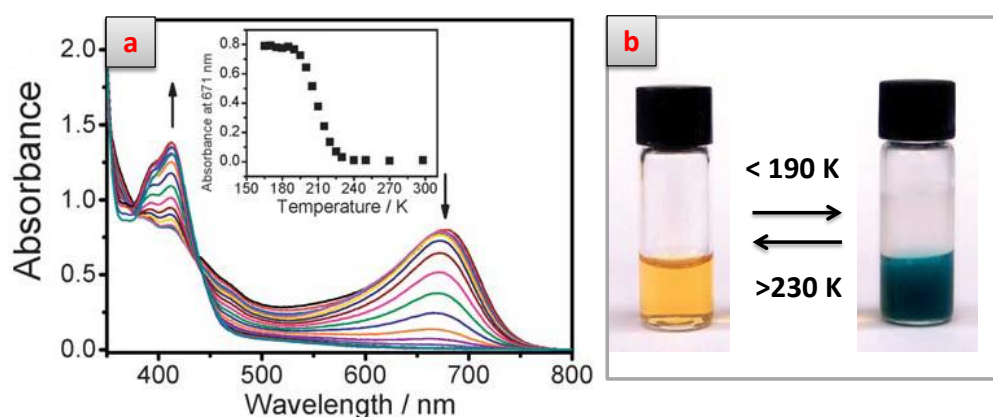


Figure 4.1: a) variable-temperature UV-Vis spectra of the Pt complex in butyronitrile within the temperature range 165 to 298 K. Inset: plot of the absorbance at 671 nm vs temperature; b) photograph illustrating the colour change of alkynylplatinum(II) terpyridyl complex solution at room temperature (left) and low temperature (right) in butyronitrile. Data adapted from ref. 11.

Another possibility is by designing and synthesizing halochromic dyes that absorb in the NIR in the protonated or non-protonated state.¹² As shown in **Figure 4.2a**, Wang *et al.* reported a new family of diazapentalene-containing dyes that in solution exhibit temperature-induced variations within the visible and NIR spectral region (500–1200 nm) around 50–60 °C. **Figure 4.2b** shows the spectra recorded at different temperatures (from 120°C to RT) of a diazapentalene derivative. The color changes from greenish ($\lambda_{\text{max}} = 680 \text{ nm}$, non-protonated form at 120°C) to colorless ($\lambda_{\text{max}} = 980 \text{ nm}$, protonated form) when the temperature drops to RT.

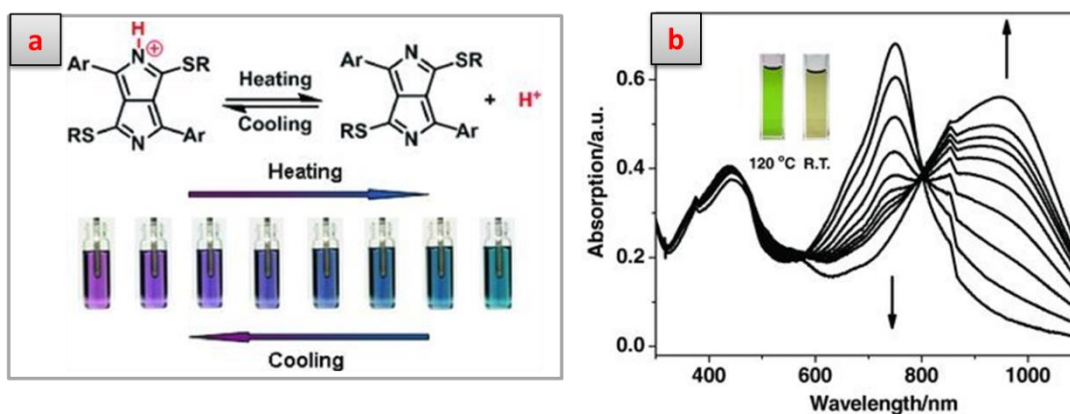


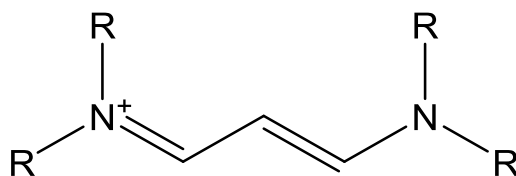
Figure 4.2: a) general structure of diazapentalene dyes before and after a temperature-induced loss of proton and the corresponding color changes observed in solution (chlorobenzene), b) changes in absorption spectra in chlorobenzene ($\sim 10^{-5}$ M) upon cooling from 120 °C to room temperature of a diazapentalene derivative. Inset: photographs of the protonated compound in chlorobenzene at low and high temperatures, respectively. Data adapted from ref. 12.

In summary, though successful, the strategies showed above have been explored to obtain switchable NIR thermochromic systems in solution (e.g., organic solvents) and not in solid materials, which are eventually more relevant. This has become a real challenge for these materials having real applications.

Cyanine dyes could represent a promising family of dyes to be used in thermochromic materials. The absorption and emission spectra are easily modulable by changing the conjugation length. The optical properties of these dyes are also very dependent on the pH and polarity of the medium in which are dissolved. If a strategy, that through the temperature, the color change of these cyanine dyes could be modulated, a new generation of highly tunable thermochromic materials would be achieved.

4.1.2 Cyanine Dyes

Cyanine dyes are molecules containing a polymethine-bridge, which is made up from an odd number of methine groups (CH) bound together by alternating single and double bonds, connecting two nitrogen atoms, usually belonging to heterocyclic rings.



Scheme 4.1: general structure of cyanine dyes.

One of the two nitrogen is in its cationic ammonium form (with an electron-withdrawing character), and the other is in its tertiary amine structure (electron-donating effect) providing a delocalized charge (**Scheme 4.1**). They have outstandingly high extinction coefficients often exceeding $100,000 \text{ L}\cdot\text{mol}^{-1}\text{cm}^{-1}$. The absorption and emission wavelength can be finely tuned by a proper selection of the substituents in the extremes of the molecule and by the length of the conjugated chain. Because the magnitude of the shift can be as high as several tenths of nanometers, cyanine dyes are nowadays one of the most used type of dye absorbing and/or emitting in the near infrared (NIR) region.

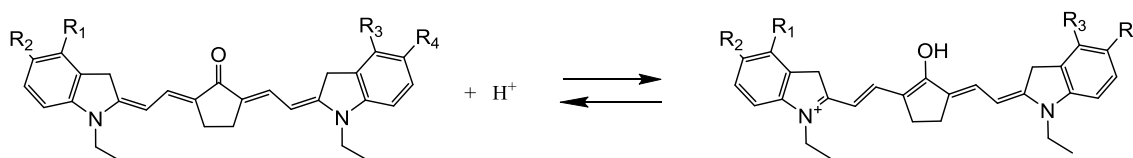
These dyes can be used in a wide range of applications, like sensitizers in organic solar cells¹³, as well as in up-converting materials¹⁴, due to their intense and broad absorption bands in the visible and NIR regions, as indicators for solvent polarity¹⁵/pH sensing¹⁶ due to their high sensitivity on the medium and its solvatochromic properties, and recently they have been also used for labelling nucleic acids¹⁷ or as novel dyes for photodynamic therapy in bioapplications.¹⁸

4.1.3 Ketocyanine Dyes

Among all the family of cyanine dyes, ketocyanine dyes were selected as the case of study in this work. Ketocyanine dyes were initially reported and studied in the early 2000 by Sergei Militov *et al.*¹⁹ Apart from the typical solvatochromism, these dyes are able to switch significantly the optical properties depending on the pH of the medium. In acidic solution these dyes are in a keto-enol equilibrium between two forms (**Scheme 4.2**): the highly conjugated protonated form (the protonation occurs in the carbonyl of the cyclopentanone), absorbing at longer wavelength (**Scheme 4.2**), and the non-protonated form, that absorbs at higher energy (**Scheme 4.2**). Depending on the pH of the medium, the equilibrium is shifted towards one form or the other.

Similarly to other cyanine dyes, these present very high extinction coefficients for both forms ($2.7 \times 10^5 \text{ L} \cdot \text{mol}^{-1} \cdot \text{cm}^{-1}$), which allows the fabrication of deep-colored pH chromic sensors using very small dye concentrations. These dyes, which usually present also luminescent properties have been used extensively as optical sensors (pH, solvent polarity)²⁰ and proton selective ionophores in waveguide devices and in polyvinylchloride membranes.^{21,22}

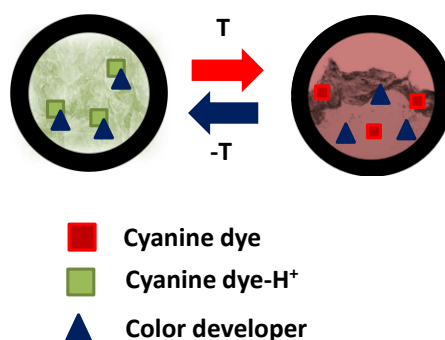
However, as far as we know, there are no examples of ketocyanine dyes where the shift of the equilibrium shown in **Scheme 4.2** is achieved by the temperature-induced melting/solidification of media able to selectively protonate the dye, which would be the base to build cyanine -based thermochromic materials.



Scheme 4.2: chemical structure of the equilibrium of the two forms of ketocyanine dyes in the presence of an acid. Data adapted from ref. 21.

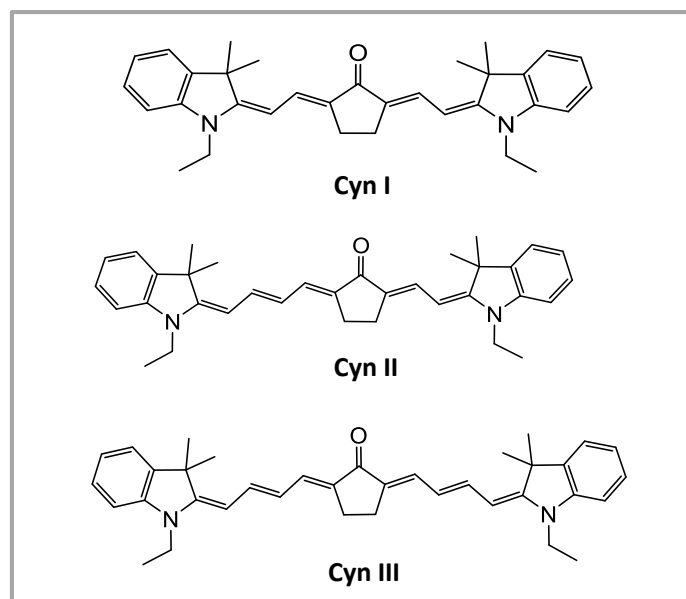
4.1.4 Designing cyanine-based thermochromic materials

In this chapter we propose the use of cyanine dyes. The color change obtained in these thermochromic systems arises from acid-base reactions or complex formations of cyanine dyes with acids or hydrogen-bonding molecules. This design is inspired from phase change material mixtures used in leuco dyes-based commercially available thermochromic materials (explained in the introduction, section 1.3.3). Therefore, for the material to be developed it is required: i) **cyanine dyes**, which must be halochromic and of different conjugation length to be able to cover distinct spectral regions (from visible to NIR) in one of the two states of the thermochromic transition, ii) a **color developer** that interacts in two different ways in the solid and in the liquid state of the solvent and iii) a solvent or phase change material (**PCM**) that through its solid-liquid transition triggers the dye-color developer interactions. The encapsulation, as showed in the previous chapter, would allow transferring the behavior observed in bulk mixture to solid functional materials (**Figure 4.3**).



Scheme 4.3: representation of the designed NIR switchable thermochromic system based on cyanine dyes.

In this work three ketocyanine dyes, synthesized and provided by the “Integrated Analytical Microsystems group” (from the Sensors & Biosensors Group at the UAB, in collaboration with Sergey Miltsov from the Organic Department of the Saint Petersburg State University), with different conjugated chain lengths were studied: **Cyn I**, **Cyn II** and **Cyn III** (Scheme 4.4). These dyes were selected with different conjugated chain length to cover absorption properties and spectral shifts upon exposition to pH changes in a broad range of the spectrum, from the visible, up to the NIR region. These dyes, in solution, absorb and in some cases emit up to above 700 nm in the protonated state, which makes them potentially very interesting for their dual response (absorption or emission) also in the NIR region. Due their electronic structure, these ketocyanine dyes are also highly solvatochromic and with an increase of the polarity of the media their absorption spectra shift to higher wavelengths (positive solvatochromism). Both the halochromism and the solvatochromism of these dyes could be exploited to produce a new generation of thermochromic materials based on cyanine dyes.



Scheme 4.4: chemical structure of the ketocyanine dyes used in this work (Cyn I, Cyn II and Cyn III).

4.2 Objectives

The objective of this chapter is to *develop temperature-responsive (pH and temperature) chromogenic solid materials based on ketocyanine dyes*. Given the intrinsic pH-sensitive properties of ketocyanine dyes, the study of this work was focused on obtaining switchable temperature-responsive solid materials. To achieve this objective, the following studies were carried out:

- i) to demonstrate that the ketocyanine dyes (**Cyn I, II and III**) could be used in tri-component thermochromic mixtures (dye, phase change materials, color developer) to obtain cyanine-based thermochromic materials
- ii) to demonstrate that the high sensitivity of the optical properties of the ketocyanine dyes on the conjugation length and the medium, could be exploited to accomplish highly tunable thermochromic mixtures by modifying the dye, phase change material and color developer
- iii) to structure the bulk mixtures in core-shell capsules preserving the thermochromic performances and tunability of the bulk mixture.

4.3 Results and discussion

4.3.1 Tri-component bulk mixtures of ketocyanines

The parent **Cyn I** is the simplest ketocyanine dye, with no substituents in the pyrrole moiety (**Scheme 4.4**) and for this reason was first studied. In ethanol, the non-protonated form of **Cyn I** predominates, reason why it exhibits a pink color ($\lambda^{\text{abs}}_{\text{max}} = 568 \text{ nm}$, **Figure 4.3a-b**). Acidification of the solution leads to the formation of the protonated form (**Cyn I-H⁺**) that absorbs largely in the NIR region and only manifest a residual green color ($\lambda^{\text{abs}}_{\text{max}} = 715 \text{ nm}$, **Figure 4.3a-b**).

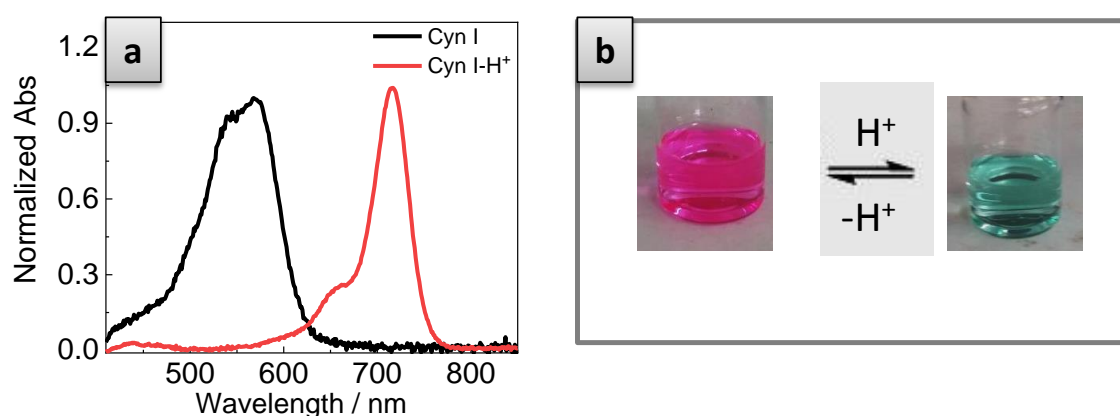


Figure 4.3: a) absorption spectra and b) digital images of **Cyn I** in ethanol solution before and after the addition of a strong acid (HCl_{aq} , 37 wt. %).

In order to obtain the same color switch but induced by temperature we prepared a **Cyn I**-based thermochromic system. This was inspired by the commercial thermochromic tri-component mixture (explained in the introduction chapter, section 1.3.3) based on a dye-developer duo and a PCM matrix, which triggers the interaction between the other two molecules and thus, the color change. 1-tetradecanol (TDOH), a 14 carbon alcohol ($T_m = 38^\circ\text{C}$),²⁵ was selected as the initial PCM and bisphenol-A (BA) was chosen as color developer.

Cyn I was dissolved in TDOH (0.08 mg/mL, 0.16 mM) at 45°C at different BA concentrations (2-80 mM). In the liquid state ($T=45^\circ\text{C}$), no apparent differences in the absorption spectrum of the prepared solutions were detected ($\lambda^{\text{abs}}_{\text{max}} = 533 \text{ nm}$, **Figure 4.4a**). The small shoulder at $\lambda_{\text{should}} = 500 \text{ nm}$, attributed to the formation of the **Cyn I**-dimer,²⁰ decreases upon increasing the amount of BA (**Figure 4.4a**). This was ascribed to an increase of the medium polarity that favors

the solvation of the dye, which otherwise has poor solubility in TDOH, and avoids thus, the formation of dimers. When the solution was cooled below the T_m^{TDOH} (solid mixture), a bathochromic shift of the absorption maximum (from $\lambda_{\text{max}}^{\text{abs}} = 533$ to 578 nm) was observed. This red shift enlarges as the amount of BA increases (**Figure 4.4b**) due to the higher polarity of the medium induced by the presence of a larger number of BA molecules interacting with **Cyn I** molecules.

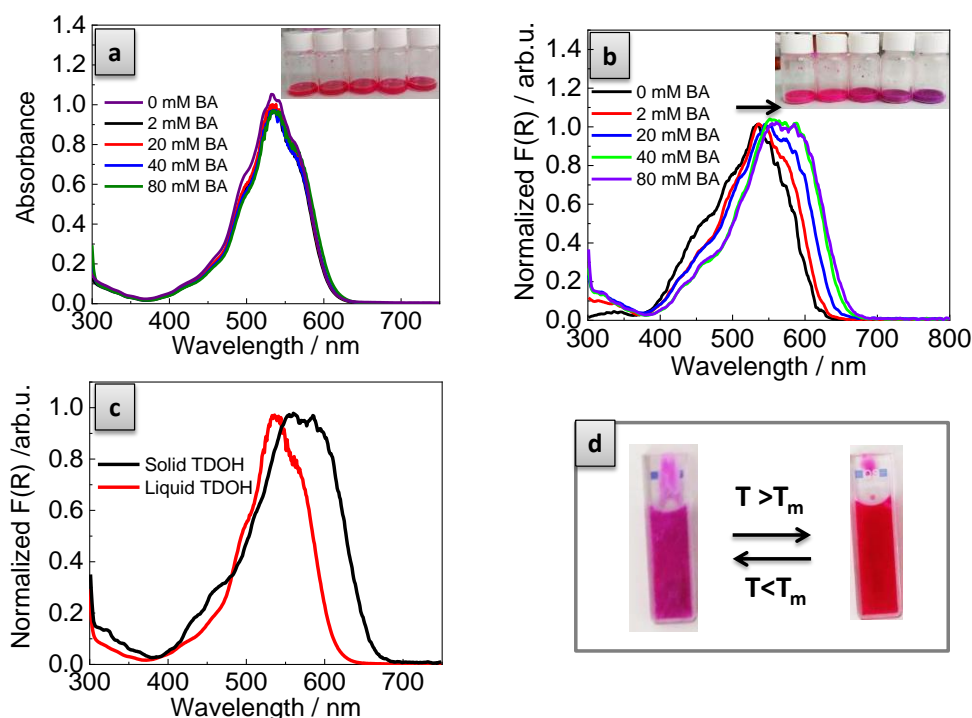


Figure 4.4: absorption spectra of Cyn I/BA@TDOH mixture a) above (45°C) and b) below T_m^{TDOH} in the presence of different amounts of BA (2-80 mM), c) absorption spectra and d) digital images of the **Cyn I/BA@TDOH** mixture with the highest concentration of BA (80 mM) above (45°C) and below T_m^{TDOH} .

Given the larger red shift produced in the solid state by the mixture with the highest BA concentration, this **Cyn I/BA@TDOH** solution showed a color change from magenta ($\lambda_{\text{max}}^{\text{abs, sol}} = 578$ nm, **Figure 4.4c-d**) to red ($\lambda_{\text{max}}^{\text{abs, liq}} = 533$ nm, **Figure 4.4c-d**), evident enough, that could be appreciated by naked-eye upon melting of the TDOH. This spectral change was attributed to the loss of interaction between BA and **Cyn I**, in the liquid state, confirming the initial hypothesis and the potentiality of ketocyanine dyes to be used for thermochromic materials.

When **Cyn II** and **Cyn III** (Scheme 4.4), which have similar structure as **Cyn I**, but with longer conjugated alkenic chains (11 and 13 carbons, respectively), were dissolved (at 45°C) in the same BA (80 mM)@TDOH mixture (Cyn/BA@TDOH), the analogous bathochromic shifts were detected upon cooling down below the T_m of TDOH. In the case of **Cyn II/BA@TDOH**, the color changed from magenta ($\lambda^{\text{abs}}_{\text{max, liq}} = 560 \text{ nm}$, 45°C, **Figure 4.5a**) to blue ($\lambda^{\text{abs}}_{\text{max, sol}} = 610 \text{ nm}$, 25°C, **Figure 4.5a**), whereas in the case of **Cyn III/BA@TDOH** the blue liquid solution ($\lambda^{\text{abs}}_{\text{max, liq}} = 600 \text{ nm}$, 45°C) turned to a pale bluish (almost colourless, $\lambda^{\text{abs}}_{\text{max, sol}} = 670 \text{ nm}$) solid after cooling down to RT (**Figure 4.5b**). The higher the number of alkenic carbons in the conjugated chain of the dye molecules, the higher the shift obtained when passing from liquid to solid.

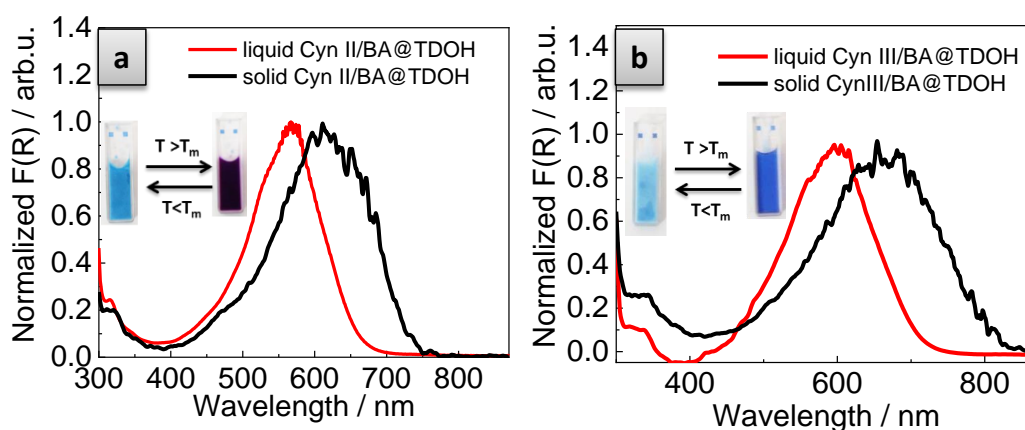


Figure 4.5: normalized absorption spectra of a) **Cyn II** and b) **Cyn III** in the solid (RT) and liquid (45°C) state of BA@TDOH.

Noticeably, taking advantage of the high sensitivity of cyanines to solvent polarity, quite large spectral shifts (70 nm) could be thermally induced simply by modifying the immediate chemical surround, without involving isomerization reactions (e.g. ring opening reactions). Worth to mention though is also that by simply changing the cyanine dye (i.e. polymethine chain length) it was possible to tune the absorption maximum of both the liquid (from $\lambda^{\text{abs}}_{\text{max, liq}} = 533\text{-}600 \text{ nm}$ **Figure 4.6a**) and solid state (from $\lambda^{\text{abs}}_{\text{max, sol}} = 574\text{-}670 \text{ nm}$, **Figure 4.6b**).

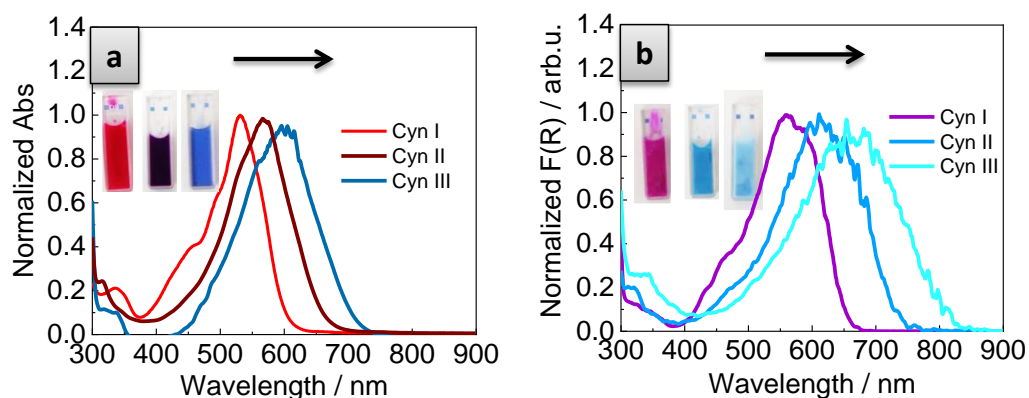
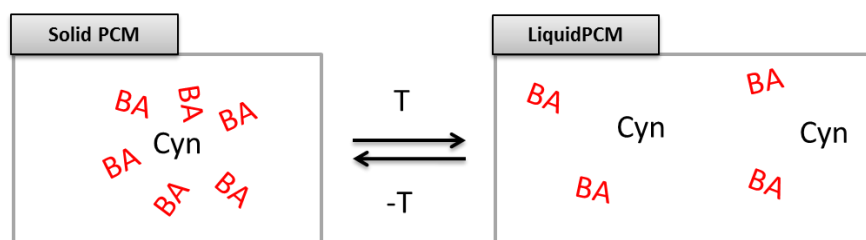


Figure 4.6: absorption spectra of **Cyn I-III/BA@TDOH** in the a) liquid and b) solid state of the mixture.

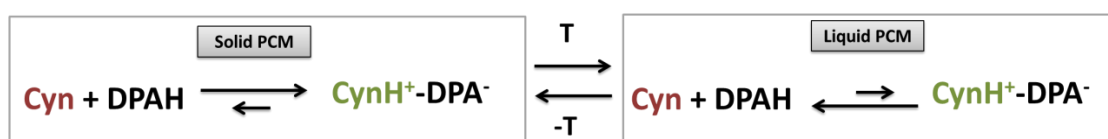
However, as already reported in the literature, in polar solvents (e.g. ethanol), ketocyanine dyes exhibited much higher bathochromic shifts when the solutions are acidified (protonation of the dye molecules, **Figure 4.3**). This spectral shift was not accomplished using BA as proton donor because its acidity (sufficient to open the lactone ring of crystal violet lactone) was not high enough to protonate the carbonyl of the cyclopentanone ring of the dyes. The smaller shift observed was instead attributed to the solvatochromic effect that BA has on the dye molecules, which is higher in the solid TDOH (**Scheme 4.5**). Our hypothesis behind this effect is that in the solid Cyn/BA@TDOH mixture, the lower solubility of the dye and BA components, induces their phase segregation (this is also observed in other PCM-based thermochromic systems). In the segregated phase, the BA is not acidic enough to protonate the Cyn dyes, but is able to establish interactions with them (through for example hydrogen-bonding) and create a microenvironment around the dye molecules sufficiently polar to induce solvatochromism. In the liquid state such solvatochromic effect is not so evident as the dye molecules are surrounded mainly by TDOH (**Scheme 4.5**).



Scheme 4.5: representation of the enhanced solvatochromic effect of BA molecules to Cyn dyes in the solid state of the PCM matrix.

In order to provide the thermochromic transition expected for the protonated/non-protonated forms of the cyanine dyes, BA was replaced the more acidic developer, dodecylphosphonic acid (DPA). DPA was selected because has smaller pKa (2.80) than BA (9.6) and its demonstrated capability to force protonation of the merocyanine form of, even when their phenolates were not very basic (Chapter 3).

After dissolving all the components, the molten **Cyn I/DPA@TDOH** mixture presented the same absorption band as before at $\lambda^{\text{abs}}_{1, \text{max, liq}} = 533 \text{ nm}$ (**Figure 4.7a-b**), related to the non-protonated dye molecules, and a smaller one at lower energies ($\lambda^{\text{abs}}_{2, \text{max, liq}} = 705 \text{ nm}$) deriving from the protonated **Cyn I-H⁺** form, which confirmed the capability of DPA to protonate **Cyn I** molecules. When the solution was solidified ($T = 25^\circ\text{C}$), the number of protonated dye molecules increased and a pale magenta color ($\lambda^{\text{abs}}_{\text{max, sol}} = 705 \text{ nm}$, **Figure 4.7a-b**) was developed. This suggested that the acid-base reaction between the DPA and the dye was favored in the solid state, possibly due to the formation of a complexed salt, formed from the precipitation of the dye and the acid, that suffer lower solubility in the solid TDOH (**Scheme 4.6**). Nevertheless, the absorption spectrum of the solid mixture revealed still an important contribution of non-protonated molecules ($\lambda^{\text{abs}}_{2, \text{max, sol}} = 533 \text{ nm}$) and a new band in the NIR region ($\lambda^{\text{abs}}_{3, \text{max, sol}} = 818 \text{ nm}$, **Figure 4.7a**). The latter band was attributed to the formation of dye J-aggregates in the mixture, which are known to form even in more polar media for highly concentrated solutions of protonated ketocyanine dyes.²¹



Scheme 4.6: representation of the equilibrium between the Cyn and DPA (in this scheme indicated as DPAH) molecules and the complexed salt $\text{CynH}^+ - \text{DPA}^-$ in the liquid and solid state of the PCM matrix.

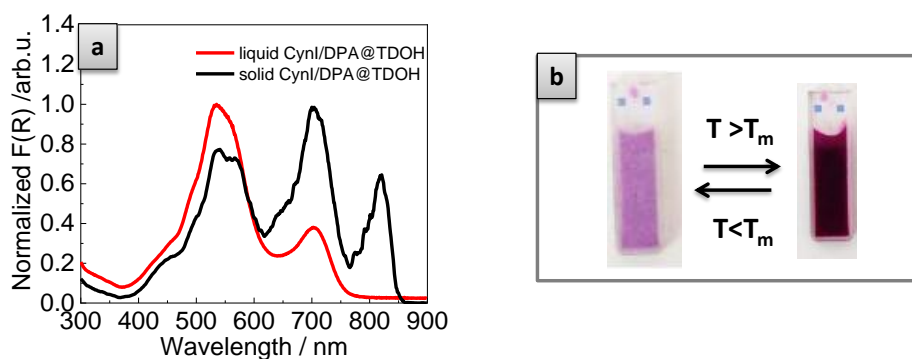


Figure 4.7: a) absorption spectra and b) digital images of **Cyn I/DPA@TDOH** mixture in the solid and liquid state.

In order to avoid the contribution of the non-protonated form in the solid mixture, we aimed to enhance the interaction between DPA and the dye. TDOH, as well as other long-chain 1-alkanols experience two exothermic transitions during the cooling process: i) a first transition, from the liquid phase to the hexagonally packed solid phase (SHEX) and a second solid-solid transition, from SHEX to the orthorhombically packed solid phase (red line, **Figure 4.8**).^{23, 24} In the case of the **Cyn I/DPA@TDOH** mixture, in which TDOH is being plasticized by DPA and the dye, the solid-solid transition is shifted towards lower temperatures (blue line, **Figure 4.8**). During the heating process an endothermic peak appeared around 20°C), which means that due to the presence of the DPA plasticizer, the mobility of the dyes at around room temperature temperature is much higher than in a solid rigid matrix and this liquid-like behavior of some of the dye molecules is avoiding the interaction with DPA.

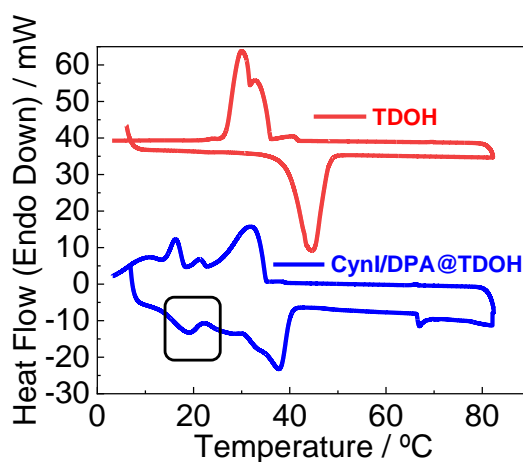


Figure 4.8: DSC curves of TDOH (red line) and of the **Cyn I/DPA@TDOH** mixture (blue line) with the peak at 20°C marked.

To avoid the spectral contribution of the non-protonated dye molecules and to favor the interaction of the dye with DPA, we decided to use a matrix with a higher T_m than TDOH to assure a matrix with high rigidity even at RT. For this, 1-hexadecanol (HDOH), an alcohol with a larger carbon chain and thus a higher melting point ($T_m = 49^\circ\text{C}$),²⁵ already used in thermochromic commercial systems, was selected. As observed for TDOH, the cooling process of the **Cyn I/DPA@HDOH** mixture in DSC measurements, also revealed that the solid-solid transition was shifted to lower temperatures (blue line, **Figure 4.9**). However, in this case, during the heating process no significant endothermic peak appeared at 20°C .

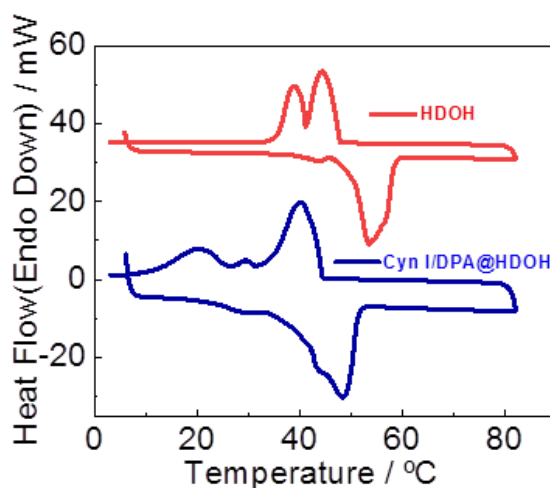


Figure 4.9: DSC curves of HDOH (red line) and of the **Cyn I/DPA@HDOH** mixture (blue line).

The spectral change of new **Cyn I/DPA@HDOH** mixture was thus investigated above and below the T_m^{HDOH} . Effectively, the red liquid solution ($T = 60^\circ\text{C}$) turned to a blue solid (**Figure 4.10b**) after cooling ($T = 25^\circ\text{C}$) the **Cyn I/DPA@HDOH** mixture, and the band at $\lambda_{\text{max}} = 530 \text{ nm}$ (red line, **Figure 4.10a**) totally disappeared in the solid state, while the corresponding **Cyn I-H⁺** band at $\lambda_{\text{max}} = 710 \text{ nm}$ increased. This color transition resembled that observed in organic solvents (i.e. ethanol) before and after the addition of a strong acid (**Figure 4.3**), confirming the successful control of the equilibrium between the protonated and non-protonated forms of **Cyn I**, upon thermally induced phase transition of the **Cyn I/DPA@HDOH** mixture.

However, the absorption spectrum of the solid **Cyn I/DPA@HDOH** still revealed an important contribution of J-aggregates ($\lambda_{\text{max, sol}}^{\text{abs}} = 810 \text{ nm}$, **Figure 4.10a**) of

the protonated dye and a residual component of the tail in the visible region that provides the bluish coloration to the mixture. At this point, it was decided to reduce the number of aggregates in the solid **Cyn I/DPA@HDOH** mixture accomplish pure reproducibility of the pH-induced spectral changes observed in solution and to prevent dye degradation, which is known to be more favored by the presence of aggregates.

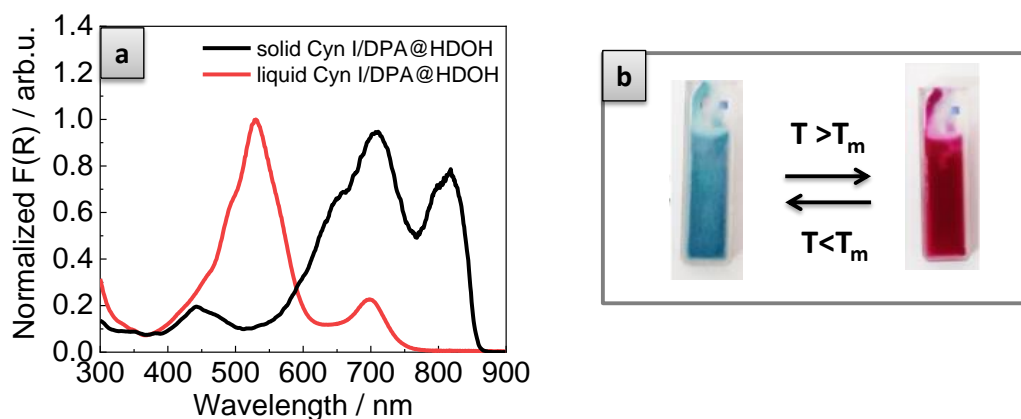


Figure 4.10: a) absorption spectra and b) digital images of **Cyn I/DPA@HDOH** mixture in the solid and liquid state.

To diminish the contribution of **Cyn I-H⁺** in the liquid state of the **Cyn I/DPA@HDOH** mixture ($\lambda^{\text{abs } 2_{\text{max, liq}}} = 700 \text{ nm}$, red line **Figure 4.10a**) the concentration of DPA was reduced 5-fold (from 5 to 1 wt. %). Interestingly by adding this it was decreased the number of protonated dye molecules in the liquid state (lower absorption at $\lambda^{\text{abs } 2_{\text{max}}} = 700 \text{ nm}$, **Figure 4.11a**), as well as the number of aggregates of these in the solid HDOH (**Figure 4.11b**).

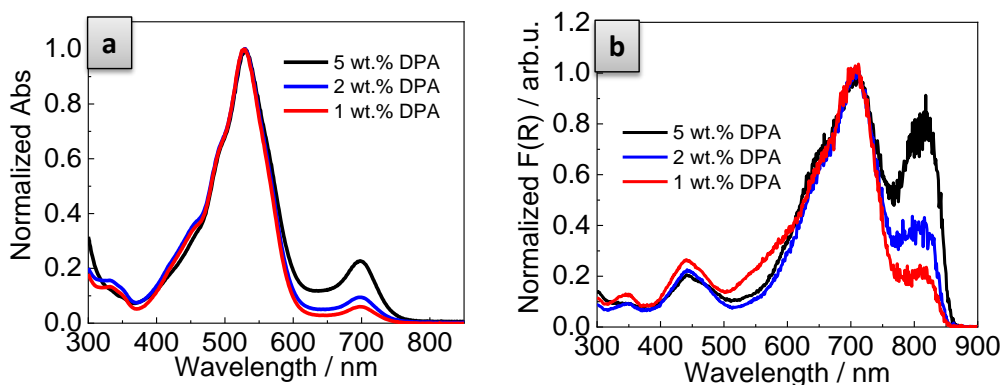


Figure 4.11: absorption spectra of **Cyn I@HDOH/DPA** with different concentration of DPA (5, 2, 1 wt. %) in the a) liquid (60°C) and b) solid state (RT) of the mixtures.

Unfortunately, in the solid HDOH mixtures containing 2 and 1 wt. % of DPA, the band at $\lambda_{\max} = 800$ nm, deriving from the J-aggregates of the protonated dye molecules, increased with time stabilizing at a plateau of absorbance after 25 minutes (**Figure 4.12a-b**). Probably, in the rigid solid matrix, the protonated molecules were diffusing with time forming the more thermodynamically stable aggregates. This result could be exploited in the future for understanding the dynamics of dyes (and other molecules) diffusion and aggregation in PCMs in their solid state. This could be used for example to evaluate the stability of molecules (e.g. drugs) in solid lipid particles, nowadays proposed for several applications. The driving force of the aggregation could be the low dye solubility in the solid PCM, which pushes away the molecules from the matrix originating segregated aggregates.

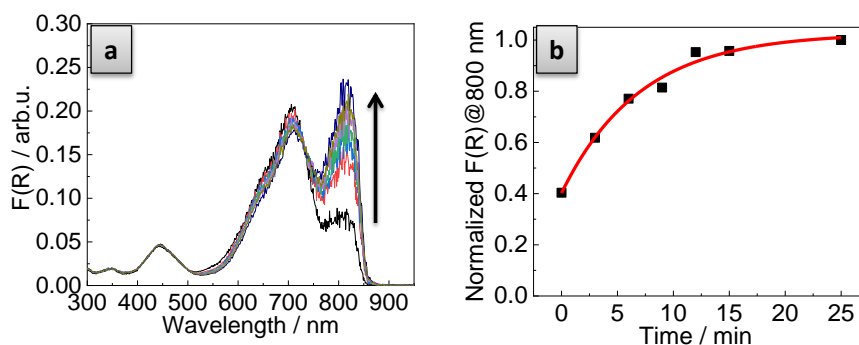


Figure 4.12: a) absorption spectra at different times and b) variation of the formation of Cyn I-H⁺ aggregates at $\lambda_{\max} = 800$ nm of Cyn I/DPA@HDOH (2 wt. %) mixture in the solid state, upon time.

Therefore, to avoid the formation of aggregates in the solid Cyn I/DPA@HDOH containing the lowest amount of DPA (1 wt. %), the dye concentration was also decreased 4-fold (from 0.08 to 0.02 mg/mL). As expected, the absorption spectrum of the so prepared solid Cyn I/DPA@HDOH (at low concentrations of Cyn I) revealed the total removal of aggregates (neither after letting the mixture stabilizing during 30 min), since no contribution of the band at $\lambda_{\max} = 800$ nm could be detected (**Figure 4.13**). Moreover, the band absorption at $\lambda_{\max} = 700$ nm was narrower than that observed for the previous solid mixtures (reducing significantly the residual color), further proving the reduced amount of aggregated species. Upon melting, the protonated form ($\lambda_{\max}^{\text{abs}} = 700$ nm) converted completely into the non-protonated species ($\lambda_{\max}^{\text{abs}} = 532$ nm) producing a thermally induced spectral shift of 168 nm. By using DPA as color developer,

HDOH as PCM and controlling the concentration of both DPA (1 wt. %) and **Cyn I** (0.02 mg/mL) it was possible to accomplish a bulk thermochromic system that mimics the spectral changes of the dye observed in solution upon pH variations.

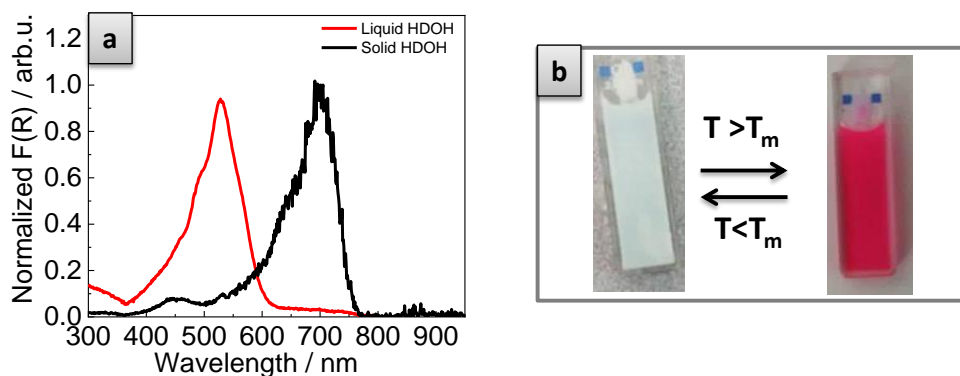


Figure 4.13: a) absorption spectra and b) digital images of **Cyn I/DPA@HDOH** mixture in the solid (RT) and liquid (60°C) state.

Overall, during the bulk optimization of the thermochromic material with **Cyn I**, different colors (from magenta to pale blue) could be effectively developed in the solid state of the mixtures. By simply varying the length of the hydrocarbon chain of the PCM (TDOH or HDOH), the type of interaction of the dye with the color developer (i.e. solvatochromism with BA or halochromism with DPA) and the concentration of dye and color developers, spectral shifts of different amplitudes and occurring in different spectral regions could be easily obtained (**Table 4.1**, **Figure 4.14a-b**) with one single dye.

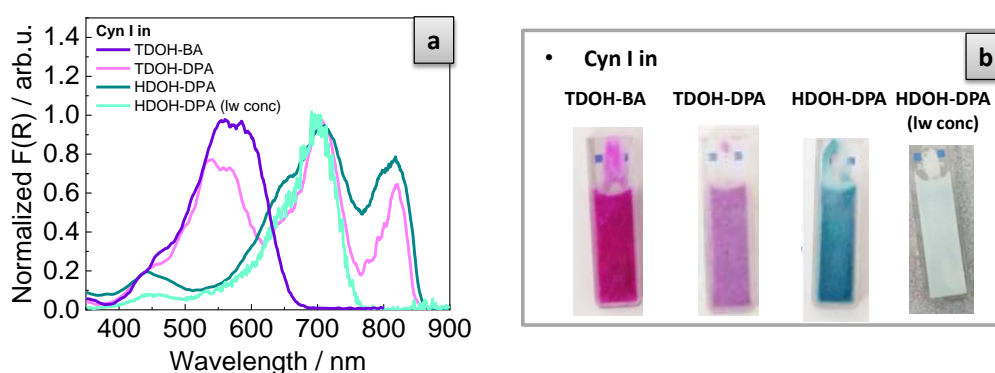


Figure 4.14: a) absorption spectra and b) digital images of **Cyn I** in different solid PCM-color developer mixtures.

To explore the universality of **DPA** as color developer for ketocyanine dyes and achieve further spectral modulation using the same strategy, the HDOH mixture

was prepared using a ketocyanine dye with longer conjugated alkenic chain: **Cyn III**. **Cyn III** was selected because already manifested the largest spectral shift of the **Cyn/BA@TDOH** mixtures after being solvated by BA molecules in the solid state of TDOH (**Figure 4.5b**). To prepare the **Cyn III/DPA@HDOH** mixture, **Cyn III** was mixed with DPA (5 wt. %) and dissolved in molten HDOH (0.02 mg/mL).

Noteworthy, a blue liquid solution ($\lambda_{\text{max, liq}}^{\text{abs}} = 590 \text{ nm}$, **Figure 4.15a-b**) is obtained upon dissolution of the dye in the DPA@HDOH mixture. The higher conjugation of Cyn III than Cyn I induced a red shift (of 57 nm) of the absorption band in the liquid state. The solution turned to pale blue solid material mainly absorbing in the NIR ($\lambda_{\text{max, sol}}^{\text{abs}} = 870 \text{ nm}$, **Figure 4.15a-b**), after cooling to RT. The residual band at 600 nm, causing the pale blue color of the solid mixture indicates the presence of non-protonated species. This bulk mixture showed the largest spectral shift of the studied mixtures (280 nm), considering the λ_{max} of the absorption spectra, generated upon thermally induced liquid-solid transition of the PCM.

Interestingly, the colorless-to-colored thermochromic transition resemble the effect usually obtained from standard bi-component thermochromic mixtures, that pass from absorbing in the UV (colorless) to the visible region, upon heating (positive thermochromism), but in this case it is achieved through negative thermochromism (from absorbing in the NIR to the visible region). This is a promising result since it could open to a new class of thermochromic materials.

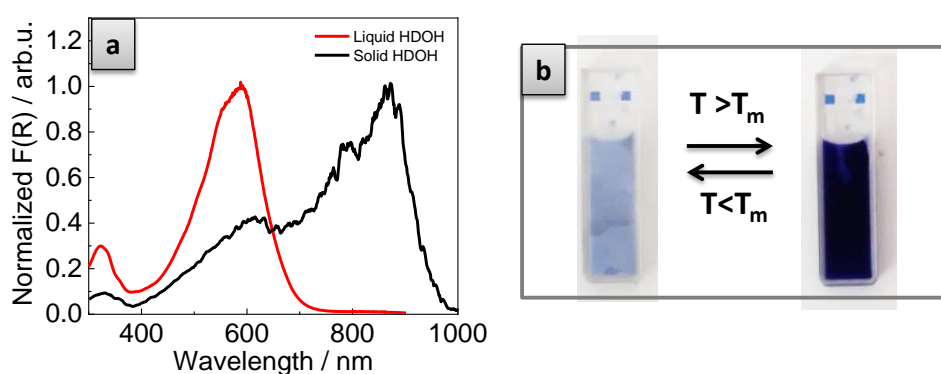


Figure 4.15: a) absorption spectra and b) digital images of **Cyn III/DPA@HDOH** mixture in the solid (RT) and liquid (60°C) state.

Therefore, the dye adds another tool to tune colors and spectral shift amplitudes of these multi-component mixtures (**Table 4.1**).

	Cyn I				Cyn II	Cyn III	
Dye conc (mM)	0.16			0.04	0.16	0.16	0.04
Mixture (solid)	TDOH-BA	TDOH-DPA	HDOH-DPA	HDOH-DPA	TDOH-BA	TDOH-BA	HDOH-DPA
λ_{\max} (nm)	578	$\lambda_{\max}^1=705$ $\lambda_{\max}^2=533$ $\lambda_{\max}^3=818$	$\lambda_{\max}^1=710$ $\lambda_{\max}^2=810$	705	610	670	870
Mixture (liquid)	TDOH-BA	TDOH-DPA	HDOH-DPA	HDOH-DPA	TDOH-BA	TDOH-BA	HDOH-DPA
λ_{\max} (nm)	533	$\lambda_{\max}^1=533$ $\lambda_{\max}^2=705$	$\lambda_{\max}^1=531$ $\lambda_{\max}^2=700$	527	560	600	590

Table 4.1: summary of the λ_{\max} obtained with different PCM/dye mixtures and different concentration of Cyn dyes.

After demonstrating the potentiality of these bulk systems as thermochromic materials with liquid-to-solid shifts as high as large as 178 nm for **Cyn I** and 280 nm for **Cyn III** (**Table 4.1**), we decided to proceed with the encapsulation of the mixtures to obtain solid materials manifesting these thermochromic properties. We started encapsulating the **Cyn I/DPA@HDOH** mixture which reproduces the behavior observed in ethanol solution upon addition of a strong acid. The encapsulation of the mixture i) prevents the leakage of the PCM during the phase transition; ii) allows integrating the mixture in polymeric materials and iii) reduces/prevents the reactivity with the surrounding media.

4.3.2 Structuration of the bulk mixture

In **Chapter 2** attempts of the encapsulation of HDOH via phase separation method were showed. Unfortunately, though different shell-forming polymers and different ratios polymer/PCM were tested, we had not been able to encapsulate properly this compound. Thus, we decided to change the encapsulation method to *in situ* polymerization. In this method, i) the oil in water (O/W) emulsion of PCM is prepared in water and then ii) the pre-polymer/monomer is added into the emulsion to encapsulate the PCM core within a solid shell through polymerization reaction. This method is used to encapsulate PCMs with polystyrene, melamine-formaldehyde resin and poly(methyl methacrylate) shell materials. Initial attempts

were carried out using melamine-formaldehyde (MF) as shell material, using a methodology already optimized in the group to encapsulate high boiling point oils.²⁶

4.3.2.1 *In-situ* polymerization: MELAMINE-FORMALDEHYDE

We first proceed with the protocol developed by A. Ayala,²⁶ which involves three basic steps: i) the formation of an O/W emulsion, with stearic-maleic anhydride (SMA) copolymer as stabilizer, at a $T > T_m$ of the material to be encapsulated, ii) the addition of the pre-polymer (PP) to the emulsion, and finally iii) the decrease of the pH to induce the polymerization of the PP in the interface of the PCM droplets. The SMA also provides the electrostatic interactions to keep the PP around the emulsified PCM and should guarantee the polymerization around the droplets rather than in the bulk volume. The first attempt of synthesis, **Cyn I/DPA@HDOH@MF** capsules (see conditions, **Table 4.2**), yielded several small particles of MF and very low amount of HDOH was encapsulated. The problem of this synthesis was the rapid addition of the acid (formic acid, within 2 min), which induced a fast polymerization of the pre-polymer in the form of small MF particles (3-5 μ m, **Figure 4.16a-b**). Considering that these conditions (**Table 4.2**) were optimized for the encapsulation of a liquid oil core at RT, the higher temperature at which the synthesis was carried out (60°C) could have enhanced the polymerization rate inducing the consequent precipitation of polymer in the form of particles, before reaching the droplets surface.

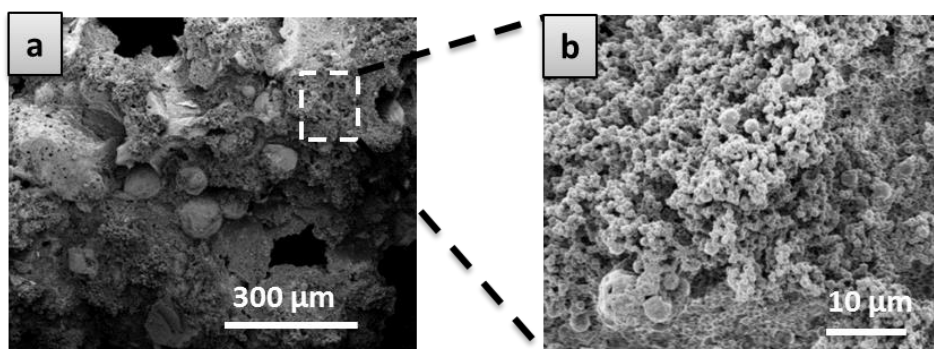


Figure 4.16: SEM images of the mixture deriving from the attempted synthesis: **Cyn I/DPA@HDOH@MF** capsules.

Therefore, in a second attempt, we used the experimental conditions established by Yin *et al.*²⁴ to encapsulate HDOH through *in-situ* polymerization of MF resin. They optimized the encapsulation efficiency testing different shell-core ratios obtaining the best results with the ratio 1:3. After using the new conditions (**Table 4.2**), starting from an acidic solution of SMA (pH 4-5) and slowly adding the pre-polymer (during 2h), the synthesis of **Cyn I/DPA@HDOH@MF_02** showed the formation of some small particles combined with larger microspheres (30-40 μm) that presented a clear cleft (**Figure 4.17a-b**), typical of the core-shell structure of MF capsules. The obtained white capsules tend to flocculate with time to the air-water interface. Unfortunately, when the suspension was heated above the T_m^{HDOH} , no color change was observed. During this synthesis, part of the emulsion was broken and the PCM droplets coalesced without being encapsulated. The lack of the thermochromic activity was ascribed to the loss of the thermoresponsive mixture during the capsules synthesis and/or to the migration of the color developer DPA (it has a partial amphiphilic character).

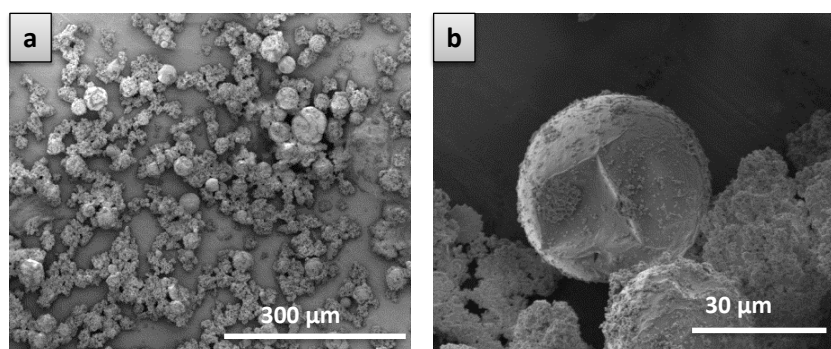


Figure 4.17: SEM images of the mixture deriving from the attempted synthesis of **Cyn I/DPA@HDOH@MF_02** capsules.

In order to avoid the rupture of the emulsion and to encapsulate better the HDOH mixture, we increased the amount of surfactant to improve the stability of the PCM droplets during the emulsion at high T (60 $^{\circ}\text{C}$), and the amount of DPA to compensate the possible loss due to migration to water and to assure its encapsulation. After these changes, microspheres (50-100 μm) with less contribution of the smaller MF particles were detected (**Figure 4.18a-b**). Nonetheless, again the capsules appeared without color.

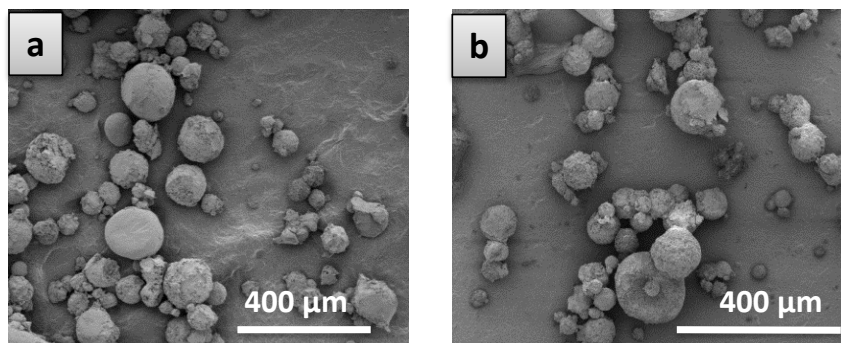


Figure 4.18: SEM images of the mixture deriving from the attempted synthesis of Cyn I/DPA@HDOH@MF_03 capsules.

In all attempted synthesis almost colorless capsules and/or small polymeric MF particles were obtained and no temperature-induced color change was detected. This could be attributed to i) the non-encapsulation of DPA due to its tendency to go to the water phase or ii) the degradation of the dye after all the synthesis procedure in which high temperature and pH changes are employed.

Synthesis code	Core (HDOH/DPA/Dye I) (mg)	Stabilizer (SMA sol 1%) (g)	MF PP solution (g)	Addition time of PP (min)	Formic acid solution (10%) (g)
Dye I@HDOH/DPA_MF	5000/50/0.5	25 (pH 9-10)	2	5	2
Dye I@HDOH/DPA_MF_02	2000/20/0.2	16 (pH 4-5)	3	120	-
Dye I@HDOH/DPA_MF_03	2000/100/0.2	32 (pH 4-5)	3	120	-

Table 4.2: main experimental parameters used for the capsules syntheses with the polymerization of melamine-formaldehyde.

4.3.2.2 *In-situ* polymerization: RADICAL POLYMERIZATION of styrene

To avoid the modification of the mixture pH (at which the Cyn I dye is very sensitive), we planned to change the encapsulation strategy to the radical polymerization method, which basically consists of i) the preparation of an O/W emulsion in which the organic phase contains the tri-component mixture, the monomer (i.e. styrene) and the radical initiator, and ii) the subsequent polymerization of the monomer, under N₂ atmosphere, to avoid oxygen scavenging of the radicals, and at high temperatures, at which the initiator decompose to radical species. The pH was kept neutral during the reaction.

In the first attempt we were able to obtain spherical and nanometer size capsules (50-60 nm, **Figure 4.19**). However, again no color in the final suspension was observed possibly due to the degradation of the dye caused by the radical species formed during polymerization. After various unsuccessful attempts it was decided to abandon also this strategy due to the highly possible dye degradation.

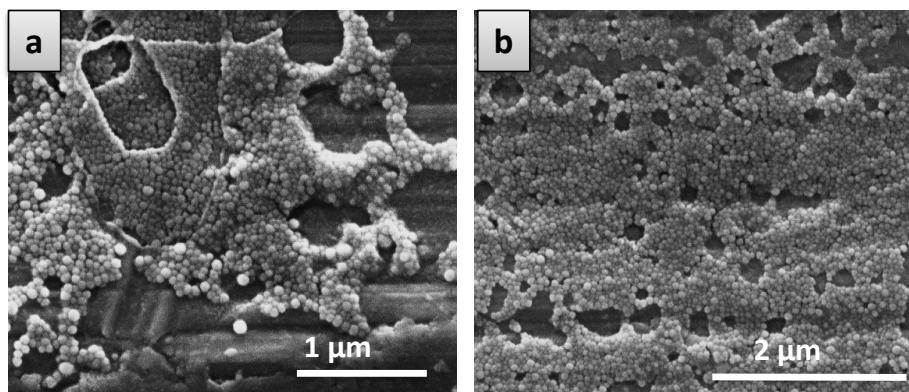


Figure 4.19: SEM images of the reaction mixture deriving from attempts to obtain the **Cyn I/DPA@HDOH@PS** capsules.

4.3.3 Structuration of the bulk **Cyn/DPA@HDOH** as solid lipid microparticles

4.3.3.1 **Cyn/DPA@HDOH SLMs**

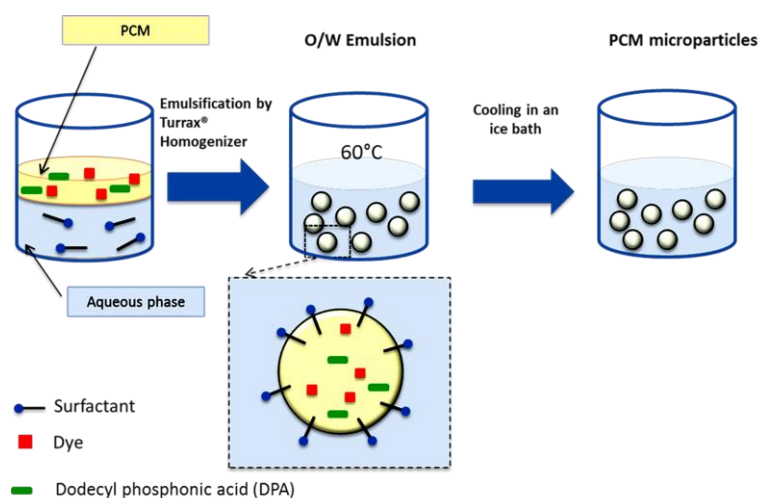
After failing on the encapsulation of the **Cyn I/DPA@HDOH** mixture while preserving the thermochromic properties, we decided to structure the bulk system in the form of spherical solid lipid microparticles (SLMs). Given the solid nature of the HDOH mixture, SLMs of this could be prepared and eventually:

- i) be directly embedded in flexible polymeric materials, analogously to what we usually do with capsules but, avoiding the step of the formation of a protective polymeric shell.
- ii) be alternatively encapsulated after their formation *via* coacervation method (see introduction section **1.4.2**).

Both strategies would i) guarantee the trapping of the SLMs within a polymeric matrix, allowing the solid-to-liquid transition without PCM leakage and ii) allow the use of water soluble pre-formed hydrophilic polymers which avoid the use of

organic solvents and reactive monomeric species, which dissolve the SLMs and degrade the Cyn dyes, respectively

For the preparation of the SLMs, we selected a widely known and reaction-free method called emulsion-cooling method,²⁷ which basically consists on: i) an emulsification at high temperature ($T > T_{m, PCM}$) in the presence of a surfactant, and subsequently ii) the rapid cooling of the emulsion by adding cold water (2-5°C), during which the droplets of the emulsion precipitates in the form of particles (**Scheme 4.7**, for more details see experimental section 7.3.4.1).



Scheme 4.7: schematic representation of the emulsion-cooling method for the preparation of SLMs.

- **Temperature-responsiveness of the Cyn I/DPA@HODH SLMs suspension**

After the synthesis, the suspension of the spherical SLMs (of size 20-50 μm as confirmed by SEM, **Figure 4.19a-b**) showed bluish color at RT, suggesting the presence of the protonated **Cyn I-H⁺** molecules. This means that during the emulsification cooling process, enough DPA remained within the SLM to induce the dye protonation. The suspension color changed to red-pink when was heated above the T_m^{HDOH} (60°C, **Figure 4.20c**), successfully preserving the behaviour observed in the bulk system before structuration. The color change was reversible and surprisingly the particles maintained the shape and structure after cooling, possibly due to the stability that conferred the surfactant in the water suspension.

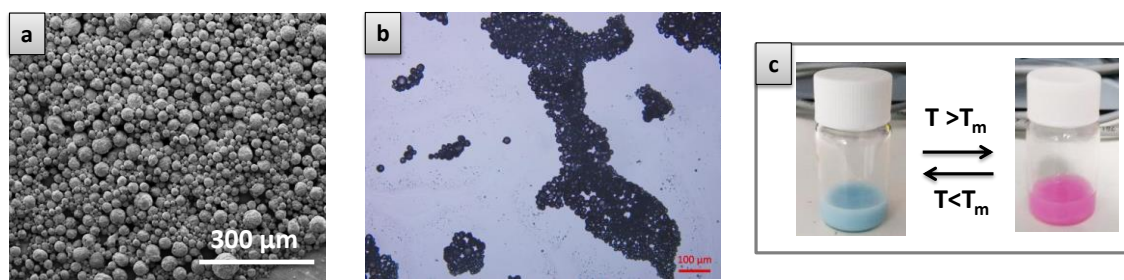


Figure 4.20: a) SEM and b) optical microscope images of the SLMs and c) digital images of the suspension of the **Cyn I@HDOH/DPA** SLMs before and after heating above the T_m^{HDOH} (60°C).

The powder obtained after freeze-drying the suspension of the SLMs presented similar blue color at RT ($\lambda_{\text{max}} = 700 \text{ nm}$, **Figure 4.21**), which confirmed that the dye was trapped in the HDOH particles and was maintaining the interaction with DPA after structuration. In this case the temperature-induced color change of the particles was not measured due to the loss of structuration that the SLMs would experiment upon heating.

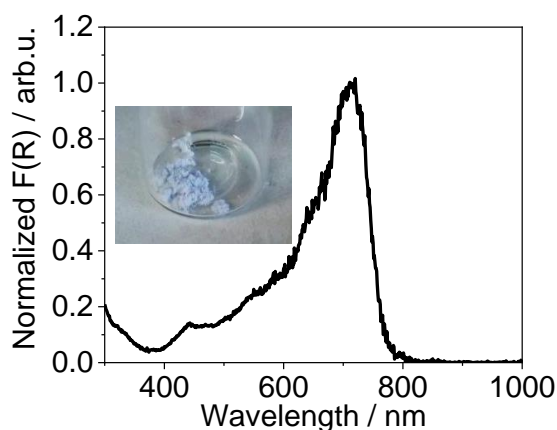


Figure 4.21: absorption spectrum at RT of the freeze-dried **Cyn I/DPA@HDOH** SLMs.

- **pH-responsiveness of the Cyn I/DPA@HODH SLMs powder**

Ketocyanine dyes are generally known for their pH-responsive properties, which have been widely studied in organic solutions,^{20,22} and are exploited in this work to obtain a new family of halochromic-based thermochromic materials. We expected, then, that besides being temperature-responsive these SLMs will change their color upon pH variation.

In order to induce change of the pH of the powdered particles, we exposed these to vapours of a strong base (ammonia). The bluish color of the particles (**Cyn I-H⁺**) turned to pink (**Figure 4.22**) after 20 min of exposure to NH_3 vapors obtained from

an ammonia solution (23 wt. %). This suggested a displacement of the equilibria towards the non-protonated form of **Cyn I**. Interestingly, upon exposition of the powder to another 20-30 min of HCl vapors (from an aqueous solution of HCl, 37 wt. %), the particles recovered the initial color confirming the reversibility of the system and the pH-response in the solid state.



Figure 4.22: digital images of the **Cyn I/DPA@HDOH** microparticles in presence of NH_3 and HCl vapors.

After demonstrating the capability of **Cyn I/DPA@HDOH** particles to respond to different stimuli (i.e. pH and temperature) we decided to prepare particles with **Cyn III** (see experimental conditions 7.3.4.1), which presented the largest spectral shift of the investigated bulk mixture during the solid-to-liquid transition (**Figure 4.5**). The suspension of the **Cyn III/DPA@HDOH** SLMs (30-60 μm , **Figure 4.23a**) showed almost no color (in agreement with the absorption of the protonated **Cyn III** mainly in the NIR region, **Table 4.1**) after the synthesis and turned to blue (non-protonated **Cyn III**) when reaching the T_m^{HDOH} (**Figure 4.22b**), mimicking faithfully the bulk behavior. Again reversibility of the suspension was confirmed when the suspension was cooled to RT.

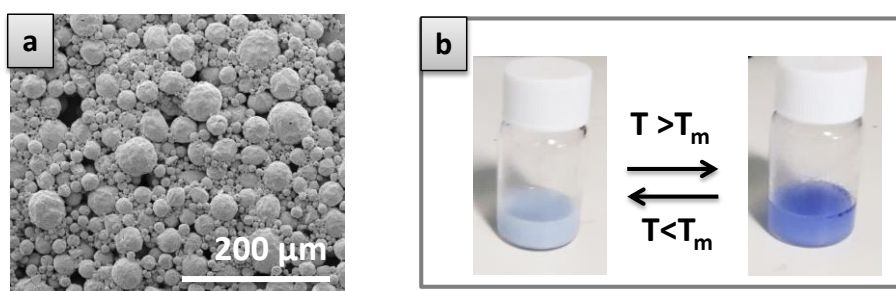


Figure 4.23: a) SEM images of **Cyn III/DPA@HDOH** microparticles and b) digital images of the suspension of the particles at RT and above the T_m of HDOH (60°C).

Once successfully prepared thermochromic microparticles based on different ketocyanine dyes, which also responded to pH changes under acidic/base atmosphere, we aimed to transfer this multi-responsive behaviour to the solid

state, by confining the SLMs within polymeric materials that confer reversibility avoiding the loss of structuration during the PCM melting.

Previous to the preparation of polymeric films or capsules (via coacervation) with the SLMs, we decided to check the chromogenic stability of these in hydrophilic-polymer concentrated water solutions.

Surprisingly, when a few droplets of the PVA concentrated water solution were added to the **Cyn I/DPA@HDOH** SLMs suspension, a slightly color change from bluish to magenta was observed, which turned to pink upon addition of a few more droplets (**Figure 4.24**), indicating the formation of the non-protonated form of **Cyn I**. A possible explanation for this phenomenon is the loss of interaction between the DPA and **Cyn I** molecules when PVA was added. The PVA could be extracting DPA from the SLMs and disrupting the salt formed with the dye in the solid HDOH. Polar compounds, such as DPA, are hardly solubilized within the SLMs and the presence of surfactant in the aqueous suspension might favor the extraction of DPA, especially if it is pushed to migrate to the surface of the SLMs by the low solubility in the PCM. Supporting this hypothesis, similar behavior was observed with other water-soluble polymers solutions such as polyacrylamide (PA, 5 wt. %) or gelatine (2.5 wt. %). Gelatine is a widely known hydrophilic polymer used together with gum Arabic for the encapsulation oil-based mixtures via complex coacervation method.²⁸

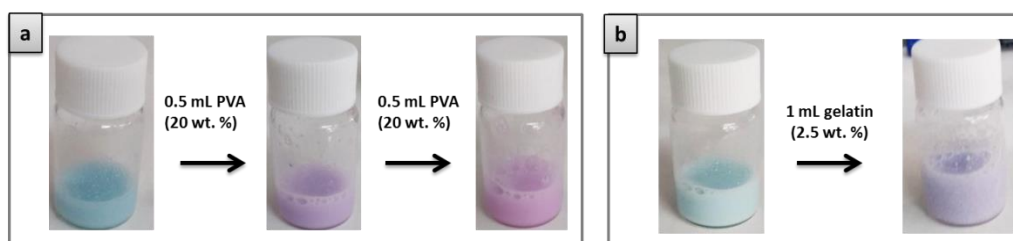
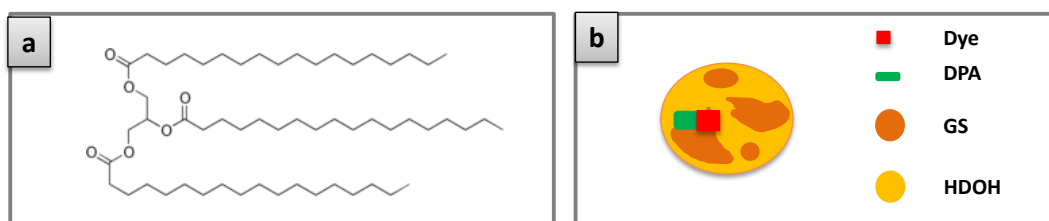


Figure 4.24: digital images of the suspension of the **Cyn I/DPA@HDOH** SLMs after the addition of a) 1 mL PVA solution (20 wt. %) and b) 1 mL of a gelatin solution (2.5 wt. %).

No PVA films, neither capsules (through coacervation) could then be obtained using these materials, without losing the thermochromic properties. At this point, a step back was needed for the optimization and preparation of more stable particles against extracting additives (i.e. water-soluble polymers, proteins, etc.).

4.3.3.2 Mixture of PCMs: Cyn/DPA@HDOH_GS

To prevent the DPA extraction from the SLMs, particles made of a mixture of PCMs were prepared. It has been reported that by using a mixture of PCMs defects are created in the solid matrix due to the non-good packing of PCM molecules of different types. This should help better encapsulation of even hydrophilic molecules (i.e. dyes, drugs).²⁹ If the dye and DPA are well encapsulated in these defects, the solvation and loss of the dye-DPA interaction by external polymers (i.e. PVA, gelatine) should be avoided. Glyceryl tristearate (GS, $T_m^{GS}=54-72^\circ\text{C}$, **Scheme 4.8**) a triglyceride deriving from three units of stearic acid was selected as the mixing PCM with HDOH (50:50 in weight).



Scheme 4.8: a) chemical structure of GS and b) schematic representation of the particles made of a mixture of PCMs.

Initially, the same quantity of DPA (5 wt. %), used for the preparation of HDOH microparticles (see experimental section 7.3.4.1), was tested in the bulk mixture **Cyn I/DPA@HDOH_GS**. A small broad shoulder at $\lambda = 550$ nm (**Figure 4.25a**, blue line) coming from residual non-protonated **Cyn I** molecules was detected. This was ascribed to the GS that was acting as plasticizer forming a eutectic mixture with HDOH ($T_m^{HDOH,GS} = 46^\circ\text{C}$), lowering the HDOH matrix rigidity (indicated by the loss of the solid-to-solid transition typical for long chain *n*-alcohols) when cooling (**Figure 4.25b**) and partially inhibiting the interaction between the dye and the DPA.

To tackle this problem, the quantity of DPA was doubled (10 wt. %) and, in the solid state of the mixture, the shoulder at $\lambda_{\text{max}} = 550$ nm disappeared (green line, **Figure 4.25a**) and the band narrowed down. When the mixture was heated above 55°C ($T > T_m^{HDOH,GS}$), the bluish color turned to magenta and the corresponding band at $\lambda_{\text{max, liq}}^{\text{abs } 1} = 530$ nm appeared in the absorption spectrum. A small contribution of the protonated **Cyn I-H⁺** molecules ($\lambda_{\text{max, liq}}^{\text{abs } 2} = 700$ nm, red line

Figure 4.25c) was also observed, suggesting the presence, in this case, of an excess of DPA.

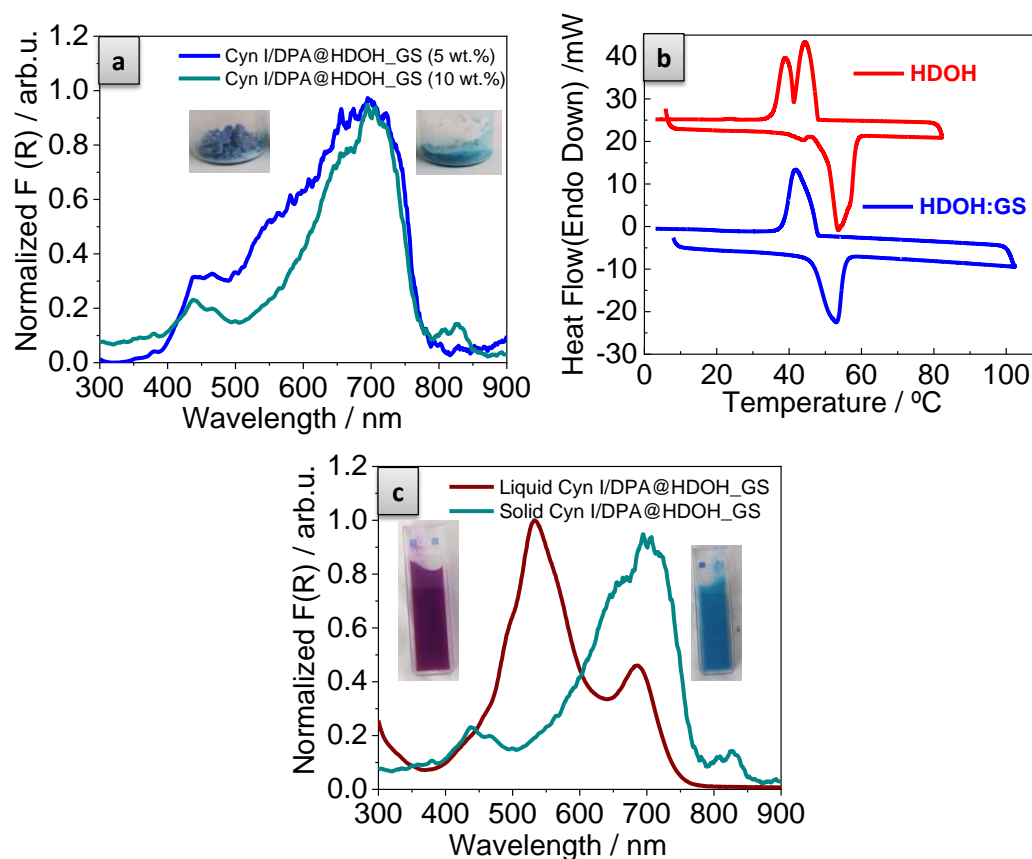


Figure 4.25: a) absorption spectra of the bulk solid mixtures **Cyn I/DPA@HDOH_GS** with 5 (blue line) and 10 wt. % (green line) of DPA at RT; b) DSC of bulk HDOH:GS mixture compared with DSC of HDOH; and c) absorption spectra of mixture **Cyn I/DPA@HDOH_GS** with 10 wt. % of DPA before and after heating above the T_m of HDOH_GS.

Despite the complete thermally induced transition between the non-protonated and protonated **Cyn**, upon **HDOH_GS** melting, we decided to proceed with the preparation of SLMs (see experimental section 7.3.4.2) to corroborate the preservation of the thermochromic properties after the addition of water-soluble polymers.

- **Cyn I/DPA@HDOH_GS microparticles**

Cyn I/DPA@HDOH_GS SLMs, with round shape and sizes between 20-40 μm (by SEM and OM, **Figure 4.26a-b**), were thus prepared with the previously explained emulsion-cooling method. The bluish suspension of the particles at RT turned to magenta when heating above the melting point of the **HDOH_GS** mixture

(55°C) and turned back to the initial state when cooling, mimicking the behaviour observed in the bulk mixture (**Figure 4.26c**).

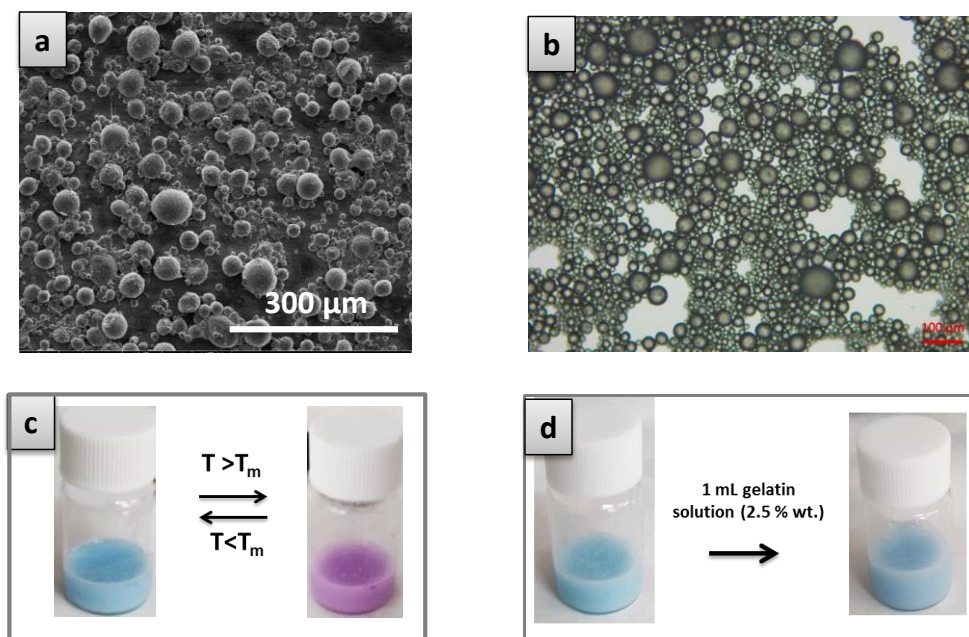


Figure 4.26: a) SEM and b) optical microscope images of **Cyn I/DPA@HDOH_GS** SLMs and c) digital images of the suspensions of the SLMs before and after heating above the $T_m^{\text{HDOH_GS}}$ and d) before and after adding 1 mL of gelatin solution (2.5 wt. %).

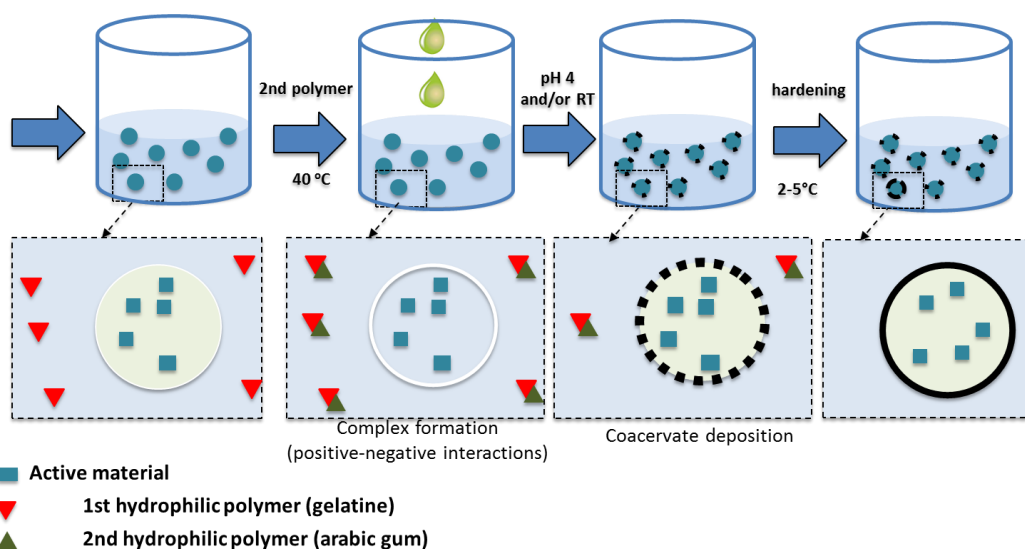
Interestingly, when the **Cyn I/DPA@HDOH_GS** SLMs were mixed with 1 mL of gelatine solution (2.5 wt. %), no apparent color change was observed by naked eye (**Figure 4.26d**). This experiment confirmed and demonstrated the potentiality of these particles, made with mixture of PCMs, to better encapsulate the dye and the DPA avoiding interaction with external compounds (and extraction), such as the gelatin or water soluble polymers. Therefore, we proceed to encapsulate these particles via complex coacervation.

4.3.4 Preparation of multi-responsive functional capsules

4.3.4.1 Cyn I/DPA@HDOH_GS@GEL_GA

The coacervation method, which has been previously optimized in the group, allows encapsulating solid particles through the formation of coacervates in their surface and the consequent reticulation (gelation), forming a protective polymeric shell. In complex coacervation, the coacervates are made by insoluble polymeric materials that contain high amount of water and are formed when the isoelectric point of two initially water-soluble polyelectrolytes, at a certain pH and

temperature, is reached (see introduction section 1.4.2). Gelatin and gum Arabic were used for the preparation of the capsules.²⁸ A schematic representation of the procedure followed is presented in **Scheme 4.9**. Cyn I/DPA@HDOH_GS SLMs were re-suspended in 10 mL of a gelatin solution (2.5 wt. %) at 40°C (below the $T_m^{\text{HDOH_GS}}$). Successively, 10 mL of a solution of gum Arabic (2.5 wt. %) were added, after which the polymers start establishing electrostatic interactions. Subsequently, the pH was reduced to 4 to maximize this interaction (the isoelectric point of the two polymers), and the temperature was let to drop up to RT, during which the coacervates deposits in the surface of the SLMs forming a thin polymeric film. Finally after cooling with ice (2-5°C), the polymer jellifies forming a stable and robust polymeric shell (for more detail see experimental section 7.3.4.3). Noticeably, the temperature of the process was kept along all process below the $T_m^{\text{HDOH_GS}}$ preventing the melting of the SLMs.



Scheme 4.9: schematic representation of the complex coacervation method used for the encapsulation of the SLMs.

The microcapsules (MCs) obtained after the synthesis evidenced a core-shell structure, with a thin transparent layer around the particles (**Figure 4.27a**), which was clearly observed by direct inspection, with the optical microscope. They presented spherical shape and sizes slightly larger (20-50 μm) than the naked SLMs (**Figure 4.27b**).

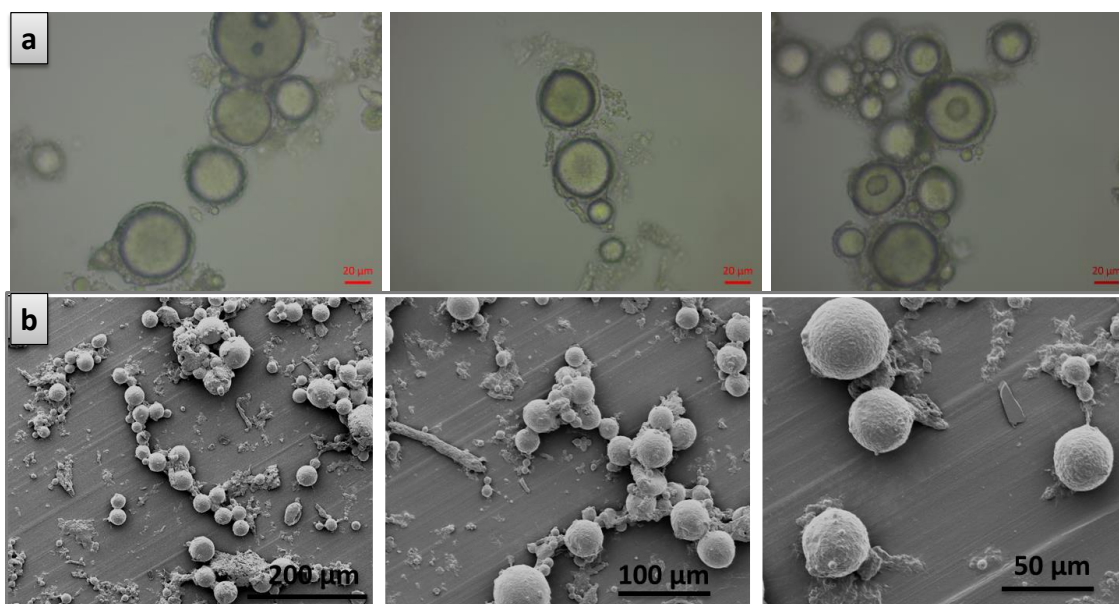


Figure 4.27: a) optical microscope and b) SEM images of the **Cyn I/DPA@HDOH_GS@GEL_GA** MCs.

$^1\text{H-NMR}$ spectrum was acquired to confirm the presence of the **HDOH_GS** mixture within the core of the gelatine-gum Arabic (**GEL_GA**) polymeric MCs. Because of the poor solubility of the porous polymeric shell in CDCl_3 , when the capsules were stirred in CDCl_3 , only the inner part (**HDOH_GS**) was expected to be extracted and dissolved. However to facilitate the extraction of the core materials, the capsules were suspended in CDCl_3 and then mixed with the vortex before running $^1\text{H-NMR}$ spectrum. **Figure 4.28a** compares the spectra of the treated capsules with the spectra of pure **HDOH** and **GS**. The $^1\text{H-NMR}$ spectrum of the capsules showed the presence of the characteristic peaks of **HDOH** at 3.63 ppm ($-\text{CH}_2-$, m) and **GS** at 4.10-4.29 ppm ($-\text{CH}_2\text{COO}$, m). The amount of material encapsulated (payload) was calculated to be approximately 55 wt. % of the total weight of the capsules. A well-defined T_m at 43°C , coming from the mixture **HDOH_GS**, was observed in the DSC of the capsules (**Figure 4.28b**). This same peak was obtained for the structured SLMs, which confirmed that **HDOH_GS** stays in a separated phase and that was not mixing with the polymeric shell.

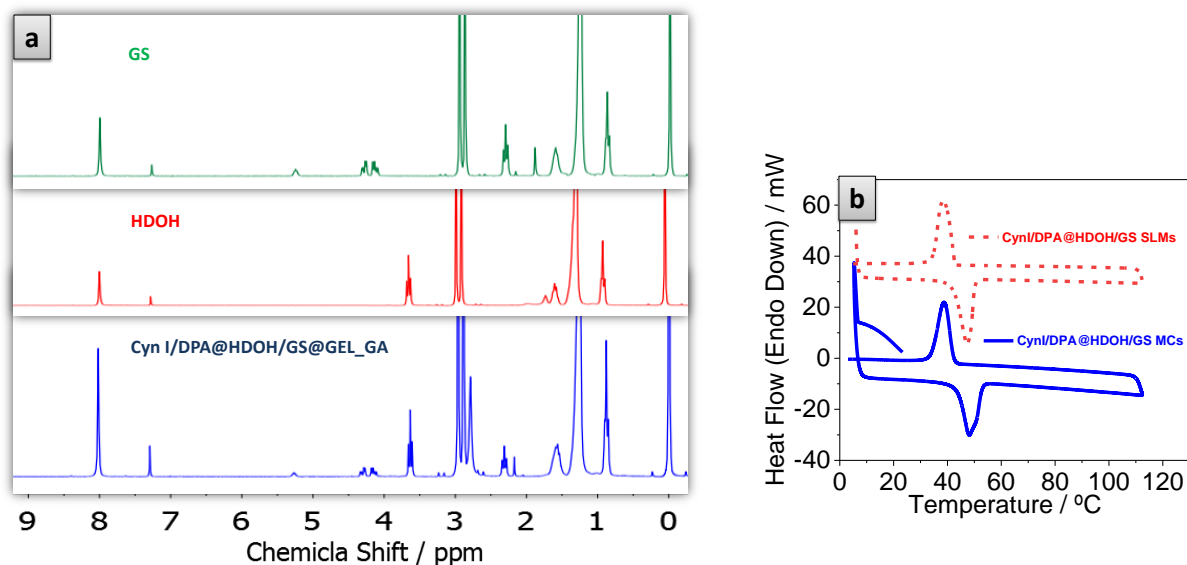


Figure 4.28: a) ¹H-NMR of the **Cyn I/DPA@HDOH_GS@GEL_GA** MCs, HDOH and GS for comparison. The corresponding ¹H-NMR peaks of **GS** appeared at $\delta = 0.87$ (t, 3H, (CH₃)₃), 1.25-1.29 (s, 26H, (CH₂)₁₃), 1.60 ppm (m, 6H, (CH₂)₃), 2.31(m, 6H, (CH₂)₃), 4.1-4.2 9(m, 4H (CH₂COO)₂), 5.2 (m, H, CHCOO) and the **HDOH** ones at $\delta = 0.88$ (t, 3H, (CH₃)) 1.26 (s, 26H, (CH₂)₁₃), 1.53 (m, 2H, CH₂) and 3.63 ppm (m, 2H, OCH₂); b) DSC of the **Cyn I/DPA@HDOH_GS@GEL_GA** MCs (blue line) and the **Cyn I/DPA@HDOH_GS** SLMs (dashed red line) for comparison.

- **Thermochromic properties**

The freeze-dried MCs preserved the bluish color of the suspension and of the initial bulk mixture. The absorption spectrum showed the characteristic band ($\lambda^{\text{abs}}_{\text{max}} = 710$ nm, **Figure 4.29a**) of the **Cyn I-H⁺**. The powder turned to reddish-magenta color ($\lambda^{\text{abs}}_{\text{max}} = 526$ nm, **Figure 4.29a-b**) after heating above the $T_m^{\text{HDOH/GS}}$ (43°C).

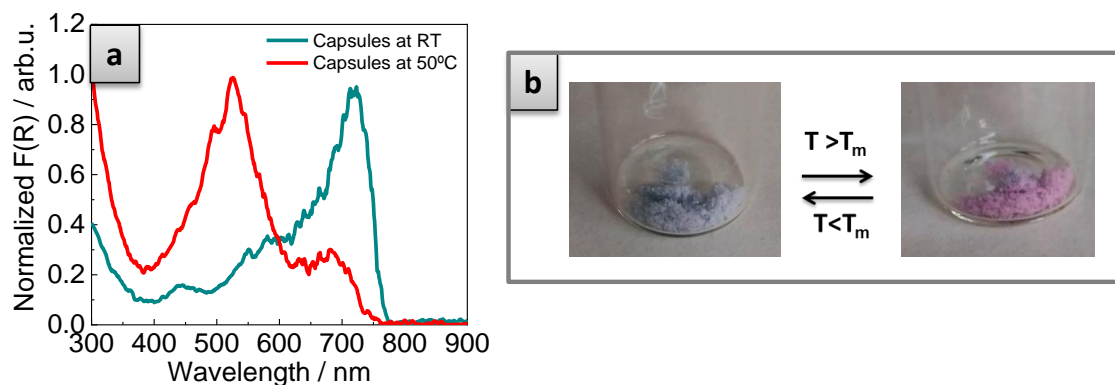


Figure 4.29: a) absorption spectra and b) digital images of the **Cyn I/DPA@HDOH_GS@GEL_GA** MCs at RT and after heating at 50°C.

In addition, the full recovery of the absorption bands of both protonated ($\lambda^{\text{abs}}_{\text{max}} = 710 \text{ nm}$) and non-protonated ($\lambda^{\text{abs}}_{\text{max}} = 526 \text{ nm}$) species, upon three heating-cooling cycles (**Figure 4.30a-b**) confirmed the reversibility of the system and the thermal stability of the dye upon temperature variation. No leaking of the HDOH_GS mixture was observed after heating the MCs above the $T_m^{\text{HDOH_GS}}$. As far as we know this is the first switchable thermochromic solid material based on ketocyanine dyes and produces a spectral shift as large as 210 nm.

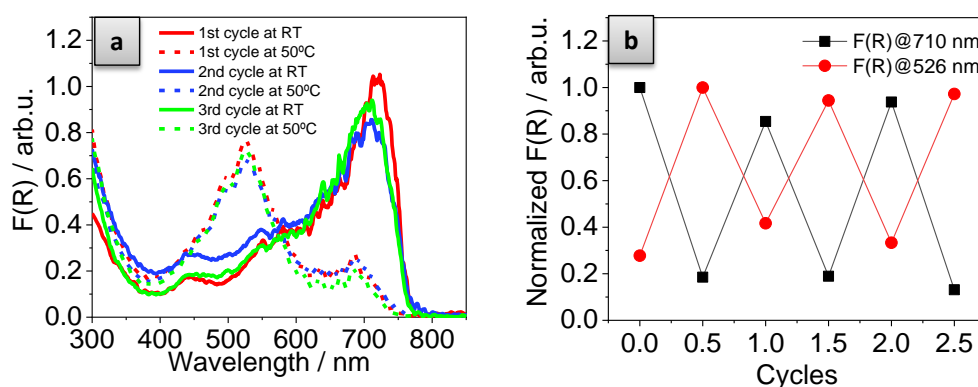


Figure 4.30: a) absorption spectra of **Cyn I/DPA@HDOH_GS@GEL_GA** MCs after three heating-cooling cycles and b) normalized absorption at $\lambda_{\text{max}} = 710$ and 526 nm after three heating-cooling cycles.

- **Halochromic properties**

The blue MCs containing the solid **Cyn I/DPA@HDOH_GS** mixture (at RT) were exposed to NH_3 vapours collected from an ammonia solution (23 wt. %). Captivatingly, they turned, within 20 minutes of exposure, to pink (**Figure 4.31b**), indicating that the NH_3 vapours were able to displace the equilibria towards the non-protonated form of **Cyn I** ($\lambda^{\text{abs, NH}_3}_{\text{max, sol}} = 510 \text{ nm}$, **Figure 4.31a-b**) by diffusing inside the capsules (through the shell) and competitively interacting with DPA (acid-base reaction). The high permeability of the polymeric shell towards the exposed vapours was something crucial for obtaining the pH-induced color change. However, this process was irreversible and after the loss of interaction between the **Cyn I** and **DPA**, the thermochromic properties were inhibited.

On the contrary, non-treated (with NH_3) capsules kept at 50°C converted from reddish to greenish upon 20 minutes of exposure to HCl . This confirmed the

formation of **Cyn I-H⁺** molecules through the exposure to acidic vapors. Noticeably, with this system one (pH or temperature) or two simultaneous stimuli (pH and temperature) could be used to induce color changes. Again the thermochromic behavior was lost after HCl-treatment obtaining an irreversible pH-responsiveness in the same material. This system could be used as complex anti-counterfeiting strategy or as indicator that records the material has been exposed at some point to acidic/basic vapours. Indeed the material shows reversible thermochromic properties until it is exposed to acid/base vapours.

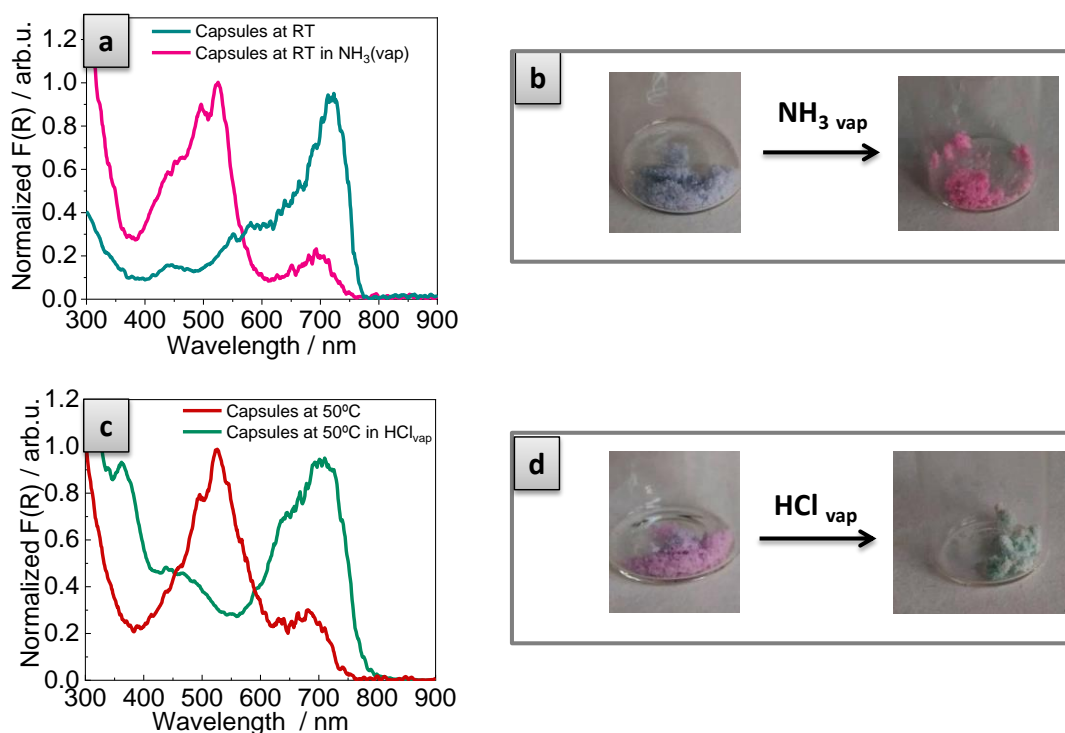


Figure 4.31: a) normalized absorption spectra and b) digital images of **Cyn I/DPA@HDOH_GS @GEL_GA** MCs at RT and after being exposed to NH₃ vapors; c) normalized absorption spectra and d) digital images of **Cyn I/DPA@HDOH_GS @GEL_GA** MCs at 50°C and after being exposed to HCl vapors.

4.3.4.2 Tunability of the chromogenic properties of the capsules

Once demonstrated the capability of these capsules to respond to different stimuli (i.e. temperature, pH) we intended to explore the tunability of the chromogenic properties of the capsules.

- **Switching temperature**

We changed the nature of the encapsulated PCM mixture in order to vary the temperature at which the color change is observed. Stearic acid (SA), a long hydrocarbon chain acid, which exhibits a melting point at 69°C, was selected and mixed with GS and **Cyn I**. When mixed with GS two melting transitions were detected by DSC (**Figure 4.32**) at 50 and 65°C.

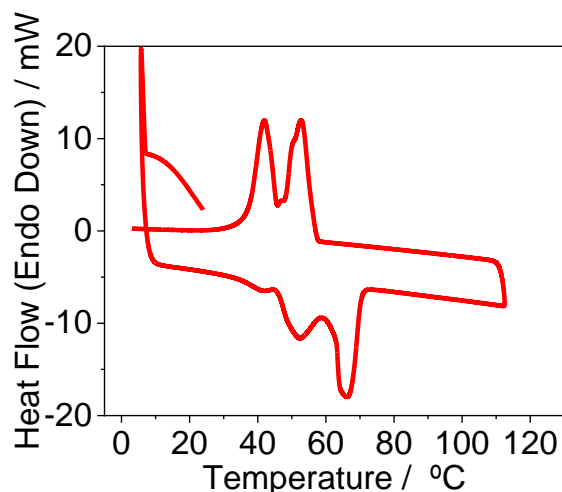


Figure 4.32: DSC of the SA_GS mixture. Two T_m (50 and 65°C) were observed.

As usual, before encapsulating, the study of the optical properties of the bulk mixtures was carried out. In this case, only 5 wt. % of DPA was needed to protonate **Cyn I** molecules in the solid SA_GS mixture. The greenish solid ($\lambda^{\text{abs}}_{\text{max, sol}}=714$ nm) turned to a blue liquid ($\lambda^{\text{abs}}_{1, \text{max, liq}}=550$ nm, $\lambda^{\text{abs}}_{2, \text{max, liq}}=714$ nm) when heated above the $T_m^{\text{SA_GS}}$ (which in this case was 65°C, **Figure 4.33a-b**). By changing the PCM mixture we were able to modify the temperature at which the switching is produced. In the liquid state of the mixture there was a significant contribution of **Cyn I-H⁺**, which could be ascribed due to the intrinsic acidity of the new matrix ($\text{pK}_a^{\text{SA}} 10.15 < \text{pK}_a^{\text{HDOH}} 16.2$). This produced a new color and a color transition, besides it occurred at a different temperature. Once proved the thermally induced change of the new mixture we proceed to the encapsulation.

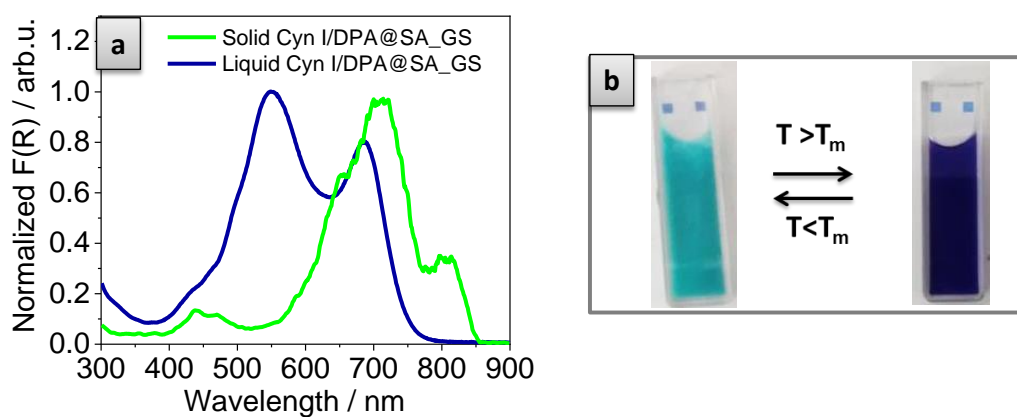


Figure 4.33: a) normalized absorption spectra and b) digital images of the **Cyn I/DPA@SA_GS** bulk before and after heating at 65°C.

4.3.4.2.1 Cyn I/DPA@SA_GS@GEL_GA

The SLMs and the corresponding capsules (containing them) of the obtained **SA_GS** mixture were successfully obtained with a well-defined core-shell structure (**Figure 4.34a-b**), oval shape and sizes ranging from 50-80 μm .

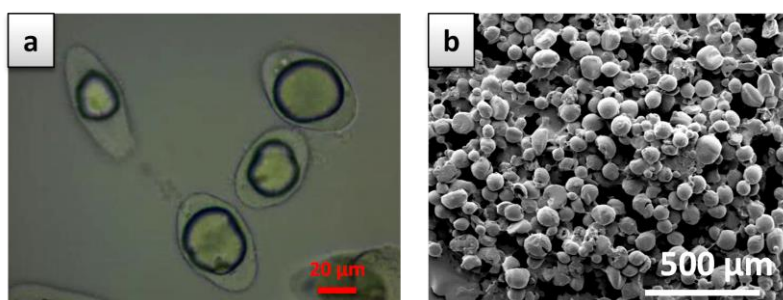


Figure 4.34: a) optical microscope and b) SEM images of the **Cyn I/DPA@SA_GS @GEL_GA** capsules.

$^1\text{H-NMR}$ spectrum in CDCl_3 was acquired to calculate the efficiency of the encapsulation of the **SA_GS** mixture (**Figure 4.35a**). Since all the characteristic peaks of SA overlapped with the ones of GS, we decided to compare the spectrum of the capsules with that of a controlled amount of **SA_GS** mixture (60 mg) assuming that the initial **SA_GS** ratio used for the synthesis is maintained in the capsules. The same amount of DMF (10 μL) was added as the reference (signals at 7.96 (m), 2.97 (s), 2.88 (s) ppm) in both tubes in order to determine the relation between the peaks. The peak at 1.61 ppm (of SA and GS, CH_2 , m) was selected to calculate the quantity of **SA_GS** encapsulated (payload), which was around 54% of the total weight of the capsules. On the other hand, the DSC of the capsules

exhibited two defined melting points at 50°C and 65°C characteristic of the SA_GS mixture (**Figure 4.35b**).

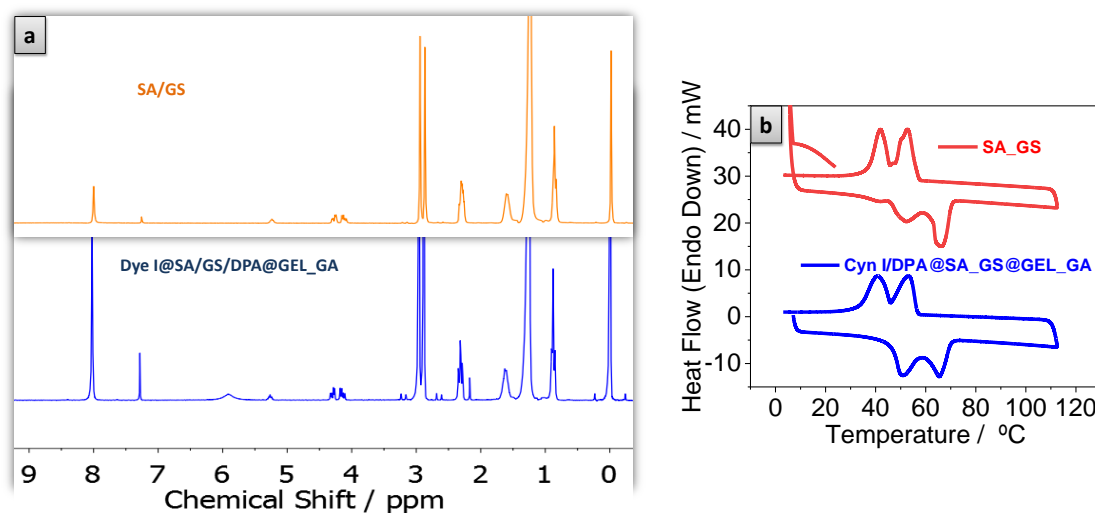


Figure 4.35: a) ¹H-NMR spectrum and b) DSC of the **Cyn I/DPA@SA_GS@GEL_GA** capsules and SA_GS mixture for comparison. The corresponding ¹H-NMR peaks of **GS** appeared at $\delta = 0.87$ (t, 3H, (CH₃)₃), 1.25-1.29 (s, 26H, (CH₂)₁₃), 1.60 ppm (m, 6H, (CH₂)₃), 2.31 (m, 6H, (CH₂)₃), 4.1-4.2 (m, 4H (CH₂COO)₂), 5.2 (m, H, CHCOO) and the ones of **SA** at $\delta = 0.88$ (t, 3H, (CH₃)) 1.26 (s, 28H, (CH₂)₁₄), 1.64 (m, 2H, CH₂) and 2.35 ppm (m, 2H, CH₂COOH).

The freeze-dried capsules showed greenish color and absorption spectra with $\lambda^{\text{abs}}_{\text{max}} = 720$ nm (**Figure 4.36a-b**), and turned to blue, ($\lambda^{\text{abs}}_{1\text{max}} = 550$ nm, $\lambda^{\text{abs}}_{2\text{max}} = 720$ nm, **Figure 4.36a-b**), when the powder was heated above the $T_m^{\text{SA}_\text{GS}}$ (65°C), reproducing nicely the thermochromic transition of the bulk solution during the solid-to-liquid phase change. Again no leaking of the SA_GS mixture was observed in the MCs after heating above the $T_m^{\text{SA}_\text{GS}}$.

As previously done for the **Cyn I/DPA@HDOH_GS@GEL_GA** MCs, four heating-cooling cycles were performed. The recovery of the characteristic absorption spectrum of both protonated and non-protonated species after each cycle, confirmed the reversibility of the system and the absence of degradation of the **Cyn I** molecules even at this higher switching temperature (**Figure 4.37a-b**).

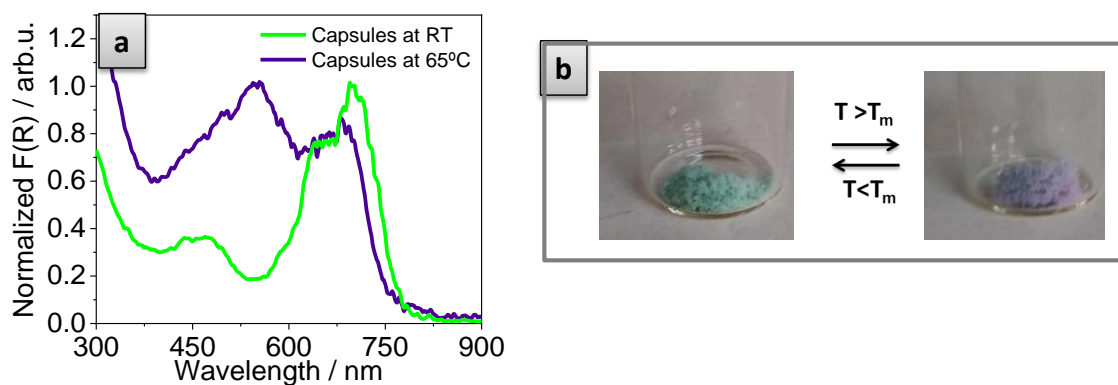


Figure 4.36: a) normalized absorption spectra of the **Cyn I/DPA@SA_GS @GEL_GA** MCs at RT and at 65°C and b) digital images of the freeze-dried MCs before and after heating above the $T_m^{SA_GS}$.

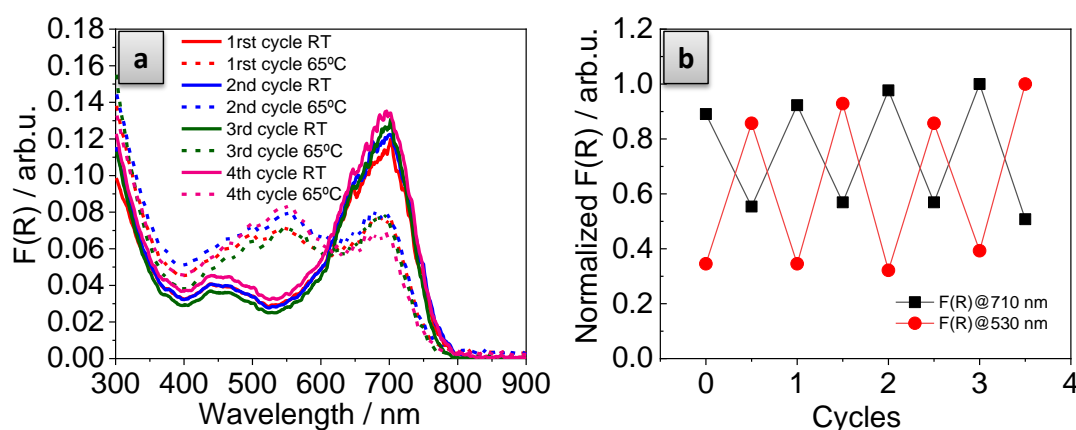


Figure 4.37: a) absorption spectra of **Cyn I/DPA@SA_GS @GEL_GA** MCs after four heating-cooling cycles and b) normalized absorbance at $\lambda_{max} = 710$ and 530 nm after four heating-cooling cycles.

When the MCs were exposed during 20 minutes at RT to NH_3 vapors from ammonia solution (23 wt. %), they turned from greenish ($\lambda_{max, sol}^{abs} = 720$ nm) turned to intense pink color ($\lambda_{max, sol}^{abs, NH_3} = 510$ nm, **Figure 4.38a-b**).

On the other hand when the MCs were exposed to HCl vapors, while heated at 65°C, the magenta color switched to greenish and presented partial absorption in the NIR region ($\lambda_{max, sol}^{abs, HCl} = 720$ nm, **Figure 4.38a-b**). Also in this case the thermochromic transition was lost after the treatment with NH_3 and HCl vapors.

Overall, we were able to obtain core-shell capsules of two different Cyn I/DPA-based mixtures. The capsules present pH-responsiveness and thermochromic transitions whose switching temperature could be modulated by changing the PCM mixture.

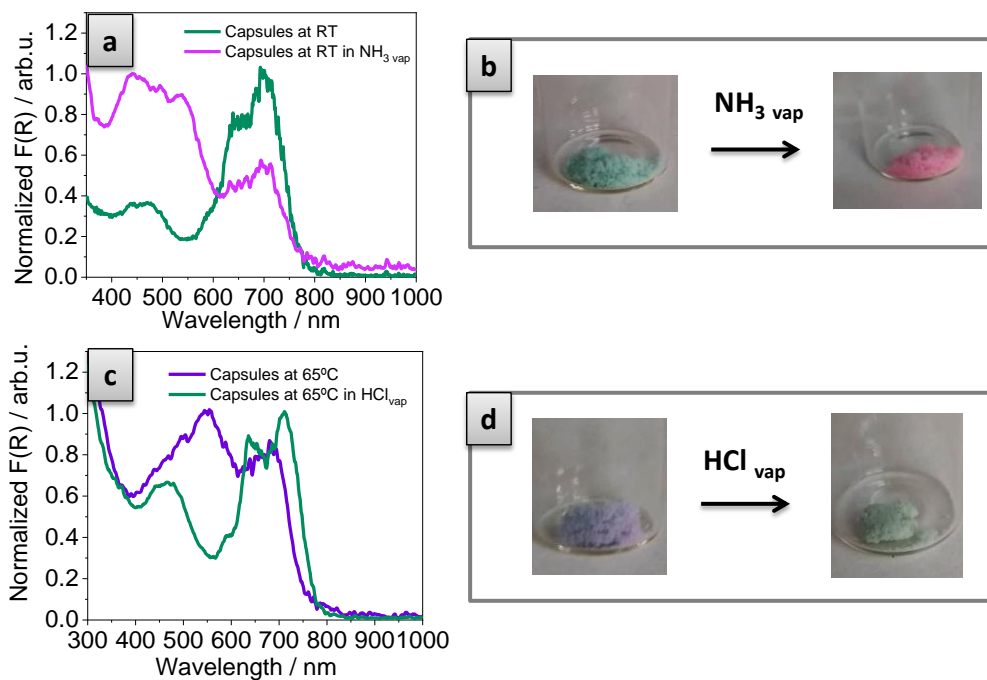


Figure 4.38: a) absorption spectra and b) digital images of **Cyn I/DPA@SA_GS @GEL_GA** MCs before and after being exposed to NH_3 vapors and c) absorption spectra and d) digital images of **Cyn I/DPA@SA_GS@GEL_GA** capsules and after being exposed to HCl vapors, while heated at 65°C .

- **Switching colors**

4.3.4.2.2 **Cyn I/BA@HDOH_GS@GEL_GA**

At the beginning of this chapter (section 4.3.1) it was showed that the mixture **Cyn/BA@TDOH** had also thermochromic properties, though yielded different colors at RT, respect to the **Cyn/DPA@HDOH** mixture. The encapsulation of this would provide another material with distinct thermochromic properties, though using, again, the same dye. However, as showed before the use of a mix of PCMs guarantees a more efficient encapsulation of the components. Therefore, the study of the bulk **Cyn I/BA@HDOH_GS** was required prior to encapsulation.

The solvatochromic effect of BA molecules on Cyn I dye and the thermochromic transition were confirmed even for the solid **Cyn I/BA@HDOH_GS** mixture, which reproduced the magenta color ($\lambda_{\text{max, sol}}^{\text{abs}} = 584 \text{ nm}$, **Figure 4.39**) of the solid HDOH-only mixture (**Cyn I/BA@HDOH**) and the blue-shift of the absorption band $\lambda_{\text{max, liq}}^{\text{abs}} = 530 \text{ nm}$ upon melting

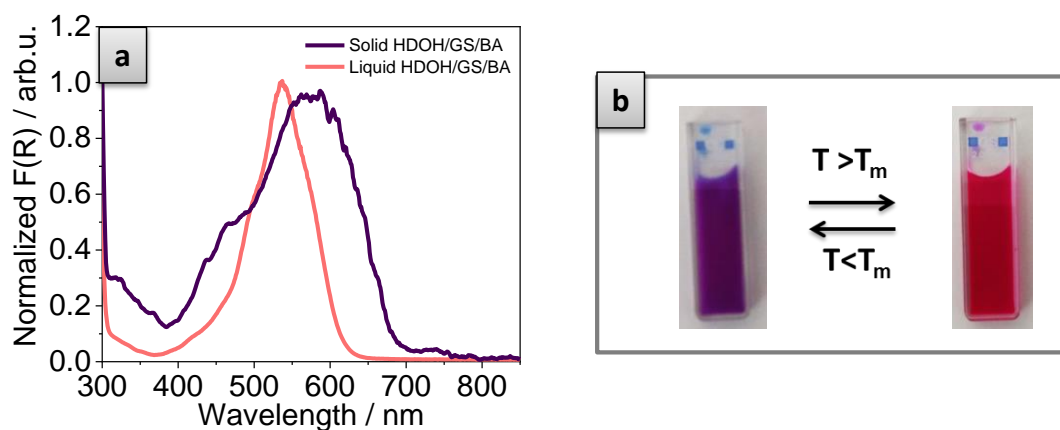


Figure 4.39: a) absorption spectra and b) digital images of the **Cyn I/BA@HDOH_GS** bulk mixture at RT and after heating at 55°C.

In the first attempt to prepare the MC with **Cyn I/BA@HDOH_GS**, from the preformed SLMs, we realized that after the coacervation process, no interaction between the SLMs and the coacervates (which stay separated from the SLMs) occurred. From the optical microscope images it could be distinguished a separation of the two materials (**Figure 4.40**).

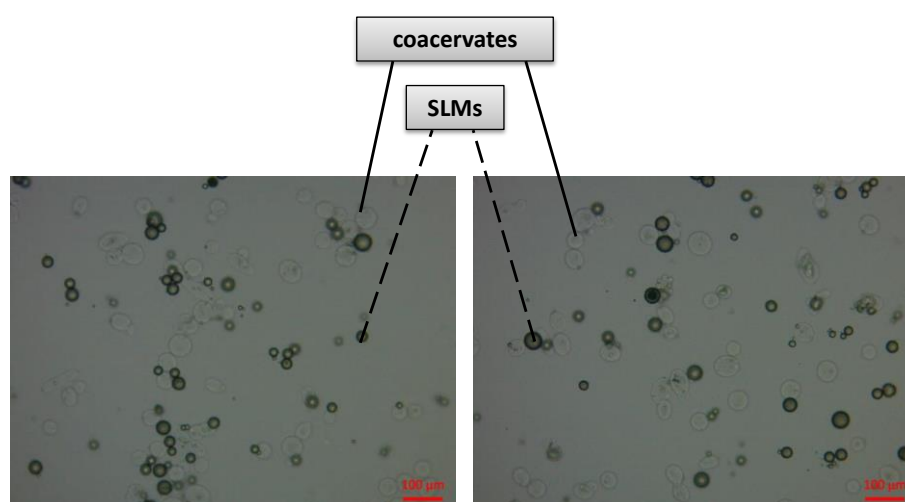


Figure 4.40: optical microscope images showing lack of interaction between the preformed **Cyn I/BA@HDOH_GS** SLMs and the coacervates.

The only difference between the preparation of these and the **Cyn I/DPA@HDOH_GS @GEL_GA** capsules was the presence of BA, instead of DPA, in the initial SLMs. Presumably, some of DPA molecules, layering on the SLMs surface were acting as surfactant and conferring negative charge to the surface, which must help the interaction with the coacervates and the consequent deposition. This

was not the case of the non-charged BA, which has lower tendency to migrate to the surface and does not have permanent negative charge. Moreover, the stabilizer used (PVA), a neutral polymer, also was not helping the establishment of interactions between the coacervates and the surface of the particles. For this reason, we decided to change the surfactant to sodium dodecyl sulphate (SDS), a widely known anionic surfactant often used in the group for the stabilization of O/W emulsions, to compensate the lack of negative charge on the surface.

Changing the surfactant and reducing the stirring rate (from 3000 to 500 rpm, see experimental section 7.3.4.5) during the formation of the particles (SDS has higher emulsification power), **Cyn I/BA@HDOH_GS@GEL_GA** MCs with core-shell structure (**Figure 4.41a-b**), round shape and sizes ranging from 30-60 μm were obtained.

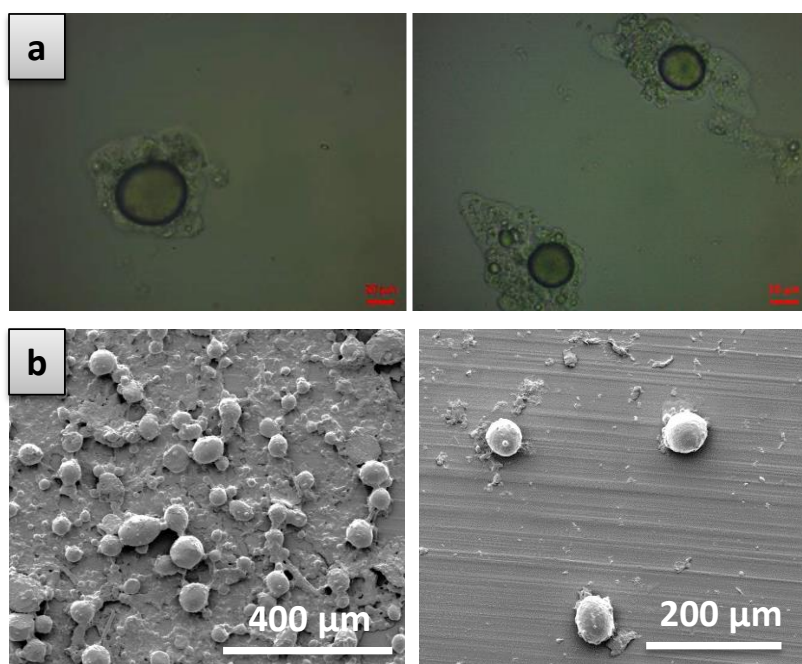


Figure 4.41: a) optical microscope and b) SEM images of **Cyn I/BA@HDOH_GS@GEL_GA** MCs.

The encapsulation of **HDOH_GS**, was confirmed by $^1\text{H-NMR}$ (payload of 52 wt. %, **Figure 4.42a**) and by the observation, in DSC measurements, of a well-defined peak at 46°C (**Figure 4.42b**) corresponding to the $T_m^{\text{HDOH_GS}}$. Worth to mention that the T_m observed for **HDOH_GS** in these capsules was slightly higher than the one reported in the **HDOH_GS** capsules with **DPA**. A possible explanation is the stronger plasticizing effect of **DPA**, which reduced the T_m of the mixture.

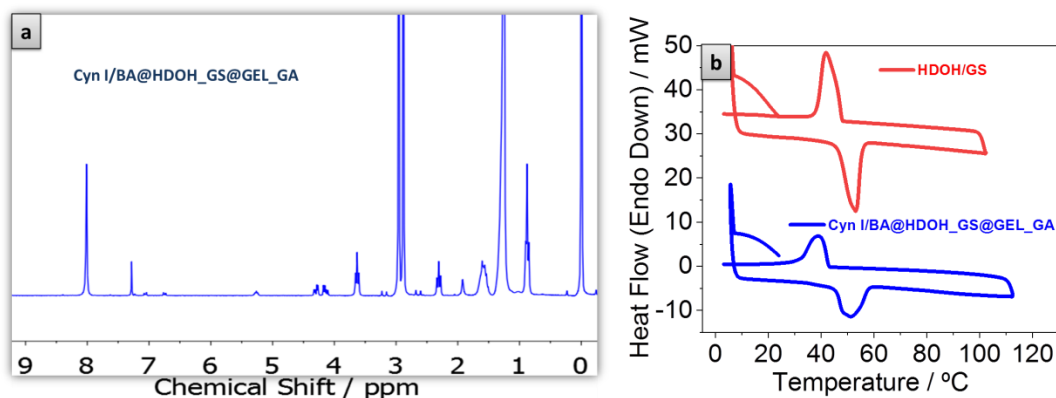


Figure 4.42: a) $^1\text{H-NMR}$ spectrum and b) DSC of the **Cyn I/BA@HDOH_GS@GEL_GA_01** MCs. The corresponding $^1\text{H-NMR}$ peaks of **GS** appeared at $\delta = 0.87$ (t, 3H, $(\text{CH}_3)_3$), 1.25-1.29 (s, 26H, $(\text{CH}_2)_{13}$), 1.60 ppm (m, 6H, $(\text{CH}_2)_3$), 2.31(m, 6H, $(\text{CH}_2)_3$), 4.1-4.2 (m, 4H $(\text{CH}_2\text{COO})_2$), 5.2 (m, H, CHCOO) and the ones of **HDOH** at $\delta = 0.88$ (t, 3H, (CH_3)) 1.26 (s, 26H, $(\text{CH}_2)_{13}$), 1.53 (m, 2H, CH_2) and 3.63 ppm (m, 2H, OCH_2).

- **Thermochromic properties**

At room temperature the magenta color of the powder (**Figure 4.43a**) indicated that the BA molecules were solvating the non-protonated form of **Cyn I** in the solid state of the **HDOH_GS**. By contrast, when the powder was heated above the **HDOH_GS** melting point (50°C), the capsules became pink and the absorption band blue shifted 40 nm ($\lambda^{\text{abs}}_{\text{max}}=530$ nm, **Figure 4.43b**) because of the loss of the solvation by BA. This process was done several times confirming the reversibility of the system and the absence of degradation of **Cyn I** (**Figure 4.43**).

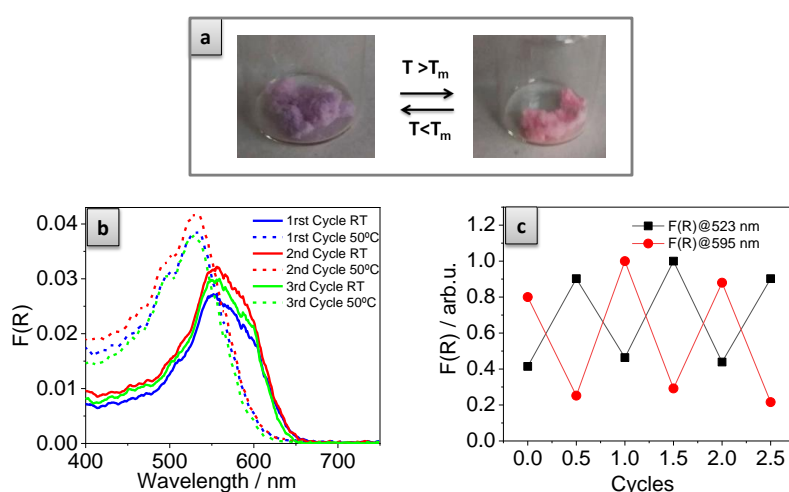


Figure 4.43: a) digital images of the **Cyn I/BA@HDOH_GS @GEL_GA_01** MCs before and after heating at 55°C ; b) absorption spectra and c) normalized absorbance at $\lambda_{\text{max}} = 595$ and 523 nm of **Cyn I/BA@HDOH_GS@GEL_GA** MCs after three heating-cooling cycles.

- **Halochromic properties**

Surprisingly, when the MC powder (at RT) was exposed 20 minutes to NH_3 vapors of ammonia solution (23%), no apparent color change by naked eye was detected. This result could be explained by the fact that in the solid state of the **Cyn I/BA@HDOH_GS** mixture, the stabilized isomer is the non-protonated form of **Cyn I**, solvated by BA. Therefore, even if a strong base was added to the capsules, the non-protonated stabilized isomer will remain unaltered.

In contrast, when the powder was exposed to HCl vapors (37 wt. % aq), it turned to greenish, almost colorless, due to the formation of the low-energy absorption band ($\lambda^{\text{abs}}_{\text{max}} = 724 \text{ nm}$, **Figure 4.44b**). It is important to notice that the band with $\lambda^{\text{abs}}_{\text{max}} = 724 \text{ nm}$ is shifted to longer wavelengths in comparison with the λ_{max} of the absorption band of the **Cyn I-H⁺** in the **Cyn I/DPA@HDOH_GS** mixture, again due to the solvation of the BA molecules in the solid state of the mixture. Moreover, when the greenish MCs powder (**Figure 4.44a**) was exposed to ammonia vapors (23%), reverted back to the initial magenta state. The recovery of the respective absorption spectra upon various cycles of exposure to HCl (37% aq, 10 min), and NH_3 (23%, 10 min) vapors, confirmed the reversibility of the material even upon strong pH changes (**Figure 4.44c**).

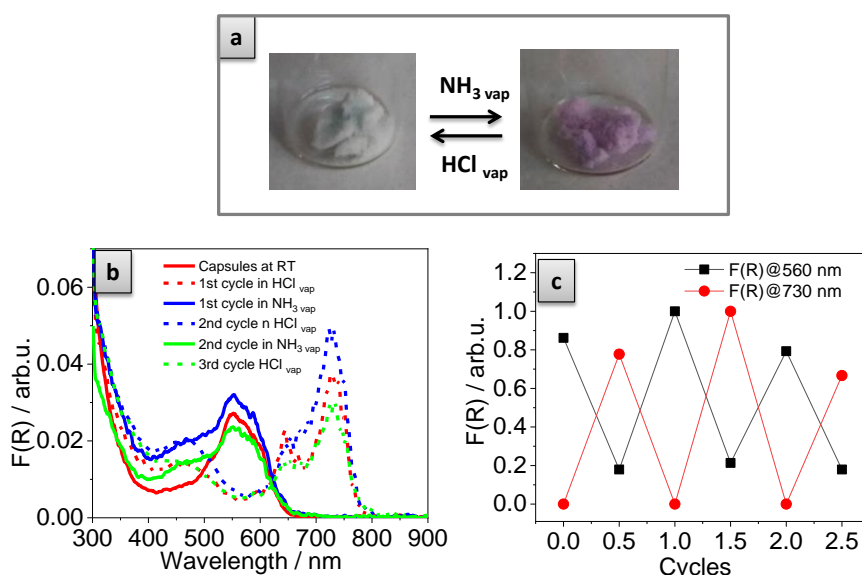


Figure 4.44: a) digital images of **Cyn I/BA@HDOH_GS@GEL_GA** MCs before and after being exposed to HCl_{vap} and successively to NH_3 vap; b) absorption spectra and b) normalized absorbance at $\lambda_{\text{max}} = 730$ and 560 nm of **Cyn I/BA@HDOH_GS@GEL_GA** capsules after three NH_3/HCl cycles.

Interestingly, after the exposure of **Cyn I/BA@HDOH_GS@GEL_GA** MCs to NH_3 vapors the system recovered the initial magenta color at RT and also the thermochromic properties. This is a very different aspect respect to the **Cyn I/DPA@PCM** MCs, which lost the thermochromic activity once subjected to any NH_3/HCl vapors.

Therefore, with BA as the color developer in the mixture we ended up with a three-state colored capsules-based solid material (**Figure 45a-b**):

- i) non-protonated **Cyn I**, solvated by **BA** (magenta color),
- ii) non-protonated **Cyn I**, non-solvated by **BA** (pink colored MCs), accomplished upon heating the powder above the T_m^{PCM} ,
- iii) protonated **Cyn I-H⁺** solvated by **BA** (greenish, almost colorless MCs), obtained at RT under HCl vapors.

Amazingly, it is possible to reversibly switch from one state to the other by changing either pH or/and temperature (**Figure 4.45a-b**).

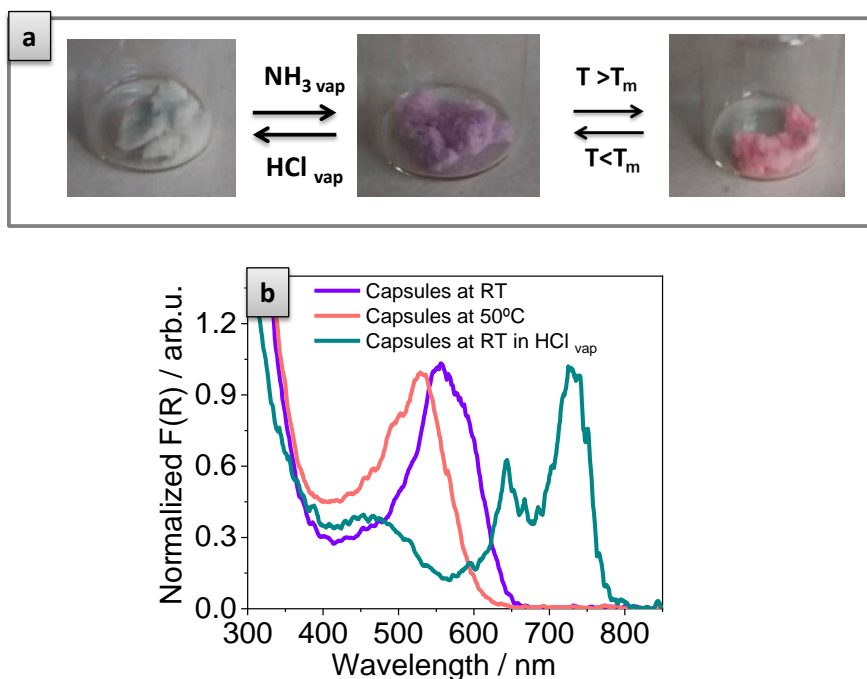


Figure 4.44: a) digital images and b) absorption spectra of the **Cyn I/BA@HDOH_GS@GEL_GA** capsules before and after heating at 55°C and after the exposure the MCs to HCl vapours, at RT.

4.4 Summary

In this part of the thesis we have reported the development of a novel and general methodology for the preparation of multi-responsive chromogenic materials, which respond alternatively or simultaneously to two stimuli (pH and/or temperature) by changing their absorption properties. The main conclusions drawn from this study conducted for this methodology are summarized below:

- i) we proved the thermochromic behavior of ketocyanine dyes when embedded in a tri-component thermochromic system. Taking advantage of the high sensitivity of the optical properties of ketocyanine dyes on the medium and the modulability of the type of interactions (solvatochromism/acid/base reactions) of these dyes with the surrounding species; we demonstrated very high tunability of the absorption properties of the mixture by suitably choosing the type and concentration of the dye, color developer and type of PCM.
- ii) we managed to structure the bulk mixtures in the form of solid lipid particles conferring them stability against external agents by mixing two different PCMs that create defects in the matrix and encapsulate more efficiently the dye and the color developer.
- iii) we successfully encapsulated the SLPs through a reaction-free encapsulation method that prevents any possible dyes degradation.
- iv) with the encapsulation we were able to transfer the bulk behavior of these mixtures to solid materials, thus obtaining, as far as we know, also the first NIR-absorbing thermo/pH-sensitive solid material based on ketocyanine dyes.
- v) We finally demonstrated the tunability of the chromic response of the material (transition-temperature and color) by simply changing the components of the mixture encapsulated either the nature of the PCMs or the interaction with the color developer.

The ketocyanine dyes used along this work are also fluorescent. For this, future work will be focused on studying the fluorescent properties of the capsules at

different temperature and pH conditions. If, as expected, these changes are also observed in emission, these capsules will exhibit not only **multi-stimuli** but also **dual** (absorption and emission) response, what increases even more the complexity and the interest of these smart materials. Finally, given the easy tenability of the optical properties of ketocyanine dyes upon extension of the conjugation length, both absorption and emission changes could be further dipped in the NIR region.

4.5 References

1. P.-A. Bouit, K. Kamada, P. Feneyrou, G. Berginc, L. Toupet, O. Maury, C. Andraud *Adv. Mater.* **2009**, 21, 1151.
2. S. Achilefu, R. B. Dorshow, J. E. Bugaj, R. Rajagopalan, *Invest. Radiol.* **2000**, 35, 479.
3. J. Lee, B. Yoo, H. Lee, G. D. Cha, H.-S. Lee, Y. Cho, S.Y. Kim, H. Seo, W. Lee, D. Son, M. Kang, H. M. Kim, Y. I. Park, T. Hyeon, D.-H. Kim *Adv. Mater.* **2017**, 29, 1603169.
4. J. Fabian, H. Nakazumi, M. Matsuoka, *Chem. Rev.* **1992**, 92, 1197.
5. M. Matsuoka, *Infrared Absorbing Dyes*, Plenum, New York, **1990**.
6. G. M. Fischer, E. Daltrozzo, A. Zumbusch, *Angew. Chem., Int. Ed.* **2011**, 50, 1406.
7. G. Qian, Z. Zhong, M. Luo, D. Yu, Z. Zhang, Z. Y. Wang, D. Ma, *Adv. Mater.* **2009**, 21, 111.
8. G. Qian, H. Abu, Z. Y. Wang, *J. Mater. Chem.* **2011**, 21, 7678.
9. H. Meng, D. Tucker, S. Chaffins, Y. Chen, R. Helgeson, B. Dunn, F. Wudl, *Adv. Mater.* **2003**, 15, 146.
10. H. Wang, T. E. Kaiser, S. Uemura, F. Würthner, *Chem. Commun.* **2008**, 1181.
11. K. H.-Y. Chan, H.-S. Chow, K. M.-C. Wong, M. C.-L. Yeung, V. W.-W. Yam, *Chem. Sci.* **2010**, 1, 477.
12. G. Qian, Z.Y. Wang, *Adv. Mater.* **2012**, 24, 1582.
13. A. Mishra, M. K. R. Fischer, P. Bäuerle *Angew. Chem.* **2009**, 48, 2474.
14. Y. Liu, M. Chen, T. Cao, Y. Sun, C. Li, Q. Liu, T. Yang, L. Yao, W. Feng, F. Li, *J. Am. Chem. Soc.* **2013**, 135, 9869.
15. C. Reichardt *Chem. Rev.* **1994**, 94, 2319.
16. S. A. Hilderbrand, R. Weissleder *Chem. Commun.* **2007**, 2747.
17. F. Hövelmann, I. Gaspar, J. Chamiolo, M. Kasper, J. Steffen, A. Ephrussi, O. Seitz *Chem. Sci.* **2016**, 7, 128.
18. L. Jiao, F. Song, J. Cui, X. Peng, *Chem. Commun.* **2018**, 54, 9198.
19. S. Miltsov, C. Encinas, J. Alonso-Chamarro, *Tetrahedron Lett.* **2001**, 42, 6129.
20. M. Puyol, C. Encinasa, L. Riveraa, S. Miltsov, J. Alonso *Sensor Actuat B-Chem* **2006**, 115, 287.
21. M. Puyol, S. Miltsov, I. Salinas, J. Alonso *Anal. Chem.* **2002**, 74, 570.

22. L. Rivera, M. Puyol, S. Miltsov, F. Villuendas, J. Alonso, *Sensor Actuat B-Chem* **2006**, 114, 705.
23. L. Carreto, A. R. Almeida, A. C. Fernandes, W. L. C. Vaz, *Biophys. J.* **2002**, 82, 530.
24. D. Yin, L. Ma, W. Geng, B. Zhang and Q. Zhang *Int. J. Energy Res.* **2015**, 39, 661.
25. CRC Handbook of Chemistry and Physics, Internet Version, <http://www.hbcnpnetbase.com> (accessed November 6, **2019**)
26. A. Ayala-Garcia, “Desarrollo de microcápsulas de fragancias con materiales de alta disponibilidad comercial para su uso en detergencia”, Universitat Autònoma de Barcelona, **2019**.
27. S. A. Wissing, O. Kayser, R. H. Müller, *Adv. Drug Deliv. Rev.* **2004**, 56, 1257.
28. C. G. de Kruif, F. Weinbreck, R. de Vries, *Curr. Opin. Colloid Interface Sci.* **2004**, 9, 340.
29. C. Zhu, D. Huo, Q. Chen, J. Xue, S. Shen, Y. Xi, *Adv. Mater.* **2017**, 29, 1703702.

CHAPTER 5

Nanostructured High-Temperature thermofluorochromic Sensors

A versatile threshold temperature fluorescent sensor based on the glass transition temperature-triggered emission activation of a dye/developer duo, encapsulated in polymeric nanoparticles was developed along this chapter. The emission enhancement, detectable even by unaided eye is completed within a narrow temperature range and activates at adjustable threshold temperatures up to 200 °C. Fluorescence is chosen as sensing probe because of its high detection sensitivity and advanced spatial and temporal resolution. The strategy is based on nanoparticles prepared from standard thermoplastic polymers, a fluorescence developer, and the commercially available Rhodamine B base dye, a well-known and widely used highly fluorescent molecule. By making nanoparticles of different thermoplastic polymers, fast, abrupt, and irreversible disaggregation-induced fluorescence enhancement, with tunable threshold temperature depending on the nanoparticles polymer glass transition temperature is achieved. As a proof-of-concept for the versatility of this novel family of nanoparticles, their use for sensing the thermal history of environments and surfaces exposed to multi-threshold temperature is showed.

5.1 Introduction

Temperature tunable chromogenic and/or emissive materials have been proposed during the last decades on a fast, easy and reliable tool to measure¹ and/or indicate instantaneous temperature changes (reversible systems) or thermal histories (irreversible systems), without the need of intrusive and expensive techniques.² These emerging materials can be used in a wide range of sensing applications, from smart food packaging^{1b} to fluorescent thermometers³ or temperature indicators.^{4,5} Among all, those showing thermally-induced emission changes (thermofluorochromic materials) reveal very attractive for practical applications, given the fast acquisition, high sensitivity in detection and spatial and temporal resolution of luminescence-based signals. Some temperature-sensitive luminescent materials such as organic polymers and dyes,⁶ nanotube-based systems,⁷ quantum dots,⁸ inorganic phosphors and organic-inorganic hybrid materials⁹ are already used to measure real time temperatures or reached temperature peaks.

Still, to widen the applicability of these materials, it is imperative to find simpler, more robust and time/cost-effective synthetic strategies that permit their scale-up and commercialization in different areas of interest. This is particularly necessary for high-temperature fluorescent sensors which, though would be relevant in many technological applications (such as monitoring electronic components, measure thermal exposure of vehicle parts or as indicator in sterilization processes, among many others),^{1,2,4} only a scarce number of examples have been reported, up to date.

5.1.1 Polymers as tool for high-temperature fluorescent sensing

One of the most fruitful approaches, so far, to obtain such high-temperature fluorescent sensors consists in the development of polymeric temperature tunable emissive materials.² In these systems, the temperature induced optical variations (fluorescence shift, activation/quenching) arise from changes in the polarity¹⁰ and/or viscosity¹¹ of the dye-containing polymeric matrix, which in turn triggers differential polymer-dye interactions^{2,12} (proton transfer, hydrogen bonding). A very nice example of the latter approach is the work reported by G. Ruggeri *et al.*,¹³ in which a water soluble perylene derivative, *N, N'*-bis(2-(1-piperazino)ethyl)-3,4,9,10-perylenetetracarboxylic acid diimide dichloride (PZPER), dispersed in

poly(vinyl alcohol) (PVA) displayed an emission enhancement after heating the film from 25°C to 115°C (**Figure 5.1a**). At 25 °C the film showed a prevalent emission band at longer wavelengths ($\lambda_{\text{max}} = 600 \text{ nm}$) caused by the presence of H-type aggregates (**Figure 5.1a-b**). The PZPER aggregates, which are promoted mostly by hydrogen bonding interactions between the side units of the molecules, are favored at room temperature (RT) due to the high polarity of PVA. When the temperature rised, the overall emission of the film increased, due to the more fluorescent monomeric PZPER (**Figure 5.1a-b**), favoured by the higher molecules mobility and the decrease of the intermolecular interactions between perylene molecules.

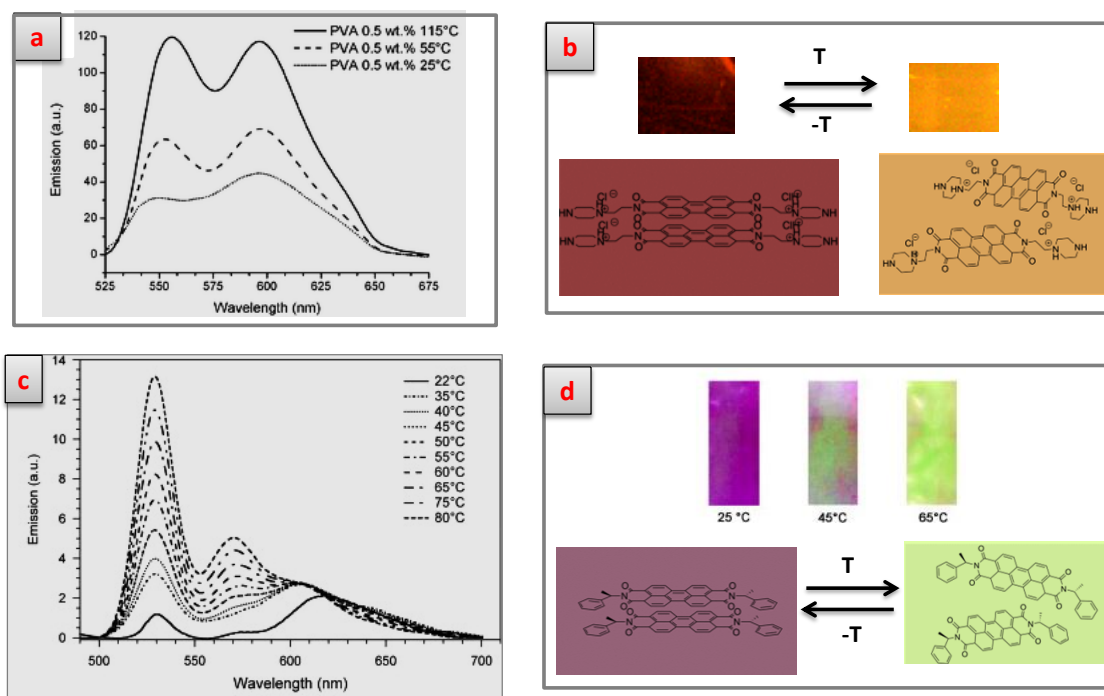


Figure 5.1: a) temperature-dependent emission ($\lambda_{\text{exc}} = 450 \text{ nm}$) spectra of a PVA film containing of PZPER (0.5 wt. %), b) digital images of the PVA film at RT and after heating at 110°C ($\lambda_{\text{exc}} = 366 \text{ nm}$) and proposed scheme of the aggregated-disaggregated state of the PZPER molecules within the film (data adapted from ref. 13); c) temperature-dependent emission spectra ($\lambda_{\text{exc}} = 300 \text{ nm}$) of a LLDPE film containing the R-Pery (0.1 wt. %); d) digital image of the same film ($\lambda_{\text{exc}} = 366 \text{ nm}$) at different temperatures; and scheme of the aggregated-disaggregated state of the R-Pery molecules within the film. Data adapted from ref. 14.

A similar work reported by the same authors demonstrated the temperature-dependent emission of a chiral perylene derivative, that is, *N, N'*-bis-(*R*)-(1'-phenylethyl)-perylene-3, 4, 9, 10-tetracarboxydiimide (**R-Pery**) dispersed into a linear low-density polyethylene matrix (LLDPE).¹⁴ At 22 °C the film presented the

prevalence of the emission band at about 620 nm attributed to the presence of a significant amount of R-Pery aggregates. Upon heating, the emission bands at about 530 and 570 nm (characteristic of the monomeric units) started to be predominant already at annealing temperatures of 35 °C (**Figure 5.1c-d**). During heating, the enhanced solubility of R-Pery in the polymer and the increased mobility of the macromolecular structure of LLDPE resulted in temporarily breaking off the dye aggregates and the inhibition of intermolecular interactions.

Though successful, sensing materials based on this approach require specific chemical functionalities in the polymer and/or dye, one of the key limitations for their implementation in real applications. Moreover, the reversibility of these systems does not allow recording the thermal history of surfaces or environments. In order to overcome these limitations, Weder *et al.*^{1,4,15} found a polymer independent approach based on cyano-oligo *p*-phenylene vinylene (COPV) dyes that produces an irreversible luminescence shift or activation/quenching when the temperature rises. The optical variations came from different aggregation states of the dye molecules^{1,2,4,16} due to viscosity decrease that the polymer suffers when the glass-transition temperature (T_g) is surpassed. Such temperature-triggered dye aggregation uses the tendency of the aromatic molecules initially kinetically trapped within the matrix in the disaggregated state (achieved upon fast cooling of the embedding matrix), to yield the thermodynamically favored aggregated state once the T_g is reached. **Figure 5.2** shows the emission shift (from the monomeric blue fluorescence to the aggregate green emission) of a COPV-containing polycarbonate (PC) sheet upon reaching the matrix T_g .

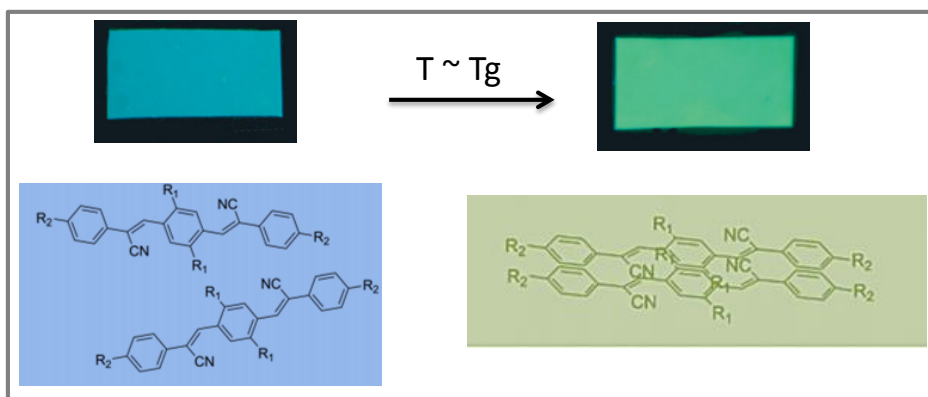


Figure 5.2: Emission color ($\lambda_{exc}= 365$ nm) of COPV-containing PC film before and after heating above the T_g of the polymer and scheme of the disaggregated/aggregated state of the COPV molecules in the polymeric matrix. Data adapted from ref. 1.

However, this strategy also suffers of drawbacks, such as the tiny and/or linear optical shifts (of mixed monomer/aggregate emission),^{1,4} the requirement of opportunely designed and synthesized dyes (e.g. cyano-oligo *p*-phenylene vinylene)^{1,2,4} and the thermodynamic tendency to yield stable aggregates already at RT with time (the sensor would expire after certain time due to the slow tendency of the dyes to form the aggregated state even at RT).¹⁷ Moreover, though many examples of T_g -triggered irreversible temperature indicators operating around RT^{15c} or slightly above 100 °C^{15a,b} have been reported, only a few examples can be found for high threshold-temperature sensors (≥ 130 °C).⁴

5.1.2 Designing polymeric NPs as novel off/on fluorescent sensors

In order to tackle all the problems mentioned above and to develop an off/on fluorescent sensor activated at high temperatures ($>130^\circ\text{C}$) with fast and abrupt emission enhancement, in this work we designed a system based on three components:

i) a fluorescent commercially available organic **dye**, composed of planar aromatic rings, and that emits efficiently in dilute solutions, while, at higher concentrations, due to the formation of aggregates, which facilitate exciton interactions and nonradiative pathways, the emission is weakened or even totally quenched.¹⁸ This phenomenon is referred to as aggregation-caused quenching (**ACQ**). Therefore, in the proposed system, by playing with the aggregated-dissaggregated state of the dye, a low (off) or a highly (on) emissive state should be generated, respectively.

ii) a high T_g **thermoplastic polymer** (matrix), which triggers the aggregated-disaggregated state of the dyes during its phase transition (glass transition temperature).

iii) **additives**, if required, such as long hydrocarbon chain molecules with hydrogen bonding ability to help the mobility and the disaggregation of the dye during the phase transition of the polymer.

Finally, in order to generate an ink with the capability to irreversibly sense high temperature changes and to get closer to a real application, all these components must be nanostructured in the form of nanoparticles (NPs) to have a water-based suspension stable over time.

In a recent work, Klymchenko *et al.* reported polymeric NPs containing cationic Rhodamine B octadecyl derivative (R18) whose fluorescence could be fine-tuned by controlling their aggregation state.¹⁹ At high dye loads and with the use of small counter-anions, non-fluorescent NPs are obtained due to the ACQ of the R18 dye. Nevertheless, dilution of the dye and/or use of bulkier counter-anions that favor disaggregation, allowed the preparation of bright and emissive NPs (**Figure 5.3**).¹⁹

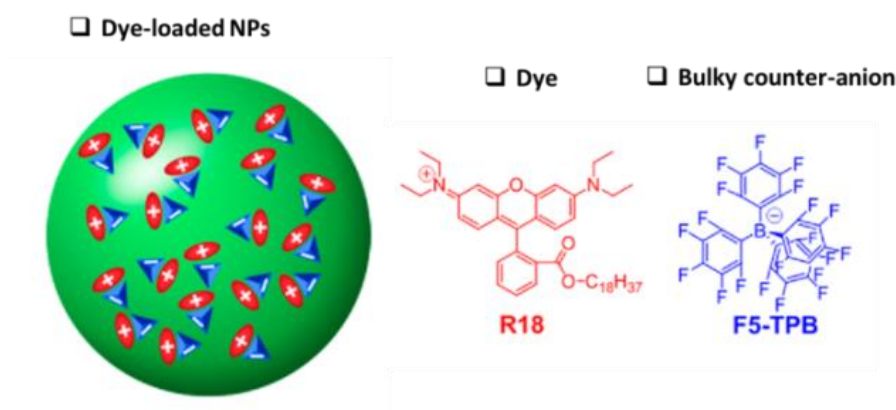


Figure 5.3: schematic representation of dye-doped fluorescent NPs using cationic R18 and bulky counter-anions and the structure of the dye and the bulky counter-anion. Data adapted from ref. 15.

In this work we hypothesize that the strategy reported by Klymchenko *et al.*, which allows a static interconversion (so far induced only upon specific synthetic conditions) can be converted into a dynamic interconversion between the non-emitting (aggregated) and emitting (disaggregated) states of the dye, upon a temperature increase above the T_g of the hosting polymer. Starting from non-fluorescent polymer nanoparticles containing highly concentrated dye, once reached the polymer glassy state, the dye molecules should start diffusing disaggregating and triggering an abrupt emission enhancement. Upon rapid cooling of the polymer material back to RT, the disaggregated state should remain kinetically trapped. In this way an off/on finely tunable irreversible threshold temperature sensor functioning up to really high temperatures ($\sim 200^\circ\text{C}$), could be obtained by using commercial components (**Figure 5.4**).

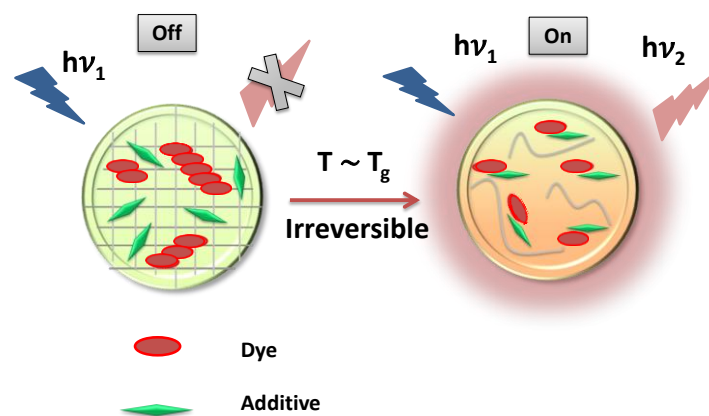
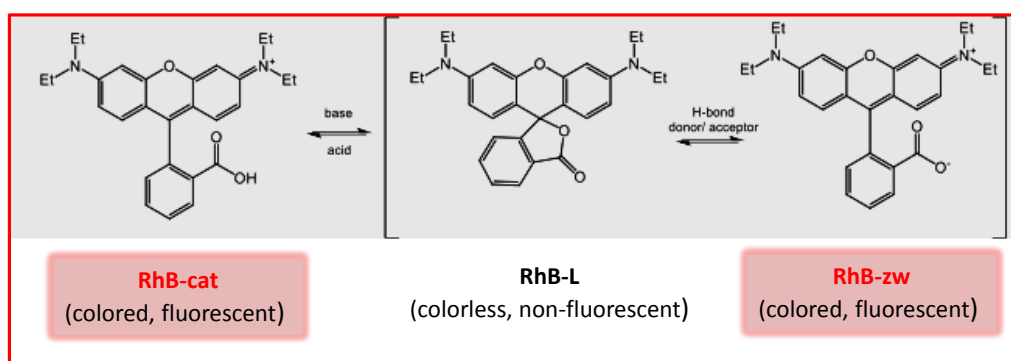


Figure 5.4: proposed scheme for the off/on fluorescent NPs.

Rhodamine B base (**RhB**), a rhodamine derivative xanthene dye, was selected as the dye of interest for this work since it presents a high extinction coefficient, high emission quantum yield (QY) in the visible region (easy to detect) and is commercially available. RhB exhibits several equilibria in solution and the emission and absorption spectra of the dye is known to depend on temperature, solvent, pH and concentration. In protic or chlorinated solvents RhB exists as an equilibrium mixture of a colorless lactone (RhB-L) and a pink colored highly emissive zwitterion (**RhB-Zw**, **Scheme 5.1**). The position of the equilibrium depends on both solvent hydrogen-bond donating ability and the solvent dielectric/polarizability characteristics. As temperature increases the equilibrium shifts toward the less polar lactone. In acidic media a new equilibrium appears due to the protonation of the lactone ring and the formation of the cationic Rhodamine B (RhB-cat), which as well as RhB-zw is colored and highly emissive.



Scheme 5.1: equilibrium between the different forms of RhB: zwitterionic (obtained in polar protic and chlorinated solvents), lactone (non-polar solvents) and cationic (in very acidic conditions).

5.2 Objectives

The aim of the work described along this chapter is to develop tunable high temperature fluorescent sensors with permanent, abrupt, well-defined optical variations (i.e. off/on fluorescence). To fulfill this general objective, different specific targets were pursued:

- i) preparation of highly-loaded RhB polymeric nanoparticles with a) low fluorescent state at RT due to ACQ and b) high emissive state at high T,
- ii) demonstrate that the fluorescent activation temperature can be tuned by simply changing the polymer type of the nanoparticles. These nanoparticles could then be used to trigger the fluorescence at certain selected temperatures between 100°C and 200°C,
- iii) development of a functional material/device to be used as high-temperature off/on threshold fluorescent sensor.

5.3 Results and discussion

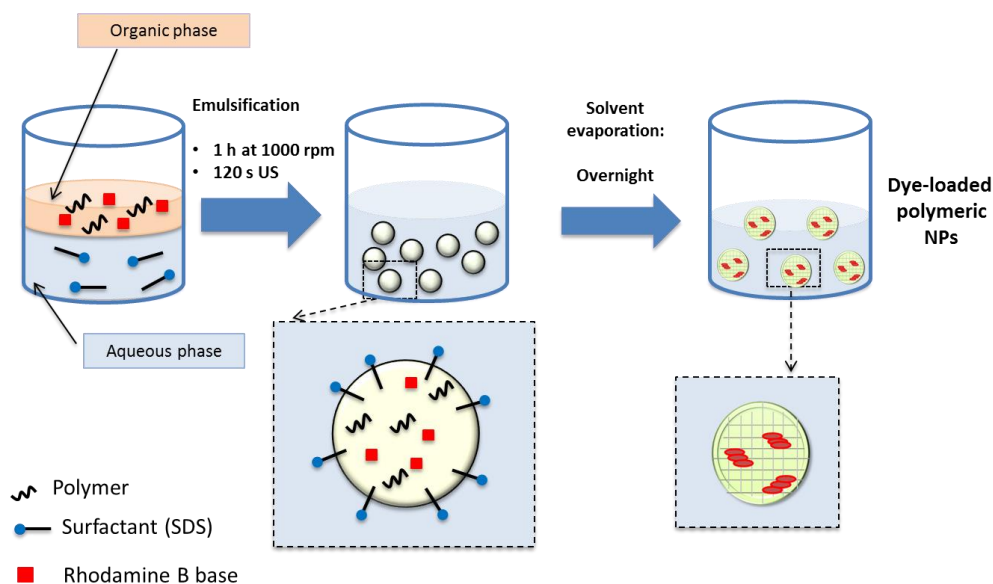
5.3.1 RhB-loaded polymeric NPs

In order to confirm the feasibility of our approach, we first needed to corroborate the ACQ of rhodamine b base in nanostructured polymers. Polystyrene (PS, $T_g = 100^\circ\text{C}$)²⁰ was selected as the starting polymeric encapsulating matrix since it is a standard, easily and commercially available thermoplastic polymer and it has been demonstrated in previous studies its capability to encapsulate dyes with hydrophobic and aromatic moieties, such as Nile Red or fluorescein, which present similar chemical structure and optical properties as rhodamine b base.²¹

Inmaculada García-Moreno and co-workers already encapsulated a Rhodamine derivative (Rhodamine 6G) in polymeric NPs of various sizes (20-160 nm), and showed that for the dye loading in the range of 0.066 - 0.4 wt. %, the emission QY remained stable (68-78%), thus showing no sign of self-quenching.²² On the other hand it has been reported that higher loading (>1 wt. %) of dyes (rhodamines,²³ cyanines, ²⁴ Nile Red,²⁵ etc.) in polymeric NPs leads to ACQ in most of the cases reducing strongly the QY. As expected, higher dyes loading in the polymer matrix favours ACQ.

The minimum concentration at which ACQ is induced is dependent on the dye solubility and this itself depends on the dye and matrix type. Therefore, a concentration study of RhB in PS NPs was carried out to determine the amount of dye to be used in the NPs to ensure negligible emission at RT.

RhB-loaded polystyrene nanoparticles (**RhB@PS**) with high (2 wt. %) and low (0.4 wt. %) concentration of dye were prepared through the reaction-free emulsion-solvent evaporation method adapted from the literature.²⁶ Basically the polymer and the dye are dissolved in dichloromethane, which is immiscible with water and suitable for dissolving PS, and a subsequently O/W nanoemulsion (with the use of ultrasounds) is prepared out. Finally the organic solvent is evaporated inducing the precipitation of the polymer in the form of the NPs (matrix-type capsules) and trapping the dye within the matrix (**Scheme 5.2**, see the experimental section **7.3.5** for the detailed synthesis).



Scheme 5.2: schematic representation of the synthesis followed for the preparation of polymeric NPs containing RhB.

The reddish suspensions obtained after the evaporation of the organic solvent were freeze-dried and in both cases a colored pink powder was obtained. SEM (**Figure 5.4a-b**) corroborated the formation of the NPs (80-150 nm) and the absorption (**Figure 5.4c**) in the visible region ($\lambda_{\max} = 557$ nm, pink color) confirmed the encapsulation of the dye on its coloured zwitterionic RhB-zw form (**Scheme 5.1**). Interestingly, the high concentrated **RhB@PS** (2 wt. %) NPs showed:

- a broader absorption band in the visible region ($\lambda_{\max}^{\text{abs}} = 557$ nm, **Figure 5.4c**) with an intense shoulder at 518 nm (in line with the presence of non-fluorescent aggregates)^{19, 27} and,
- a 7 times weaker, broader and slightly red-shifted fluorescence band ($\lambda_{\max}^{\text{em}} = 610$ nm, **Figure 5.4d**) compared to the less concentrated NPs ($\lambda_{\max}^{\text{em}} = 604$ nm, **Figure 5.4d**). Both the low intensity and the red-shift of the emission band are characteristic of the non-emitting RhB-zw aggregated state. This study indicated that **RhB@PS** NPs with RhB concentration of at least 2wt. % were needed to ensure negligible emission at RT.

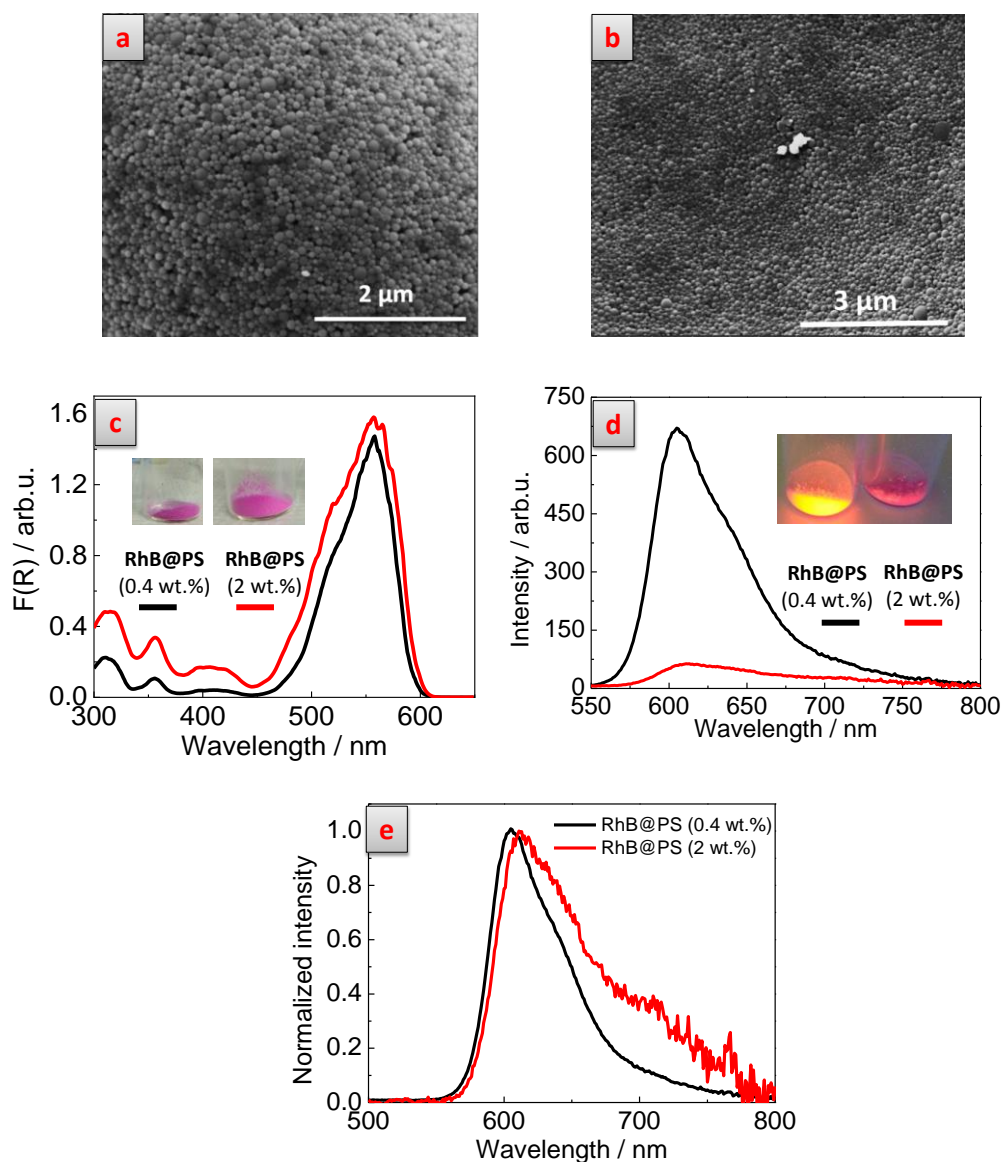


Figure 5.4: SEM images of a) **RhB@PS** (2wt. %) and b) **RhB@PS** (0.4 wt. %) NPs; c) absorption and d) fluorescence spectra and e) normalized fluorescence spectra of **RhB@PS** NPs at two different dye concentration (0.4 and 2 wt. %). Inset: digital images of the freeze-dried NP powders appearance under c) visible light and d) under UV light (365 nm).

Once **RhB@PS** NPs with 2 wt. % of dye-loaded were selected, we aimed to study the temperature-dependent emission through fluorimetry. For this study, the NPs were first heated for 10 min at increasing selected temperatures, from 25°C to 120°C and then cooled down rapidly at RT. The fluorescence of the heated NPs was measured at RT and the emission intensity was compared with the fluorescence of the non-heated NPs. The integrated emission enhancement (ΔF) of the NPs heated at certain T was obtained from the equation: $\Delta F(T) = (F_T - F_{RT})/F_{RT}$, and ΔF_{\max} was defined as the maximum enhancement observed. In the case of **RhB@PS** a

progressive fluorescence enhancement was observed (**Figure 5.5a**), with a $\Delta F^{\max} = 47\%$, obtained after heating the NPs at 105°C . Such enhancement was attributed to the dye molecules disaggregation process occurring upon matrix softening and increase of the mobility of the polymeric chains around the reported polystyrene T_g (100°C).²⁰ The softening of the polymer was clearly demonstrated by the complete loss of the NPs shape once this temperature was reached (**Figure 5.5b**). Interestingly, the enhanced emission was observed after cooling (the fluorescence measurements were carried out at RT), evidencing the irreversibility of the emission activation after the loss of structure of the particles. Concomitant processes accounting for this temperature-induced fluorescence increase were discarded. Indeed, enhancement of the RhB fluorescence due to temperature dependency was excluded as it generally follows the opposite trend.²⁸ On the other side, the simultaneous existence of an equilibrium shift from the non-fluorescent lactone (colorless) to the emitting zwitterionic (colored) isomer was also left out as the latter is the original form already trapped along the formation of the NPs (accounting for their pink color).

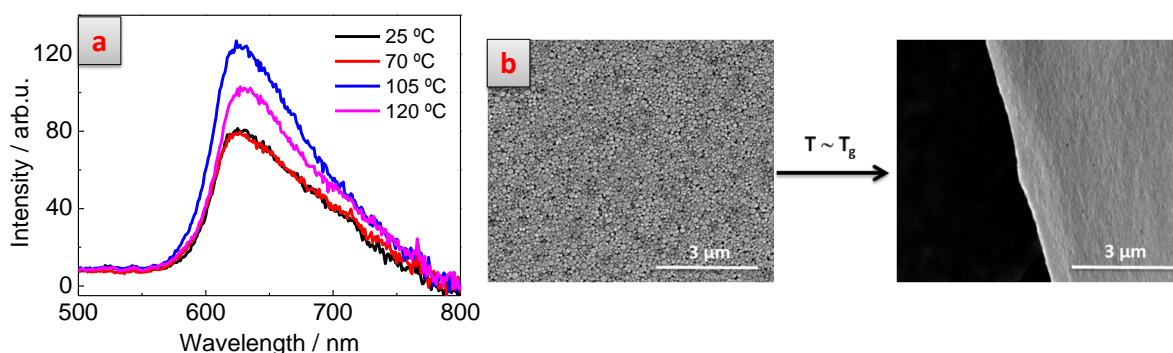


Figure 5.5: a) emission spectra recorded at RT after heating the NPs at different temperatures (from 25°C to 120°C) and b) SEM images before and after heating the **RhB@PS** (2 wt. %) NPs above their T_g .

Though irreversible fluorescence enhancement was measured, the increase of the fluorescence intensity after heating above the T_g of the polymer was not easy to appreciate by naked eye and was not as strong as desired. Indeed, the less concentrated and non-heated **RhB@PS** NPs (0.4 wt. % of dye) were already 6-fold brighter (**Figure 5.4d**) than the heated concentrated **RhB@PS** (2 wt. %, **Figure 5.5a**, blue line) indicating a much higher degree of disaggregated RhB molecules.

This means that only few RhB molecules were undergoing disaggregation in **RhB@PS** (2 wt. %) NPs after the softening of the polymer at high T.

To overcome this limitation, we proposed the co-encapsulation of additives in the particles favoring the diffusion and the disaggregation of RhB at higher temperatures. As a candidate we considered dodecanoic acid (DA), a twelve-carbon non-volatile weak acid with melting point (T_m) of 43.8 °C.²⁹ The reason for this choice is threefold. Above its T_m , DA is expected to act as i) plasticizer of the polymer, increasing the RhB molecules mobility, ii) intercalates between the RhB molecules through the formation of hydrogen-bonds and iii) it is also known to form complexes with spirolactones and spiropyrans molecules through hydrogen-bonding interactions, inducing the opening to the colored and fluorescent form.³⁰

5.3.2 RhB/DA@PS NPs

Following the protocol adopted along this thesis, before the nanostructuration, the behavior of RhB in DA was investigated in bulk solutions, both in solid ($T < T_m^{DA}$) and liquid state ($T > T_m^{DA}$). The pink and highly fluorescent ($\lambda_{\max}^{\text{emi}} = 595$ nm) solution obtained by dissolving the RhB-base in liquid DA ($T > T_m^{DA}$, 47 μM) was in agreement with the formation of mostly the RhB-zw form (**Figure 5.6a, c**). The lack of any fluorescence enhancement upon addition of glacial acetic acid (AA, **Figure 5.6b**), which is described to boost the formation of the RhB-zw form,³¹ confirmed that the formation of this species was almost quantitative already in liquid DA. At lower temperatures ($T < T_m^{DA}$), the solution solidified while maintaining the pink color characteristic of the RhB-zw form. However, in this case, the fluorescence was almost completely quenched ($\lambda_{\max}^{\text{emi}} = 627$ nm) most likely due to the formation of the insoluble aggregates (**Figure 5.6a**). These results confirmed the influence of DA on the ACQ properties of RhB.

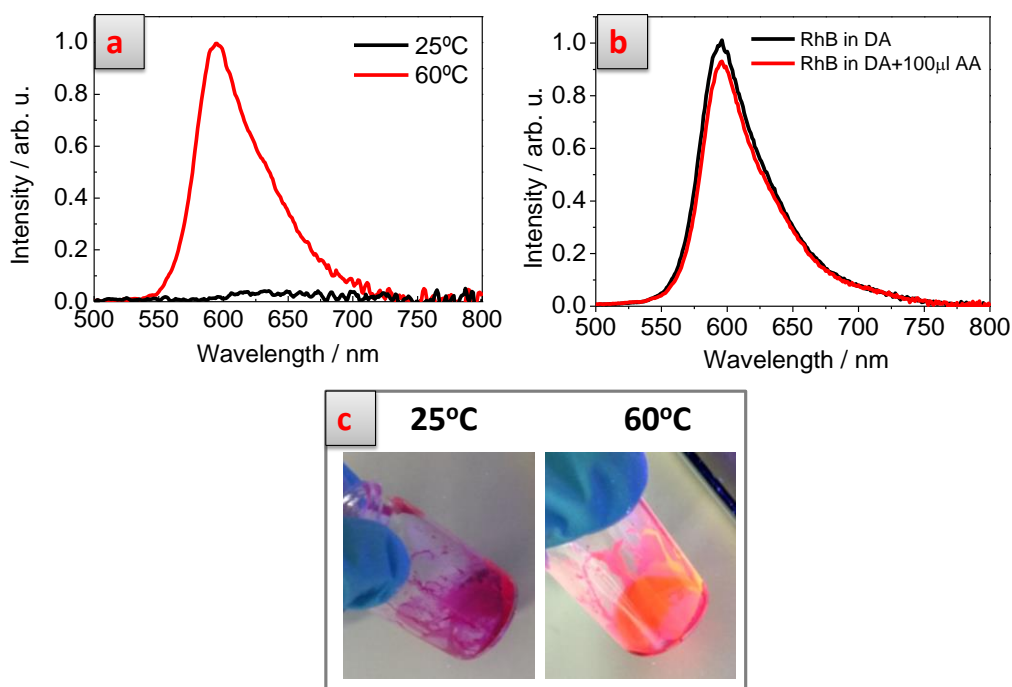


Figure 5.6: a) emission spectra recorded below and above the T_m^{DA} , b) emission spectra recorded before and after the addition of 100µL of AA to liquid **RhB@DA** solution and c) digital images under UV light of the **RhB@DA** solution below (25°C) and above (60°C) T_m^{DA} .

Once proved DA could be used to tune the optical properties of RhB-zw, a synthesis of DA-containing matrix-type capsules was carried out using PS as matrix (**RhB/DA@PS**) and following the same methodology used for **RhB@PS** NPs (2 wt. % RhB respect to PS), but adding in this case DA to the dichloromethane mixture, just before the emulsification process (**Scheme 5.2**, see experimental section **7.3.5**). Such addition resulted in an immediate fluorescence enhancement due to the DA-induced equilibrium displacement towards the dissolved RhB-zw form. Dichloromethane solutions with increasing concentration of DA (0 to 50 mM) were prepared to determine the required DA amount to assure the maximum formation of the RhB-zw form (**Figure 5.7a**). This concentration was 50 mM (**Figure 5.7b**), which and was used for the synthesis of RhB/DA-containing NPs.

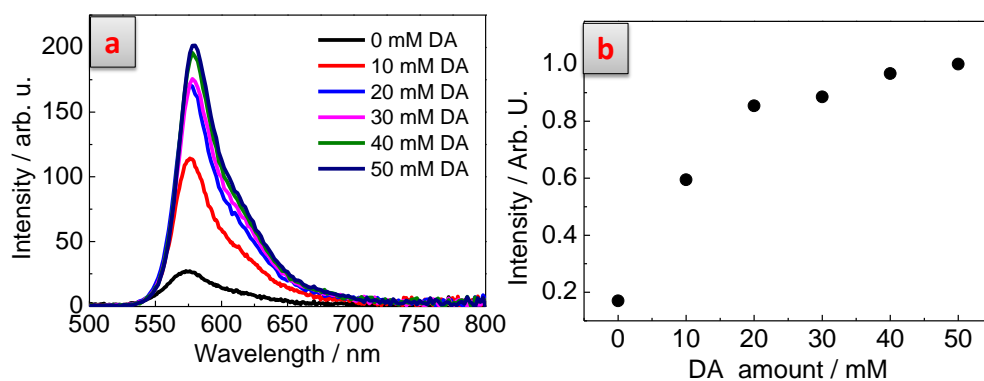


Figure 5.7: a) emission spectra ($\lambda_{\text{exc}} = 355 \text{ nm}$) and b) integrated emission intensities of RhB in a dichloromethane solutions (5 mL, 4.5 mM) containing different quantities of added DA.

The formation of the **RhB/DA@PS** NPs (120–200 nm) was corroborated by SEM (**Figure 5.8a**). The pink NPs showed only residual fluorescence ($\lambda_{\text{max}}^{\text{emi}} = 622 \text{ nm}$) due to a large presence of aggregates of RhB-zw molecules (**Figure 5.8b**). Once more, the influence of the aggregation state on the emission properties of the nanoparticles was confirmed upon decreasing (diluting) the percentage of the dye (0.4 wt. % of RhB with respect to PS, **Figure 5.8b**). In this case, a much more intense and narrower fluorescence emission ($\lambda_{\text{max}}^{\text{emi}} = 605 \text{ nm}$) was found at room temperature (**Figure 5.8b**, left image). The high concentrated **RhB/DA@PS** (2 wt. %) NPs were selected for a deeper characterization given the non-fluorescent state (off state) at RT potentially useful for an off/on threshold temperature irreversible fluorescent sensors.

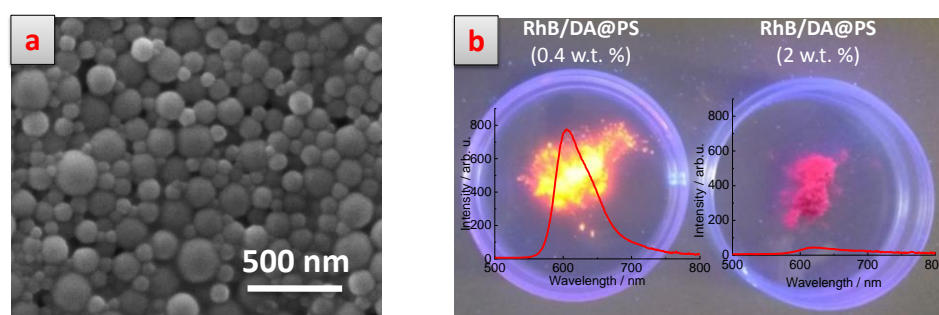


Figure 5.8: a) SEM image and b) digital image with the emission spectra of **RhB/DA@PS** NPs prepared with two different dye concentrations (0.4 and 2 wt. %).

$^1\text{H-NMR}$ of the **RhB/DA@PS** (2 wt. %) NPs, dissolved in CDCl_3 , was recorded to determine the amount of DA encapsulated. The spectrum of the NPs was compared with the spectra of pure DA and PS (**Figure 5.9**). As expected, the particles presented the characteristic peaks of PS and DA. By using an internal reference

(dimethylformamide, DMF), the amount of encapsulated DA was determined to be 9 wt. % respect the total weight of the NPs, which confirmed the good encapsulation efficiency (90%) of this molecule within the polymeric matrix.

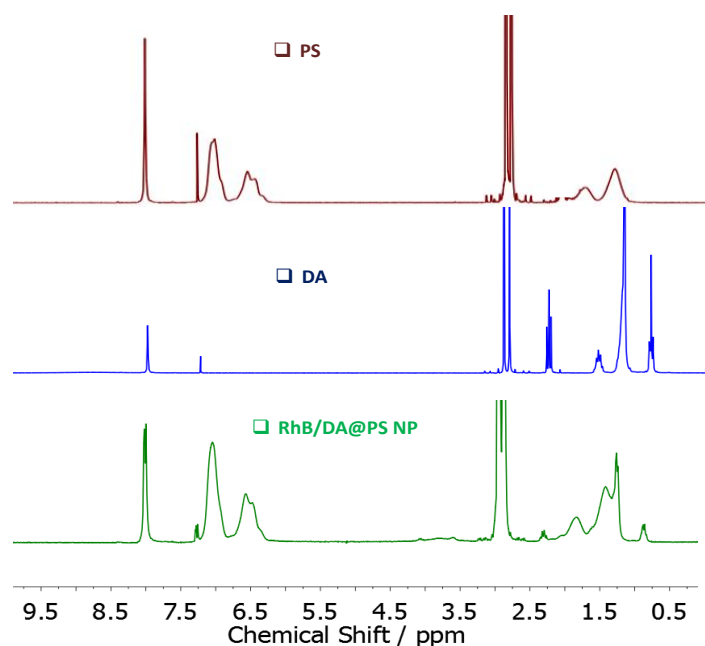


Figure 5.9: ^1H -NMR spectra (250 MHz, CDCl_3) of dissolved **RhB/DA@PS** NPs, pure PS and DA. Characteristic peaks of **PS** at $\delta = 1.45$ (br., s, 2H, CH_2), 1.85 (br. s, 1H, CH), 6.5 (m, 2H, ArH) and 7.15 ppm (s, 3H, ArH) and of **DA** at $\delta = 0.79$ (m, 3H, CH_3), 1.25 (br. s, 16H, $(\text{CH}_2)_8$), 1.6 (m, 2H, CH_2) and 2.40 ppm (t, 2H, COCH_2). The peaks at $\delta = 2.88$ (s, 3H, CH_3), 2.97 (s, 3H, CH_3) and 7.96 (s, 1H, CH) were related to DMF, used as internal reference.

- **Thermofluorochromism of the RhB/DA@PS NPs**

Once the characterization of the morphological properties and the chemical composition of the NPs were achieved, the fluorescence spectra of **RhB/DA@PS** NPs at increasing selected temperature within the 25°C-110 °C range, were recorded (**Figure 5.10a**). For these measurements, again, the NPs powder was kept for 10 minutes at the selected temperature (e.g. 100 °C) and after letting to cool down to RT, the emission was recorded.

Between 25 °C and 70 °C, the fluorescence intensity remained practically constant with a partial narrowing of the emission band, just above the melting point of the DA (43.8 °C). Tangible emission enhancement was observed above 80°C ($\Delta F = 69\%$) and became much more evident ($\Delta F = 231\%$) once the NPs were heated for 10 min at 90 °C (**Figure 5.10a-c**) and leveled at its maximum value at 100-110 °C ($\Delta F_{\text{max}} = 266\%$). In this case the enhancement was high enough as to be

detectable even by naked eye (**Figure 5.10b-c**). The increase of the fluorescence intensity, which was also irreversible, was accompanied by a little blue shift (from $\lambda_{\max} = 627$ nm to 618 nm) and a further narrowing of the emission band (**Figure 5.10d**), which are further indications of disaggregation of RhB.

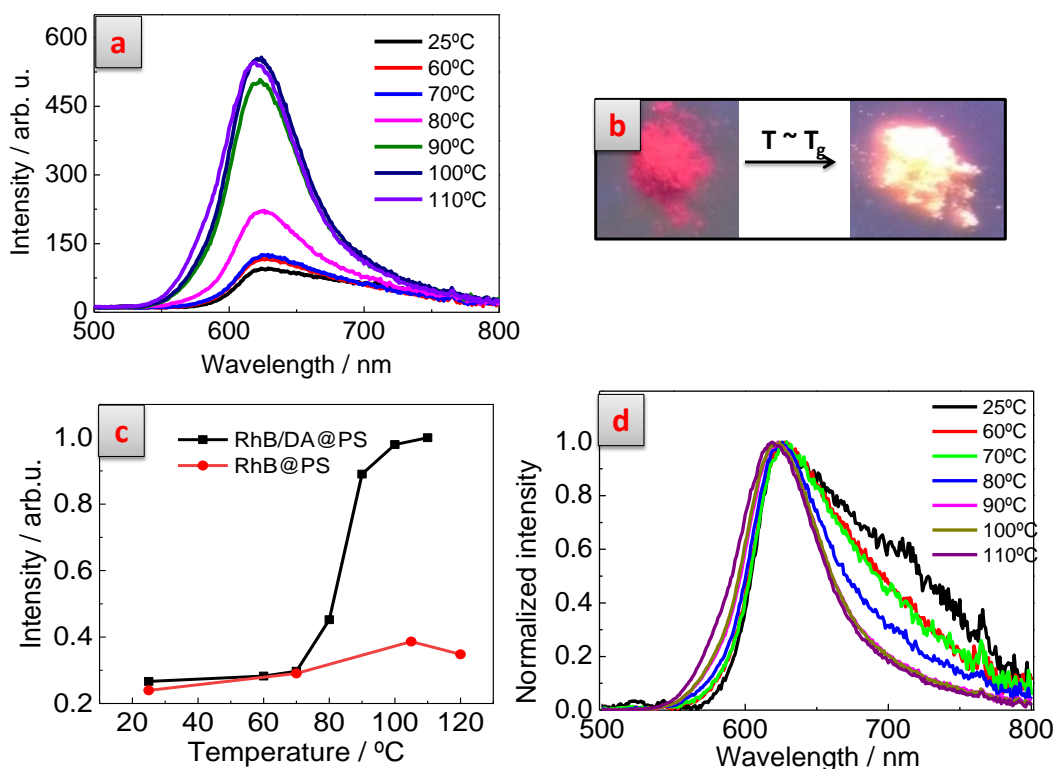


Figure 5.10: a) emission spectra ($\lambda_{\text{exc}} = 355$ nm) of the RhB/DA@PS NPs (2 wt. %), recorded at RT after heating the NPs at different temperatures; b) digital photographs of RhB/DA@PS taken at RT before (25 °C) and after (90 °C) heating, under UV light ($\lambda_{\text{exc}} = 365$ nm); c) integrated intensities of the temperature-dependent emission spectra of RhB/DA@PS and RhB@PS NPs and d) normalized emission spectra of RhB/DA@PS NPs (2 wt. %) after being heated at different temperatures

The NPs were exposed at the minimum trigger temperature (90°C, **Figure 5.11**) for different times. After an inertial period (3 minutes), during which the fluorescence intensity did not increase, the enhancement was observed up to reaching a maximum value after 10 minutes (**Figure 5.11b**). In the future a more detailed study could be carried out to see if from 3 to 10 minutes there is a linear correspondence of intensity vs time. This would make these NPs suitable for being used as time-temperature indicators.

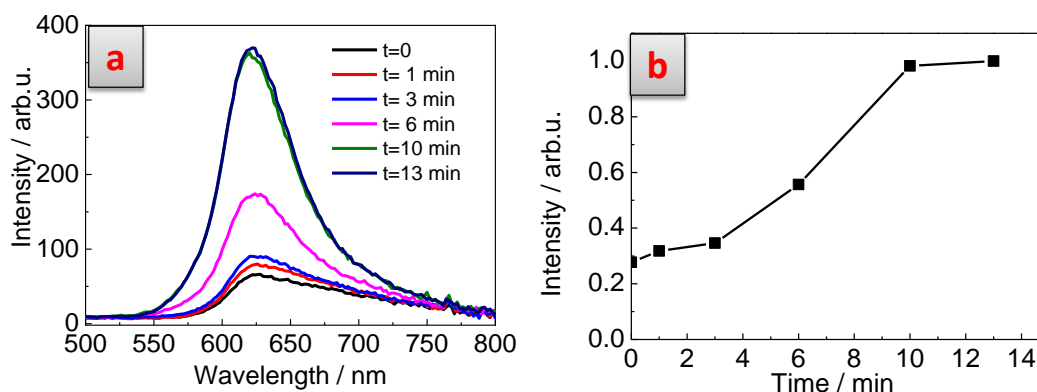


Figure 5.11: a) emission spectra and b) normalized integrated emission intensity of the **RhB/DA@PS** NPs kept at 90°C different times.

The maximum fluorescent enhancements were obtained at 100-110°C, which fitted nicely with the T_g of the **RhB/DA@PS** NPs recorded in the DSC (93°C, **Figure 5.12a**). SEM also confirmed how at this temperature (100°C) the spherical structure of the NPs was lost (**Figure 5.12b**), confirming the crossing of the NPs T_g .

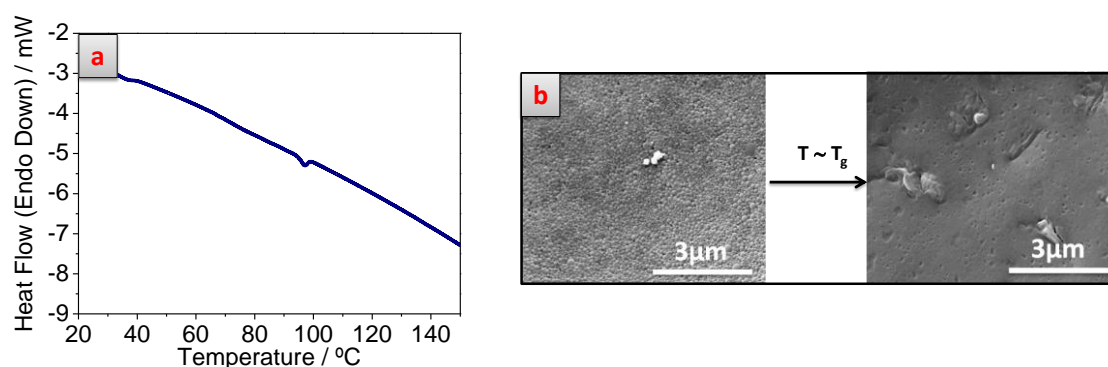


Figure 5.12: a) DSC analysis of **RhB/DA@PS** NPs between 20 and 150 °C (T_g around 93°C) and b) SEM images of **RhB/DA@PS** NPs before (25°C) and after (100°C) heating.

Interestingly, the addition of DA to the NPs strongly increased the fluorescence difference between the maximum emitting and non-emitting ($\Delta F^{\max} = 266\%$ obtained at 100-110 °C) states in comparison to the corresponding NPs lacking DA ($\Delta F^{\max} = 47\%$, at 105 °C). In both **RhB/DA@PS** and **RhB@PS** NPs the initial fluorescence was negligible; therefore, the ΔF difference was related to the intensity of emission of the heated state. As expected, DA was helping on the disaggregation of RhB by plasticizing the matrix and intercalating between RhB molecules.

The irreversible fluorescence activation (it remains high after cooling to RT) was thus ascribed to the immobilization of RhB molecules during cooling, that prevents their re-aggregation within the rigid polymer matrix. To prove this we aimed to investigate the effect on the final fluorescence on the cooling rate of the NPs. For this purpose, the **RhB/DA@PS** NPs were heated above their T_g (100 °C) and then, let cooling down under three different regimes: a) by putting the NPs container in ice (fast cooling), by keeping the container at RT (the standard procedure used for all NPs) and c) keeping the containing vial in the heated bath slowly cooled down to RT (≈ 1.3 °C·min⁻¹, slow cooling). Interestingly, fast cooling and RT-equilibration provided similar final fluorescence intensities and emission enhancement ($\Delta F = 374$ and 342%, respectively), while a lower emission was obtained upon slow cooling ($\Delta F = 228$, **Figure 5.13**). This was ascribed to the higher capability of the RhB molecules to re-aggregate during the slow cooling (**Figure 5.13a-b**) due to the slow re-establishment of a rigid polymeric matrix. On the other hand ice cooling and reequilibration at RT induced the fast increase of the matrix rigidity and the immobilization of the disaggregated RhB molecules.

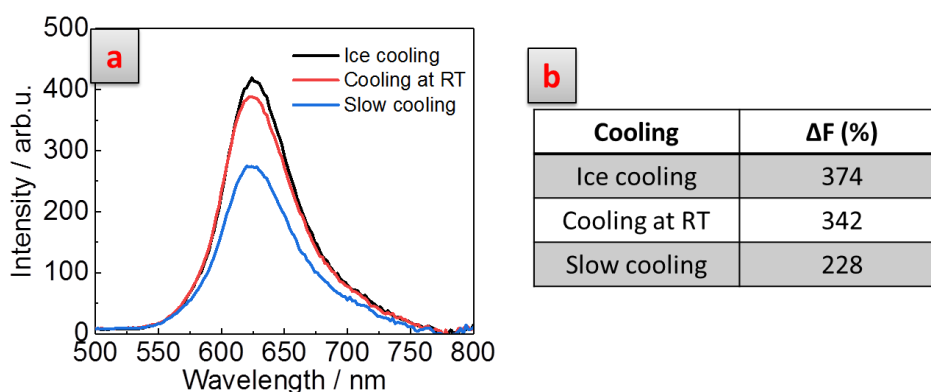


Figure 5.13: a) emission spectra of the **RhB/DA@PS** NPs after being heated at 100°C and cooled under different regimes and b) table with the ΔF values obtained at different cooling regimes.

This means that the RhB molecules were kinetically trapped in the disaggregated state, similarly to what Weder *et al.*¹ achieved for the preparation of fluorescent COPV-containing polymers through hot extrusion/fast cooling. However, while in the reported examples the kinetic trapping provided the initial state (pre-heating stage) of the polymer sensor, in our system the NPs are prepared in the thermodynamically stable aggregated state. This should guarantee a stable off state of the sensor upon time during storage or while it is not detecting high

temperatures. Actually, emission signal of the NPs before and after heating were stable upon time. Indeed, the fluorescence intensity of the NPs left at RT during 12 days did not change (**Figure 3.14a-b**). Moreover, when a portion of the NPs from the same batch was heated after a few days of storage, similar fluorescence intensity (and thus, enhancement) was observed (**Figure 5.14b**). This experiment confirmed that the **RhB/DA@PS** behavior is reproducible after several days of storage.

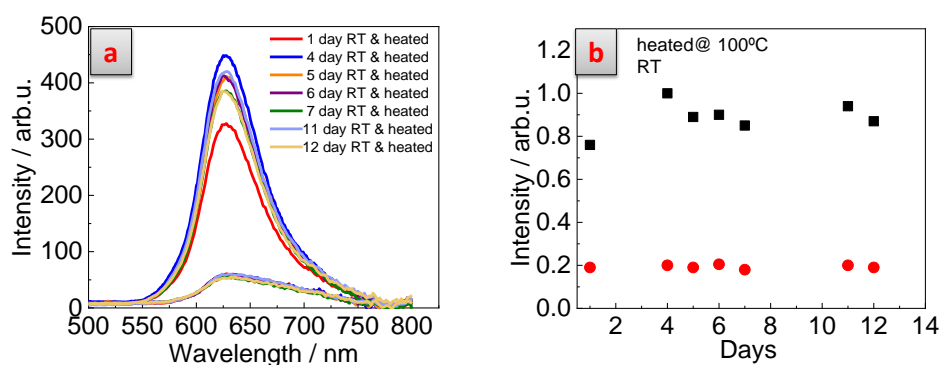


Figure 5.14: a) fluorescence spectra (recorded at RT) of non-heated and heated **RhB/DA@PS** NPs stored up to 12 days at RT; b) integrated intensities of the fluorescence spectra recorded at RT of the non-heated and heated **RhB/DA@PS** NPs stored during 12 days at RT.

Finally, any chemical degradation of RhB into different and more fluorescent species that account for the emission enhancement was discarded by analyzing the negligible changes of the RhB absorption spectra before and after annealing in both the solid state and dissolved in CHCl_3 (**Figure 5.15a-b**).

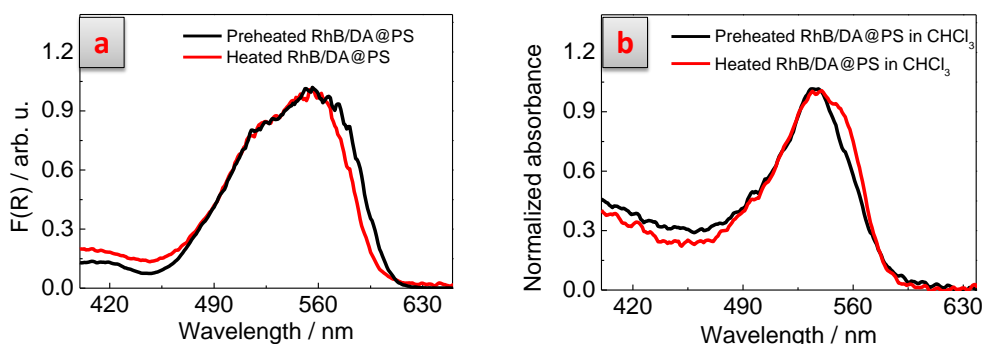


Figure 5.15: normalized absorption spectra of the preheated and heated **RhB/DA@PS** NPs a) powder and b) dissolved in CHCl_3 .

To prove the importance of using DA as additive to increase the fluorescence enhancement, other possible plasticizing additives were tested. Nonanoic acid

(**NA**), a 9-carbon carboxylic acid with a shorter hydrocarbon chain than DA and liquid at RT; 1-tetradecanol (**TDOH**), a 14-carbon alcohol often used in thermochromic systems (Chapter 4) as species competitively interacting with color developer in its liquid state, and Myglyol®812, a hydrophobic oil (a caprylic/capric triglyceride, **M812**), which does not have hydrogen bonding groups.

As done for **RhB/DA@PS**, the NPs encapsulating RhB and selectively one of these additives (**RhB/NA@PS**, **RhB/TDOH@PS** and **RhB/M812@PS**) were prepared and freeze-dried to obtain the corresponding powders. Temperature-dependent fluorescent studies were carried out for all obtained NPs, in the same manner as done before. Interestingly, only the NA-doped NPs showed an evident off/on fluorescence enhancement ($\Delta F^{\max} = 313\%$), most likely due to its similar chemical structure of DA and its tendency to form hydrogen bonds with RhB. In contrast, TDOH ($\Delta F^{\max} = 104\%$) and M812 ($\Delta F^{\max} = 7.4\%$) induced a more linear or almost no fluorescence increase (**Figure 5.16a-d**). This means that not only a plasticizer is required to facilitate the molecular motion of the dye when the T_g^{PS} is reached, but specific hydrogen-bonding interactions are required to increase the disaggregation efficiency.

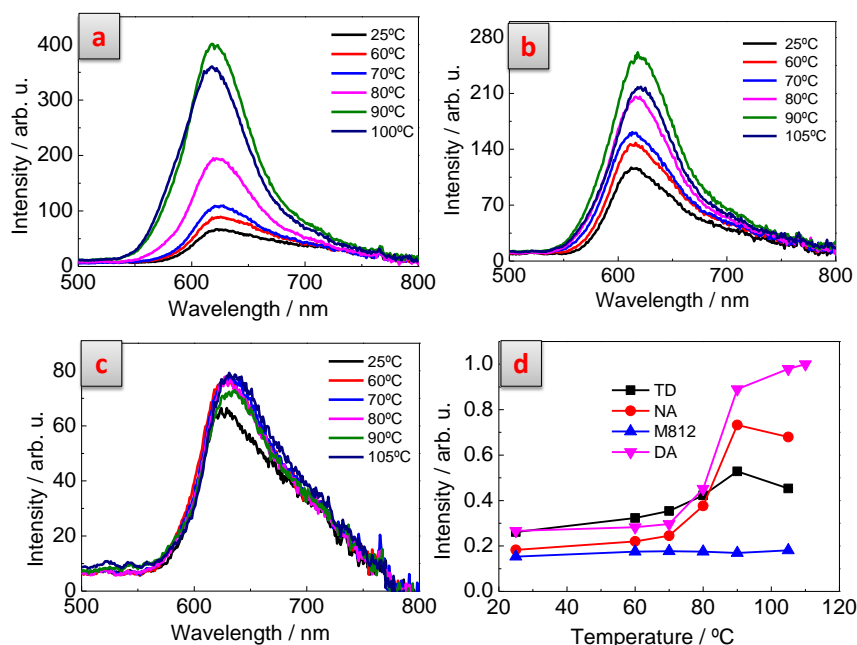


Figure 5.16: emission spectra ($\lambda_{\text{exc}} = 355 \text{ nm}$) of a) **RhB/NA@PS**, b) **RhB/TDOH@PS** and c) **RhB/M812@PS** NPs (2 wt. %), recorded at RT after being heated at different temperatures; d) integrated emission intensities (normalized respect to the highest emission intensity) vs temperature.

Once demonstrated that DA as additive gave the best results in terms of ΔF after heating above the T_g of PS (**RhB/DA@PS**) we decided to prove the universality of the system by using different polymeric matrices. The reason was twofold: i) to confirm that the behaviour observed was independent of the chemical composition of the matrix and ii) to see if we could obtain an off/on fluorescent transition at different temperatures, which ideally would depend on the T_g of the polymeric matrix used.

5.3.3 RhB/DA@polymeric NPs

Poly(methyl methacrylate) (PMMA, $T_g = 105\text{ }^\circ\text{C}$)¹⁷ and poly(bisphenol A carbonate) (PC, $T_g = 150\text{ }^\circ\text{C}$)¹⁷ were selected as they are standard commercially available polymers that allow for straightforward syntheses of NPs. Polyethersulphone (PES) and polyetherimide (PEI), engineering polymers with very high T_g (180 $^\circ\text{C}$ ²² and 215 $^\circ\text{C}$,²² respectively), were chosen because they could provide higher sensing temperatures. All these polymers are thermoplastic and are expected to induce the same RhB fluorescence enhancement when the respective T_g is reached. In all the cases, **RhB/DA@PMMA**, **RhB/DA@PC**, **RhB/DA@PES** and **RhB/DA@PEI** (2 wt. % of RhB) NPs could be successfully obtained (80-200 nm, **Figure 5.17a-d**) with the same method described above (see experimental section 7.3.5), with the exception of PEI, for which CHCl_3 was used to ensure a proper dissolution of the less soluble polymer.

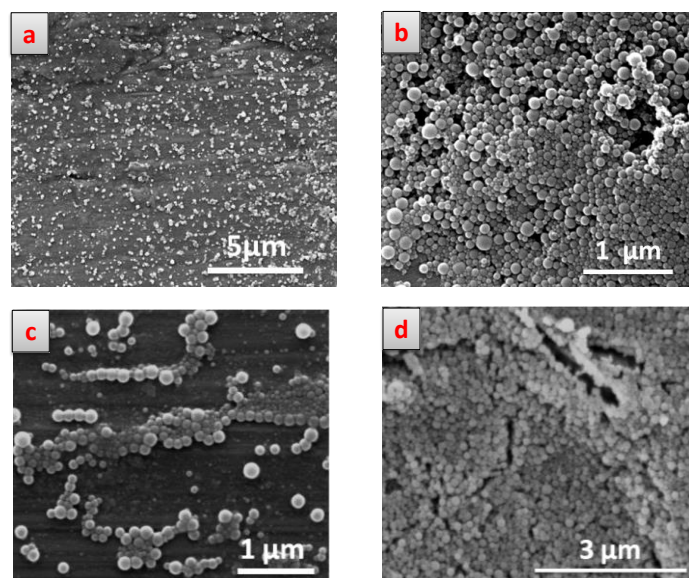


Figure 5.17: SEM image of the a) **RhB/DA@PMMA**, b) **RhB/DA@PC**, c) **RhB/DA@PES** and d) **RhB/DA@PEI** NPs.

Notably, despite the well-known costs and difficulties for the PES and PEI processability in standard extrusion/injection molding processes, the highly loaded **RhB/DA@PES** and **RhB/DA@PEI** NPs were very easy to achieve through a scalable method. As previously done for **RhB/DA@PS**, $^1\text{H-NMR}$ (**Figure 5.18**) was performed to calculate the quantity of DA encapsulated using the same amount of internal standard (DMF, $10\mu\text{L}$). In all cases (PMMA, PC, PES, PEI) the encapsulation of DA was confirmed by the presence of one of the characteristic peaks of DA at $\delta=2.40$ ppm (t, 2H, COCH_2), which in none of the spectra was overlapping the peaks of the polymers, allowing the confirmation of the DA encapsulation and its amount determination. The calculated payloads (8.6, 7.4, 8.7, 9.0 wt. %, respectively) obtained from the $^1\text{H-NMR}$, were close to the theoretical value (10 wt. %) extrapolated by considering that all DA added at the beginning of the synthesis was encapsulated.

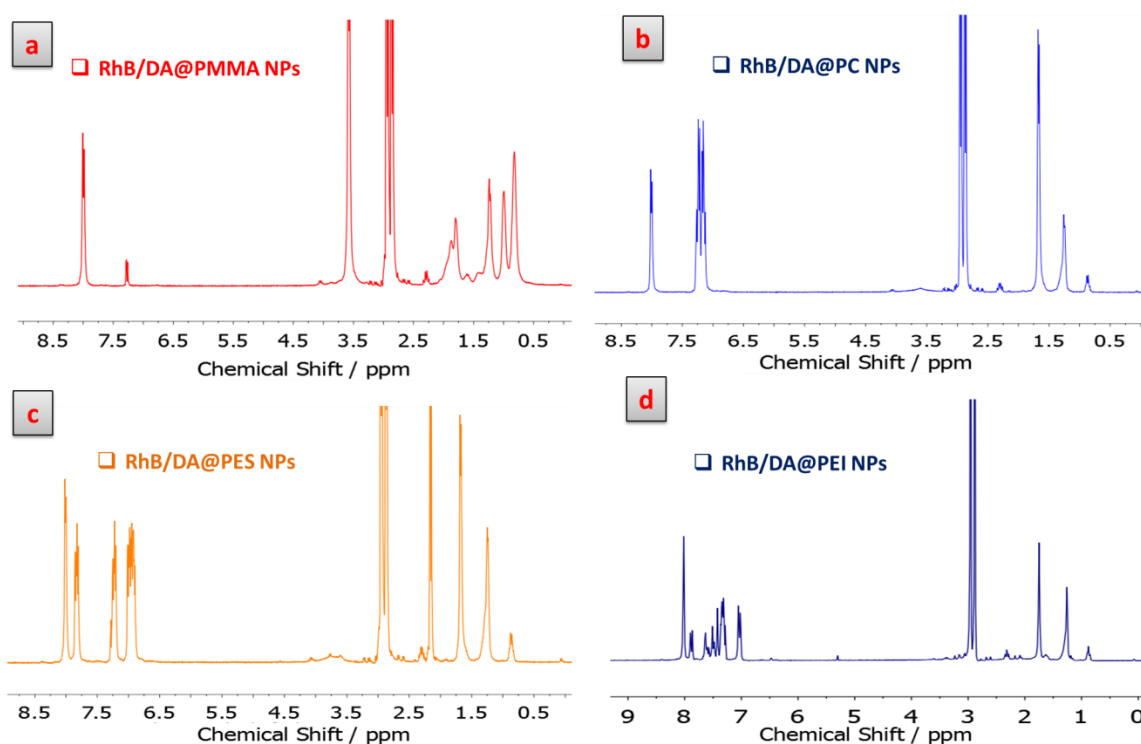


Figure 5.18: $^1\text{H-NMR}$ spectra (250 MHz) of dissolved a) **RhB/DA@PMMA** b) **RhB/DA@PC**, c) **RhB/DA@PES** and d) **RhB/DA@PEI** NPs in CDCl_3 . Characteristic peaks of **PMMA** at $\delta = 0.80\text{-}0.98$ (m, 3H, CH_3), 1.68-2.02 (m, 2H, CH_2) and 3.62 ppm (s, 3H, OCH_3), of **PC** at $\delta = 1.6$ (s, 6H, CH_3) and 7.1 ppm (m, 8H, ArH), of **PES** at $\delta = 1.6$ (s, 6H, (CH_3)), 6.9 (m, 8H, ArH), 7.1(m, 4H, ArH) and 7.9 ppm (m, 4H, ArH), of **PEI** at $\delta = 1.69$ (s, 6H, (CH_3)), 6.96 (m, 8H, ArH), 7.3(m, 2H, imide ArH), 7.4 ppm (d, 2H, Imide ArH) and 7.9 ppm (d, 2H, Imide ArH) and of **DA** at $\delta = 0.79$ (t, 3H, CH_3), 1.25 (s, 16H, (CH_2)₈), 1.6 (m, 2H, CH_2) and 2.40 ppm (m, 2H, COCH_2).

The DSC analysis of the NPs showed that DA plasticizes the polymers, inducing therefore changes in the measured T_g of the NPs polymer (93, 95, 100-150, 150 and 186 °C), making them lower (in the case of PS, PMMA, PES and PEI NPs)^{17, 22} or broader (PC)¹⁷ than the reported values for the corresponding plain bulk polymers (**Figure 5.19**). These are the temperatures around which the fluorescence enhancements of the NPs are expected to occur.

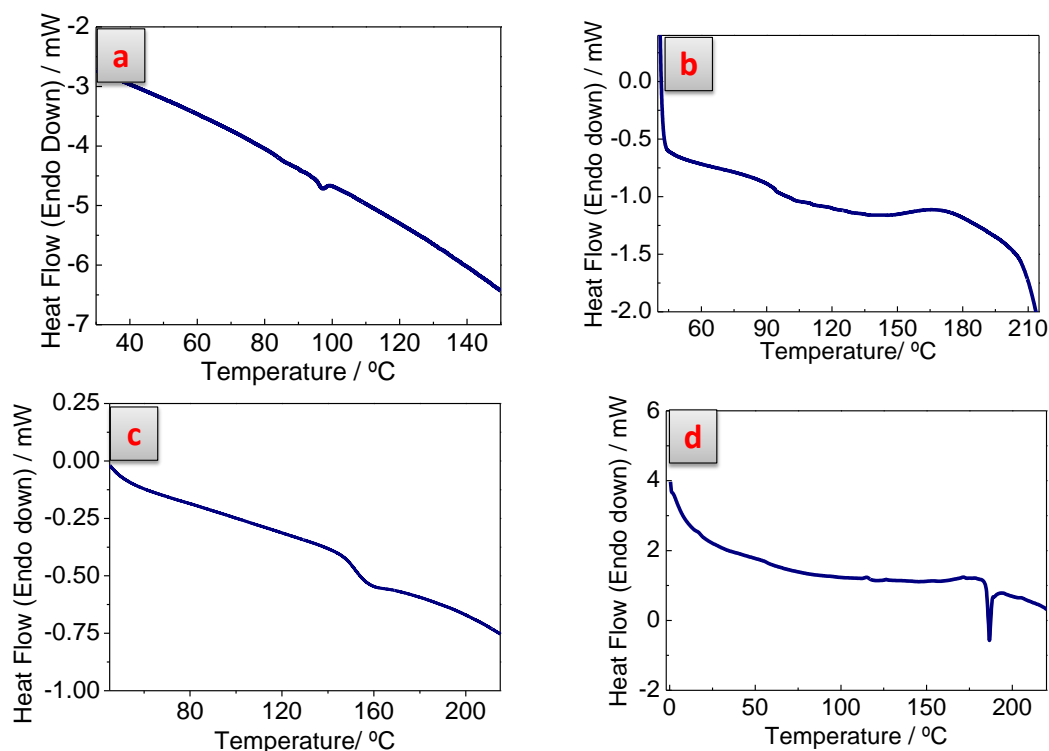


Figure 5.19: DSC of the a) **RhB/DA@PMMA** ($T_g = 95$ °C), b) **RhB/DA@PC** (T_g between 100-150 °C), c) **RhB/DA@PES** ($T_g = 150$ °C) and d) **RhB/DA@PEI NPs** ($T_g = 186$ °C).

- **Thermofluorochromism of RhB/DA@polymer NPs**

All NPs were pink colored after freeze-drying and showed only a little fluorescence emission ($\lambda_{\max}^{\text{PMMA}} = 619$ nm, $\lambda_{\max}^{\text{PC}} = 624$ nm, $\lambda_{\max}^{\text{PES}} = 621$ nm and $\lambda_{\max}^{\text{PEI}} = 623$ nm), indicating again the encapsulation of RhB-zw molecules (2 wt. %) as non-emitting aggregates under these conditions (**Figure 5.20a-d**). Variable-temperature emission spectra of **RhB/DA@PMMA**, **RhB/DA@PC**, **RhB/DA@PES** and **RhB/DA@PEI NPs** were studied and showed to exhibit the same behaviour:

i) no significant fluorescence changes were observed until 5-10 °C below the corresponding measured polymer T_g s (95 °C, 100-150 °C, 150 °C and 186 °C respectively, **Figure 5.20e**).

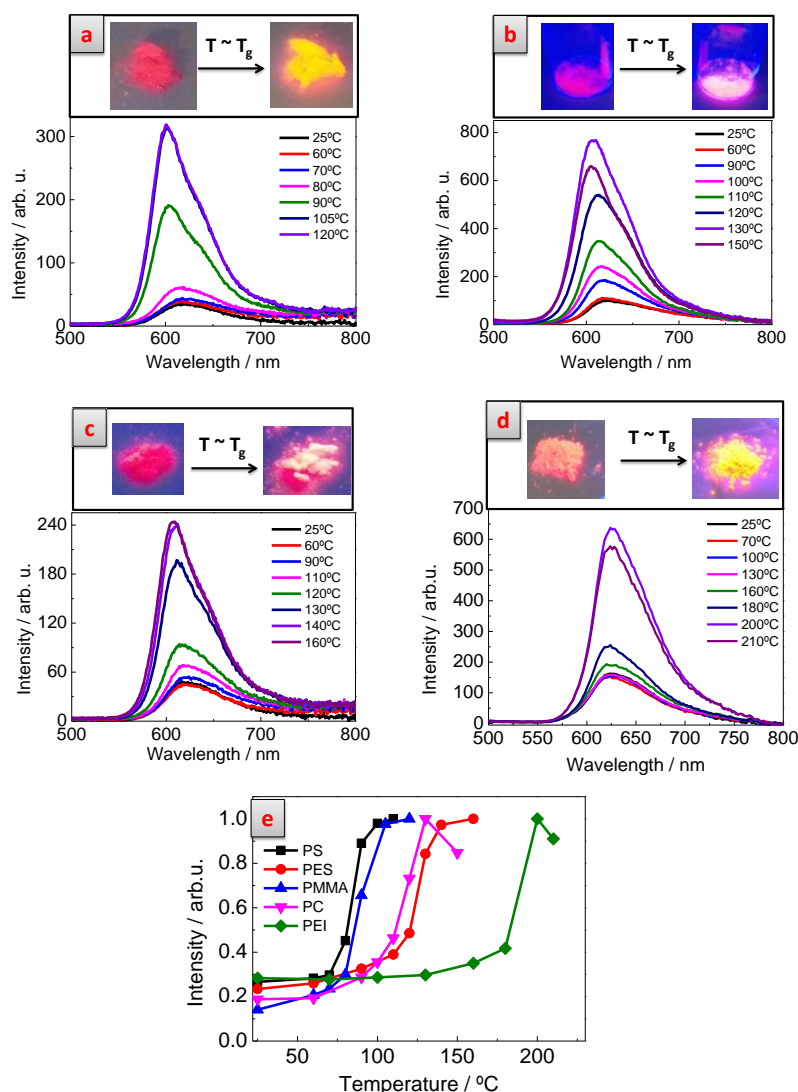


Figure 5.20: emission spectra ($\lambda_{exc} = 355$ nm) recorded at RT after heating the NPs at different temperatures and digital photographs under UV irradiation before and after heating above the T_g of a) **RhB/DA@PMMA**, b) **RhB/DA@PC**, c) **RhB/DA@PES** and d) **RhB/DA@PEI** NPs and e) integrated emission intensities of all RhB/DA@polymer NPs at different temperature.

ii) once the T_g of the NPs polymer was overcome, the induced emission enhancement was fast (~ 10 min), abrupt (within 20°C), and very high; ΔF_{max} as high as 611%, 438%, 328%, 253% for **RhB/DA@PMMA** NPs (at 120 °C, **Figure 5.20a**), **RhB/DA@PC** NPs (at 130 °C, **Figure 5.20b**), **RhB/DA@PES** NPs (at 160 °C, **Figure 5.20c**) and **RhB/DA@PEI** NPs (at 200 °C, **Figure 5.20d**), respectively. In almost all the cases the fluorescence increase was accompanied by a narrowing and blue-shifting of the bands (**Figure 5.21**). Notably, the maximum fluorescent

enhancement (ΔF_{\max}) was between 10 and 25 °C above the measured T_g of the NPs polymer. This little discrepancy between the measured T_g of the NPs polymer and the threshold fluorescence activation, was ascribed to the equipment and different heating procedures used in the two types of measurements. While in DSC the NPs were heated at 10 °C min⁻¹ in a closed aluminum sample holder, in fluorescence experiments the NPs were heated at a set temperature in a glass vial for 10 min.

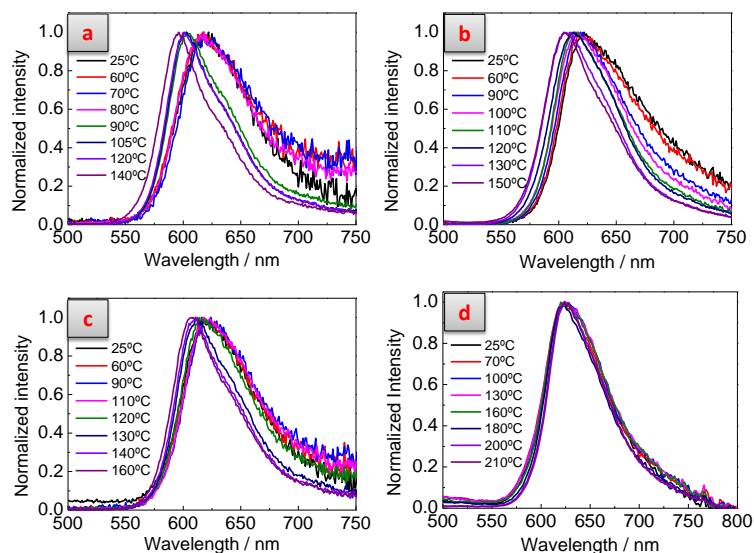


Figure 5.21: normalized spectra of a) RhB/DA@PMMA, b) RhB/DA@PC, c) RhB/DA@PES and d) RhB/DA@PEI NPs after being heated at different temperatures.

iii) the fluorescence is retained upon cooling down to room temperature, when the spherical morphology of the initial nanoparticles is already lost according to SEM images (Figure 5.22).

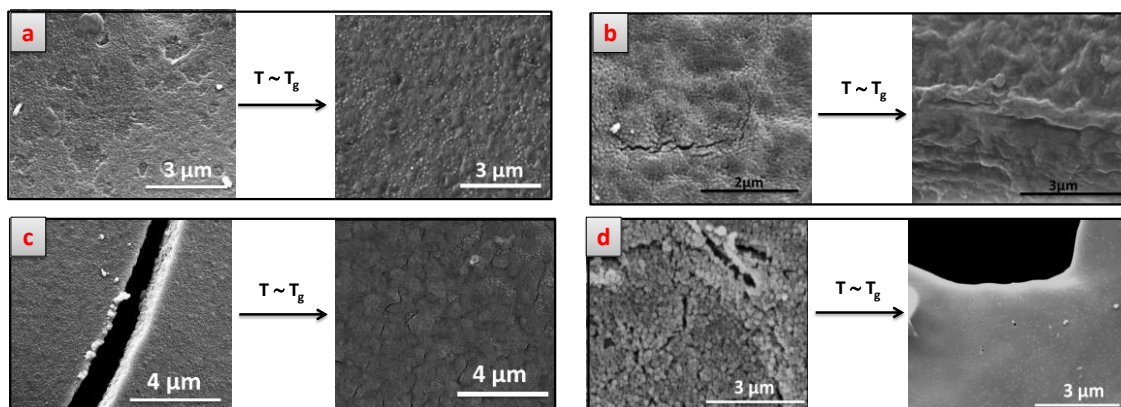


Figure 5.22: SEM images of a) RhB/DA@PMMA, b) RhB/DA@PC, c) RhB/DA@PES and d) RhB/DA@PEI NPs before and after the annealing observed at the temperature at which the respective ΔF_{\max} are reached.

These experiments showed that i) once reached the NP polymer T_g , the softening of the matrix allows the RhB disaggregation (which is further favored by the presence of DA) and the increase in the fluorescence; ii) the type of thermoplastic polymer could be used to tune the emission enhancement triggering temperature; iii) the fast re-equilibration of the matrix at RT blocks the isolated RhB molecules preventing their re-aggregation and assuring the maintenance of the enhanced fluorescence once the NPs are cooled to RT (kinetically trapping). To prove the importance of DA in the enhancement mechanism, control experiments were also carried out with polymer NPs not containing DA.

RhB@PMMA, **RhB@PC**, **RhB@PES** and **RhB@PEI** NPs were prepared as before but without DA (see experimental section 7.5.3). As expected the morphological and size (80-200 nm) properties of the particles were similar to those containing DA (**Figure 5.23**).

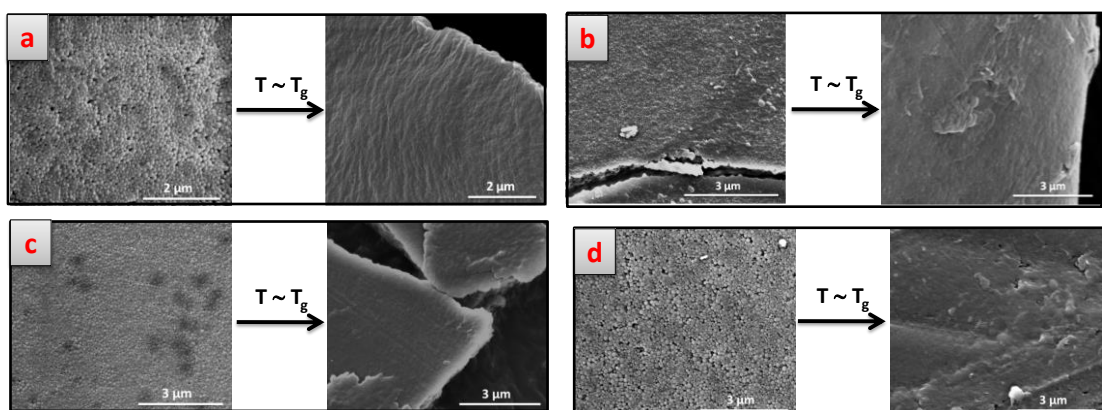


Figure 5.23: SEM images of a) **RhB@PMMA**, b) **RhB@PC**, c) **RhB@PES** and d) **RhB@PEI** NPs before and after the annealing observed at the temperature at which the respective ΔF max are reached.

Temperature- dependent emission measurements showed maximum fluorescence enhancements ΔF^{\max} of 194% (at 120 °C), 68% (140 °C), 132% (160 °C) and 292% (210 °C), respectively (**Figures 5.24, Table 5.1**), with emission activation temperatures strongly correlated with the nature of the polymer.

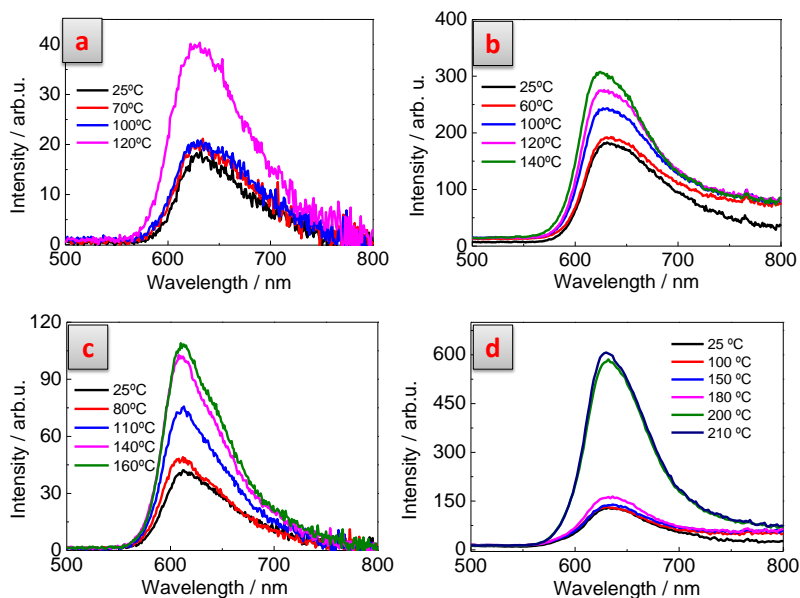


Figure 5.24: emission spectra ($\lambda_{\text{exc}} = 355 \text{ nm}$) recorded at RT after heating the a) **RhB@PMMA**, b) **RhB@PC**, c) **RhB@PES** and d) **RhB@PEI** NPs at different temperatures.

In all cases, the SEM of the NPs heated at the respective temperatures at which ΔF^{max} was observed, showed the loss of the NPs structure, indicating that the complete enhancement is achieved upon reaching the NPs polymer T_g s (**Figure 5.23**).

These experiments confirmed the importance of adding DA in the matrix-type capsules: these DA-free NPs generally presented i) much lower ΔF^{max} and ii) far less abrupt emission changes (which complete in $\geq 40^\circ\text{C}$), most of the times gradual (**Figure 5.25a-b**), than those observed for the respective DA-containing NPs (the only exception is given by PEI, which gave similar enhancement features with and without DA). Only **RhB@PEI** NPs ($\Delta F^{\text{max}} = 292\%$) exhibited the complete off/on fluorescence switch within just 20°C also in the absence of DA (**Table 5.1**). This was ascribed to: i) the high rigidity of PEI, which does not allow the dye molecules to diffuse until the polymer reaches its T_g and ii) the higher temperature needed to reach the T_g , which in turn tips the system with more energy to efficiently disaggregate the dyes. These results confirmed the need to use DA for developing precise off/on temperature threshold fluorescent sensors based on polymer NPs, in which it not only acts as plasticizer (favoring the RhB mobility) but also helps the disaggregation of the RhB molecules intercalating between them by forming hydrogen-bonding interactions.

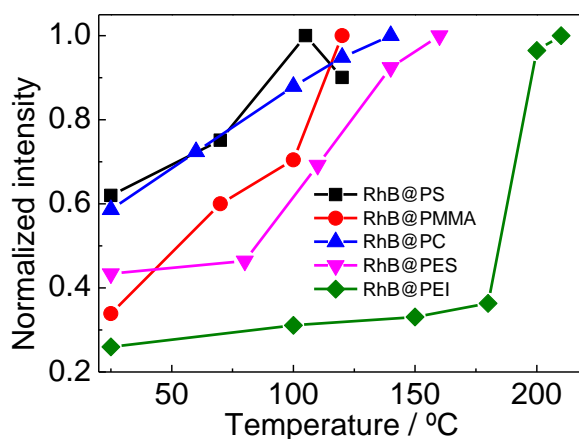


Figure 5.25: integrated emission ($\lambda_{\text{exc}} = 355 \text{ nm}$) of the **RhB@Polymeric** NPs at different temperatures

Polymer	ΔF^{max} (%) of RhB@polymer	ΔF^{max} (%) of RhB/DA@polymer
PS	27	266
PMMA	194	611
PC	68	438
PES	132	328
PEI	292	253

Table 5.1: table of the comparison of the ΔF^{max} obtained for the **RhB@polymers** and **RhB/DA@Polymers**.

5.3.4 Tunable threshold temperature sensors

The glass transition dependency of the irreversible fluorescence activation permits the use of these **RhB/DA@polymer** NPs for the implementation of threshold temperature sensors. The proof-of-concept of the threshold temperature sensor was obtained by layering **RhB/DA@PMMA** NPs (which gave the highest ΔF^{max}), on top of a thermally conductive aluminum bar (**Figure 5.26**). A thermopar attached to the bar, close to the NPs position, allowed for the direct measurement of the surface temperature. When the bar was held between 70 and 80 °C for four minutes no fluorescence changes were observed. On the contrary, the emission of the NPs clearly increased within a minute while the temperature reached 120 °C,

with the fluorescence completely and irreversibly turned on already at 110 °C. The fluorescence enhancement was clearly detectable by naked eye and maintained once the bar was cooled back to lower temperatures (i.e. 70 °C).



Figure 5.26: digital snapshots showing the fluorescence enhancement occurring while heating the powder from 90 to 120 °C and the fluorescence maintenance once the **RhB/DA@PMMA** NPs were cooled down to lower temperatures ($\lambda_{\text{exc}} = 365 \text{ nm}$).

Similarly, with nanoparticles of different polymers (and different T_g s), we were able to prepare a multiple threshold fluorescent sensor with the scope to permanently detect the history of a surface or environment exposed to increasing temperatures (**Figure 5.27**). In this case **RhB/DA@PMMA**, **RhB/DA@PES** and **RhB/DA@PEI** NPs were layered in three aluminum metal containers and simultaneously subjected (for 10 min) at increasing temperatures inside an oven. Thus, we were able to observe, by naked eye, selective fluorescence turning on upon temperature increase, with **RhB/DA@PMMA** activating first ($T = 100 \text{ °C}$), then **RhB/DA@PES** NPs ($T = 140 \text{ °C}$) and finally **RhB/DA@PEI** NPs ($T = 200 \text{ °C}$).

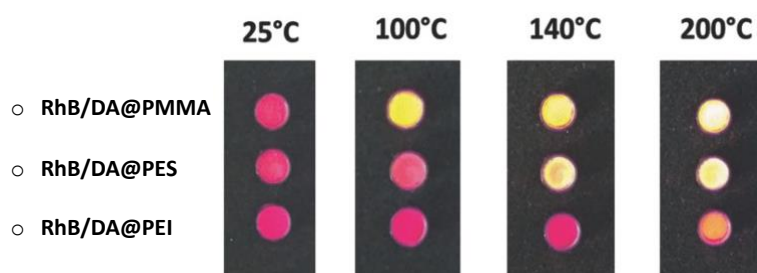


Figure 5.27: digital photographs of the **RhB/DA@PMMA**, **RhB/DA@PES**, and **RhB/DA@PEI** NPs in aluminum containers after being exposed to different temperatures ($\lambda_{\text{exc}} = 365 \text{ nm}$).

Notably, independently on the heat transfer mechanism (conduction or convection) the NPs gave the same response upon overcoming the glass transition temperature

of the NPs polymer. As far as we know, this is the first RhB-based solid fluorescence thermometer revealing threshold temperatures as high as 200 °C.

5.3.5 Preparation of a thermofluorochromic device

In order to prepare functional devices the NPs must be embedded in a polymeric matrix or deposited onto a substrate. The embedment of the NPs in a polymeric matrix was initially attempted following the same procedure used to obtain other chromogenic films (e.g. photochromic films, **Chapter 3**): casting an aqueous suspension of the NPs, also containing a film-forming polymer, onto a substrate and letting the water evaporate (see experimental section 7.3.6). As film-forming polymer polyvinyl alcohol 4-88% (PVA 4-88%, $T_g \sim 70^\circ\text{C}$) and polyacrylamide (PAA, $T_g \sim 150^\circ\text{C}$) were chosen. Though PVA 4-88% has lower T_g than the T_g of all polymeric NPs, it was selected to verify the behaviour of the NPs when embedded in solid matrices.

RhB/DA@PMMA NPs were selected for the preparation of the films since they presented the higher ΔF^{max} recorded after heating. Surprisingly, when a few droplets of the PVA concentrated solution were added to the suspension with the **RhB/DA@PMMA** NPs, a slightly color change (from reddish to pink) and fluorescence activation (**Figure 5.28a**, under UV light $\lambda_{\text{exc}} = 365 \text{ nm}$) were observed. Moreover, after water evaporation, the formed PVA film was already highly fluorescence at RT without heating (**Figure 5.28b**). Unfortunately, similar behaviour was observed for PAA after the evaporation of the water obtaining again a highly fluorescent film at RT (**Figure 5.28c**). Given the high fluorescence of the films prior heating, these materials could not be used as threshold temperature sensors.

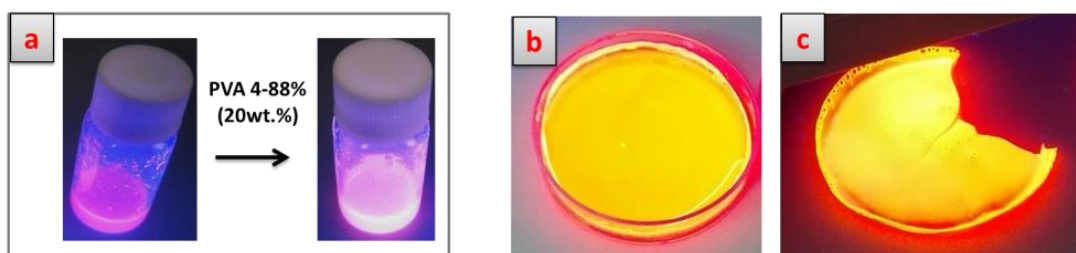


Figure 5.28: digital photographs (under UV light) of the a) suspension of **RhB/DA@PMMA** NPs before and after adding 10 droplets of PVA 4-88%, b) PVA and c) PAA film with the **RhB/DA@PMMA** NPs.

An explanation was attempted to justify this phenomenon. Upon the addition of the hydrophilic polymers, the RhB molecules are extracted from the NPs and solvated in the water by the polymer chains. The presence of these polymers in the aqueous phase increases the RhB solubility in water, where it diffuses without forming aggregates and yielding fluorescence increase. When the film formed, the RhB remained molecularly dissolved in the matrix, maintaining the fluorescence properties. This method could not be used to obtain devices from the **RhB/DA@PMMA** NPs.

In order to tackle the impossibility to embed the NPs into hydrophilic polymeric matrices, we decided to obtain the device by trapping the NPs into porous cellulose paper and/or textile material. To prepare functional thermofluorescent papers and fabrics the freeze-dried NPs (**RhB/DA@PMMA** and **RhB/DA@PES**) were spread on top of the substrate (filter paper with porous size $\sim 100 \mu\text{m}$ or textile) obtaining a homogeneous distribution of the NPs (homogeneous coloration, **Figure 5.29a-b**). On the one hand a portion of the filter paper with **RhB/DA@PMMA** NPs (**Figure 5.29a**) was heated at 120°C ($T > T_g$) showing the local irreversible activation of the fluorescence, which could be detected clearly by naked eye. On the other hand these NPs and **RhB/DA@PES** NPs were spread as well on top of a textile. Thus, we were able to observe, by naked eye, selective fluorescence turning on upon temperature increase, the textile with **RhB/DA@PMMA** activating first ($T = 100^\circ\text{C}$), and the textile with **RhB/DA@PES** NPs activating secondly ($T = 140^\circ\text{C}$).

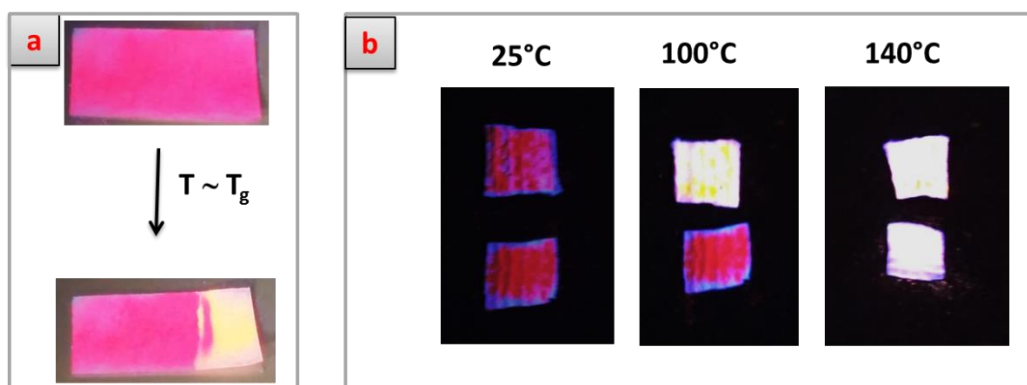


Figure 5.29: a) digital photographs of the **RhB/DA@PMMA** NPs-based functional filter paper before and after heating a piece above the T_g of the NPs and b) digital photographs of the **RhB/DA@PMMA** and **RhB/DA@PES** NPs-based functional adsorbing paper after being heated at different temperatures.

The functional paper/textile (device) demonstrated that the NPs developed in this work can be suitable to obtain precise off/on temperature multi-threshold (depending on the polymer matrix) fluorescent sensors. Again we showed the possibility to integrate the NPs into devices that might be used in real applications.

5.4 Summary

In summary, in this part of the thesis we reported a novel, general, and straightforward methodology for the development of fluorescent tunable threshold temperature sensors able to record the thermal history of surfaces and environments over a broad range of temperatures, from 90 up to almost 200 °C, unusually high for a molecular-based sensor. The strategy is based on the encapsulation of Rhodamine B base, together with a developer (dodecanoic acid) within matrix-type capsules, easily prepared with a time and cost-effective method from commercially available polymers, without requiring additional design and/or synthesis of new molecular dyes. The obtained NPs provide:

- a) abrupt (30 °C) and fast (<10 min) fluorescence enhancements upon reaching the glass transition temperature due to the developer-facilitated disaggregation of RhB molecules within the polymer,
- b) easy tunability of the threshold fluorescence activation temperature by simply changing the constituent thermoplastic polymer,
- c) an irreversible fluorescent activation (it remains once the NPs are cooled down) that allows recording the thermal history of surfaces and/or environments exposed to overheating.

Interestingly, the fluorescence appearance from the polymeric NPs can be detected by unaided eye (upon irradiation with UV) without the need of any auxiliary equipment and can be easily adapted to any thermoplastic polymer, copolymer, and blend suitable for NPs synthesis. This also includes scarcely reported very high temperatures (140–200 °C) sensing systems based on molecular materials and easily prepared NPs made by high T_g polymers which are normally costly and difficult to process in conventional ways.

Finally, the developed NP powders can be easily applied onto porous papers or textiles to obtain functional devices that could be used for multi-threshold sensing applications that require irreversible high-temperature detection.

5.5 References

1. a) B. R. Crenshaw, C. Weder, *Adv. Mater.* **2005**, 17, 1471; b) Food Process Modelling (Eds: L. M. M. Tijskens, M. L. A. T. M. Hertog, B. M. Nicolai), Woodhead Publishing Limited, Cambridge, UK 2001, Ch. 19.
2. A. Seeboth, D. Löttsch, R. Ruhmann, O. Muehling, *Chem. Rev.* **2014**, 114, 3037.
3. J. Feng, L. Xiong, S. Wang, S. Li, Y. Li, G. Yang, *Adv. Funct. Mater.* **2013**, 23, 340.
4. C. E. Sing, J. Kunzleman, C. Weder, *J. Mater. Chem.* **2009**, 19, 104.
5. a) M. A. White, M. LeBlanc, *J. Chem. Educ.* **1999**, 76, 1201; b) F. Azizian, A. J. Field, M. Heron, C. Kilner, *Chem. Commun.* **2012**, 48, 750; c) F. Azizian, A. J. Field, M. Heron, *Dyes Pigm.* **2013**, 99, 432.
6. A. J. Qin, L. Tang, J. W. Y. Lam, C. K. W. Jim, Y. Yu, H. Zhao, J. Z. Sun, B. Z. Tang, *Adv. Funct. Mater.* **2009**, 19, 1891.
7. S. J. Lee, J. E. Lee, J. Seo, I. Y. Jeong, S. S. Lee, J. H. Jung, *Adv. Funct. Mater.* **2007**, 17, 3441.
8. L. M. Maestro, E. M. Rodríguez, F. S. Rodríguez, M. C. Lglesias-dela Cruz, A. Juarranz, R. Naccache, F. Vetrone, D. Jaque, J. A. Capobianco, J. G. Solé, *Nano Lett.* **2010**, 10, 5109.
9. a) H. S. Peng, M. I. J. Stich, J. B. Yu, L. N. Sun, L. H. Fischer, O. S. Wolfbeis, *Adv. Mater.* **2010**, 22, 716; b) J. B. Yu, L. N. Sun, H. S. Peng, M. I. J. Stich, *J. Mater. Chem.* **2010**, 20, 6975; c) R. Contreras-Caceres, I. Pastoriza-Santos, J. Pérez-Juste, J. Pacifico, A. Fernández-Barbero, L. M. Liz-Marzán, *Adv. Funct. Mater.* **2009**, 19, 3070.
10. Y. Shiraishi, R. Miyamoto, X. Zhang, T. Hirai, *Org. Lett.* **2007**, 9, 3921.
11. C. C. White, K. B. Migler, W. L. Wu, *Polym. Eng. Sci.* **2001**, 41, 1497.
12. A. Seeboth, D. Löttsch, R. Ruhmann, *J. Mater. Chem. C* **2013**, 1, 2811.
13. F. Donati, A. Pucci, G. Ruggeri, *Phys. Chem. Chem. Phys.* **2009**, 11, 6276.
14. A. Puccia, F. Donati, S. Nazzi, G. U. Barretta, G. Pescitelli, L. Di Bari, G. Ruggeri, *React Funct Polym.* **2010**, 70, 951.

15. a) J. Kunzelman, B. R. Crenshaw, M. Kinami, C. Weder, *Macromol. Rapid Commun.* **2006**, 27, 1981; b) M. Kinami, B. R. Crenshaw, C. Weder, *Chem. Mater.* **2006**, 18, 946; c) B. R. Crenshaw, J. Kunzelman, C. E. Sing, C. Ander, C. Weder, *Macromol. Chem. Phys.* **2007**, 208, 572.
16. S.-h. Guo, F.-y. Zheng, F. Zeng, S.-z. Wu, *Chin. J. Polym. Sci.* **2016**, 34, 830.
17. A. Pucci, F. Signori, R. Bizzarri, S. Bronco, G. Ruggeri, F. Ciardelli, *J. Mater. Chem.* **2010**, 20, 5843.
18. G. Chen, W. Li, T. Zhou, Q. Peng, D. Zhai, H. Li, W. Z. Yuan, Y. Zhang, B. Z. Tang, *Adv. Mater.* **2015**, 27, 4496.
19. a) A. Reisch, P. Didier, L. Richert, S. Oncul, Y. Arntz, Y. Mély, A. S. Klymchenko, *Nat. Commun.* **2014**, 5, 4089; b) I. Shulov, S. Oncul, A. Reisch, Y. Arntz, M. Collot, Y. Mély, A. S. Klymchenko, *Nanoscale* **2015**, 7, 18198.
20. Polymer Data Handbook (Ed: J. E. Mark), Oxford University Press, New York **1999**.
21. Q.-H. Liu, J. Liu, J.-C. Guo, X.-L. Yan, D.-H. Wang, L. Chen, F.-Y. Yan, L.-G. Chen, *J. Mater. Chem.*, **2009**, 19, 2018.
22. V. Martín, J. Bañuelos, E. Enciso, I. L. Arbeloa, A. Costela, I. García-Moreno *J. Phys. Chem. C* **2011**, 115, 3926.
23. R. I. Macdonald, *J. Biol. Chem.* **1990**, 265, 13533.
24. A. Wagh, S. Y. Qian, B. Law, *Bioconj. Chem.* **2012**, 23, 981.
25. A. S. Klymchenko, E. Roger, N. Anton, H. Anton, I. Shulov, J. Vermot, Y. Mely, T.F. Vandamme, *RSC Adv.* **2012**, 2, 11876.
26. a) Y. Zhao, J. Fickert, K. Landfester, D. Crespy, *Small* **2012**, 8, 2954; b) R. H. Staff, D. Schaeffel, A. Turshatov, D. Donadio, H.-J. Butt, K. Landfester, K. Koynov, D. Crespy, *Small* **2013**, 9, 3514; c) M. Hu, S. Peil, Y. Xing, D. Döhler, L. C. da Silva, W. H. Binder, M. Kappla, M. B. Bannwarth, *Mater. Horiz.* **2018**, 5, 51.
27. J. L. Dela Cruz, G. J. Blanchard, *J. Phys. Chem. A* **2002**, 106, 10718.
28. R. F. Kubin, A. N. Fletcher, *J. Lumin.* **1982**, 27, 455.
29. J. R. Rumble CRC Handbook of Chemistry and Physics, CRC Press, Boca Raton, **2005**.

30. a) M. A. White, M. LeBlanc, *J. Chem. Educ.* **1999**, 76, 1201; b) F. Azizian, A. J. Field, M. Heron, C. Kilner, *Chem. Commun.* **2012**, 48, 750; c) F. Azizian, A. J. Field, M. Heron, *Dyes Pigm.* **2013**, 99, 432.
31. I. Rosenthal, P. Peretz, K. A. Muszkat, *J. Phys. Chem.* **1979**, 83, 350.

CHAPTER 6

General Conclusions

6.1 Summary and general conclusions

During the present doctoral thesis we demonstrated that assembling in micro/nanostructures conventional dyes with interacting media (phase change materials or polymers with additives, when needed) is a successful, straightforward approach to develop solid materials with advanced chromogenic properties. Through the encapsulation of these mixtures into core-shell or matrix-type polymeric capsules, the advanced chromogenic and fluorogenic properties of bulk mixtures are successfully transferred into the solid state. In all developed materials it is showed how the chromogenic/emissive properties (i.e. color, response rate, activation temperature, etc.) could be easily tuned by modifying the capsules components, without requiring time-consuming chemical modifications of the dye or the matrix of the final solid material. Based on this approach, three different types of advanced chromogenic or fluorogenic materials have been prepared in this thesis:

i) highly **tunable** and temperature-controlled **switchable reverse photochromic solid materials** were developed through the encapsulation of different dyes and interacting media (**Figure 6.1a-b**), which allowed controlling the photochromic properties (colors, rates, and type of photochromism). The subsequent incorporation of these capsules in polymeric matrices allowed fabricating a proof-of-concept of a multicolored rewritable device (**Figure 6.1c**). With this strategy we were able to prepare films that allow on demand reversible UV-light writing (direct photochromism), visible-light writing (reverse photochromism) and temperature-induced thermochromic transitions (**Figure 6.1d**)

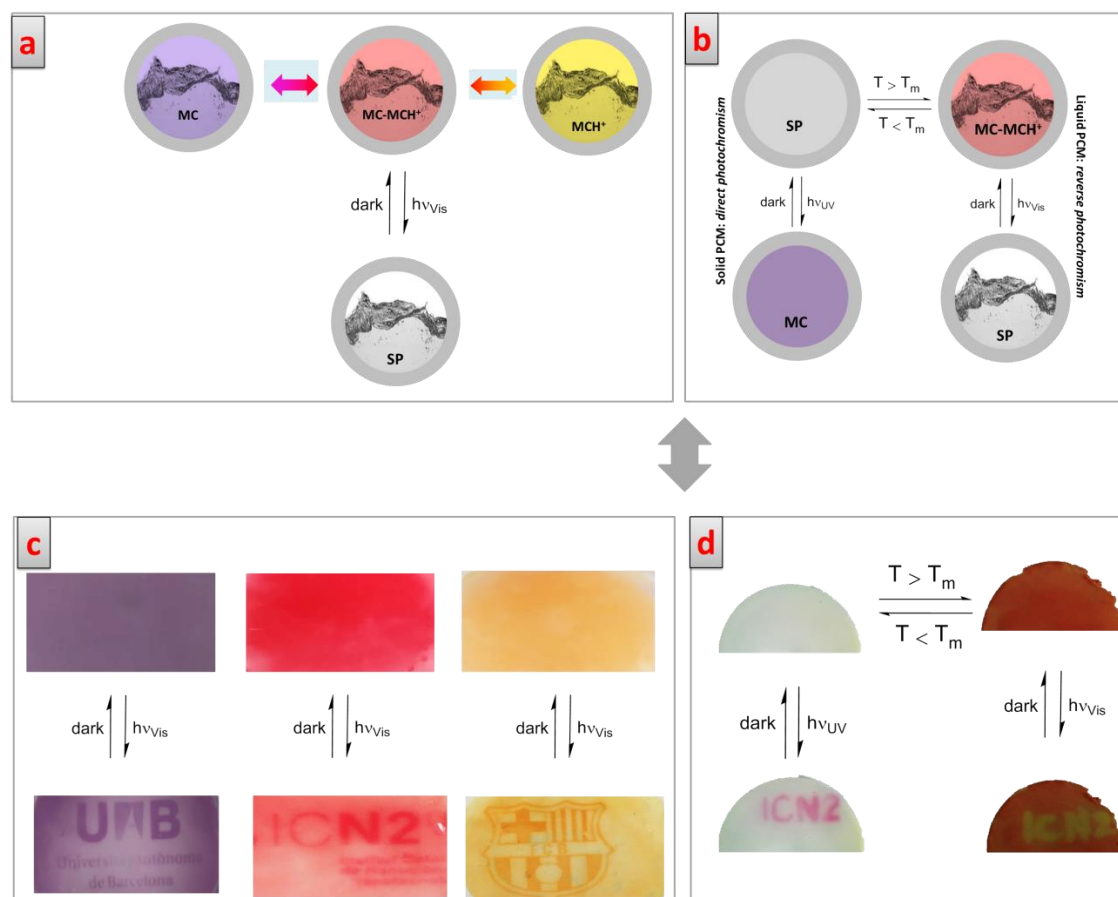


Figure 6.1: a) schematic representation of the a) tunability of reverse photochromism and the b) temperature-induced switchable photochromism exhibited by the capsules prepared in **Chapter 3**; polymeric films prepared from photochromic core-shell capsules and displaying c) highly tunable reverse photochromism and d) switchable photochromism.

ii) **multiresponsive and tunable thermochromic materials** based on ketocyanine dyes were obtained by the structuration of bulk mixtures in solid lipid microparticles and the subsequent encapsulation within polymeric capsules. Tunable transition temperatures and colors (ranging from visible to the NIR region) were obtained by playing with the interacting mixture inside the capsules. The capsules could be designed and prepared to present temperature and pH responsiveness, which could be reversible (**Figure 6.2**) or irreversible (loss of the thermochromic properties) depending on the type of media of the capsules core.

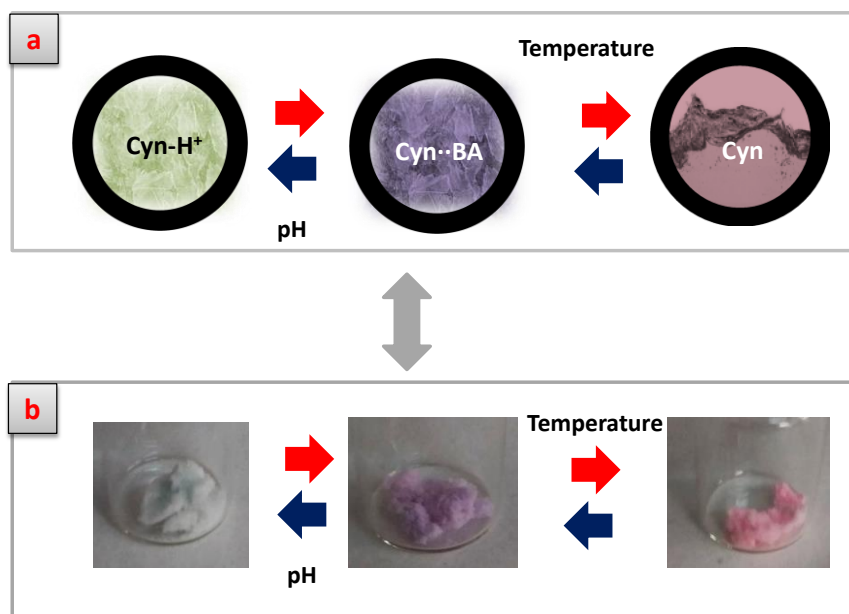


Figure 6.2: a) schematic representation of the multiresponsive capsules based on ketocyanine dyes obtained in **Chapter 4** and b) photographs of the solid powder of the capsules after being exposed to different stimuli (pH and temperature).

iii) **high threshold temperature off/on irreversible fluorescent nanoparticles** have been prepared (**Figure 6.3**). The overcome of the glass transition temperature of the thermoplastic polymer matrix of the nanoparticles (matrix-type capsules) triggers the fluorescence activation. By changing the polymer matrix, the switching activation temperature could be easily tuned between 100 and 200°C. By using this approach, multithreshold irreversible fluorescent temperature sensors could be prepared.

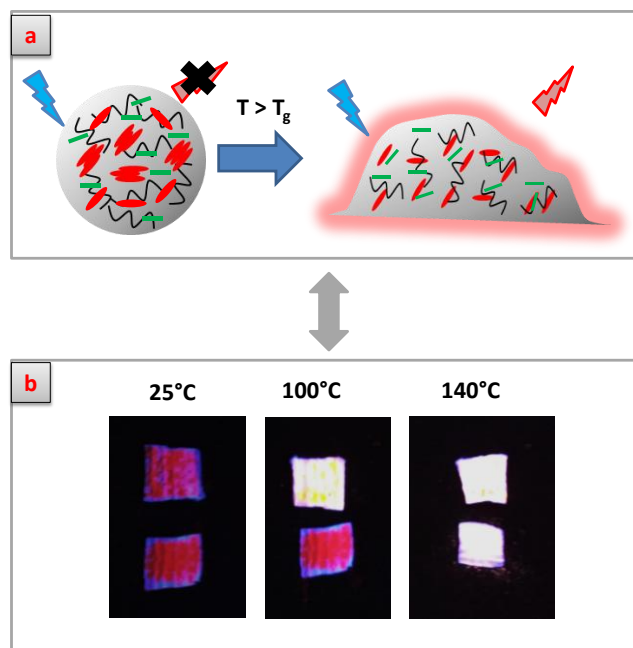


Figure 6.3: a) schematic representation of the irreversible temperature off/on fluorescent behaviour of the dye-loaded polymeric nanoparticles prepared in **Chapter 5** and b) photographs of a textile with the NPs adsorbed which can be potentially used as multi-threshold high-temperature fluorescent sensing devices.

Very promising results obtained for these three systems and the possibility to transfer the advanced chromogenic and fluorogenic behaviour observed in bulk mixtures to functional solid prototypes, make these new materials almost usable in potential applications such as anti-counterfeiting technologies, rewritable devices, and high temperature sensing.

However, due to the high demanding requirements of the industry for real products, several aspects must be still investigated before the developed materials can be integrated in the final products, such as the scalability of the capsules, the fatigue resistance of the dyes, the incorporation of the materials in the products and the integration into the industrial manufacturing processes.

CHAPTER 7

Experimental Section (Materials and methods)

7.1 Materials

7.1.1 Polymers, surfactants and monomers

Polymethyl methacrylate (**PMMA**, MW = 120000), polybisphenol-A carbonate (**PC**, MW = 45000), polyethersulfone (**PES**, MW = 22000), polystyrene (**PS**, MW = 190.000), polyetherimide (**PEI**), gelatin from porcine skin (**GEL**, gel strength 175 g Bloom, Type A), gum arabic from acacia tree (**GA**), polyvinyl alcohol (**PVA**, Mowiol® 4-88, 85% hydrolyzed, medium molecular weight), polyacrylamide (**PA**, MW = 150000), styrene (**Sty**, ≥99%) and azobisisobutyronitrile (**AIBN**, 98%) were acquired from Sigma Aldrich. Sodium dodecyl sulphate (**SDS**) was purchased from Fisher. Saduren®163 (melamine-formaldehyde pre-polymer) was acquired from BASF.

7.1.2 Color developers and phase change materials

Bisphenol-A (**BA**, 99%), dihydroxy-terminated poly(dimethylsiloxane-co-diphenylsiloxane) (**PDMS-OH**), glyceryl tristearate (**GS**) and dodecanoic acid (**DA**, 98%) were purchased from Sigma Aldrich. Nonanoic acid (**NA**, 97%), 1-tetradecanol (**TDOH**, 97%), 1-hexadecanol (**HDOH**, 97%), *n*-dodecylphosphonic acid (**DPA**, 95%) and *n*-octyl 4-hydroxybenzoate (**Benz**, 98%), stearic acid (**SA**, >90%) were acquired from Alfa Aesar. Miglyol®812 (**M812**) was bought from oximedexpres. Trilaurin (**TA**, >98%) was obtained from TCI chemicals.

7.1.3 Dyes

Photochromes 1',3',3'-trimethyl-6-nitrospiro[1(2H)-benzopyran-2,2'-indoline] (**SP-1**), 1'-(2-hydroxyethyl)-3',3'-dimethyl-6-nitrospiro[1(2H)-benzopyran-2,2'-indoline] (**SP-2**), 1',3'-dihydro-8-methoxy-1',3',3'-trimethyl-6 nitrospiro [2H-1-benzopyran-2,2-(2H)-indole] (**SP-3**), 1',3',3'-trimethylspiro[1(2H)-benzopyran-2,2'-indoline] (**SP-4**), (6-bromo-1',3',3'-trimethylspiro[1(2H)-benzopyran-2,2'-indoline] (**SP-5**) and 8-methoxy-1', 3', 3'-trimethylspiro[1(2H)-benzopyran-2,2'-indoline] (**SP-6**) were all obtained from TCI chemicals. The fluorescent dye Rhodamine b base (**RhB**) was purchased from Sigma Aldrich. Ketocyanine dyes (**Cyn I**, **II** and **III**) were synthesized by the "Integrated Analytical Microsystems group" (from the Sensors & Biosensors Group at the UAB, in collaboration with

Sergey Miltsov from the Organic Department of the Saint Petersburg State University).

7.1.4 Solvents

The organic solvents used during the synthesis procedures, dichloromethane (DCM) and chloroform, were acquired from Scharlau. All commercial solvents and chemicals were used without any further purification. Distilled water or MiliQ water was used in all syntheses. Deuterated solvents were acquired from Euriso-Top.

7.2 Characterization techniques

7.2.1 Optical Microscopy: optical microscopy images were collected using a Zeiss Primo Star equipped with a camera AxioCam ERc 5s. Approximately 1 drop of the suspension of particles/capsules was poured on top of a glass slide and observed before and after drying. The objective magnification used for collecting the images was between 4x and 40x.

7.2.2 Scanning electron microscopy (SEM): SEM images were collected on the scanning electron microscope FEI Quanta 650 FEG at acceleration voltages between 2-10 kV. Samples were mounted on SEM metal stubs covered with aluminum or carbon tape and they were coated with a thin layer of platinum (~ 5 nm). Microcapsules and nanoparticles suspensions (100 μ L) were deposited on the stub by drop casting, allowing solvent evaporation in air at room temperature. For solid powders, approximately 1 mg of microcapsules or nanoparticles was deposited on the adhesive carbon tape.

7.2.3 Absorption spectra of the solid and liquid samples were obtained from a Cary 60 spectrophotometer. Liquid homogeneous solutions were measured in transmittance mode and using the solvent as blank. Solid samples were measured through diffuse reflectance mode, using an external integrating sphere connected with a fiber optic. As a reference, the same material (i.e. phase change materials, capsules, films) without the dye, was used. The absorption spectra were estimated from the measured diffuse reflectance spectra through the Kubelka-Munk equation ($F(R) = (1-R)^2/2R$). To determine the color change kinetics, the maximum of absorption (or $F(R)$) was plotted against time. The curve was fitted with

exponential functions [$y = A_1 \cdot \exp(x/t_1) + y_0$] using the software Origin 8. The k value was calculated from [$k = 1/t_1$].

7.2.3.1 Time-dependent absorption measurements were performed using the spectrophotometer in scan mode. For all the photochromic materials, their thermal back-isomerization was monitored by recording the absorption (or reflectance) spectra at different time delays, in the dark after reaching their photostationary state.

7.2.3.2 Temperature-dependent absorption spectra were recorded by layering the capsules powder holder on top of a heating/cooling plate and placing the integrating sphere on top of the capsules powder. The sample temperature was controlled through a recirculating thermostat (Huber MPC-K6) coupled to the sample holder or through a heating plate, and monitored with a thermometer set on top of the surface of the heating plate.

7.2.4 Fluorescence spectra were recorded on a PTI QuantaMaster 300 phosphorescence/fluorescence spectrophotometer (Horiba Ltd.). The excitation (355 nm) for emission measurements was provided from a Xenon lamp (75 W).

7.2.4.1 Temperature-dependent fluorescence measurements: solid preheated and heated NPs were measured at room temperature (RT) in a triangular 1 x 1 cm cuvette with the width face, placed at 45° respect to both the excitation beam and the detection direction. The fluorescence measurements were carried out at RT. The emission enhancement at a given temperature ΔF (T) was calculated with the equation ΔF (T) = $(F_T - F_{RT})/F_{RT}$, where F_T and F_{RT} are the integrated emission intensities obtained from the emission bands after heating the NPs at the specific temperature T and at RT, respectively.

7.2.4.2 Heating process of the RhB-containing nanoparticles (NPs) for temperature-dependent fluorescence study: the NPs were put in a vial which was immersed for 10 min in a preheated oil bath. After heating, the solid material was transferred to the triangular measuring cuvette for fluorescence or reflectance measurements at RT.

7.2.5 Proton nuclear magnetic resonance ($^1\text{H-NMR}$): $^1\text{H-NMR}$ spectra were recorded using the following spectrometers located at the Servei de Resonància Magnètica Nuclear of the UAB: Bruker DPX250 (250 MHz for $^1\text{H-NMR}$) and Bruker DPX400 (400 MHz for $^1\text{H-NMR}$) and 20-30 mg of microcapsules or nanoparticles were dissolved in CDCl_3 . The spectra are given in chemical shifts, δ (ppm). The peaks are defined as singlets (s), triplets (t) or multiplets (m). 10 μl of DMF ($\delta = 7.96$ (s, 1H, CH), 2.97 (s, 3H, CH_3), 2.88 (s, 3H, CH_3)) were added to the samples, as an internal reference, for quantitative determination of the microcapsules payload. The payload was calculated as $[\text{g encapsulated material}]/[\text{g capsules}] \%$.

7.2.6 Differential Scanning Calorimetry (DSC) measurements were carried out in a TA Instruments Q20 differential scanning calorimeter. Approximately between 4-7 mg of a sample were deposited on a 0.5 cm-in-diameter aluminum pan. An empty pan was used as a reference. The scanning rate was 10 K/min for both the heating and cooling processes. The scanned temperature range depended on the sample.

- The melting/crystallization point were calculated from the intersection between two tangents (one is the tangent of the endo- or exothermic peak and the other is the straight line of the baseline).

- The glass transition temperature (T_g) values of the polymers were determined from the temperature at which the curve slope starts to change was taken.

7.3 General procedures

7.3.1 Lyophilisation of the microcapsules and nanoparticles was carried out in a TELSTAR CRYODOS-50 freeze dryer with one single stage compressor, giving a refrigerator power of 450 W and a final temperature of 223 K. This dryer is coupled to an Edwards RV12 vacuum pump, with which a final pressure of $2 \cdot 10^{-3}$ mbar is achieved.

7.3.2 Irradiation methods: irradiations were carried out using a low pressure mercury lamp (365 nm, 2.7 mW/cm^2 , 1 cm of distance from the sample), a laser pointer (Laser 303, 405 nm, 1.3 W/cm^2), a green laser pointer (JD-850, 532 nm,

570 mW/cm²) and a non-coherent flashlight torch (UltraFire CREE XM-LT6, 1 cm of distance from the sample).

7.3.3 Synthesis of photochromic microcapsules

- **7.3.3.1 Synthesis of SP-X/NA@PMMA:** in a typical experiment PMMA (0.5 g) was dissolved in DCM (5 mL) upon magnetic stirring while the photochrome of interest (30 mg for **SP-1** and **SP-4**, 10 mg in the case of **SP-5**) was dissolved in NA (0.903 g). During photochrome dissolution, colour development was observed. Once all the photochrome was dissolved, the NA solution was poured into the DCM solution. The final organic mixture was subsequently added to a previously prepared PVA (4-88%) water solution (10 mL, 1 wt. %). The mixture was homogenized (T18 Ultra-Turrax® IKA, 5000 rpm) at room temperature for 10 minutes to induce the formation of the oil-in-water (O/W) emulsion. Successively, the whole emulsion was transferred into a round bottom flask and was heated at 44 °C under vacuum for 20 minutes, during which DCM evaporated and the PMMA precipitated around the NA droplets. The obtained microcapsules suspension was diluted with water (30 mL) and centrifuged at 4000 rpm during 10 minutes. This process was repeated three times redispersing the capsules with water (10 mL). After freeze-drying the resulting suspension in the dark, a coloured, fine solid powder was obtained.
- **7.3.3.2 Synthesis of SP-1/NA-DPA@PMMA:** the synthesis of these microcapsules was carried out as in 7.3.3.1 with the exception of the addition of DPA (25 mg) in the initial **NA/SP-1** solution. During the DPA addition the photochromic solution changed from red to yellow. The amount of dye (SP-1) was 10 mg.
- **7.3.3.3 Synthesis of SP-1/PDMS-OH@PMMA:** the synthesis of these microcapsules was carried out as in 7.3.3.1 with the following exceptions:

 - the PMMA amount was increased to 0.75 g,
 - NA (0.903 g) was substituted by PDMS-OH (1.05 g),
 - the amount of SP-1 was maintained at 30 mg,
 - the homogenization step was carried out emulsifying at 3000 rpm.

- **7.3.3.4 Synthesis of SP-4/TDOH-BA@PC and SP-5/TDOH-BA@PES:** the syntheses of these capsules was carried out as showed in 7.3.3.1 but:
 - PMMA was substituted by 0.25 g of PC (for **SP-4/TDOH-BA@PC** capsules) or PES (**SP-5/TDOH-BA@PES**),
 - NA was substituted by a solution of TDOH (0.5 g) and BA (30 mg),
 - the TDOH/BA solution was prepared at 50°C,
 - the homogenization step was carried out emulsifying at 3000 rpm for 5 min.
- **7.3.3.5 Synthesis of SP-X/DA@PMMA:** the synthesis was carried out as in 7.3.3.1 with the following exceptions:
 - NA was substituted by DA (0.883 g),
 - the DA/SP solution was prepared at 50°C,
 - the DCM solution (10.4 mL) and the amount of water phase (15 mL) were increased.

7.3.4 Thermo and pH-responsive solid lipid microparticles (SLMs) and microcapsules (MCs)

- **7.3.4.1 Synthesis of Cyn/DPA@HDOH SLMs:** in a typical experiment, DPA (100 mg) and Cyn (0.2 mg) were dissolved in molten HDOH (2 g) at 60°C. The final mixture was subsequently added to a previously prepared PVA (4-88%) water solution (10 mL, 1 wt. %) and was homogenized (T18 Ultra-Turrax® IKA, 3000 rpm) at 60°C during 5 min. Successively, the whole emulsion was transferred to 20 mL of cold water (2-5°C), where the HDOH droplets precipitate trapping the DPA and the dye.
- **7.3.4.2 Synthesis of Cyn/DPA@HDOH_GS particles:** the synthesis was carried out as in 7.3.4.1 but:
 - substituting the HDOH with a mixture of HDOH (1 g) and GS (1 g),
 - obtaining the O/W emulsion by stirring at 1000 rpm.
- **7.3.4.3 Synthesis of Cyn/DPA@HDOH_GS@GEL_GA capsules:** the synthesis of the capsules is divided in two steps: the formation of the solid lipid microparticles (SLMs) and the consequent coacervation process.

1. **Preparation of Cyn/DPA@HDOH_GS SLMs:** this step was carried out as in 7.3.4.1 but doubling the amount of DPA (400 mg) and Cyn (0.2 mg). The resulting suspension of the SLMs was let to flocculate during 2-3 hours to the air-water interface. Almost all the water was removed with a syringe leaving 2-3 mL of a very concentrated SLMs suspension (~1 g/mL).
 2. **Shell formation of the MCs:** the concentrated SLMs suspension (~1 g/mL) was dispersed in a previously prepared gelatine Milli-Q water solution (2.5 wt. %, 10mL) at 40°C (below the T_m of the HDOH_GS mixture). Then, a gum Arabic solution (2.5 wt. %, 10mL) at 40°C was added stepwise. The pH of the total suspension was reduced to approximately 4 (3 drops of acetic acid) to maximize the electrostatic interaction between the polymers and the temperature was let to drop up to RT, during which the coacervates deposits on the surface of the SLMs, forming a thin polymeric film. Finally after cooling with ice (2-5°C), the polymer jellifies forming a stable and robust polymeric shell.
- **7.3.4.4 Synthesis of Cyn/DPA@SA_GS@GEL_GA capsules:** the synthesis was carried out in two steps as showed in 7.3.4.3 but changing the following conditions for the SLMs synthesis:
 - the HDOH/GS mixture was substituted by SA (1 g) and GS (1 g),
 - the DPA was reduced to 100 mg,
 - the homogenization (1000 rpm during 5 min) is carried out at 80°C,
 - after the SLMs formation, these are let to flocculate during 3-5 hours.
 - **7.3.4.5 Synthesis of Cyn/BA@HDOH_GS@GEL_GA capsules:** the synthesis of the capsules was carried out as in 7.3.4.3 but with the following exceptions in the SLMs preparation:
 - the DPA (400 mg) was substituted by BA (100 mg),
 - the PVA water solution (10 mL) was substituted by SDS water solution (0.5 wt. %),
 - the homogenization was carried out at 500 rpm during 2 min,
 - after the SLMs formation, these are let to flocculate during 3-5 hours.

7.3.5 Synthesis of RhB@polymer NPs

In a typical experiment the polymer (PMMA, PS, PC, PES, and PEI) of interest (0.5 g) and RhB-base (10 or 2 mg, 2 or 0.4 wt. % respect to the polymer) were dissolved in DCM (5 mL) upon magnetic stirring. For PEI particles CHCl_3 was used instead because of the better polymer solubility in this solvent. During the dye dissolution, fluorescence development was observed. Once all the components were dissolved, the final organic mixture was subsequently added to a previously prepared SDS water solution (10 mL, 0.5 wt. %). The mixture was pre-emulsified (T18 Ultra-Turrax ® IKA, 1000 rpm) at RT for 60 minutes. The formed preemulsion was sonicated for 120 s (Branson Ultrasonic Sonifier, 70% amplitude, 30 s pulse on, 10 s pulse off) to produce the nanoemulsion. The obtained mixture was transferred into a vial and the organic solvent was let to evaporate overnight at RT, inducing the precipitation of the polymer and the encapsulation of the dye and the fluorescent developer (when included) in the nanoparticles. The suspension was diluted with water (10 mL) and freeze-dried for 48 h, after which a pink-colored, non-fluorescent fine solid powder was obtained. The NPs with the fluorescent developer (DA, M812, NA, TDOH, 50 mg) were prepared following the same method, starting from a solution of RhB and the fluorescent developer in CH_2Cl_2 .

7.3.6 Preparation of polymeric films

- **7.3.6.1 PVA films preparation:** a fraction of the obtained suspension (2.5 mL) of the photochromic microcapsules (300 mg) was dispersed homogeneously with the vortex in a previously prepared PVA solution (3.3 g, 20 wt. %). This solution was slowly transferred to a plastic Petri plate (diameter of 5.5 cm) and water was allowed to evaporate on a flat surface at room temperature during 24 h. The final film was easily removed from the Petri plate once it was dry.

- **7.3.6.2 PA film preparation:** the films were prepared as shown in 7.3.6.1 with the following exceptions:
 - The PVA solution was substituted by a PA solution (10 g, 2 wt. %),
 - The evaporation time was increased from 24 to 48 h.